



# Impact of anthropogenic organic matter on the fluorescence in coastal zone

Ibrahim El-Nahhal

## ► To cite this version:

Ibrahim El-Nahhal. Impact of anthropogenic organic matter on the fluorescence in coastal zone. Biodiversity and Ecology. Université de Toulon, 2018. English. NNT : 2018TOUL0005 . tel-02134307

**HAL Id: tel-02134307**

**<https://theses.hal.science/tel-02134307>**

Submitted on 20 May 2019

**HAL** is a multi-disciplinary open access archive for the deposit and dissemination of scientific research documents, whether they are published or not. The documents may come from teaching and research institutions in France or abroad, or from public or private research centers.

L'archive ouverte pluridisciplinaire **HAL**, est destinée au dépôt et à la diffusion de documents scientifiques de niveau recherche, publiés ou non, émanant des établissements d'enseignement et de recherche français ou étrangers, des laboratoires publics ou privés.

# Thèse de Doctorat

Pour obtenir le grade de  
**Docteur de L'Université de Toulon**

Discipline et Spécialité : Chimie, Chimie de l'environnement

Présentée par :

**Ibrahim Yasser Zidan El-Nahhal**

---

**Impacte de la matière organique anthropique issue des stations  
d'épurations sur la fluorescence de la matière organique en zone côtière**

---

Directeur de Thèse : **Dr. Stéphane Mounier**

Présentée et Soutenue publiquement  
Le 10 Juillet 2018

**Jury de Thèse:**

<b>Mme. Madeleine Goutx</b> Directrice de Recherche au CNRS (France),	Examinatrice
<b>M. Stéphane Mounier</b> Maître de conférences HDR, Université de Toulon (France) ,	Directeur
<b>M. Abdelkrim Ouammou</b> Professeur de l'Enseignement Supérieur (PES), Université Sidi Mohamed Ben Abdellah (Maroc) ,	Rapporteur
<b>Mme. Claire Richard</b> Directrice de Recherche, CNRS, ICCF, Université de Clermont Auvergne (France) ,	Rapporteur
<b>M. Davide Vione</b> Associate Professor, Università degli Studi di Torino (Italie),	Examineur
<b>Mme. Florence Vouvé</b> Maître de conférences, Université de Perpignan (France) ,	Examinatrice





This page is intentionally left blank ...

رَبِّ أَوْزِعْنِي أَنْ أَشْكُرَ نِعْمَتَكَ الَّتِي أَنْعَمْتَ عَلَيَّ وَعَلَىٰ وَالِدَيَّ وَأَنْ أَعْمَلَ صَالِحًا تَرْضَاهُ وَأَدْخِلْنِي  
بِرَحْمَتِكَ فِي عِبَادِكَ الصَّالِحِينَ

**Permetts-moi Seigneur, de rendre grâce pour le bienfait dont  
Tu m'as comblé ainsi que mes père et mère, et que je fasse  
une bonne œuvre que tu agrées et fais-moi entrer, par Ta  
miséricorde, parmi Tes serviteurs vertueux**

## Dedication

إلى آبائي الأولين

I dedicate this PhD thesis to my beloved father Dr Yasser EL-Nahhal and to the spirit of my grandfather Zidan Salem EL-Nahhal .

## Remerciements

Tout d'abord, j'exprime mon grand gratitude envers ALLAH , le tout puissant , de m'avoir donné le courage d'endurer et d'accomplir tous les différents tâches de ma thèse de doctorat , et de m'avoir béni de de nombreux gens de grand esprit qui étaient et sont encore le grand soutien et source d'encouragement dans ma vie personnelle ainsi que ma vie professionnelle.

Je tiens à remercier mon directeur de thèse Monsieur Stéphane Mounier , Professeur à l'Université de Toulon, qui m'a encadré tout au long de cette thèse et qui m'a fait partager ses brillantes intuitions. Qu'il soit aussi remercié pour sa gentillesse, sa disponibilité permanente et pour les nombreux encouragements qu'il m'a prodiguée.

J'adresse tous mes remerciements à Monsieur Abdelkrim OUAMMOU , Professeur de l'Enseignement Supérieur (PES) à l'Université de Sidi Mohamed Ben Abdellah , ainsi qu'à Madame Richard Claire, Directrice de Recherche à l'Université Clermont Auvergne , de l'honneur qu'ils m'ont fait en acceptant d'être rapporteurs de cette thèse . Mes sincères remerciements s'adressent aux autres membres de mon jury de thèse : Madame Florence VOUVÉ, Madame Madeleine Goutx et Monsieur Davide Vione d'avoir accepté de juger la qualité de mes travaux de thèse.

Il faut pas oublier l'accueil chaleureux dans les premier jours des mon arrivée en France par Monsieur Dr. Cedric Garnier qui m'a bien accueilli et aidé dans le côté administratif ainsi que son épouse Madame Dr. Véronique le Noble

Je remercie également Monsieur Christian Martino, pour sa disponibilité dans toutes les sortie de prélèvement ainsi que pour son soutien technique dans la instrumentation des matériaux nécessaires pour l'achèvement des travaux de cette thèse et de son esprit accueillant . Gaël Durrieu est aussi remercié pour sa participation aux sortie de prélèvement.

Je remercie également Monsieur Roland Redon, pour ses conseils à l'amélioration de la présentation de soutenance .

Je remercie aussi le programme Hermes/Erasmus Mundus pour le financement de cette thèse . j'aimerais aussi remercier tout le personnel au CROUS Nice-Toulon.

## Table of Contents

<b>Table of Contents</b>	<b>7</b>
<b>List of Abbreviations</b>	<b>10</b>
<b>List of Figures</b>	<b>11</b>
<b>List of Tables</b>	<b>17</b>
<b>List of Annexes</b>	<b>19</b>
<b>Chapter 0 : Introduction</b>	<b>20</b>
<b>Chapter 1 - State of the Art and Literature Review</b>	<b>24</b>
I.1 The coastal Zone :	25
I.2 Carbon Cycle	28
I.3 Biogeochemical and ecological importance of the DOM in the coastal ocean	30
I.4 Organic matter	30
I.4.1 Complexity of the organic matter	32
I.4.2 Dissolved organic matter (DOM)	33
I.4.3 Chromophoric Dissolved Organic Matter CDOM	34
I.4.4 The optical properties of Organic matter	36
I.4.4.1 Fluorescent dissolved organic matter (FDOM)	36
I.4.4.2 Composition of fluorescent dissolved organic matter	36
I.4.4.3 Principle of Fluorescence Spectroscopy	36
I.4.4.4 Jablonski Diagram	37
I.4.4.5 Methods of analysis of 3D excitation and emission matrix spectra of fluorescence.	39
I.5 Irradiation in Environment	47
I.5.1 Solar irradiation	47
I.6 Principle of photochemistry	51
I.6.1 Photodegradation of Dissolved Organic matter DOM	51
I.6.2 Kinetic rate order determination of Photodegradation of DOM	53
<b>Chapter 2 : Materials and methods</b>	<b>55</b>
II.1 Study Area	56
II.1.1 Gapeau River	56
II.1.2 Tributaries of The river Gapeau	57
II.1.2.1 The Le Real Martin tributary	57
II.1.3 Wastewater treatment Plant of La Crau city - Département du Var - Southeastern France	60
II.1.4 The Coastal zone of Hyeres City	61
II.2 Solar Irradiation Experiments	62
II.2.1 Sampling Sites	62
II.2.2 Irradiation experiments	66
II.2.3 Materials of irradiation experiment	66
II.2.4 Filtration/without filtration mixture	67
II.2.5 Preparation of the mixtures	69

II.2.6 Exposing the mixtures to Sunlight	71
II.2.7 Experiment notation/codification	73
II.2.8 Preparation of chemical actinometer	73
II.2.9 Preparation of solar energy sensor : Physical actinometer	76
II.2.9.1 The Relationship between our physical actinometer and Météo-France data	77
II.2.10 Excitation Emission Matrix fluorescence spectroscopy	79
II.2.10.1 Sampling the quartz vials	79
II.2.10.2 Three dimensional excitation emission matrix (3D EEM) acquisition	80
II.2.10.2.1 First EEM data acquisition : “Elnahhal” method	81
II.2.10.2.2 Second EEM data acquisition: “Croatie” method	81
II.2.10.2.3 Third data acquisition method : two dimensional fluorescence	82
II.2.11 PARAFAC modelling of the data	83
II.2.12 Normalization of Contribution of CP/PARAFAC components of irradiation experiments	85
II.2.13 Multi-linear regression modelling of the CP/PARAFAC Components with two endmember mixing composition.	87
II.2.14 Kinetics or Pseudo-Kinetics order determinations	90
II.3 Geographical field experiment	91
II.3.1 Choosing the sampling sites	91
II.3.2 Electrical Conductivity and pH of Geographical field experiment	95
II.3.3 3D excitation emission matrix of fluorescence spectroscopy of Geographical field experiment	95
II.4 Temporal variations Field experiment	96
II.4.1 Preparing bottles of the autosampler	96
II.4.2 Sampling of three Endmembers during a 48 hour cycle	97
II.4.3 Filtration/Non filtration of the samples of the temporal variations of the sources (Endmember mixing components)	99
II.4.3.1 Measurement of non-filtered (NF) samples	100
II.4.3.2 Measurement of the filtered (F) samples	100
II.4.4 Electrical Conductivity and pH measurement	101
<b>Chapter 3 : Photodegradation of DOM from three endmembers and multilinear regression</b>	<b>102</b>
III.1 Introduction	104
III.2. Material and methods	105
III.2.1 Sampling Sites	105
III.2.2 Materials of irradiation experiment	107
III.2.2.1 Filtration	107
III.2.2.1 Preparation of mixtures	107
III.2.2.3. Experiment notation/codification	107
III.2.2.4. Irradiation experiments	108
III.2.2.5. Solar irradiance measurement	109
III.2.3. Excitation Emission Matrix EEM fluorescence spectroscopy	109
III.2.3.1. Sampling	109
III.2.3.2. Data processing	110
III.2.4. Multi-linear regression	111
III.2.4.1. Multilinear regression of three endmember	111
III.2.5. Kinetics	113
III.3. Results and Discussion	113
III.3.1. EEMs Results	113
III.3.2 Multivariate Linear Regression Parameters	116
III.3.3. Determination of coefficient kinetic decay and order	117
III.4. Conclusions	120
<b>Chapter 4 - Temporal and Spatial investigations on the river Gapeau</b>	<b>130</b>
IV.1 Temporal Field experiment	131
IV.1.1 Variation of the conductivity during temporal field experiment	134
IV.1.2 Variation of the pH values during temporal field experiment	135
IV.1.3 EEMs temporal determination	137

IV.1.4 EEMs temporal variation	140
IV.1.4.1 Gapeau River	141
IV.1.4.2 Wastewater Treatment plant	142
IV.1.4.3 Confluence Gapeau River & Le Réal Martin	144
IV.1.4.4 Sea Water	146
IV.2 Geographical field experiment results	148
IV.2.1 Description of the weather during the sampling for the spatial “geographical” field experiment .	148
IV.2.2 pH results of the Geographical field experiment	150
IV.2.3 Electrical Conductivity for Geographical field experiment	151
IV.2.4 Geographical variation of temperature	152
IV.2.5 CP/PARAFAC Components results of the decomposition of the geographical field experiment	153
IV.2.6 Variation with Geographical Distance of CP/PARAFAC Components	156
IV.2.6.1 The 1st CP/PARAFAC component	156
IV.2.6.2 The 2nd CP/PARAFAC component	157
IV.2.6.3 The ratio of the 1st and 2nd CP/PARAFAC Components	159
<b>Chapter 5 - Estimation of annual inputs</b>	<b>161</b>
V.1 The multilinear regression model used here	162
V.2 Annual variation modeling	165
V.2.1 Variation in the presence of UV irradiation	165
V.2.2 Importance of the irradiation in the model	172
V.3 Geographical field experiment : modelling based on the multilinear regression model	173
<b>Conclusions and Perspectives</b>	<b>180</b>
<b>References</b>	<b>186</b>
<b>ANNEX I : fRW and fSW Permutation</b>	<b>205</b>
<b>ANNEX II : fWW and fSW Permutation</b>	<b>218</b>
<b>ANNEX III : fRW and fWW Permutation</b>	<b>231</b>
<b>ANNEX IV : EGU poster</b>	<b>244</b>
<b>ANNEX V</b>	<b>246</b>
<b>ANNEX VI : Kinetic constants</b>	<b>250</b>
<b>Abstract</b>	<b>255</b>



## List of Abbreviations

NOM : Natural Organic Matter

DOM : Dissolved Organic Matter

CDOM: Chromophoric Dissolved Organic Matter

FDOM : Fluorescent Dissolved Organic Matter

PARAFAC : Parallel Factor Analysis

DOC : Dissolved Organic Carbon

DON : Dissolved Organic Nitrogen

DOP : Dissolved Organic Phosphorus

POC : Particulate Organic Carbon

WWTP : Wastewater Treatment Plant

UV : Ultra Violet

PCA : Principal Component Analysis

PLS : Partial Least Squares

EEM : Excitation Emission Matrix

FRI : Fluorescence Regional Integration

RW : River Water

SW : Sea Water

WW : WasteWater treatment plant effluent

$f_{RW}$  : Content Fraction of River Water

$f_{WW}$  : Content Fraction of WasteWater treatment plant effluent

$f_{SW}$  : Content Fraction of Sea Water

CR : Croatia method of EEM data acquisition which is an arbitrary name

EN : Elnahhal method of EEM data acquisition which is an arbitrary name

## List of Figures

**Figure I.1:** Geographic distribution of the global coastal population and the shoreline development

**Figure I.2 :** The contemporary global carbon cycle through the major reservoirs of planet Earth. Units are Pg C or Pg C yr<sup>-1</sup>

**Figure I.3 :** The carbon cycle in nature

**Figure I.3:** The relationship between various Natural organic matter fractions which is represented as acronyms . TOM: Total Organic Matter , TOC: Total Organic Carbon , DOM: Dissolved Organic Matter , DOC: Dissolved Organic Carbon which comprises (humic acid, fulvic acid, and humin) and non-humic material , POC: Particulate Organic Carbon , DON: Dissolved Organic Nitrogen , DOP: Dissolved Organic Phosphorus .

**Figure I.4 :** Hypothetical and Theoretical structure of the humic acid according to Stevenson, (1982) cited in (Aiken, 1985)

**Figure I.5 :** Hypothetical and Theoretical fulvic acid proposed in (Aiken, 1985)

**Figure I.6:** Schematic figure to make clear the relationship and the overlap between the different fractions of organic matter . Figure has been taken from (P. Coble, Lead, Baker, Reynolds, & Spencer, 2014). DOM: dissolved organic matter , CDOM : chromophoric dissolved organic matter , FDOM : fluorescent dissolved organic matter

**Figure I.7 :** A typical Jablonski diagram of singlet electron energy states which shows an increase in the energy level by going from down to the upside. The ground state is indicated by  $S_0$  the first excited singlet electronic state by  $S_1$

**Figure I.8 :** The localization of the components of fluorescent organic matter , and regions in the fluorescence map in addition to the first and second order of Rayleigh and Raman scattering. Source: Ferretto, N. (2014)

**Figure I.9 :** figure showing the first and second Rayleigh and Raman scattering and fluorescence

Image adapted from : [\(Larsson et al. 2007\)](#)

**Figure I.10:** Example of combining EEMs into a three-dimensional cube of data ( $x_{ijk}$  in Eq. 1) adapted from (Stedmon & Bro, 2008)

**Figure I.11:** Flowchart showing the logical steps necessary for the PARAFAC analysis of the excitation emission matrices of the fluorescence datasets Source : (Stedmon & Bro, 2008)

**Figure I.12 :** A cube of the excitation emission matrices EEMs dataset which is decomposed to parallel five distinct CP/PARAFAC components Source of the image : (Murphy, Stedmon, Graeber, & Bro, 2013)

**Figure I.13:** The incoming solar radiation (insolation) received in various latitudes during an equinox date

**Figure I.14:** The variation of the average daily insolation ( $\text{W/m}^2$ ) with latitude and with time of the year

**Figure I.15 :** Solar irradiance spectrum which shows the solar irradiance in  $\text{Watt/m}^2/\text{nm}$  as a function of the electromagnetic wavelength. It represents the received solar irradiance at the atmosphere and at the surface of the earth.

**Figure I.16 :** Solar radiation map of France

**Figure II.1:** Water catchment of the Gapeau River and the principal sources of the water catchment of the Gapeau river. Gapeau river is situated in the (Southeastern France , Département du Var, Région PACA). Map source : [\(Ollier 1972\)](#)


**Figure II.2 :** The Mean monthly Flow ( $\text{m}^3/\text{s}$ ) of the Gapeau river measured for 56 years from 1961 to 2016 at the hydrological station Y4624010 - le Gapeau à Hyères [Sainte-Eulalie] for a catchment area of  $517 \text{ km}^2$  and at 9 m of altitude, and this station is located after the confluence of the Gapeau river with the Real Martin river

**Figure II.3 :** Wastewater treatment plants found in the watershed of the Gapeau River . this figure shows thirteen wastewater treatment plants.

Source : report from Syndicat Mixte du Bassin Versant du Gapeau

**Figure II.4 :** Bird's eye view picture by satellite of the wastewater treatment plant for the La Crau commune and for la communauté de communes de la vallée du Gapeau. This Satellite pictures shows the treatment tanks and the administrative building of the wastewater treatment plant. This WWTP outputs its effluent directly in the Gapeau river which is obscured by the trees on its path.

**Figure II.5:** Google map showing the three islands which surround the coastal zone of the city of Hyeres. Port-Cros , Le levant , Porquerolles, Presqu'île de Giens

**Figure II.6:** Map showing approximate locations of the study area and the sampling sites of the three endmember mixing components from upward to downward , the Gapeau river , the wastewater treatment plant of the city of la Crau and the Sea water at the city of hyeres ( Rade d'Hyeres) . (  ) shows where samples were collected . Map made by using Google Maps™ a web mapping service.

**Figure II.7:** Pictures of the sampling of the three endmember for the solar irradiation experiments . Pictures shows also the bottle used in the sampling campaigns

**Figure II.8:** Image showing the installation of the wooden plank on the roof of the MIO laboratory (Ex-Protee) ( $43^\circ 08' 11.2'' \text{ N } 6^\circ 01' 16.7'' \text{ E}$ ).

**Figure II.9:** Ternary diagram of the mixing percentages of three endmember mixing components (freshwater (RW), wastewater treatment plant (WW), seawater (SW)). Each intersecting point represents a solution that contains the mentioned and calculated percentages of each water source

(endmember).

**Figure II.10:** Picture showing the quartz tube put upside down in a wooden plank on the roof of the laboratory MIO (ex-PROTEE) at the Universite de Toulon ; for solar irradiation for different periods of time .

**Figure II.11 :** Image showing the coloration of the actinometer solution (Potassium Ferrioxalate) which occurred very fast in the same day of the installation of the irradiation experiment

**Figure II.12:** The solar panel in the right and the data logger inside the small box, in the picture in the left , a birds' eye view of the solar panel and the USB data logger .

**Figure II.13:** Correlations between insolation data of Meteo-France and insolation from our solar cell physical actinometer . Blue points and line : correlation between nice and La Garde. Orange points and dotted line : correlation between insolation of Marignane and La Garde.

**Figure II.14 :** Pictures showing the quartz cuvettes, the “tourelle” and the F-4500 spectrofluorometer. The arrows shows the sequence of measurement.

**Figure II.15:** The fluorescence landscape with the square inside showing the region of focus for the method of data acquisition named “Elnahhal” ( $\lambda_{EX}=200-400$  nm), ( $\lambda_{EM}=220-420$  nm) in green. The whole square shows the region of focus for the data acquisition named “Croatie” ( $\lambda_{EX}=200-600$  nm), ( $\lambda_{EM}=200-800$  nm) the whole picture. Vertical axis represents excitation wavelengths  $\lambda_{EX}$  and horizontal axis represents emission wavelengths  $\lambda_{EM}$

**Figure II.16 :** The sunlight irradiation experiments protocol for all the experiments, in addition that another method of fluorescence data acquisition is used which is croatie which has a broader windows on both the excitation and the emission wavelengths.

**Figure II.17 :** Figure showing the first CP/PARAFAC component C1 contribution in the mixtures samples for day zero (Normalized and non-normalized contributions) as an example from the irradiation experiment I000

**Figure II.18 :** Figure showing the first CP/PARAFAC component C1 contribution in the mixtures samples for day zero (Normalized and non-normalized contributions) as an example from the irradiation experiment I000 with the Contribution of C1 Normalized put onto the secondary axis.


**Figure II.19:** Map showing the sampling sites for the geographical field experiment along the pathway of the river Gapeau tills its river mouth at the city of Hyeres. The map shows also the relative site of the sampling sites with respect to France. Sampling sites were at the southeastern part of France in Region PACA

**Figure II.20 :** Figure showing the pictures of the sampling campaign for the geographical field experiment .

**Figure II.21:** Picture of the autosampler used for sampling . It has the capacity of 24 plastic bottles of 1L. It was programmed to take one sample every two hour to cover a range of 24 bottles which

corresponds to 48 hours sampling campaign.

**Figure II.22** : Photos of the temporal variation field experiments of the waters of the Gapeau river and wastewater treatment plant of La Crau city and the confluence of the Gapeau river and its tributary Le Real Martin, and the seawater at the city of Hyeres .

**Figure III.1** : Map showing approximate locations of sampling sites of three endmember from upward to downward , Gapeau river, wastewater treatment plant of la Crau city and Sea water at Hyères city (Rade d'Hyères) .(  ) shows where samples were collected. Map made by using Google Maps

**Figure III.2.** Contour plots of CP/PARAFAC components identified from the decomposition of all EEM datasets. Spectral loadings of excitation and emission wavelengths of the three identified CP/PARAFAC in the present study. Excitation loading for CP/PARAC component are solid lines whereas emission loadings are shown in dotted lines.

**Figure IV.1** : Figures showing photos of the sampling campaigns for the temporal field experiment of the four water sources on the gapeau river (a): Gapeau River, (b): WWTP of La Crau City,(c ): Confluence (Gapeau-Le Réal Martin), (d): Sea (L'Aiguade at Hyeres city).

**Figure IV.2** : Diurnal (48 h cycle) variation of the conductivity values in  $\mu\text{S}/\text{cm}$  of the four water sources (endmembers) sampled for the temporal field experiment

**Figure IV.3** : Diurnal (48 h cycle) variation of pH values of the four water sources (endmembers) sampled for the temporal field experiment

**Figure IV.4** : CP/PARAFAC results by the PROGMEEF software showing the loading for the two parafac components and the concordia results (72.82% for two components)

**Figure IV.5.** Contour plots of CP/PARAFAC components identified from the decomposition of all EEM datasets of the Temporal field experiments of the Gapeau river , Confluence (Gapeau river, Le Réal Martin), wastewater treatment plant of La Crau city, Sea water at Hyères city. Spectral loadings of excitation and emission wavelengths of the two identified CP/PARAFAC in the temporal field experiment are also shown. Excitation loading for CP/PARAFAC component are solid lines whereas emission loadings are shown in dotted lines.

**Figure IV.6** : Four figures of the normalized contribution of CP/PARAFAC components C1 and C2 for the temporal field experiment of the Gapeau River . Figures on the left hand side shows the variations of C1 and C2 for the nonfiltered Gapeau Samples whereas the right hand side shows the variations of C1 and C2 for the filtered Gapeau Samples. Units of Fluorescence contributions of C1 and C2 are arbitrary units

**Figure IV.7** : Four figures of the normalized contribution of CP/PARAFAC components C1 and C2 for the temporal field experiment of the wastewater treatment plant WWTP of La Crau city . Figures on the left hand side shows the variations of C1 and C2 for the nonfiltered Gapeau Samples whereas the right hand side shows the variations of C1 and C2 for the filtered Gapeau Samples. Units of Fluorescence contributions of C1 and C2 are arbitrary units

**Figure IV.8** : Four figures of the normalized contribution of CP/PARAFAC components C1 and C2 for the temporal field experiment of the Confluence of Gapeau River and Le Real Martin tributary . Figures on the left hand side shows the variations of C1 and C2 for the nonfiltered Gapeau Samples whereas the right hand side shows the variations of C1 and C2 for the filtered Gapeau Samples. Units of Fluorescence contributions of C1 and C2 are arbitrary units

**Figure IV.9** : Four figures of the normalized contribution of CP/PARAFAC components C1 and C2 for the temporal field experiment of the sea water samples at St.Louis, Hyeres city . Figures on the left hand side shows the variations of C1 and C2 for the nonfiltered Gapeau Samples whereas the right hand side shows the variations of C1 and C2 for the filtered Gapeau Samples. Units of Fluorescence contributions of C1 and C2 are arbitrary units

**Figure IV.10** : Some photos of the geographical field experiment during the two sampling campaigns of 19-august-2016 and 22-august-2016. In addition, the left hand corner pictures shows the downstream of the anti-salt dam(barrage) on the Gapeau river estuary. Moreover, photos shows also the sampling rod “stick” used.

**Figure IV.11** : Figure showing the variation of the pH with distance in kilometers for the first (19-august-2016) and the second (22-august-2016) geographical field sampling experiment

**Figure IV.12** : Figure showing the variation of the electrical conductivity EC  $\mu\text{S}/\text{cm}$  with distance in kilometers for the first (19-august-2016) and the second (22-august-2016) geographical field sampling experiment

**Figure IV.13** : Figure showing the variation of the temperature  $^{\circ}\text{C}$  with distance in kilometers for the first (19-august-2016) and the second (22-august-2016) geographical field sampling experiment

**Figure IV.14** : Progmeef results windows showing the concordia graph on the lower right hand corner and the value of the concordia test for two CP/PARAFAC components is shown above this graph (99.75%). Loadings of the two CP/PARAFAC components are also shown.

**Figure IV.15**. Contour plots of CP/PARAFAC components identified from the decomposition of all EEM datasets of the Spatial (geographical) field experiments. Spectral loadings of excitation and emission wavelengths of the two identified CP/PARAFAC in the spatial “geographical” field experiment are also shown. Excitation loading for CP/PARAC component are solid lines whereas emission loadings are shown in dotted lines.

**Figure IV.16** : Figure showing graphs of the geographical variation of the contribution of CP/PARAFAC component C1 with distance in kilometers along the pathway of Gapeau river till the sea at l’ayguade at Hyeres city. The geographical field experiment of 19-august-2016 doesn’t have a filtration dataset.

**Figure IV.17** : Figure showing graphs of the geographical variation of the contribution of CP/PARAFAC component C2 with distance in kilometers along the pathway of Gapeau river till the sea at l'ayguade at Hyeres city. The geographical field experiment of 19-august-2016 doesn't have a filtration dataset.

**Figure IV.18** : Figure showing graphs of the geographical variation of the ratio of CP/PARAFAC component C1/C2 with distance in kilometers along the pathway of Gapeau river till the sea at l'ayguade at Hyeres city. The geographical field experiment of 19-august-2016 doesn't have a filtration dataset

**Figure V.1** : figure showing histogram of the irradiation in volts for each month of the year

**Figure V.2** : figure showing the variation of the content fraction or discharges of the wastewater treatment plant WWTP , seawater SW and river water RW as a function of month of the year

**Figure V.3** : figure showing the variation of the contribution of CP/PARAFAC C1 and C2 as a function of month of the year for two irradiation experiments I000 and I111 for the first case of mixing (mixing of only river water and wastewater treatment plant) . These variation are produced from the multilinear regression model.

**Figure V.4** : figure showing the variation of the contribution of CP/PARAFAC C1 and C2 as a function of month of the year for two irradiation experiments I000 and I111 for the second case of mixing (mixing of river water and wastewater treatment plant and sea water ). These variation are produced from the multilinear regression model.

**Figure V.5** : figure showing the ratio between C1 and C2 which is  $C1/C2$  for two cases of irradiation ( with irradiation= $C1/C2+UV$ ; without irradiation= $C1/C2-UV$ ) as a function of month of the year. The ratio varies from zero and one.

**Figure V.6** : Figure showing the variation with distance of the normalized C1 contribution for the irradiation experiment I111 based upon the multilinear regression model. Blue curve shows the variation of normalized C1 in the month of august in the summer whereas the red curve shows the variation of normalized C1 in the month of december

**Figure V.7** : Figure showing the variation with distance of the normalized C1 contribution for the irradiation experiment I000 based upon the multilinear regression model. Blue curve shows the variation of normalized C1 in the month of august in the summer whereas the red curve shows the variation of normalized C1 in the month of december

## List of Tables

**Table I.1:** The designated Peaks in letters by (P. G. Coble, 1996) study and the exact position of their fluorescence maxima in the fluorescence map . Their names in letters because their chemical composition was not known at the time of this study (P. G. Coble, 1996).

**Table I.2.** Studies which studied photodegradation of DOM coupled with EEM technique

**Table II.1 :** All of solar irradiation experiments and their corresponding dates and state of filtration of Endmembers.

**Table II.2:** Types of irradiation experiments according to which endmember was filtered . Bold means that the irradiation experiment was conducted in the present works of this PhD thesis where non bold means the experiment was not conducted

**Table II.3** The percentages in solution of each endmember mixing components of the fifteen samples used in this study

**Table II.4** The percentages in solution of each endmember mixing components of the fifteen samples used in this study taken by weight in mg

**Table II.5 :** Dates of irradiation experiments.

**Table II.6 :** table showing the absorbance values of the solution for the measurement of the iron ions  $Fe^{2+}$  in the irradiated potassium ferrioxalate solution using colorimetric method of the O-Phenanthroline at 510 nm ([Bowman and Demas 1976](#))

**Table II.7 :** Table showing whether or not a solar irradiation experiment had a control group. In addition to the mode of measurements

**Table II.8 :** Table showing the number of the EEM text files in each dataset of Elnahhal and Croatie for all the irradiation experiments and the temporal field experiment and the geographical field experiment. In addition their CP/PARAFAC analysis and modelling

**Table II.9 :** Dates and day of the week of the three sampling campaigns of the geographical field campaigns

**Table II.10:** Coordinates of the sampled sites during the river path of the river Gapeau in the city of Hyeres ( southeastern of France , PACA region).

**Table II.11 :** The sampling dates and time of 1st and last sample of the temporal sampling campaigns for the Gapeau river (RW), the waste water treatment plant of La Crau (WW), the confluence (Gapeau-Réal Martin) and the seawater (SW) at L'Ayguade-Hyeres.

**Table III.1-**Content fraction of each endmember mixing components of fifteen samples used in this study

**Table III.2-**Solar Irradiation Experiment dates and types.

**Table III.3-**Descriptions of CP/PARAFAC components and comparison with literature

**Table III.4-**Multilinear regression parameters of CP/PARAFAC components found in the present study

**Table III.5-**Kinetic order of coefficients of multilinear regression for each CP/PARAFAC . "NA" means that correlation coefficient for 2<sup>nd</sup> order rate was less than 0.75, and was dismissed.

**Table III.6-**Kinetic constant for coefficients of multilinear regression for each CP/PARAFAC component. Values in parenthesis are relative standard deviation for kinetic constant

**Table III.7-**Relative standard deviation RSD for multilinear regression parameters for CP/PARAFAC components for control samples of irradiation experiments

**Table IV.1 :** The exact sampling dates of both the Temporal and Spatial"Geographical" field



experiments of the endmembers (WW, RW, Confluence and SW). S : Spatial ; T : Temporal.

**Table IV.2** : Weather conditions for the temporal field experiments of the four sampling sites.

**Table IV.3** : Rain event occurred for the temporal field experiments of the sea water at St.louis -Hyeres city . For the non-mentioned hours , there was no rain event with 0 mm precipitation.

**Table IV.4**-Descriptions of CP/PARAFAC components and comparison with literature

**Table IV.5** : Mean and standard deviation of pH, EC , C1, C2 for the four water sources “endmembers” for the temporal field experiment . C1 and C2 units are arbitrary units

**Table IV.6** : Weather conditions for the temporal field experiments of the four sampling sites.

**Table IV.7**-Descriptions of CP/PARAFAC components and comparison with literature

**Table V.1**-Multilinear regression parameters of each CP/PARAFAC components at time zero with their corresponding coefficients of correlation found in the present study from the Elnahhal method of data acquisition

**Table V.2**-Kinetic constant for coefficients of multilinear regression for each CP/PARAFAC component from the Elnahhal method of EEM data acquisition .

**Table V.3** : irradiation in volts used the modelling

**Table V.4** : Discharges of the Seawater SW , River water RW , wastewater treatment plant WWTP , units are  $\text{m}^3/\text{s}$  .

**Table V.5** : table showing the exact percentage or content fractions of Seawater SW , River water RW , wastewater treatment plant effluent for the first case of mixing mentioned above in the text of this chapter 5 which were used in the application of the multilinear regression model.

**Table V.6**: figure showing the mixing percentages or content fraction of the seawater fSW and river water fRW using in the application of the multilinear regression model for the second case of mixing mentioned above in the text of this chapter (chapter V)

**Table V.7** : table showing the factor multiplied by the distance to take into account the increase of discharge of the river a function of distance in km

**Table V.8** : Table showing the exact discharge values in  $\text{m}^3/\text{s}$  used in the application of the multilinear regression model , irradiation is in volts

**Table V.9** ; Table showing the content fractions fSW and fRW based on values from table V.x . These content fraction were used in the application of the multilinear regression model for the modelling of the geographical field of the Gapeau river.

## **List of Annexes**

**ANNEX I :**  $f_{RW}$  and  $f_{SW}$  Permutation

**ANNEX II :**  $f_{WW}$  and  $f_{SW}$  Permutation

**ANNEX III :**  $f_{RW}$  and  $f_{WW}$  Permutation

**ANNEX IV :** EGU poster

**ANNEX V**

**ANNEX VI :** Kinetic constants

---

# Introduction

---

The carbon element constitute one of the most important geochemical cycles on a planetary level. Among the different carbon reservoirs or compartments of the planet earth , the carbon element is present and exists in mineral forms mainly in the rocks and the sediments in carbonate form. The carbon element is recycled between the different planetary reservoirs through the hydrosphere. The gaseous forms of carbon are of great importance due to its role in the global warming and climate change. Biomass is an important reservoirs or compartment of carbon which is the intermediary between the gaseous and mineral forms of carbon. The only way that carbon could change from the oxidized forms ( $\text{CO}_2, \text{CO}_3^{2-}$ ) for the reduced forms is through the process of photosynthesis to become what is called organic matter. Therefore , to follow and track the organic matter in the environment and its formation processes and the processes of its transport and degradation is of immense importance for the purpose of understanding the fragile process which governs the carbon cycle

Among the important zones, where so many transformations phenomena is produced, are the coastal zones which are subjected to the greatest anthropogenic pressures. The coastal zone represents the place where the rivers rejects or outputs their inputs which are coming from their water catchments or watersheds and in so doing , they inputs the organic matter which was previously produced on the terrestrial biosphere and in the soils of their water catchments. In addition to this natural organic matter , generally organic substances barely degraded (biopolymers) and the more evolved substances (geopolymers and the humic substances) , the organic matter produced by the human activity is also added to the riverine inputs in the coastal zone. This anthropogenic organic matter is still produced increasingly and regularly since some centuries ago. The population growth in the coastal zones is growing exponentially and about 80% of the human population reside at the sea coast. This anthropogenic pressure changes the nature of the matter transported by the rivers but to what degree?! , it is still unclear .

The urban discharges , mainly from the wastewater treatment plants discharges, is one of the impact of human activity on the coastal zones; in addition to the the agriculture and the industrial pollution. In fact , all the urban discharges and the agricultural and industrial discharges come in the end to the sea and the coastal zone and in particular , the organic discharges. In Europe and in particular , in France , these organic discharges are regulated however , they are regulated only for some parameters such as : biological oxygen demand BOD , chemical oxygen demand COD , color , odor , microbial content , etc... Some other parameters are not regulated such as the metal contents or the organic pollutants such as the Polycyclic Aromatic Hydrocarbons PAHs , pharmaceutical products or phytosanitary products.

In practice , the coastal zone receives a great quantity of organic matter which gets degraded either by the biodegradation pathway or by the photochemically-induced degradation pathway or it gets flocculated and rejoin the sediments where it becomes mineralized by the

microorganisms. Through the pathways of degradation and mineralization, the organic matter provides food and nutrients for the biomass which use this transformed organic matter to proliferate in the marine medium or milieu or it gets flocculated in the oceanic seafloor.

In order to study the cycle of the organic matter and hence partially part of the carbon cycle, the UV-Visible spectroscopy is the preferred tool and the instrument of predilection. In fact, part of the organic matter possess properties which enables the interaction with electromagnetic waves of the UV-Visible domain. Hence, these properties are used in the satellite images for estimated the quantity of the organic matter and therefore, the carbon which is present in the oceans and particularly, the coastal zones. It is therefore important to know well the properties of the marine and coastal organic matter. In fact, there is a difference of properties between the coastal zone and the open sea/ocean zone, in particular due to the photodegradation and the inputs by the rivers. It is possible to follow and track the plumes of the organic matter through the measurements of its optical properties.

Part of the organic matter fluoresces and provokes interferences and overlaps in the relations which could be thought to be linear between the properties of absorbance and the concentration of the organic matter in the aquatic media. In particular in the coastal zones which have properties of fluorescence very different from the oceanic organic matter. It is also important to study the fluorescence of the organic matter discharged by the riverine inputs in the coastal zone.

Among the questions which we are justified in asking, is the question about the origin of the fluorescent organic matter which concerns the works of the present PhD thesis. In fact, which part of the fluorescent natural organic matter in measured fluorescence in the coastal zone is subjected to an important anthropogenic impact?. And also, is the behavior different between the anthropogenically-impacted organic matter and the natural organic matter in terms and in regard the photodegradation?. The fluorescence which is observed in the coastal zone and media, comes from which organic matter, the marine organic matter, or the terrestrial organic matter or the anthropogenic organic matter?

We conducted these works of the present PhD thesis in order to try to answer these questions through the trial of developing a simple model of evolution of the fluorescent organic matter in the anthropogenically-impacted coastal zone or milieu.

This manuscript is organized in the following manner :

**The first chapter** presents a general introduction and a theoretical frameworks for the works conducted in the present PhD thesis and provides the reader with a literature review in addition to the problem of the research and its environmental context and the main goal and purposes of the present PhD thesis

**The second chapter** presents the aspects of the study area from general informations to the specific information of the sampling locations in addition to most of the methods used for the data acquisition of the excitation emission matrices and the irradiation experiments conducted in this PhD thesis. Moreover, it explains the methods used and the apparatuses used for the Geographical field experiment in addition to the sampling of the temporal field experiment .

**The third chapter** presents the scientific article sent to the journal of Water Research for publication and it had the state of “under review” . It also presents the results of the irradiation experiments of the three endmember mixing components and their correspondent kinetic order .

**The fourth chapter** presents the results of both the geographical field sampling experiment of the river Gapeau and the results of the temporal field experiment of the Gapeau river , Wastewater treatment plant of La Crau city , the Confluence of Gapeau - Le Real Martin and the seawater at l'ayguade at the Hyeres city

**The fifth chapter** presents the results of the modelling of the results of the geographical field experiment and the temporal field experiment based on the multilinear regression model developed in the third chapter of the present PhD thesis.

---

# **Chapter 1 - State of the Art Literature Review**

---

## **Impact of anthropogenic organic matter on the fluorescence in coastal zone**

---

## **I.1 The coastal Zone :**

Coastal zone has been a source of attraction for humans due to rich resources for logistical reasons (e.g. access points to marine trade and transport, recreational/cultural activities, fishing activities) and due to its special sense of place being the interface between land and sea. This suggests the importance of the coastal zone. There is an increasing development and utilisation of coastal zone in the recent decades which led to the tremendous changes of the coastal zone at socio-economic and environmental levels, a trend being expected to be the same if not increasing in the near future.

First of all , the coast is intuitively understood to be where land and ocean meet. The constant movement of this line of meeting between land and ocean, makes it difficult to simply clearly drawing this on a map . This constant movement is due to the naturally occurring processes of geomorphism making the coast a region of interaction between land and sea. Some examples of the constituents of this region of interaction could be beaches, salt marshes, mangroves and coral reefs. These examples are connected and very close to the coast; however , there are also distant part from the coast which are part of the region of interaction between land and sea and plays an important role in the process of morphodynamics of the coast. These are river systems which takes part in sediment transport and bringing the fresh water to the coastal environment. Hence, the inland limit to the coast is the boundaries of the watersheds of river systems which could be thousands of kilometers inland.

The coastal zone of our planet Earth is constituted of amazing areas. It is of vital importance to almost all forms of life be it terrestrial (human species :homo sapiens and other animals) or aquatic life forms and is also a unique domain geologically, ecologically and biologically (Beatley, Brower, & Schwab, 2002). The Coastal zone is very dynamic and fragile zone which is also considered to be the interaction zone between man and nature (Peña-Cortés et al., 2013). The coastal zone comprises all the coastal regions which are the regions that are near the shore of waterbody like the sea of the ocean. They are fragile ecosystems which are very sensitive and vulnerable to natural and anthropogenic pressures that are the contributors to the deterioration of this regions near the shore and this is what has been recognized by the european Dobris assessment (Gouldson & Gouldson, 1996). If one would like to draw and precisely determine the boundary between the land and the ocean , this seems to be an



impossible task because there is no clearly defined line on the map. The coastal zone which is a gradual transitional zone between the terrestrial and the aquatic (marine/oceanic) zones of the earth, has so many definitions (scientific and cultural). Many of these definitions lack well-defined physical precise boundaries either landward or seaward and therefore are confusing and vague. In spite of the fact that the term “coastal zone” is generally understood. The coastline or the seashore can be defined as the boundary line between the lands and the ocean or the sea. Whereas, the term coastal zone designates the region where interaction of the sea and land processes takes place. The US Commission on Marine Science, Engineering and Resources, 1969 has defined the term “coastal zone” as “the part of the land affected by its proximity to the sea, and that part of the sea affected by its proximity to the land as the extent to which man's land-based activities have a measurable influence on water chemistry and marine ecology.” This definition of US commission on Marine Science, Engineering and Resources was chosen by us as the working definition of the studied area in the works of the present thesis because it perfectly applies to and fits the coastal area of the mediterranean part of France.

Some of the reasons of importance of the coastal zone is that vital ecosystems such as mangrove forests, estuarine ecosystems, coral reefs, seagrass beds among many other ecosystems are found. These ecosystems are important for the conservation of biodiversity and they provide a shielding service to the coastal zone by protecting it from the offshore waves and from harsh weather conditions. In addition, multiple products and services from various resources are produced and/or supported in the coastal zone. As a result of this, rapid population growth can be seen in the coastal areas (Masalu, 2008). It is estimated that 60% of world's population lived within 100 km of a coastline (Clayton, 1992; Hinrichsen, 2016; Laird, 1991). The coastal zone is of great importance because majority of the global population inhabit these zones and they are subjected to a process of a demographic concentration ([de Andrés et al. 2018](#); [Masalu 2008](#); [Small and Nicholls, 2003](#)). There is a higher population density in the coastal zone compared to that in non-coastal zone (hinterland) and ongoing migration to the coastal zone which is associated with global demographic changes (Hugo, 2011). The growth of population and the rate of urbanization in the coastal zone has exceeded the demographic development of the hinterland (non-coastal zone) because of the rapid economic growth and higher rate of migration to the coastal zone (McGranahan, Balk, & Anderson, 2007; Smith, 2011) which emphasize the importance of the

coastal zone. Moreover, there is a distinctive pattern in the coastal zone of population structure and development which could be linked partially to the urbanization and population growth at a global level (Neumann, Vafeidis, Zimmermann, & Nicholls, 2015). The following map (Figure I.1) shows the geographical distribution of the global coastal population.

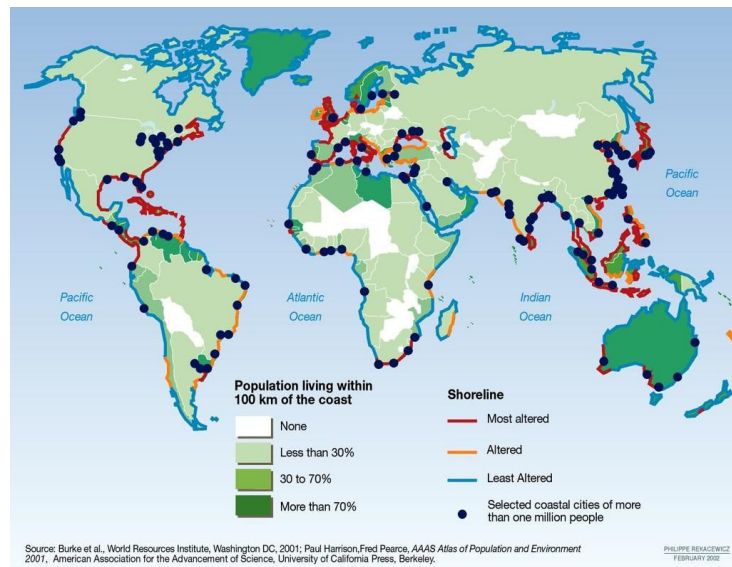


**Figure I.1:** Geographic distribution of the global coastal population and the shoreline development  
Image source : <http://www.thegeographeronline.net/crowded-coasts.html>

The human utilisation of the coastal zone could be traced to hundreds of years ago when the humans started the exploitation of the natural resources through fishing and pasturing (Kim, 2016). High pressure by the human activity is generated on the coastal ecosystems and coastal natural resources through the increased rates of pollution and utilisation of these resources by the increasingly growing population and urban development in the coastal zone (Crossland et al., 2005). The Coastal population growth subject the coastal land to increasing anthropogenic pressures and environmental degradation (Masalu, 2008). Some example of them could be high demands for housing and for food and agriculture which in turn changes the natural landscape. Agriculture has a negative impact on the biodiversity because it replaces so many diverse species with a single species crops. Urbanization also negatively impact the natural landscape by replacing the naturally occurring habitat by the cities and structural buildings which deteriorates the natural landscape and the coastal water quality through the added risks of sewage inputs (treated , partially treated). In addition, urbanization

increases the risks of dumping high loads of sludge of wastewater treatment plants into the coastal zone which in turn increases the burden of anthropogenic organic matter which causes many environmental problems (e.g. eutrophication among many others). Industrial activity has severe negative impacts also on the coastal zone. According to the impact of these anthropogenic activities in the coastal zone, there are lots of scientific studies and works regarding the coastal water quality and the sediments in the coastal area .

Being the interface between the continental/terrestrial crusts and the marine/oceanic crust; the coastal zone plays a major part in the biogeochemical cycling of the elements especially the carbon cycle.

## **I.2 Carbon Cycle**

The carbon cycle is considered, by biogeochemical scientific community, to be at the heart and of central importance in the scientific field of biogeochemistry (Schlesinger & Bernhardt, 2013). The global carbon cycle is the biogeochemical cycle of the element of carbon which can be defined by the transformation and speciation of carbon from one form to another and its exchanges among four major reservoirs and spheres of the planet earth (e.g biosphere, pedosphere, geosphere, hydrosphere, and atmosphere) (Wigley & Schimel, 2005). All living things mainly consist of carbon. The carbon cycle as the name cycle reflects is a sequence of events that enables the Earth to sustain life and this cycle describe the movement of the atmospheric carbon to the biosphere through photosynthesis by the autotrophs (e.g. plants and cyanobacteria) which is the only pathway for carbon to enter the organic carbon reservoirs and how it returns back to the atmosphere through the pathway of metabolic respiration of the animals (herbivores, carnivores and omnivores) and by plants (respiration during night) and the combustion of fossil fuels. Also the entering of atmospheric carbon to the hydrosphere and the aquatic biosphere by the dissolving of carbon dioxide into the ocean to form carbonates then this carbonates can be used to form calcium carbonates by the sea shells .

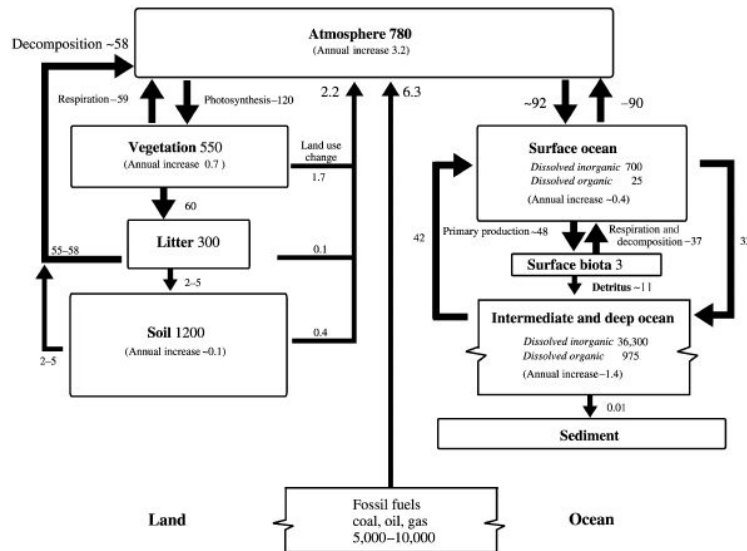


**Figure I.2 :** The contemporary global carbon cycle through the major reservoirs of planet Earth. Units are Pg C or Pg C yr<sup>-1</sup>  
Figure source : (Houghton, 2003)

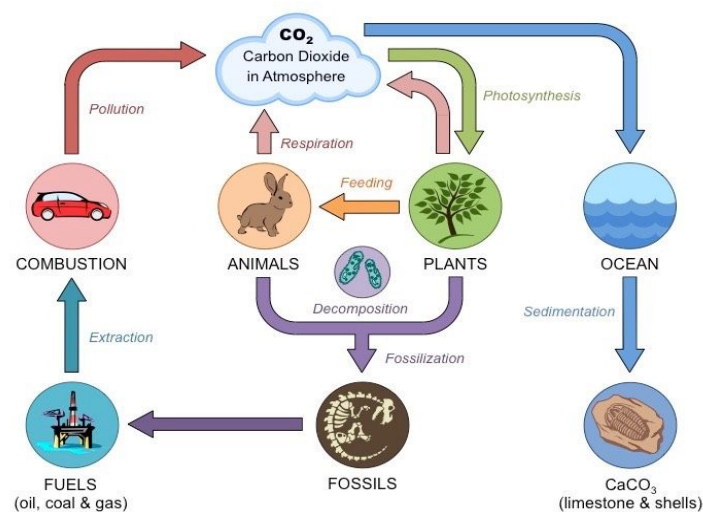


**Figure I.3 :** The carbon cycle in nature  
Image source : <http://ib.bioninja.com.au/standard-level/topic-4-ecology/43-carbon-cycling/carbon-cycle.html>

The dead plants and dead animals, that are buried, are decomposed by the decomposers and then becomes fossils by the process of fossilization. The fossils could be viewed as a frozen form of carbon which returns to the atmosphere by the anthropogenic activities (e.g.: extracting petrol, coal mining) and using it as an energy source by the combustion of this fuel, this form of carbon returns to the atmosphere in the form of carbon dioxide. In addition,

all of the combustion reactions and the metabolic respiration can be viewed as the opposite of the photosynthesis process since it is the reverse chemical reaction. In addition, carbon can enter the hydrosphere and be sedimented by the sedimentation processes and form the rocks as the limestones and be part of the rock's cycle.

Part of the carbon cycle poorly understood in the coastal zone is the dissolved organic matter which plays a major role in the carbon cycle.

### **I.3 Biogeochemical and ecological importance of the dissolved organic matter in the coastal zone**

The dissolved organic matter DOM plays a major role in the carbon cycle in the coastal zone. There are many sources of the dissolved organic matter (DOM) in the coastal zone, autochthonous sources and allochthonous sources. The autochthonous sources of DOM are the sources from which the DOM is produced in situ in the marine environments, some of these sources maybe the excretion and the exsudation from the primary producers (phytoplankton, macrophytes) in brief is the DOM produced by the autochthonous primary production. Whereas allochthonous sources of dissolved organic matter could be from vascular plant origin which is dissolved organic matter that is produced in different source land such forests.

### **I.4 Organic matter**

Organic matter, as the term may suggest, is the material which is found in the organs of living bodies which was previously the case in the vitalism point of view and the cadavers and remains of them, in short could be said to be the dead stuff of any kind. In addition, the term organic means that the material which is organic is by necessity contains carbon and hydrogen as the basic building blocks and on top of that it means also that this organic material is by necessity of biological origin (P. G. Coble, 2007). The term organic matter is the general term used to designate the whole pool of materials which includes thousands or thousands of thousands of organic compounds and when no specific chemical compound name or a specific chemical compound category can be assigned to a given sample when the sample composition is not characterized sufficiently (P. G. Coble, 2007) . In addition, (Filella, 2008) defined the natural organic matter (NOM) as the organic matter that is found in natural aquatic ecosystems like freshwater sources (e.g. rivers) or in an engineered aquatic ecosystems which is every matter except the living organisms and the anthropogenic

compounds (e.g Polycyclic aromatic hydrocarbons (PAH) among many others). Moreover, this natural organic matter is a pool of many unidentified organic compounds.

Organic matter has different properties both physical and chemical according to its origin and source, for examples the organic matter found in the river waters of a forested watershed is different from the organic matter found in the rivers whose water catchment is urbanized and from organic matter found in the river waters whose water catchment is used for agricultural purposes. The organic matter from a forested water catchment is considered to be of natural origin and pristine sources whereas the organic matter found in the river waters from urbanized or industrialized and agricultural water catchment is said to be of anthropogenic (or anthropogenically impacted) origin or sources because this organic matter has a signature of the human activity on it. In the literature (Filella, 2008), there is no method which enables the quantification of the organic matter according to its source and origin (natural , anthropogenic), rather the measurement of bulk parameters (e.g. DOC) give insightful information about the sources of the organic matter in a specific ecosystem. In addition to that there exist in the literature many studies of the molecular biomarker for each source and origin and environmental settings of the organic matter so that the source of the organic matter can be traced back to its original source. Furthermore, organic matter consists of many fractions which have varying operational definitions and represents groups of molecules that have similar physical and chemical properties. These fractions are shown and summarized in the following schematic diagram (Figure I.3). The acronyms of the fractions of the organic matter are shown in the caption of this diagram.

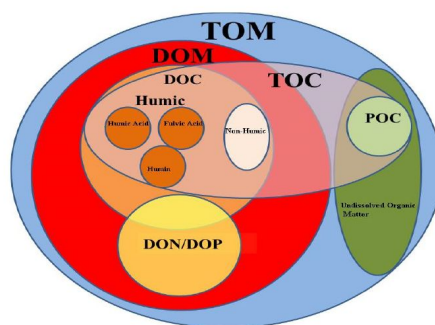


**Figure I.3:** The relationship between various Natural organic matter fractions which is represented as acronyms . TOM: Total Organic Matter , TOC: Total Organic Carbon , DOM: Dissolved Organic Matter , DOC: Dissolved Organic Carbon which comprises (humic acid, fulvic acid, and humin) and non-humic material , POC: Particulate Organic Carbon , DON: Dissolved Organic Nitrogen , DOP: Dissolved Organic Phosphorus . Figure taken from : (Pagano, Bida, & Kenny, 2014)

### I.4.1 Complexity of the organic matter

Due to the heterogeneity of sources of the organic matter in natural water, about 80 % of the organic matter molecular structure is hard to identify. Some authors proposed hypothetical structure for the humic acid as shown in figure I.4 and for the fulvic acid as shown in figure I.5.

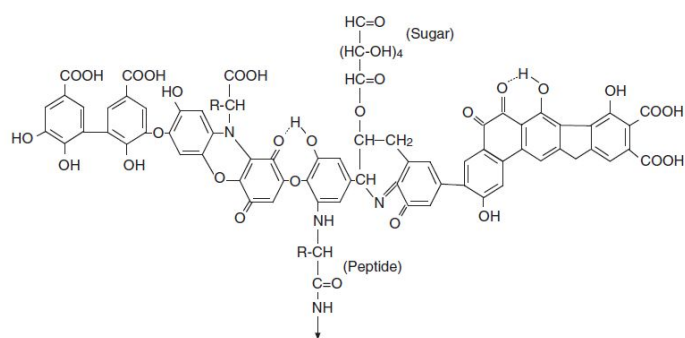


**Figure I.4** : Hypothetical and Theoretical structure of the humic acid according to Stevenson, (1982) cited in (Aiken, 1985)  
(Hudson, Baker, & Reynolds, 2007)

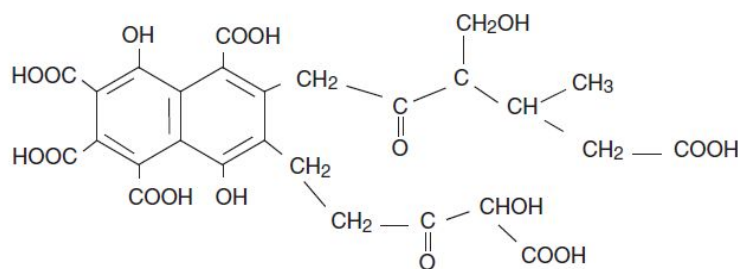


**Figure I.5** : Hypothetical and Theoretical fulvic acid proposed in (Aiken, 1985)  
(Hudson et al., 2007)

The main sources of humic and fulvic acids in the coastal environment is from riverine inputs which gets into river through the precipitation process after leaching from soils (P. Coble, Hu, Gould, Chang, & Wood, 2004; Nelson & Siegel, 2002) whereas cell autolysis of

phytoplankton is considered to be the autochthonous sources of humic and fulvic acids in the open ocean.

## **I.4.2 Dissolved organic matter (DOM)**

Dissolved organic matter (DOM) is considered to be an important reservoir of organic carbon which plays a major role in the cycling of organic carbon between the terrestrial biosphere and the oceanic biosphere (Alam, Jahangir Alam, Nagao, & Emran Quayum, 2015; Amon, 2004; Hansell, Carlson, Repeta, & Schlitzer, 2009; Romankevich, 1984; Williams & Druffel, 1988) and the exchangeability between various carbon reservoirs. In addition, it also plays several diverse roles ecologically and environmentally on a local and global scales (M. Chen & Jaffé, 2014). Dissolved organic matter is a ubiquitous component found in the natural ground and surface waters (Baker, Inverarity, Charlton, & Richmond, 2003; Boehme & Wells, 2006; Del Vecchio & Blough, 2002; Gardner, Bernard Gardner, Chen, & Berry, 2005; S. Li et al., 2016; Y. Wang, Zhang, Shen, Chen, & Feng, 2014; Whitehead & de Mora, 2004; Yan et al., 2017) and engineered waters (e.g. drinking water treatments, wastewater treatment plants, among many others) (Baghoth, Sharma, & Amy, 2011; W. Chen, Westerhoff, Leenheer, & Booksh, 2003; Stedmon, Markager, & Bro, 2003; M. Wang & Chen, 2018; L. Yang, Hur, & Zhuang, 2015; X. Yang, Meng, Huang, Sun, & Lin, 2014) and consists of a mixture of heterogeneous nature (Perminova et al., 2003) of aliphatic and aromatic compounds containing oxygen, nitrogen and sulfur functional groups (M. Chen & Jaffé, 2014; Wagner et al., 2015). The Dissolved organic matter (DOM) in aquatic environments is the organic matter that is operationally defined as the fraction that is separated by filters and passes a specific filter (0.1–0.7  $\mu\text{m}$ ) (Mostofa, Yoshioka, Mottaleb, & Vione, 2012); the permeate of that filter; while the particulate organic matter POM is the fraction that does not pass this filter (Mostofa, Yoshioka, et al., 2012) or the remaining part and it is mainly composed of phytoplankton cell, algae, plant debris, bacteria, among many other microorganisms (microfauna and microflora) (Gregorich, Beare, McKim, & Skjemstad, 2006). This POM is easily decomposed either by the photo-degradation pathway or the chemical and biological degradation pathways and therefore, it is considered as labile organic matter. DOM could be viewed as a biochemical buffer serving to keep stable the conditions for the aquatic organisms through the capacity to immobilize/mobilize heavy metals hence their bioavailable fraction and toxicity (Giacomin, Gillis, Bianchini, & Wood, 2013; Shi, Jin,



Hu, Fang, & Li, 2017). According to its origin, the place where it is produced, the DOM is classified into two or three categories. The first type of DOM is allochthonous DOM, as the term allochthonous means “of foreign land”, is of vascular plant origin produced in the soils of forested watersheds rivers and is typically referred to as terrestrially derived DOM in the literature and is constituted mainly by humic substances (Thurman, 1985). The main characteristics of this allochthonous DOM are high aromaticity, high molecular weight and low nitrogen content (Zhang, Liang, Wang, & Xu, 2015). The second category is often referred to in the literature as autochthonous DOM, as the term “autochthonous” literally means “ of the same land”, is the DOM which is produced in the same land of the aquatic environment which is the DOM produced by the microorganisms like bacteria and phytoplankton and algae and macrophytes naturally found in the ecosystem (Krupa, 2010); the main characteristics of this categories are low aromaticity, low molecular weight and high nitrogen content (Zhang et al., 2015). The third category is the dissolved organic matter of anthropogenic origin which is the organic substances synthetically produced by human activity like industry (e.g. Fluorescent whitening Agents FWA ([Holt et al. 1975](#); [Aman 2015](#); [Kramer 1992](#))) and agriculture (pesticides and herbicides) and from urbanization. In addition, DOM found in natural waters is a pool of organic compounds containing a vast range of organic compounds which have a molecular weight ranging from Low Molecular weight LMW DOM ( < 10 Da)(Hayase & Tsubota, 1985) to high molecular weight HMW DOM ( $\geq 300$  kDa) (Thurman, 1985; Hayase & Tsubota, 1985)

### **I.4.3 Chromophoric Dissolved Organic Matter CDOM**

Chromophoric and colored dissolved organic matter (CDOM), chromophoric literally means carrying a “ chromo”, a greek word for color; refers to the optical properties of CDOM. In addition, the term Chromophoric Dissolved organic matter is operationally defined as the optically active fraction of DOM which is the light-absorbing component of DOM and the fraction that can absorbs and reflect light at ultraviolet (UV) and visible wavelengths ([Grzybowski 2016](#); [Coble 2007](#)) . This CDOM is also known as gelbstoff which is the term preferred by Paula Coble, a big player in the field of the optical measurements of CDOM like the UV-vis absorbance and fluorescence spectroscopy (P. G. Coble, 2007). The relationship

between the fractions of the organic matter can be summarized by the following schematic figure (Figure I.6)

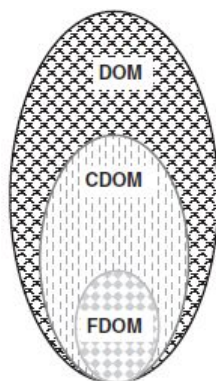


**Figure I.6:** Schematic figure to make clear the relationship and the overlap between the different fractions of organic matter . Figure has been taken from (P. Coble, Lead, Baker, Reynolds, & Spencer, 2014). DOM: dissolved organic matter , CDOM : chromophoric dissolved organic matter , FDOM : fluorescent dissolved organic matter

It is clear from figure I.6 that the dissolved organic matter fraction is the global fraction that comprises the CDOM subgroup which in turn comprises the fluorescent dissolved organic matter (FDOM) subgroup. In other words, FDOM is a fraction of the colored dissolved organic matter and CDOM, chromophoric dissolved organic matter is a fraction of DOM..

#### **I.4.3.1 The importance of chromophoric dissolved organic matter**

The importance of the study of the chromophoric or colored dissolved organic matter comes from the fact that it is an important factor controlling ocean color and its photic zone and bioavailability of light for phytoplankton and other photosynthesizing organisms; and it also carries and produces carcinogenic disinfection by-products and organic pollutants in the natural and engineered aquatic systems (S. Li et al., 2017). In addition, its study enables the expansion of our knowledge about the dynamics of the dissolved organic matter in the aquatic environments and its role in the circulations of biogeochemical elements such as carbon.

## **I.4.4 The optical properties of Coloured Dissolved Organic Matter**

### **I.4.4.1 Fluorescent dissolved organic matter (FDOM)**

Fluorescent dissolved organic matter (FDOM) is defined in the literature (Mostofa, Yoshioka, et al., 2012) as the operationally defined fraction of the CDOM which has the capacity of the emission of light upon excitation through the absorption of a photon of higher energy and has significant fluorescence efficiency at some specified location in the fluorescence excitation emission matrices or fluorescence maps .

### **I.4.4.2 Composition of fluorescent dissolved organic matter**

The major fluorophores found in the fluorescence map of the natural fluorescent organic matter are constituted of two types. The first type is the protein-like fluorescence which mainly comes from aromatic amino acids which has the capability of fluorescing in the ultraviolet region of the electromagnetic spectrum and these are tyrosine like fluorescence representing two peak regions ( B1 and B2 regions) and the tryptophan-like fluorescence representing also two regions ( T1 and T2 regions ) as it is shown in **Figure I.8** and **Table I.1**. The second type is the fluorescence of the humic substances, which is represented by Peak A region (fulvic acid-like fluorescence) and Peak C region (humic acid-like fluorescence) and Peak M1 and Peak M2 (marine humic acid-like fluorescence) as it is shown in **Figure I.8** and **Table I.1**. The above mentioned fluorophores have specific peaks characterized by couples of excitation emission wavelength. Theses peaks of fluorescence and regions in EEM are elaborated and detailed more in the section “**Methods of analysis of 3D excitation and emission matrix spectra of fluorescence**“

### **I.4.4.3 Principle of Fluorescence Spectroscopy :**

Spectroscopy is the study of light matter interaction (Herrmann & Onkelinx, 1984) which provides informations about the matter at a molecular and structural level and therefore it is a physical method for chemical analysis. The light is considered to be electromagnetic energy. Spectroscopy is divided to many fields according to the part of the electromagnetic spectrum used in the interaction with the matter in study. The fluorescence spectroscopy has been widely used in the area of study and research of chemistry since the year 1963 (Kalle, 1963) and its use has been reinforced and enhance by the development of the three dimensional

technique of excitation and emission matrix spectra (P. G. Coble, 1996). Fluorescence is a form of photo-luminescence and could be simply defined as the emission of a photon of lower energy (longer wavelength) than absorbed one (excitation) when an electron returns to its ground state. Fluorescence spectroscopy in three dimensional excitation emission matrices mode provide a three-dimensional contour maps of a given aqueous solution of the fluorescent fluorophores therein but also the Rayleigh and Raman scattering of the water (Mostofa, Yoshioka, et al., 2012) which can be clearly seen in Figure I.8 and Figure I.9. These three-dimensional contour maps are called in the literature excitation–emission matrix (EEM) which provide the fluorescence intensity as a function of the excitation wavelengths and the emission wavelengths. In addition, all the underlying principles of the fluorescence phenomenon are explained in details in previously reported literature ([Lakowicz 1983](#); [Albani 2008](#); [Mostofa et al. 2012](#); [Hudson et al. 2007](#))

The fluorescence phenomenon happens when the electrons of an organic molecule of a given chemical species; which has already a given color; absorbs light of quantized energy that correspond exactly to the difference in the energy levels or states existing in it (Senesi, 1990). Therefore, for an electron to absorb any form of energy to jump to a higher energy level, this energy has to correspond to the difference of energy between the ground electronic state and the first excited electronic state.

Fluorescence EEM are formed by registering the emission spectra for several wavelengths of excitation, or excitation spectra for several emissions. They are literally matrices as their names reflects in which excitation wavelengths are in columns and the emission wavelength are in the rows (or vice versa) and the values in each intersection of a given wavelength of excitation and emission represents the fluorescence intensity. Fluorescence as a phenomenon of photoluminescence is explained by the Jablonski diagram which is detailed in the next section.

#### **I.4.4.4 Jablonski Diagram**

The Polish Physicist Aleksander Jablonski studied the interaction of the light and matter and in the year 1933 he proposed a three energy level diagram (Frackowiak, 1988) as an attempt to explain the photoluminescence phenomenon which is generated from the interaction of the light and many organic compounds (Jablonski, 1933); and the more developed diagram

which includes the vibronic energy states is called the Jablonski diagram. What this diagram does is that it highlights the different energetic pathways a molecule can take once it interacts with light. The Jablonski diagram explains best how the mechanism of the photo-luminescence (e.g. fluorescence or phosphorescence) occurs which is how organic molecules result in the emission of visible light. This Jablonski diagram is shown in the following figure (Figure I.7) which shows the possible electronic energy states which are discrete.

There are several pathways and relaxation channels for an electron to relax when it returns back to the ground state from its excited state after the absorption of a discrete quantum of light (a given wavelength). The most common relaxation pathways have been previously described in the literature which are vibrational relaxation, internal conversion, and fluorescence ([Lakowicz 1983](#)).

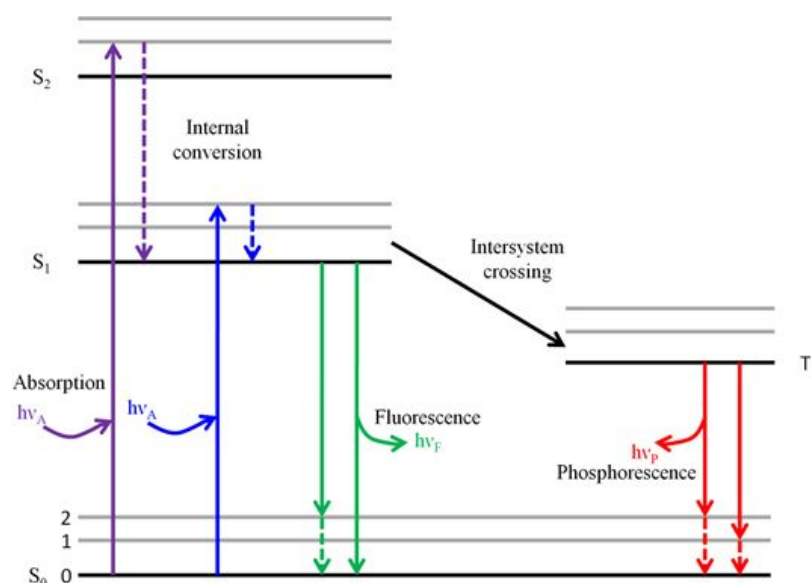


**Figure I.7 :** A typical Jablonski diagram of singlet electron energy states which shows an increase in the energy level by going from down to the upside. The ground state is indicated by  $S_0$  the first excited singlet electronic state by  $S_1$

Source : <http://nptel.ac.in/courses/102103044/module2/lec6/1.html>

When the electron relaxes within the first excited singlet state  $S_1^*$  meaning that moving down within the electronic state  $S_1$ , these pathways are vibrational relaxation and internal conversion and sometimes are called in the literature as nonradiative relaxation because there is no emission of light. On the other hand, after these nonradiative relaxation of the electron,

one of the remaining pathway is the jump of the electron from the first excited state to the ground state, this electronic jump is radiative relaxation meaning that there is an emission of energy corresponding to the difference between these electronic states. This difference in energy correspond to the visible part of the electromagnetic spectrum. Therefore, this emission of electromagnetic energy is an emission of visible light and this relaxative pathway is called fluorescence in which the molecules deal with the received photon energy by the emission of energy at a longer wavelengths (Jaffe & Miller, 1966). Senesi (1990a) called fluorescence, the reverse of absorption because it happens within the singlet electronic states and not the triplet electronic states which are phosphorescence. As a consequence of the use of EEM spectra and the plethora of information therein; there are so many methods for analysing them.

#### **I.4.4.5 Methods of analysis of 3D excitation and emission matrix spectra of fluorescence.**

There is so much information that could be extracted from an excitation emission matrix spectra of a sample. Therefore, there are several methods for the analysis of the excitation emission matrices data generated by the technique of fluorescence spectroscopy. Some of these methods are: peak picking ([Coble 1996](#)), Fluorescence Regional Integration (FRI) ([Chen et al. 2003](#)), Canonical Polyadic / PARAllel FACtor analysis (CP/PARAFAC) ([Murphy et al. 2013](#)) and Self-organizing maps (SOM) ([Bieroza et al. 2009](#)). The following are some explanations of the above mentioned methods based on the literature. The methods such as FRI and SOM won't be discussed in detail but the reader is redirected to the relevant literature published elsewhere for further details because these methods are out of scope of the present works of this PhD thesis.

##### **I.4.4.5.1 Peak Picking method**

The Peak picking method is a visual inspection/detection of peaks which are a specific position in the fluorescence space which is the three dimensional excitation and emission matrix spectra. Many couples of excitation and emission wavelengths ( $\lambda_{\text{ex}}$ ,  $\lambda_{\text{em}}$ ) which represents a specific position in the fluorescence contour maps has been named and specified by the work of (P. G. Coble, 1996) who has introduced the 3D fluorescence in the environmental geochemistry. [Coble \(1996\)](#) used this method to characterize water samples

from riverine, estuarine, coastal, marine, oceanic origins. These positions have been also named as peaks. Hence the presence of these peaks in a sample give us informations about its origin and composition. The most observed peaks in this study (P. G. Coble, 1996) are Peak A and Peak C which correspond to Humic substances; Peak T and Peak B are associated with proteins and more specifically with fluorescent amino-acids tryptophan and tyrosine amino-acids; Peak M has also been associated with marine humic substances in the previously mentioned work and recently has been associated with recent microbial activity. The position of these peaks in the fluorescence map are summarized in the following table (Table I.1) which is taken from the (P. G. Coble, 1996) study. Also, their position are shown visually in figure (Figure I.8).

**Table I.1:** The designated Peaks in letters by (P. G. Coble, 1996) study and the exact position of their fluorescence maxima in the fluorescence map . Their names in letters because their chemical composition was not known at the time of this study (P. G. Coble, 1996) .

Fluorescence Peak	$\lambda_{Ex} / \lambda_{Em}$	Name	Origin
A	260 < /448-480	Fulvic acid-like fluorescence	Terrestrial origin - degradation of plant and animal debris (humic substances)
C	320-360 / 420-460	Humic acid-like fluorescence	Terrestrial origin - degradation of plant and animal debris (humic substances)
M	250 < (290-325) / 370-430	Marine Humic acid-like fluorescence	Biological activity , anthropogenic inputs
B	225-237 (270-275) / 304-312	Tyrosine (amino acid)-like fluorescence	Microbial activity , primary production
T	225-237 (270-280) / 330-368	Tryptophan (amino acid)-like fluorescence	Microbial activity , primary production , anthropogenic inputs

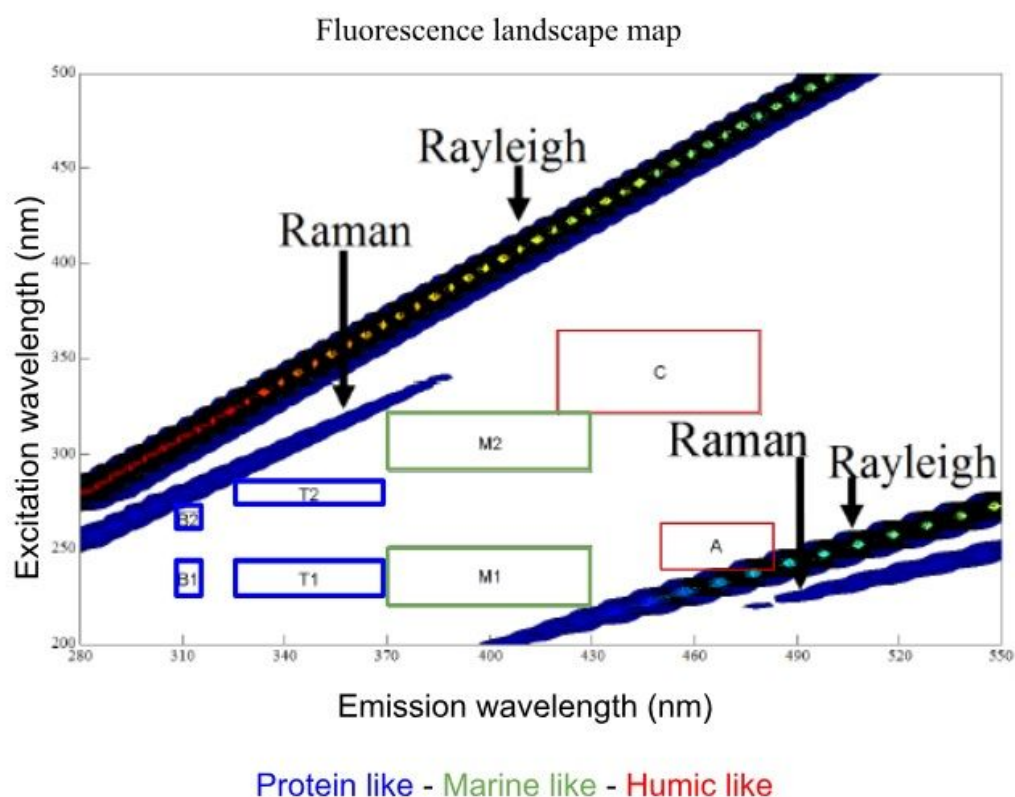


**Figure I.8 :** The localization of the components of fluorescent organic matter , and regions in the fluorescence map in addition to the first and second order of Rayleigh and Raman scattering. Source: Ferretto, N. (2014)

When dealing with large number of EEM, the method of peak-picking gets time-consuming, tedious, fatiguing and source of error depending on the sharpness of the maximum or on the matrix accuracy. Therefore the need for a more sophisticated technique for the analysis of these EEMs of fluorescence is of paramount importance such as multivariate techniques, one technique of which is CP/PARAFAC which has been developed where whole regions of three dimensional excitation emission matrix spectra of fluorescence are considered (Henderson et al., 2009).

#### **I.4.4.5.2 Canonical Polyadic / Parallel Factor analysis (CP/PARAFAC) tool :**

After the studies conducted by ([Stedmon et al. 2003](#); [Søndergaard et al. 2003](#); [Yang et al. 2015](#)); the method of decomposition (CP/PARAFAC) has also another name which is less commonly known which is CANDECOMP (CANonical DECOMPosition) which has been proposed by (Carroll et al., 1970). CP/PARAFAC can have another name which is PARAFAC. PARAFAC is a powerful multivariate modeling tool in the analysis of the EEMs



of the dissolved organic matter DOM. It has the capability of statistically decompose or separate overlapping EEM topographic signal spectra because EEMs often involve various types and fluorescent species called fluorophores which can be overlapping peaks, into individual independent fluorescent components with unique excitation emission spectra. Therefore it provides a quantitative and qualitative model of the EEM data sets ([Stedmon and Bro 2008; Cory and McKnight 2005](#)) or in another way of expressing it, PARAFAC has the ability of the isolation and quantification of individual fluorescence component signals which correspond to fluorescence intensity of FDOM in natural waters or in mixtures. PARAFAC is a mathematical technique and functions by modeling the three-way data, fitting the tree linear equation by minimizing the sum of squares of the residuals ( $\epsilon_{ijk}$ ) like any regression modeling using the following equation :

$$X_{ijk} = \sum_{f=1}^F a_{if} b_{jf} c_{kf} + \epsilon_{ijk} \quad i=1,..,I; j=1,..,J; k=1,..,K \quad \text{Eq (1.)}$$

$X_{ijk}$  is one element of the three-way data array with dimensions i, j, and k.

Fluorescence intensity of the sample i measured at emission wavelength j and excitation wavelength k is denoted by the number  $x_{ijk}$ ; whereas the final term  $\epsilon_{ijk}$  represents the error in the model which represents the unexplained signal (residuals containing noise and other un-modeled variation) (Stedmon & Bro, 2008) and the number i represents the number of the samples in the EEMs data set and the number j and k represent the emission and excitation wavelengths respectively.

The parameters a, b, and c are what is returned from the modelling process. The pseudo-concentration of each PARAFAC component (factor or some references name it as analyte) is given by the  $a_{if}$  whereas the parameters  $b_{jf}$  and  $c_{kf}$  in the above equation represent the estimated emission and excitation loadings of each component of the found PARAFAC components (factors) and it is inferred from these  $b_{jf}$  and  $c_{kf}$  information, the nature of this fluorescent component. Furthermore, F value is the maximum number of components in the validated PARAFAC model (Andersen & Bro, 2003). It is recommended by the published research conducted by ([Bro 1997; Stedmon et al. 2003](#)) that some preparations of the EEM Dataset should be done before proceeding to the PARAFAC

analysis. The first preparative step is the subtraction of the EEM data of the Milli-Q water blank from every EEM of every measured sample. The second preparative step is the elimination of the Raman and Rayleigh 1<sup>st</sup> and 2<sup>nd</sup> order light scattering from every EEM spectra of every sample because Rayleigh and Raman Scattering are wavelength dependent (not tree linear). Theses dispersions or scattering are always existing and inherent to any water sample and, from any aquatic system and can be seen in figure I.9 . The removal of these Rayleigh and Raman scattering is done according to the detailed method in the study conducted by (Zepp, Sheldon, & Moran, 2004). Inner filter effect is another problem could be facing the treatment and interpretation of the excitation emission matrix of fluorescence spectroscopy and should be taken into account and can be reduced by diluting the water samples or by applying mathematical correction ([Larsson et al. 2007](#)) .The last preparative step is the application of the constraint of non-negativity to all of the PARAFAC component because it is logical that the excitation and emission and the concentration of any PARAFAC components should and must be positive and can not have negative values.

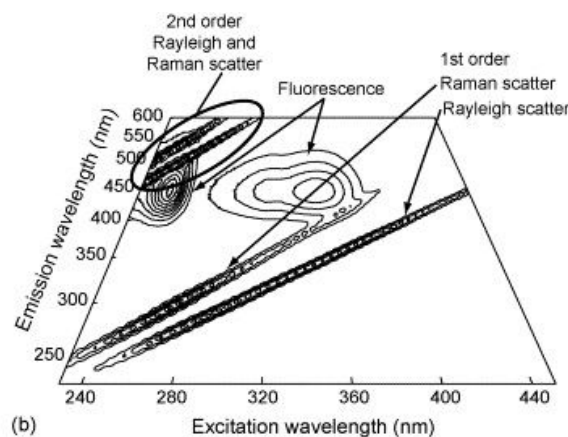


**Figure I.9** : figure showing the first and second Rayleigh and Raman scattering and fluorescence

Image adapted from : ([Larsson et al. 2007](#))

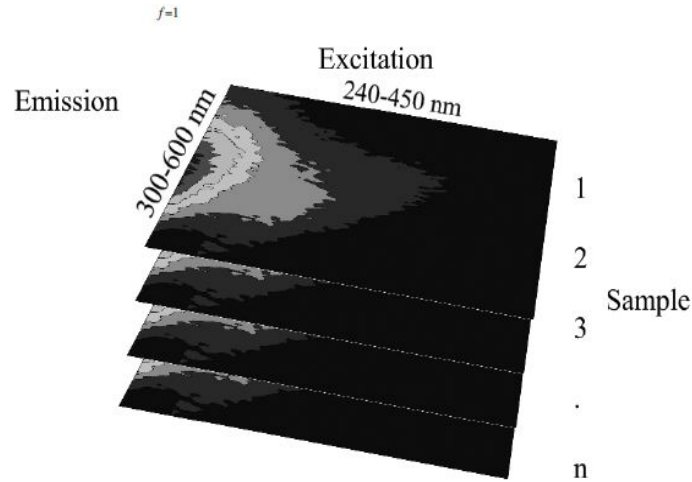


**Figure I.10:** Example of combining EEMs into a three-dimensional cube of data ( $x_{ijk}$  in Eq. 1) adapted from (Stedmon & Bro, 2008)

It is clear from the figure above (Figure I.10) that each sample has its fluorescence EEM and the aim of PARAFAC is to combine all the EEMs spectra of the sample into a three-dimensional box of data ( $x_{ijk}$  in Eq. 1), then finding or calculating the common factors shared by all the EEMs of the samples with varying contribution in each EEM .

In the following diagrams or flow chart, the detailed steps for the PARAFAC analysis are summarized and shown in (Figure I.11) .

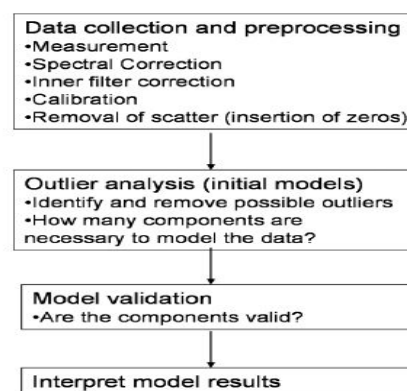


**Figure I.11:** Flowchart showing the logical steps necessary for the PARAFAC analysis of the excitation emission matrices of the fluorescence datasets Source : (Stedmon & Bro, 2008)

As it can be seen that from the above flowchart (Figure I.11) the interpretation of the model results are the last step and these steps is concerned with the identification of the PARAFAC

components and the comparison of these components with different PARAFAC components found in previous studies in the literature either the studies concerned about the PARAFAC or the studies of the fluorescence of the dissolved organic matter in whatever aquatic environment. More explanations of how the decomposition PARAFAC proceeds are as follows in the following figure (Figure I.12).

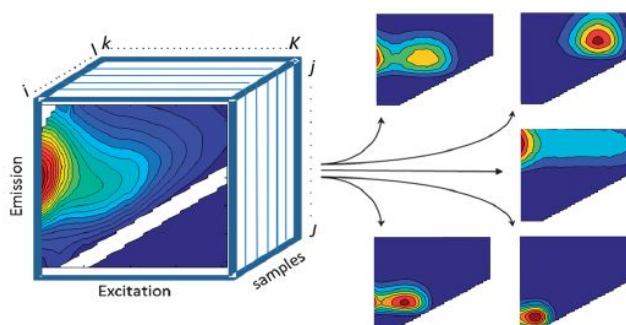


**Figure I.12 :** A cube of the excitation emission matrices EEMs dataset which is decomposed to parallel five distinct CP/PARAFAC components Source of the image : (Murphy, Stedmon, Graeber, & Bro, 2013)

The figure above (Figure I.12) shows a dataset of EEM of fluorescence that is rearranged in threeway structure or a cube of data for further analysis of the data by PARAFAC algorithm software. And on the right hand side of the figure, it can be seen five distinct PARAFAC component each one of which has clearly different excitation emission wavelengths which are found in the EEM dataset on the left hand side of the figure. Moreover, each excitation emission matrix which represent a slice of the left hand side cube, could be reconstructed using the five PARAFAC model components on the right hand side of the figure and it contains certain contribution of each PARAFAC components. The different contribution of each PARAFAC component is referred to in the literature dealing with the treatment of Datasets by PARAFAC by the terms “pseudo concentration” or contribution.

In our present study , the program “progmeef” which is runnable at any matlab platform and which was developed by Dr.Roland Redon who works at the MIO laboratory (Université de Toulon center). This software is based on differents studies of the signal treatment. Furthermore, a small description of other methods of analysis which are used for the treatment and analysis of the EEM are presented in the next following paragraphs in order just to bring the reader up date to the state of the art techniques used in the literature in this scope. For the sake of time and space, only two methods of the analysis of the EEMs will be presented in the present chapter, and these are the fluorescence regional integration and the

second method will be the self-organizing maps for dealing with EEMs. The above mentioned methods will be described briefly without the need for presenting images and figures in the process of explaining them. And the reader will be directed to different references in the literature for further information and explanation.

This PARAFAC method of dealing with and analysing the EEMs spectra of FDOM has been widely used in many natural and engineered aquatic environments such as lakes (Du, Zhang, Chen, Chang, & Liu, 2016; Z. Zhou, Guo, & Minor, 2016) rivers (Hur & Cho, 2012; Meng et al., 2013; Mostofa et al., 2009; Yu et al., 2016), estuaries (Hall & Kenny, 2007; Stedmon & Markager, 2005) , seas (Dainard & Guéguen, 2013), oceans (Dainard & Guéguen, 2013), wastewater treatment plants (Cohen, Levy, & Borisover, 2014; W.-T. Li et al., 2014; Qian, Chen, Li, & Yu, 2017; L. Yang, Han, Lee, & Hur, 2015; L. Yang, Shin, & Hur, 2014) and drinking water treatment plants (Heibati et al., 2017; Shutova, Baker, Bridgeman, & Henderson, 2014; Vera et al., 2017). In addition, this was the technique used throughout the entire present thesis to decompose the EEMs measured for this thesis works.

#### **I.4.4.5.3 Fluorescence Regional Integration FRI:**

FRI is another mathematical method used in the quantitative analysis of the spectra of FDOM. In this method the fluorescence EEM is divided into five spectral regions. Fluorescence regional integration functions by integrating the volumes beneath operationally defined EEM regions (J. Zhou, Wang, Baudon, & Chow, 2013). These volumes represent FDOM fractions in a water sample, the same as the PARAFAC components and the peaks in the peak-picking method. The relative abundance of the fractions of the fluorescent dissolved organic matter which are detected in a water sample are represented by the normalized region-specific EEM volumes (W. Chen et al., 2003) .

Other methods of analysing the excitation emission matrix of fluorescence are self-organizing maps which is not described here in this section but the reader is directed to the relevant literature published elsewhere (Bieroza, Baker, & Bridgeman, 2012).

## I.5 Irradiation in Environment

### I.5.1 Solar irradiation

It is very clear that the closest star to our planet earth is the sun. Our climate and our atmospheric motions are moved essentially by the radiant energy of the sun (Iqbal, 2012). Insolation could be viewed as an acronym for **incoming solar radiation** and it is defined as the amount of sunlight received per unit area by latitude and by season

$$Insolation = \frac{Light}{Area}$$

It is clear from this mathematical equation that the insolation has a direct proportionality with the amount of light or here in this case, the light produced by the sun which is the solar light, and in addition to that, insolation has an inverse proportionality with the area receiving sunlight.

The insolation depends upon several factors :

The angle of insolation, when the angle is close to 90 degrees, we have greater insolation values because the area of the surface receiving sunlight is the smallest whereas, when the angle of insolation is smaller , the irradiated surface and area becomes greater and therefore according to the mathematical relationship described above, the insolation becomes smaller because of its inverse proportionality with the irradiated area.

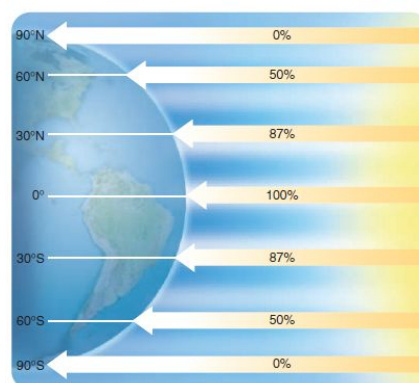


**Figure I.13:** The incoming solar radiation (insolation) received in various latitudes during an equinox date

Source : [https://www.cengage.com/resource\\_uploads/downloads/0495555061\\_137179.pdf](https://www.cengage.com/resource_uploads/downloads/0495555061_137179.pdf)

The latitude at which the insolation is measured : It is clear from the figure (Figure I.13) that the amount of the received incoming solar radiation in the equatorial line is 100% because it is perpendicular and this percentage decreases as we go from the equatorial line to the north and to the south in equal percentages

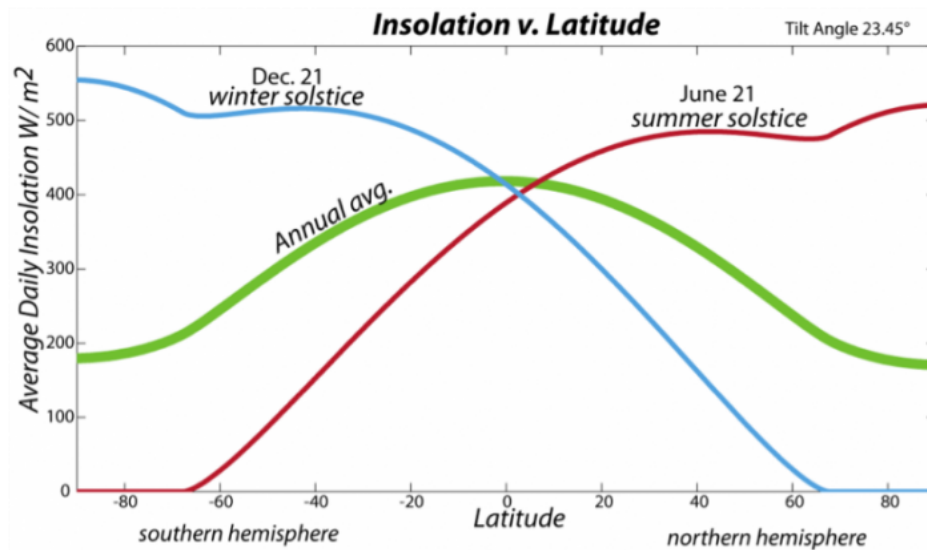


**Figure I.14:** The variation of the average daily insolation ( $\text{W/m}^2$ ) with latitude and with time of the year (Image source: <https://www.e-education.psu.edu/earth103/node/1004>)

It can be seen from the above figure (Figure I.14) that for the summer solstice in the northern hemisphere which occurs at June 21<sup>st</sup> of each year, the highest values of insolation in  $\text{W/m}^2$  is found in the north pole ( $90^\circ\text{N}$ ) than any other location of Earth indicating that the north poles gets that highest solar energy for that day. The same goes for the south pole in the summer solstice of southern hemisphere which corresponds to winter solstice in the northern hemisphere which normally occurs on December 21<sup>st</sup> in which the highest one-day energy input is received and found there. In addition, the annual average daily insolation as a function of latitude is also shown in the same figure because one-day energy inputs (insolation) do not count for much in terms of annual climate.

Time of day : it is known that the sun is at its highest height at the noon and the lowest during the first and last hours of the day and accordingly, this affect the angle of insolation and therefore, the values of insolation varies during the daylight from the lowest in the first few

hours of the daylight to the maximum values at the noon, then it goes down again until it reaches its lowest values of insolation at the twilight hours.

The seasons : Since the sun appears to have different paths according to each season this affects the angle of insolation and also affects the duration of daylight since in summer we have the longest daylight during the year and the shortest daylight in the winter and this affects the values of the daily insolation. The longer the duration of daylight, the more the insolation values received per day at the same area of measurement.

Solar irradiance can be defined as the power produced by the received sunlight in unit area or the power produced by the insolation. The integration of the solar irradiance data over time or the accumulated solar irradiance is called solar irradiation or insolation or solar exposure but in practice the two terms are being used interchangeably. And they are just different ways of saying the same thing .

### Solar irradiance spectrum

Solar spectrum or solar irradiance spectrum could be defined as the distribution of the emitted by the sun- electromagnetic radiation which is incident on the top of the atmosphere of the earth .

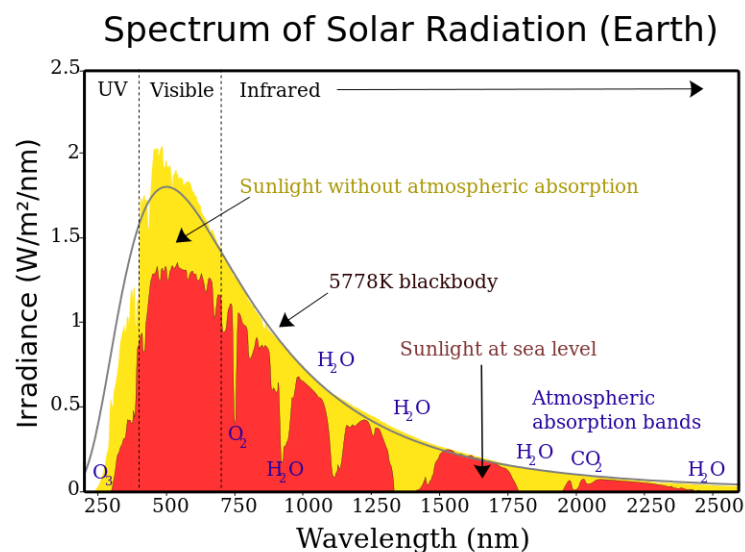


**Figure I.15** : Solar irradiance spectrum which shows the solar irradiance in Watt/m<sup>2</sup>/nm as a function of the electromagnetic wavelength. It represents the received solar irradiance at the atmosphere and at the surface of the earth.

(Figure source : [https://commons.wikimedia.org/wiki/File:Solar\\_spectrum\\_en.svg](https://commons.wikimedia.org/wiki/File:Solar_spectrum_en.svg))



The above figure (Figure I.15) shows the solar irradiance in  $\text{W/m}^2$  as a function of wavelength in nanometers. The yellow figure is the extraterrestrial solar spectrum before it enters the atmosphere of the earth or at the surface of the sun. The red figure shows the solar irradiance spectrum received at the sea level after it enters the atmosphere of the earth and it shows the atmospheric absorption bands of water molecules and carbon dioxide molecules. This red figure which represents the spectral distribution of radiation at the sea level could change and have different shapes as a function of the extraterrestrial spectral distribution of solar radiation and as a function of the atmospheric constituents (Iqbal, 2012). The smooth curve shows the irradiance spectrum of a black body; at a temperature close to that of the sun which is 5,777 Kelvin; resembles greatly and very closely the spectrum of the solar irradiance. Some of the UV radiation gets absorbed by the atmosphere.

### Insolation in France :

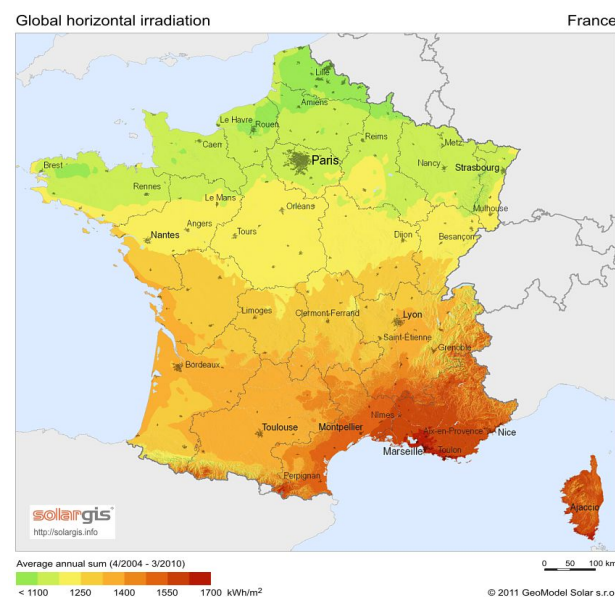


**Figure I.16 :** Solar radiation map of France

(Source : <http://www.mappery.com/map-of/Solar-Radiation-Map-of-France>)

It can be seen from the Figure I.16 that annual solar irradiance intensity increases from the north to the south of France since we go southward we approach the tropics of cancer. The north regions of France receives a lowest insolation in comparison to the southern regions. In addition, there is an increase also from the west to the east of france. It is also clear that Region PACA “Provences Alpes Côte d’Azur” has the highest solar irradiance intensities

compared to the whole of France. In this region of France, “PACA”, the whole works of the present thesis were conducted. The highest values is 1,700 kWh/m<sup>2</sup> and the lowest values that could be attained is 1,100 kWh/m<sup>2</sup> .

## **I.6 Principle of photochemistry**

Photochemistry is defined as the science of chemistry that deals with the interaction of light and matter. And it studies the chemical reactions that is caused by the absorption of any photon of light starting from the near end of the electromagnetic spectrum the ultraviolet photons whose wavelengths starts from 100 to 400 nm and the visible light (400–750 nm) and the chemical reactions caused by these two regions of the electromagnetic wavelengths are studied by the UV-Visible spectroscopy and finally the infrared electromagnetic waves (750–2500 nm) studied in the infrared spectroscopy (McNaught & Wilkinson, 1997). Photosynthesis, a natural chemical reaction that occurs due to the light; vision in the human beings and the animals, also initiated by light or photons; formation of vitamin D, also initiated by sunlight the polymerizations; all of these aforementioned reactions are some examples of photochemical reactions which are studied in the branch of chemistry which is named photochemistry (Glusac, 2016). There exist difference at the level of proceeding between the photochemical reactions and the temperature-driven or thermally-induced chemical reactions. Photochemical reactions can overcome large activation barriers in a short period of time whereas the thermally-induced chemical reactions requires a long period of time in order to be able to overcome these same activation barriers. Moreover, photodegradation of plastics is a destructive chemical reaction, in which the plastics get destroyed by the sunlight or the absorption of sufficient amount of photons and this represents an example that the photochemistry can be destructive as well as constructive .

### **I.6.1 Photodegradation of Dissolved Organic matter DOM :**

Photodegradation of DOM is the degradation induced by sunlight leading to the destruction of the colored dissolved organic matter chromophores which leads to the photobleaching of the CDOM and the loss of its optical properties like uv-vis absorption and fluorescence. It could also lead to the mineralization of the dissolved organic carbon to carbon dioxide CO<sub>2</sub>. In addition, photodegradation leads to fading of the photochemically-sensitive matter and could also result in the production of organic compounds and other materials of different

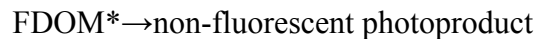
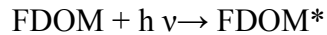
chemical and photochemical reactivity (Vidali, Remoundaki, & Tsezos, 2009). Many studies which focused on the photochemical reactions involving DOM have reported that there are changes induced by the photochemical reactions on the structures and optical properties of DOM as well as their molecular size (Del Vecchio & Blough, 2002; Helms et al., 2013). Photodegradation of DOM in aquatic systems are very important. [Blough & Del Vecchio \(2002\)](#) have summarized the importance of the process of the photochemical degradation of the CDOM and have highlighted the fact that the color oceans is kept in steady state and controlled by the photo-reactivity of the terrestrial dissolved organic matter which is the dissolved organic matter transported by the rivers. The effect of photochemical induced changes and transformations (photodegradation, photobleaching, photo-oxidation) of the dissolved organic matter is usually studied through the investigation of the creation of bioavailable fraction, the optical properties characterization, the physico-chemical properties of humic substances and the spatio-temporal changes of the above mentioned properties. In the following table (Table I.2), a summary of the studies that used fluorescence spectroscopy to study the photochemistry of dissolved organic matter in various aquatic environments and ecosystems is proposed.

**Table I.2.** Studies which studied photodegradation of DOM coupled with EEM technique

<b>Aquatic Environment</b>	<b>Reference</b>
Wetlands	(Waiser & Robarts, 2005)
Rivers	(Gao & Zepp, 1998; Meng et al., 2013; Patel-Sorrentino, Mounier, Lucas, & Benaïm, 2004; Rodríguez-Zúñiga et al., 2008; Song et al., 2017; White, Vaughan, & Zepp, 2003)
Marine	(Bertilsson, Carlsson, & Granéli, 2004; Boehme, Coble, Conmy, & Stovall-Leonard, 2004; Del Vecchio & Blough, 2004; De Souza Sierra, Donard, Lamotte, Belin, & Ewald, 1994; Ferrari, Dowell, Grossi, & Targa, 1996; Kieber, Hydro, & Seaton, 1997; Miller, Moran, Sheldon, Zepp, & Opsahl, 2002; Skoog, Wedborg, & Fogelqvist, 1996; Zanardi-Lamardo, Moore, & Zika, 2004)
Estuaries	(Moran, Sheldon, & Zepp, 2000; Skoog et al., 1996)
Humic standards	(Del Vecchio & Blough, 2002, 2004)
wastewater	(X. Yang et al., 2014)

## I.6.2 Kinetic rate order determination of Photodegradation of DOM

The kinetics of the photodegradation of the dissolved organic matter could be of first order kinetics or of a second order kinetics. For the first order kinetics, the chemical photodegradation reaction could be as follows :



Whereas for a second order kinetics , the chemical reaction could be described as



In addition to the above mentioned paragraph, the rate of DOM photodegradation is equal to:

$$r = I_a * \Phi$$

Where  $I_a$  is the rate of photons absorption and  $\Phi$  the quantum yield of the reaction.

$I_a$  is equal to  $I_0 * (1 - 10^{-A})$  with  $A = \epsilon * c * l$

$$\text{so } r = I_0 * (1 - 10^{-\epsilon * c * l}) * \Phi$$

$r$  can be simplified in two conditions.

If  $A$  is  $>2$ , then  $10^{-A} \approx 0$  and  $I_0 * (1 - 10^{-A}) \approx I_0$  thus  $r$  is independent of  $c$ , the concentration of DOM, the order of the reaction is 0 (zero<sup>th</sup>)

If  $A$  is  $<0,05$ , then  $10^{-A} \approx 1 - 2,3 * A$ , -due to the limited development  $\exp(-x) \approx 1 - x$  if  $x$  is very low- thus  $I_0 * (1 - 10^{-A}) \approx I_0 * (1 - (1 - 2,3 * A))$  and  $r$  is equal to  $I_0 * 2,3 * A$  and it is proportional to  $c$ , the concentration of DOM; the order of the reaction is 1.

However, reactions can be also more complex, For instance, if DOM sensitized its own photodegradation, the order of the reaction can be  $>1$ .

**Environmental context of the present PhD thesis works :** There is a well established literature about the key role which the marine dissolved organic matter plays in the global carbon cycle and hence its effect on the global warming. The influence of the anthropogenic activities on the composition and the distribution of the marine coloured dissolved organic matter in the coastal waters (Tedetti et al., 2012) still needs lots of research works in order to address these questions. Particularly what is the contribution of the anthropogenic FDOM to the coastal FDOM ? In our study we addressed the effects of the photochemistry on the fate of the anthropogenic fluorescent dissolved organic matter in the coastal marine waters using three endmember mixing model.

The aim of the works of the present PhD thesis was to search for differences between the natural fluorescent dissolved organic matter and the anthropogenic fluorescent dissolved organic matter in the coastal zone in terms of a fluorescence signal . This aim was divided into several objectives .

The main objective was to develop a model for the evolution of Anthropogenic Fluorescent dissolved Organic Matter from the WWTP point of leaving until the coastal zone by using coupled mixing experiments and photodegradation experiments.

The secondaries objectives were :

- 1- Application of this model by geographical field experiment of the Gapeau river path
- 2- Studying the temporal variability of fluorescence signal of the three endmember mixing components ( Gapeau river, WWTP discharge , Seawater at Hyeres city).

---

## **Chapter 2 : Materials and methods**

### **Methodology**

---

## II.1 Study Area

The studied area throughout the whole works of the present PhD thesis was the water catchment of the Gapeau River and its coastal zone. Three endmember mixing components were studied by solar irradiation experiments which were : the Gapeau river (RW), the wastewater treatment plant at the La Crau city (WW) and the seawater at the coastal zone of the Hyeres city (SW). These three endmember mixing components are described in the following sections in this methodology chapter.

### II.1.1 Gapeau River

The river Gapeau is a small coastal river which is situated in the French Var department in the Southeastern region of France named Provence-Alpes-Côte d'Azur (figure II.1) and is the second largest river in the Var department. The Gapeau river birth at its source named Beaupre at “collet du Gapeau” in the commune of Signes at a mountain range named “La Sainte Baume” in the Var department. Its climate is of mediterranean type. It empties at the city of Hyères in the Mediterranean sea in what is called in french “rade d'Hyères”. It is 47.5 kilometers long, its catchment area is 544 km<sup>2</sup> ([Ducros et al. 2018](#)).

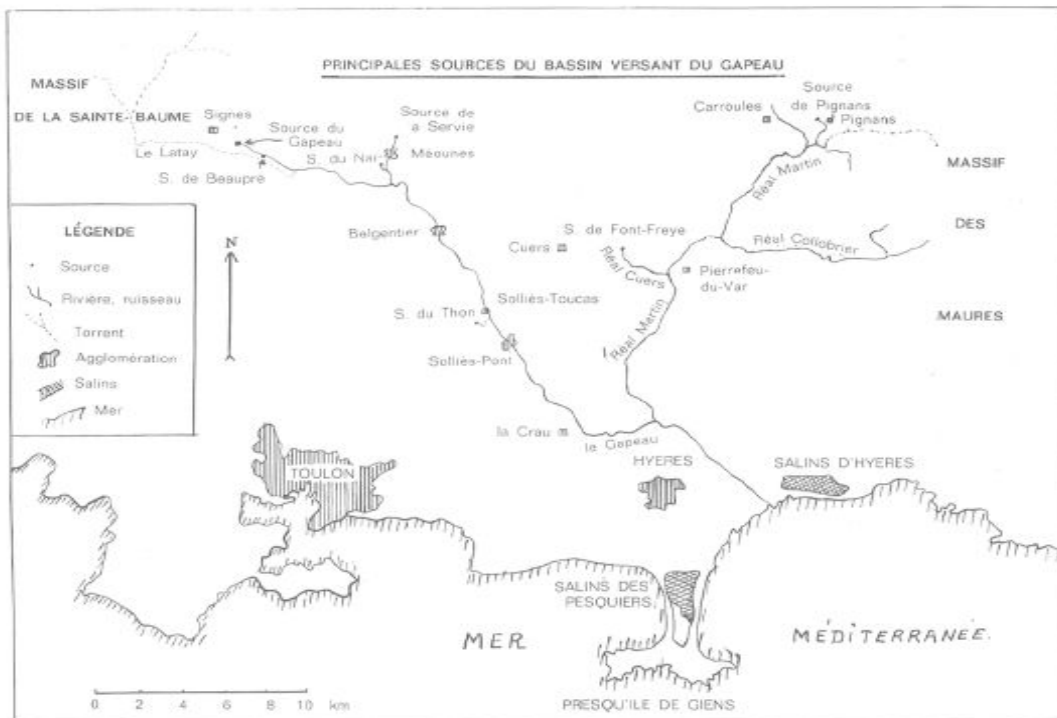


**Figure II.1:** Water catchment of the Gapeau River and the principal sources of the water catchment of the Gapeau river. Gapeau river is situated in the (Southeastern France , Département du Var, Région PACA). Map source : [\(Ollier 1972\)](#)

## II.1.2 Tributaries of The river Gapeau

The river Gapeau is the major river that flows from the city of Signes and verses its water in the sea at the city of the Hyeres. There is one main tributary of the river Gapeau; which is the Le Real Martin which , on the other hand, has it own tributary which has the name Le Real Collobrier.

### II.1.2.1 The Le Real Martin tributary

The Réal Martin tributary starts to flow and to be a river at the commune of Pignans and it has 28 km of length. The Réal Martin tributary reaches its confluence with the river Gapeau after the wastewater treatment plant of the city La Crau. Thus Réal Martin tributary is



an urbanized river since it crosses various french cities in the administrative department of Var, and these cities are Pignans, Carnoules, Puget-Ville, Pierrefeu-du-Var.

### Hydrological regime of the Gapeau River

The hydrological regime of the Gapeau river is a pluvial regime having its maximum discharge flow in the winter season in the period of rainfalls and its minimum discharge flow in the summer season because there is no rain in the summer as it can be clearly seen in figure II.2.

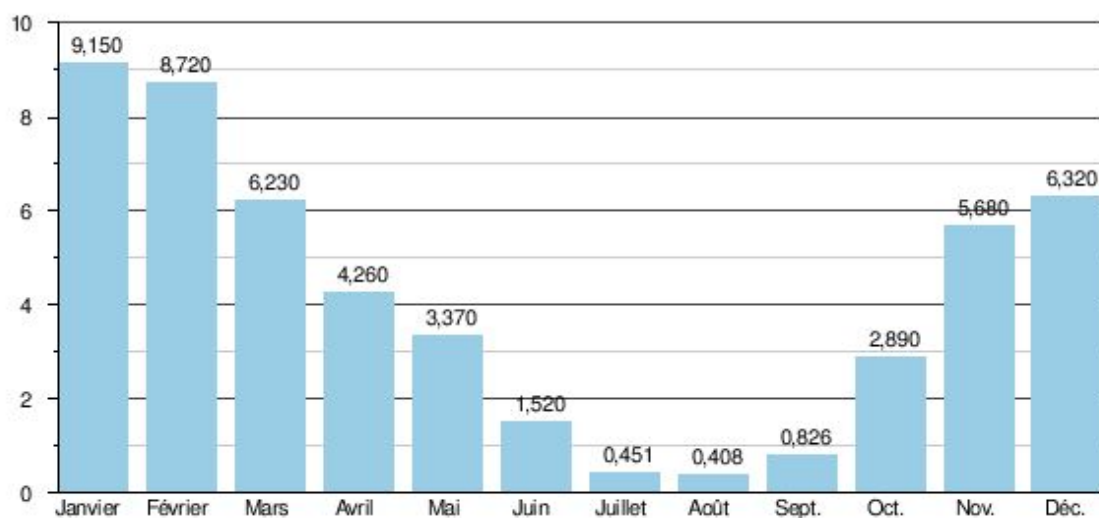


**Figure II.2 :** The Mean monthly Flow (m<sup>3</sup>/s) of the Gapeau river measured for 56 years from 1961 to 2016 at the hydrological station Y4624010 - le Gapeau à Hyères [Sainte-Eulalie] for a catchment area of 517 km<sup>2</sup> and at 9 m of altitude, and this station is located after the confluence of the Gapeau river with the Real Martin river

Source : wikipedia, banque hydrique, Ministère de l'écologie et du développement durable

<https://fr.wikipedia.org/wiki/Gapeau>

This figure II.2 describes the hydrological regime and situation of the river Gapeau at the measuring station of Sainte-Eulalie which is located after the confluence of the Gapeau river with the Real Martin river.

The water catchment of the Gapeau river is highly impacted by many anthropogenic activities such as agriculture, agro-alimentary industry, military, drinking water, wastewater treatment, tourism; which modifies the hydrological functioning of The Gapeau river. ([SAGE Gapeau, 2015](#)). Regarding the wastewaters generated by the french communes on the Gapeau river, they are collected and treated by three major company managers called “gestionnaire”. These company managers are : The first two companies are SAUR and SADE which are affiliated to the “Compagnie générale des eaux” which changed its name to the current name of “Veolia Environnement”. The third company is named Société Varoise d’Aménagement et de Gestion (SVAG). In total, there is thirteen wastewater treatment plants on the watershed of Gapeau river as it can be seen in **Figure II.3**. The principal wastewater treatment plants in the watershed of Gapeau river are found in the urban centers or urban city which are : Signes, Cuers, Méounes, Pignans, Carnoules, Collobrières, Pierrefeu-du-Var, Puget-Ville et La Crau. These are names of the communes which have their own wastewater treatment plant.



**Figure II.3 :** Wastewater treatment plants found in the watershed of the Gapeau River .  
this figure shows thirteen wastewater treatment plants.

Source : report from Syndicat Mixte du Bassin Versant du Gapeau

Most of the works presented here in this PhD thesis have focused on the wastewater treatment plant at La Crau city.

### **II.1.3 Wastewater treatment Plant of La Crau city - Département du Var - Southeastern France**

The wastewater treatment plant of the La Crau city is situated in the Var department in the region “PACA : Provinces Alpes Côte d’Azur” in southeastern France in the following longitude and latitude 43°08'43.1"N 6°05'35.4"E. This wastewater treatment plant serves several french communes collectively named in french “ La communauté de communes de la Vallée du Gapeau [www.ccvg.fr/](http://www.ccvg.fr/)” (CCVG) which could be translated to english as “ The community of the communes of the valley of the Gapeau River” which includes the following french communes : Solliès-Pont, La Farlede, Solliès-Toucas, Solliès-ville, and Belgentier. The commune of La Crau is added to them but is not an integral part of it. Each Commune is responsible for the public service of collecting the wastewater in its administrative area. The public service of transporting and the treatment of the sewage of each commune is the responsibility of the CCVG. The collected sewage is treated at the collective wastewater treatment plant which is situated in the La commune de La Crau. The public service of the treatment of the collected sewage at the wastewater treatment plant of la commune de La Crau is delegated to the company of Veolia Eau (<https://www.service-client.veoliaeau.fr/>). The total number of inhabitants of CCVG and the commune of La Crau is 50,086 inhabitants which is the served number by the collective wastewater treatment plant. Furthermore, this wastewater treatment plant of La Crau treats also industrial wastewater from the “La distillerie” which has the longer name DISTILLERIE LA VAROISE. A satellite view of this wastewater treatment plant of La Crau city is shown in **Figure II.4**



**Figure II.4 :** Bird's eye view picture by satellite of the wastewater treatment plant for the La Crau commune and for la communauté de communes de la vallée du Gapeau. This Satellite pictures shows the treatment tanks and the administrative building of the wastewater treatment plant. This WWTP outputs its effluent directly in the Gapeau river which is obscured by the trees on its path.

#### **II.1.4 The Coastal zone of Hyeres City**

The charge or the water load of the river Gapeau is disposed to the sea at the coast of the city of Hyeres which is located at the south east of the var department. This coast of the Hyeres city is surrounded by three small islands which are île de Porquerolles, île de Port-Cros and île du Levant, they make part of the natural national parc of Port Cros (PNPC).

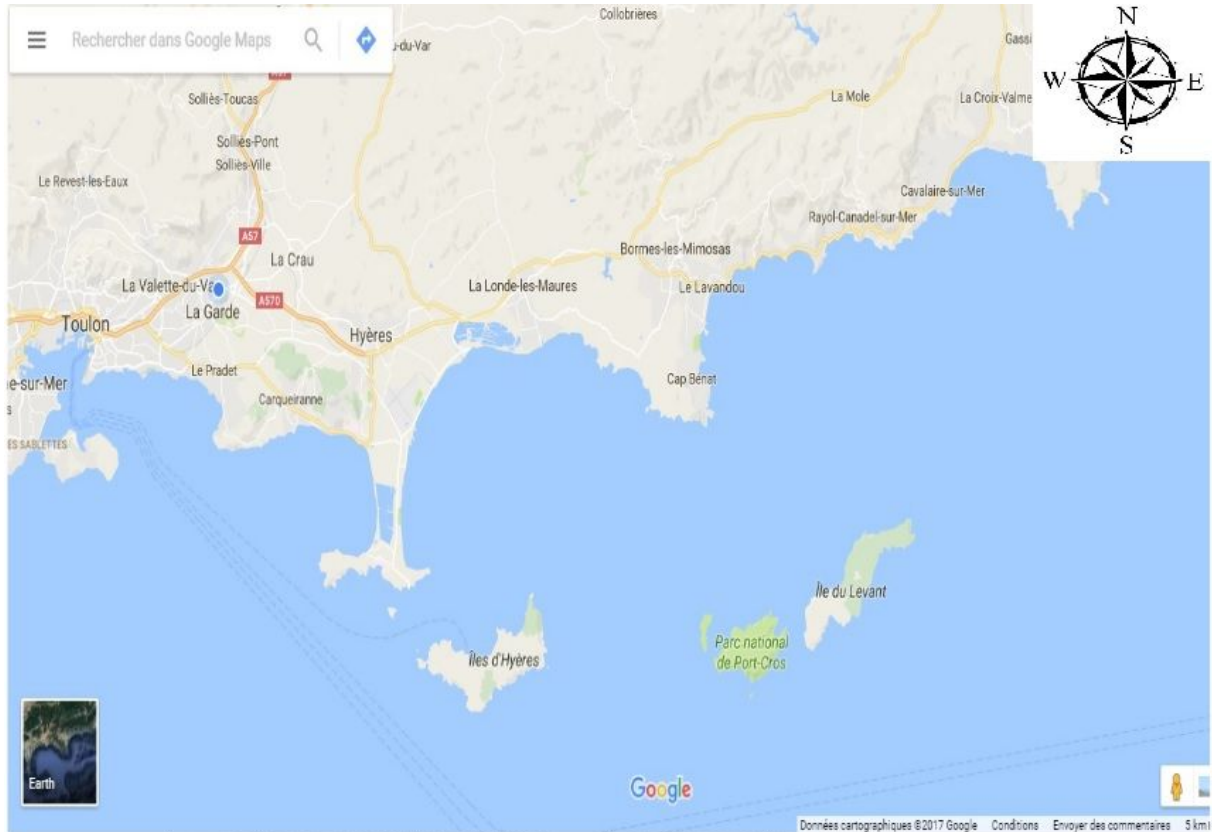


**Figure II.5:** Google map showing the three islands which surround the coastal zone of the city of Hyeres. Port-Cros , Le levant , Porquerolles, Presqu'île de Giens

There is a wastewater treatment plant WWTP at the city of Hyeres which is not found in the watershed of the Gapeau river. This wastewater treatment plant has the name STEP d'Hyères-Carqueiranne.

## II.2 Solar Irradiation Experiments


### II.2.1 Sampling Sites

The Gapeau river birth at the Signes city ( $43^{\circ} 17' 24''$  N,  $5^{\circ} 52' 59''$  E) and run till the sea water in the city of Hyères ( $43^{\circ}06'42''$  N,  $6^{\circ}11'33''$  E) in the southeastern part of France (figure II.6). The Gapeau river has a mean flow discharge of  $4.13 \text{ m}^3/\text{s}$ , a length of 47.5 km



and a water catchment of 544 km<sup>2</sup> (Ducros et al., 2018) with a pluvial hydrological regime. The endmember river water (RW) was sampled along the river roughly 500m before the wastewater treatment plant which is located at ( 43°08'38.6"N 6°05'36.1"E) where the wastewater treatment plant endmember was sampled at its output. The wastewater treatment plant (WW) of the city of La Crau has a daily volume of 14,500 m<sup>3</sup>/day (mean 0.17 m<sup>3</sup>/s) and serves 80,000 population equivalents. It inputs a treated wastewater effluent directly to the Gapeau river of the following characteristics : BOD<sub>5</sub>= 15 mg/L, COD<sub>5</sub>=50 mg/L, suspended solids= 20 mg/L (source of these data : a private report from this WWTP of La Crau). The sea water (SW) endmember was sampled at the coastal area of the city of Hyeres at roughly seven meters far from the beach ( 43°06'10.4"N 6°10'38.3"E ). Plastic bottle of one liter (cleaned with ethanol 100% and three times rinsed with 18.2 MΩ at 25 °C MilliQ water) were used to sample one liter of each endmember mixing component. Eight sampling cruises were conducted for each photochemical sunlight irradiation experiments, the sampling dates corresponding to each irradiation experiment are shown in table II.1.

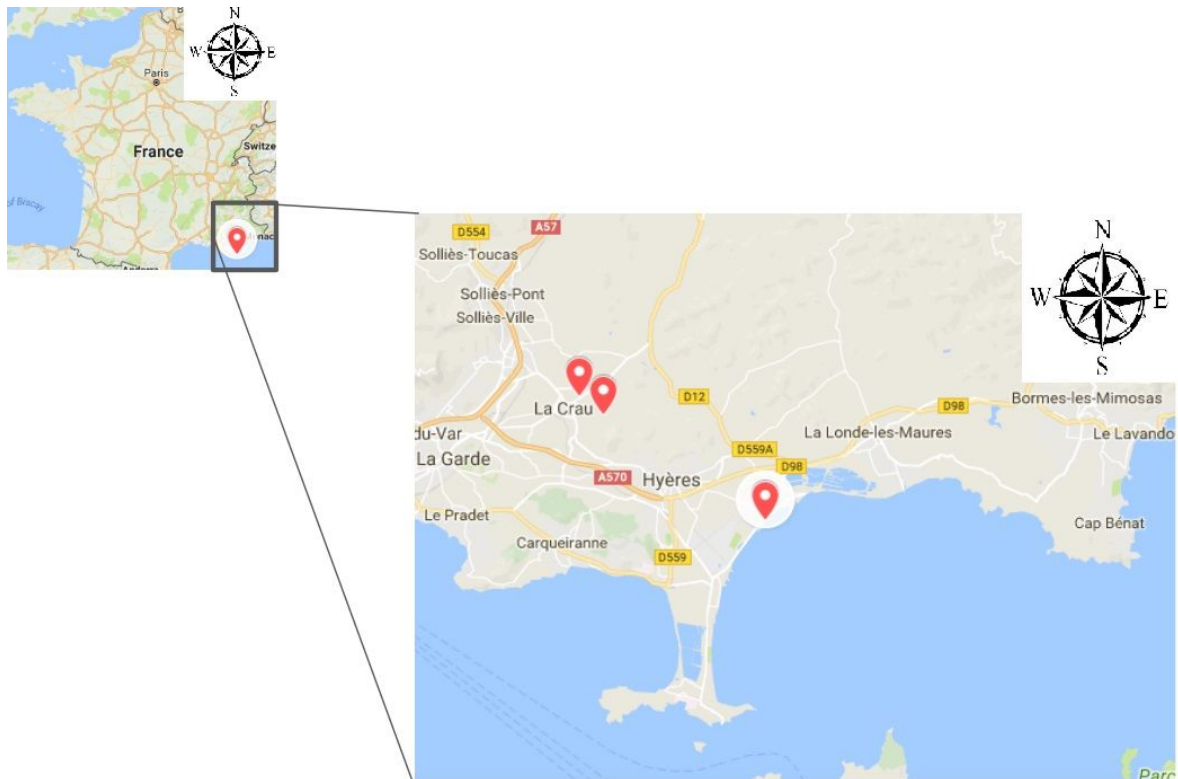
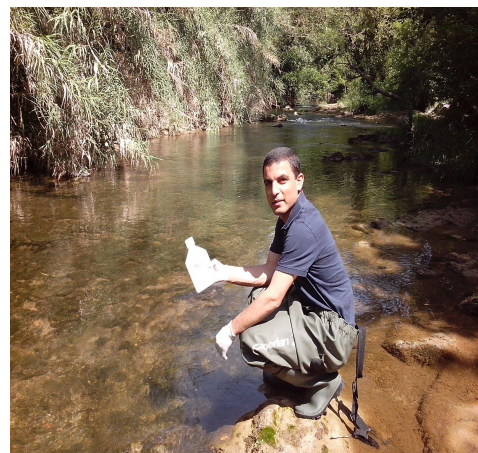


**Figure II.6:** Map showing approximate locations of the study area and the sampling sites of the three endmember mixing components from upward to downward , the Gapeau river , the wastewater treatment plant of the city of la Crau and the Sea water at the city of hyeres ( Rade d’Hyeres) . (  ) shows where samples were collected . Map made by using Google Maps™ a web mapping service.

The following figure (figure II.7) shows some pictures of three endmembers ( Gapeau river , Wastewater treatment plant of La Crau , Seawater at St.Louis at Hyeres city) used for the solar irradiation experiments

**Gapeau  
river**



**WWTP of  
La Crau**



**Sea at  
Hyeres (St.  
Louis)**



**Figure II.7:** Pictures of the sampling of the three endmember for the solar irradiation experiments . Pictures shows also the bottle used in the sampling campaigns



## II.2.2 Irradiation experiments

The effect of solar irradiation on the photodegradation of FDOM was first conducted by doing the filtrations and after that, the biodegradation of the FDOM, meaning the role of the bacteria on the degradation of these anthropogenic FDOM, was conducted by not doing the filtration of the three endmember mixing components (RW, SW and WW) mentioned in this study. Dates of the experiments are as follows:

**Table II.1** : All of solar irradiation experiments and their corresponding dates and state of filtration of Endmembers

Experiment	Beginning Date	End Date	Sampling Date	cruise	Experiment Type According to Filtration	Exp. according to table II.3.	No.
1 <sup>st</sup>	26-05-2015	05-06-2015	26-05-2015		All WW, SW and RW water are filtered	1	
2 <sup>nd</sup>	22-06-2015	04-07-2015	19-06-2015		All WW, SW and RW water are filtered	1	
3 <sup>rd</sup>	10-07-2015	17-07-2015	07-07-2015		All WW, SW and RW water are filtered	1	
4 <sup>th</sup>	27-08-2015	11-09-2015	26-08-2015		All WW, SW and RW water are filtered	1	
5 <sup>th</sup>	10-11-2015	20-11-2015	09-11-2015		Only WW not filtered	4	
6 <sup>th</sup>	03-12-2015	17-12-2015	30-11-2015		Only RW not Filtered	2	
7 <sup>th</sup>	15-02-2016	04-03-2016	12-02-2016		Only SW not filtered	3	
8 <sup>th</sup>	11-05-2016	27-05-2016	09-05-2016		All, WW, SW and RW are not filtered	8	

## II.2.3 Materials of irradiation experiment

Fifteen quartz tubes of 50 mL capacity were used to produce the mixtures within them. Another fifteen normal dark glass tubes were used to produce the same mixtures and be used as control samples. Wooden planck was used, as it is shown in **Figure II.8**, to hold the quartz tubes for the irradiation experiments and was put on the roof of MIO Laboratory.



**Figure II.8:** Image showing the installation of the wooden plank on the roof of the MIO laboratory (Ex-Protee) ( $43^{\circ} 08' 11.2''$  N  $6^{\circ} 01' 16.7''$  E).

Ice box was used to put the dark tubes within it for the control experiment near the experiment to have the same temperature conditions without the light exposition. Eight sampling cruises were conducted for the irradiation experiments .

## II.2.4 Filtration/without filtration mixture

Depending on the experiment (table II.2), all or part of the endmember sample was filtered using Millipore filters Type GNWP  $0.20\ \mu\text{m}$ , 47 mm diameter and filtration kit was previously cleaned by acidified water ( $10\% \text{HNO}_3$ ). The filtered waters of each endmember mixing components were put in a novel one liter glass bottle (pre-rinsed with  $10\% \text{HNO}_3$  and 3 times with  $18.2\ \text{M}\Omega\cdot\text{cm}$  at  $25\ ^{\circ}\text{C}$  MilliQ-water) and transferred to the refrigerator at  $4\ ^{\circ}\text{C}$  in the dark. The filtrate were used for the preparation of the mixtures in the following day. For the river water and the sea water, one filter was needed to filter one liter water bottle while two Millipore filters were needed for the wastewater for treatment plant indicated that there

was a bigger amount of dissolved organic matter or biological matter in this treated wastewater.

**Table II.2:** Types of irradiation experiments according to which endmember was filtered .  
Bold means that the irradiation experiment was conducted in the present works of this PhD thesis where non bold means the experiment was not conducted

<b>Experiment Number</b>	<b>River water</b>	<b>Sea Water</b>	<b>TWW water</b>
<b>1</b>	<b>F</b>	<b>F</b>	<b>F</b>
<b>2</b>	<b>NF</b>	<b>F</b>	<b>F</b>
<b>3</b>	<b>F</b>	<b>NF</b>	<b>F</b>
<b>4</b>	<b>F</b>	<b>F</b>	<b>NF</b>
5	<i>NF</i>	<i>NF</i>	<i>F</i>
6	<i>NF</i>	<i>F</i>	<i>NF</i>
7	<i>F</i>	<i>NF</i>	<i>NF</i>
<b>8</b>	<b>NF</b>	<b>NF</b>	<b>NF</b>

Only five types of the irradiation experiments mentioned here in this table were conducted. these types are the first four experiments and the last one which is number eight. The irradiation experiment number 1 was conducted four times to insure the reproducibility of the degradation of the fluorescence signal results. The experiment number 3 was conducted for a long period which lasted three weeks because it was conducted in the winter period in which not so much solar irradiation amounts were received by the irradiated quartz tubes. The exact types of irradiation experiments are shown and indicated in table II.2. Further works are needed to conduct these experiment to further our knowledge on the effect of particles of one endmember on the photodegradation of fluorescence of the mixtures.

## II.2.5 Preparation of the mixtures

The sixteen quartz vials were washed with osmosis water then transferred to an acid bath (nitric acid 10%  $\text{HNO}_3$ ) for twenty four hours then washed with 18.2  $\text{M}\Omega\cdot\text{cm}$  at 25 °C Milli Q-water . Then the quartz vials were inserted in an oven at 450 °C for twenty four 24 hours in order to be sure that there are/remains no traces of dissolved organic carbon to make sure that we get reliable results after that for the next experiment data collection. Fifteen mixtures were made according to ternary mixing diagram (Fig. II.9) which enables the visualization of the mixing percentages (content fraction) of three endmember mixing components. The exact mixing percentages of the three types of waters are summarized in table II.3 and the exact mixing taken by weights are shown in table II.4. Each indicated percentage of the three endmember mixing components was taken by weight, assuming a density of 1.0, 1.0 and 1.025 for the WW, RW and SW respectively. And the number of the quartz vial was given after each mixing according to the same table (table II.4).

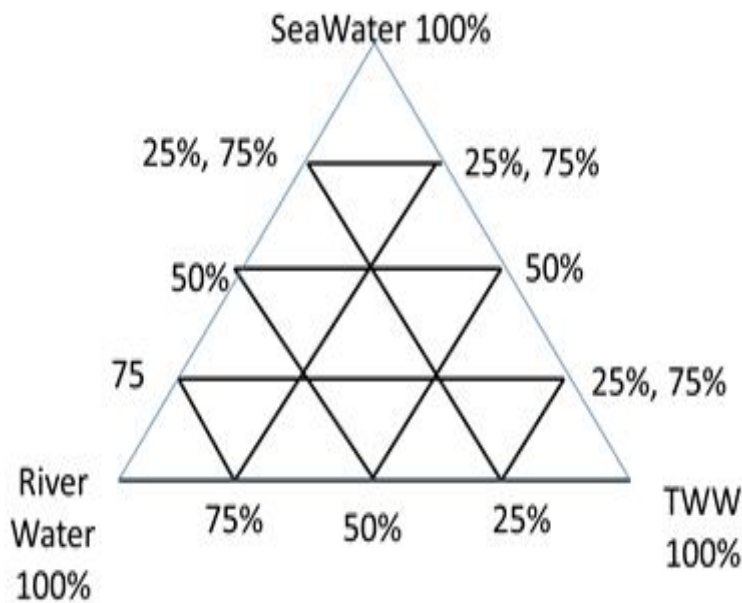


**Figure II.9:** Ternary diagram of the mixing percentages of three endmember mixing components (freshwater (RW), wastewater treatment plant (WW), seawater (SW)). Each intersecting point represents a solution that contains the mentioned and calculated percentages of each water source (endmember).



**Table II.3** The percentages in solution of each endmember mixing components of the fifteen samples used in this study

Endmember	Sample Number	1	2	3	4	5	6	7	8	9	10	11	12	13	14	15
River Freshwater		100	0	0	75	50	25	75	50	25	0	0	0	50	25	25
Sea water		0	100	0	25	50	75	0	0	0	25	50	75	25	25	50
WWTP water		0	0	100	0	0	0	25	50	75	75	50	25	25	50	25

**Table II.4** The percentages in solution of each endmember mixing components of the fifteen samples used in this study taken by weight in mg

Endmember	Sample Number	1	2	3	4	5	6	7	8	9	10	11	12	13	14	15
River Freshwater		50	0	0	37.5	25	12.5	37.5	25	12.5	0	0	0	25	12.5	12.5
Sea water		0	50	0	12.5	25	37.5	0	0	0	12.5	25	37.5	12.5	12.5	25
WWTP water		0	0	50	0	0	0	12.5	25	37.5	37.5	25	12.5	12.5	25	12.5

Each bottle of these quartz bottles were shaken gently by hand after the production of the mixtures in order to insure the homogeneity of the mixtures (having a homogenous solution).

## II.2.6 Exposing the mixtures to Sunlight

After the preparation of the mixtures, the 50 mL quartz vials were transferred and put in a wooden plank on the roof of the lab to be exposed to sunlight. The wooden plank was designed by Christian Martino, a member of the laboratory MIO (ex-PROTEE) responsible for designing the instrumentation for the experiments conducted by the laboratory. Sixteen circular opening corresponding to the size of the cap of the quartz tube were cut in the wooden plank to insure stable standing of the quartz tubes and to insure controlled conditions for the irradiation experiments. The solar irradiation of the whole (15 samples) was done for different durations of time which ,according to the meteorological conditions, affects the amount of received sunlight radiation (insolation) at the surface of the planet earth. The

irradiation dates for each irradiation experiment and the corresponding duration of irradiation are summarized in the table II.1.



**Figure II.10:** Picture showing the quartz tube put upside down in a wooden plank on the roof of the laboratory MIO (ex-PROTEE) at the Universite de Toulon ; for solar irradiation for different periods of time .

The quartz vials were put in wooden plank at sufficient distance to insure that each quartz vial receive the same amount of sunlight exposure energy. In addition, the wooden plank was used to make sure that the quartz vials are stable and to avoid the effect of strong wind in the winter and cloudy days. For all of the irradiation experiment except irradiation experiment where all the water sources (endmember) are filtered (river water is filtered ,seawater is filtered , WWTP effluent is filtered) , control samples were prepared in dark bottles and put in an icebox (doesn't contain ice) and was put beside the wooden plank on the roof of the laboratory.



## II.2.7 Experiment notation/codification :

Each photodegradation experiment concerns a 15 mixed samples with no, total or partial filtration of endmember. The following notation Ixyz was used to codify them, where x, y z correspond to the RW, SW and WW endmember respectively and indicate that the endmember is filtered with a value of 1. As an example, the experiment code I101 corresponds to the irradiation experiment in which the RW and WW endmember mixing components are filtered while the SW is not. More understanding of this notation could be withdrawn from table II.5

**Table II.5** : Dates of irradiation experiments.

Experiment Type	Start Date	End Date	Reference
RW-F SW-F WW-F	28-08-2015	11-09-2015	I111
RW-F SW-F WW-NF	10-11-2015	20-11-2015	I110
RW-NF SW-F WW-F	3-12-2015	17-12-2015	I011
RW-F SW-NF WW-F	15-02-2016	04-03-2016	I101
RW-NF SW-NF WW- NF	11-05-2016	27-05-2016	I000

\*RW: River, SW: Sea water, WW :Treated wastewater, F and NF correspond to the filtration state of each (endmember). F means Filtered , NF means NonFiltered.

## II.2.8 Preparation of chemical actinometer

It was programmed to measure the flux of photon by using a chemical actinometer. Potassium ferrioxalate ( $K_3Fe(C_2O_4)_3 \cdot 3H_2O$ ) was bought which was synthesised and purified by recrystallization ([Hatchard and Parker 1956](#)) and chosen as a chemical actinometer to measure the amount or the quantity of the received solar exposure of the samples (photonic



flux). The chemical actinometer measures the photonic flux of the sun or any light source based upon a photochemical reaction in which in our case the redox state of the iron ions is changed upon the absorption of a quantum of light according to the following photochemical reaction



Due to the fact that the quantum yield of the production of reduced iron ions has a value of 1.25 at 253.7 nm and it varies not so much between 200 nm and 400 nm; the actual reduced iron concentration is quantified using colorimetric method of the O-Phenanthroline at 510 nm ([Bowman and Demas 1976](#)). The coefficient of molar extinction of the complex/ligand  $\text{Fe}^{2+}$ /O-Phenanthroline is equal to 11,530 L mol<sup>-1</sup>cm<sup>-1</sup>. The photonic flux could be calculated through the following equation ([Braun et al. 1986](#))

$$[C] - [C_0] = \Phi / V * P_0 t$$

Where : [C] ; the concentration of the compound C at time t (mol/L); [C<sub>0</sub>] = concentration of compound C at time = 0 (mol/L); Φ : the quantum yield of the photolysis of compound C at the irradiation wavelength; P<sub>0</sub> = Photonic flux of the irradiated solution (einstein/s) (1 Einstein = 1 mole of photons); V : volume of the irradiated solution in L.

A known amount (0.10648 g) of potassium ferrioxalate was weighted using a small weighing shoe on a sensitive balance of 0.1 milligram sensitivity. Then it was transferred to a 100 mL volumetric flask and milli-Q water was added to the mark. After that, the solution was left for fifteen minutes on a magnetic stirrer to insure the homogeneity of the solution. Fifty milliliters were transferred to a quartz tube. This quartz tube which contains the potassium ferrioxalate solution was also put with the other quartz bottles on the roof of the laboratory.

Unfortunately, the reduction reaction of the iron ions in this chemical actinometer (potassium ferrioxalate) was run fast and we couldn't use this actinometer properly to the determination of the photonic flux of the sun for each solar irradiation experiments for comparison purposes as it can be seen **Figure II.11**. Some example values of the absorbance of the actinometer

solution are shown in table II.6. Therefore, we opted to use a physical actinometer as described in the next section.

**Table II.6** : table showing the absorbance values of the solution for the measurement of the iron ions  $\text{Fe}^{2+}$  in the irradiated potassium ferrioxalate solution using colorimetric method of the O-Phenanthroline at 510 nm ([Bowman and Demas 1976](#))

Date	Absorbance
25-05-2015	0.116
30-05-2015	0.267
01-06-2015	0.285
02-06-2015	0.255
03-06-2015	0.249
04-06-2015	0.306



**Figure II.11** : Image showing the coloration of the actinometer solution (Potassium Ferrioxalate) which occurred very fast in the same day of the installation of the irradiation experiment

## II.2.9 Preparation of solar energy sensor : Physical actinometer

A solar panel charging a battery (Solar Cell 9V/109 mA) (fig. II.12) with a data logger was bought and then programmed to measure the solar exposure amount in volts every two minutes. This solar panel charging a battery was put on the roof of the laboratory one day before going to the sampling sites for sampling. This solar energy sensor is a physical actinometer in which it measures the photonic flux (the received photonic energy per unit of time) based upon the photoelectric effect of Albert Einstein without the need for a photoreaction to occur.

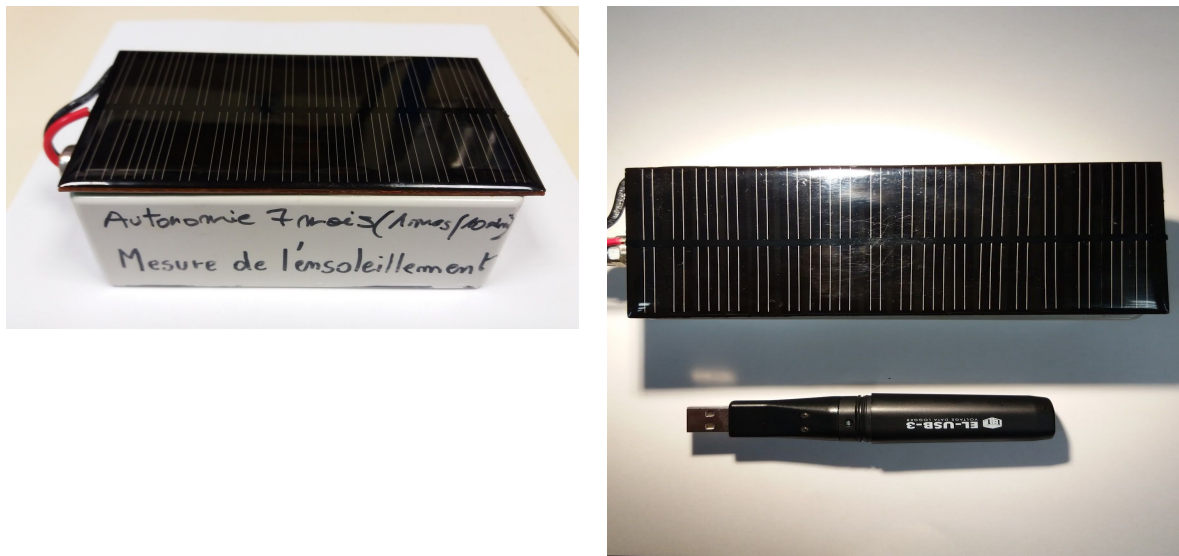


**Figure II.12:** The solar panel in the right and the data logger inside the small box, in the picture in the left , a birds' eye view of the solar panel and the USB data logger .

On the same time, the daily insolation data were asked to MétéoFrance ([www.meteofrance.com](http://www.meteofrance.com)) which is a french service of meteorological affaires. Data required were from the measuring stations at two cities near to the city of La Garde which were : the city of Nice and the city of Marignane. Linear regression analysis was carried and conducted to have the relationship between the data from the solar energy sensor and the MétéoFrance data in order to use this relationship to find data for the photochemical sunlight irradiation experiment at which there was no data from our solar energy sensor. Correlations were strong as shown in the following figure (figure II.13).

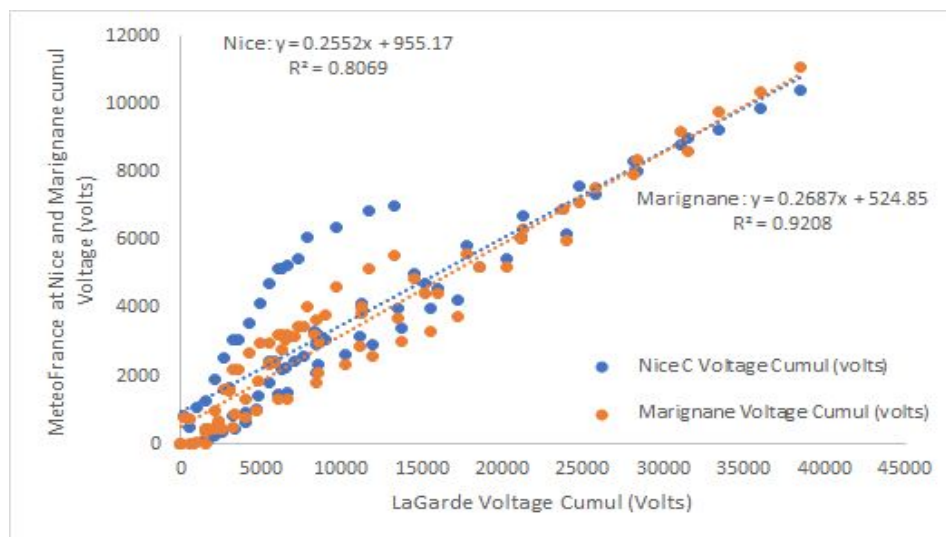


**Figure II.13:** Correlations between insolation data of Météo-France and insolation from our solar cell physical actinometer . Blue points and line : correlation between nice and La Garde. Orange points and dotted line : correlation between insolation of Marignane and La Garde.

### II.2.9.1 The Relationship between our physical actinometer and Météo-France data

It can be seen from figure II.13 that there are two existing linear regression equations with their corresponding correlation coefficients. The blue full circles marker points represent the points between the data of insulations measured in volts by our physical actinometer and the data of insolation measured in volts measured by Météo-France [www.meteofrance.com](http://www.meteofrance.com) at the city of Nice , southeastern of France . The blue dotted line represents the linear regression

line between our insolation data in volts measured at the roof of our laboratory MIO , universite de toulon at the city of La Garde and the insolation measurements at the city of Nice with the linear regression equation indicated at the upper left which is  $y = 0.26 x + 955.17$  with a correlation coefficient  $R^2 = 0.81$  . The orange full triangle marker points in the graphed chart represent the dotted lines between our insolation data measured in volts by our physical actinometer and the insolation data measured in volts by Météo-France [www.meteofrance.com](http://www.meteofrance.com) at the city of Marignane which is a suburb of the city of Marseille , southeastern France. The orange dotted line represents the linear regression line between our measured insolation data in volts by our physical actinometer (solar cell sensor) measured at the roof of our laboratory MIO (Mediterranean Institute of Oceanography) , Université de Toulon at the campus of the city of La Garde . This linear regression equation is indicated at the middle of the graphed chart which is  $y = 0.27 x + 524.85$  with a correlation coefficient  $R^2=0.92$  where y represents the insolation in volts of the measuring station of Météo-France [www.meteofrance.com](http://www.meteofrance.com) at the city Marignane and x represents the values of insolation in volts measured at our laboratory MIO (Mediterranean Institute of Oceanography) , universite de Toulon measured at the city of La Garde.

For most of the photochemical sunlight irradiation experiments, we had the measured data from our physical actinometer except for the photochemical sunlight irradiation experiment codified I111 from 28 august 2015 to 11 september 2015. After asking for the insolation/irradiance data for all of our photochemical sunlight irradiation experiments from Météo-France [www.meteofrance.com](http://www.meteofrance.com) from the nearest measuring stations to our laboratory situated at the city of La Garde which turned out to be the city of Nice, southeastern France and the city of Marignane , suburb of Marseille , southeastern of France . And after getting these insolation data , we regressed all of our existing insolation data with their corresponding insolation data from Météo-France for the two datasets (Nice , Marignane) leaving the insolation data for the codified experiment I111 ( 31-aug-2015 to 11-sept-2015) from Météo-France aside without involving them in the insolation data used to make the linear regression . After having the two corresponding linear regression equations described in the above part of this section . We used the linear regression equation with the measuring station at the city of Marignane to make predictions for our missing physical actinometer insolation data for the photochemical sunlight irradiation experiment codified

I111 (31-aug-2015 to 11-sept-2015) because the correlation coefficient ( $R^2=0.92$ ) turned out to be greater than that of Nice. By transforming the Marignane

After data treatment, Météo-France insolation were extrapolated into physical actinometer values using the following regression equation :

$$x = (y - 524.85) / 0.27 \quad \text{or in other terms} \quad \text{Ins}^{\text{LaGarde}} = (\text{Ins}^{\text{Marignane}} - 524.85) / 0.27 \quad (\text{eq.}\#)$$

By substituting for y values by the values of insolation in volts from the Météo-France at Marignane, we got our predicted values of insolation in volts for the photochemical sunlight irradiation experiment codified I111 (28-aug-2015 to 11-september-2015). These insolation data in volts were used for further data analysis in this present study.

## **II.2.10 Excitation Emission Matrix fluorescence spectroscopy**

After the preparation of the mixtures described in the ternary of mixtures, 3 ml were sampled for the measurement of excitation emission matrix of fluorescence and these aliquots (the sampled 3 ml from each corresponding quartz vial) constituted time zero measurements. However, some of the irradiation experiments, there was no time zero measurements.

### **II.2.10.1 Sampling the quartz vials**

The next day (after the start date of each irradiation experiment) , 3 ml was taken as aliquots of each quartz vial (which are 15 quartz vial corresponding to 15 different mixtures ) and transferred to 3 mL quartz cuvettes in a 16 cuvettes rack. Sodium azide (100  $\mu\text{L}$  of 1M  $\text{NaN}_3$ ) was added to the cuvettes in order to stop the biological/microbial activity and to kill all the living microbes in the solution for the irradiation experiments in which at least one water source is not filtered whereas for the experiment in which all the sources are filtered (I111), we made a convention that there is no microbial activity due to filtration and all the microbes were taken away from solution by the filter (we chose to do so arbitrary without verifying it) .

**Table II.7** : Table showing whether or not a solar irradiation experiment had a control group. In addition to the mode of measurements

<b>Irradiation Experiment</b>	<b>Control / dark incubation</b>	<b>Fluorescence measurement</b>
I111	No control/dark incubation	No Alteration between odd and even samples
I110	yes	Alteration between odd and even samples from day to day of measurement
I011	yes	Alteration between odd and even samples from day to day of measurement
I101	yes	Alteration between odd and even samples from day to day of measurement
I000	yes	Alteration between odd and even samples from day to day of measurement

Most of the fluorescence measurement were done in the evening and beginning of the night because the fluorescence apparatus (spectrofluorimeter) was occupied by other laboratory users. Therefore, we couldn't measure 3D EEM fluorescence of all of the fifteen 15 mixtures for both the solar irradiation experiment and its corresponding 15 mixtures of the control/dark incubation at the same time or at the same day or even in a consecutive days. Because of that, we chose to make an alteration between the sample; that is to say, we measured the odd numbered irradiated samples and the remaining samples were the even numbered control/dark incubation samples and the following measurements were the inverse thing , that is to say , (even numbered irradiated samples + odd numbered control/dark samples). Table II.7 shows the solar irradiation experiments in which such alteration was done.

### **II.2.10.2 Three dimensional excitation emission matrix (3D EEM) acquisition**

The fluorescence was measured using a Hitachi F-4500 fluorescence spectrophotometer, which is equipped with a double excitation monochromator, a single emission monochromator, and a photomultiplier assembly. It is also equipped by a 16 cuvette cells holder (torelle), enabling the measurement of 16 samples in automatic mode. In the 16 cells one is systematically occupied by an ultrapure water cell from Perkin Elmer which is used as reference to check the spectrofluorimeter stability. Two methods of fluorescence data

acquisition were used, the 1<sup>st</sup> one is called “Elnahhal” (EN) method and the 2<sup>nd</sup> one is named “Croatie” (CR) which are arbitrary names to distinguish between them. In the following figure (figure II.14), the general mode of EEM acquisition is summarized.

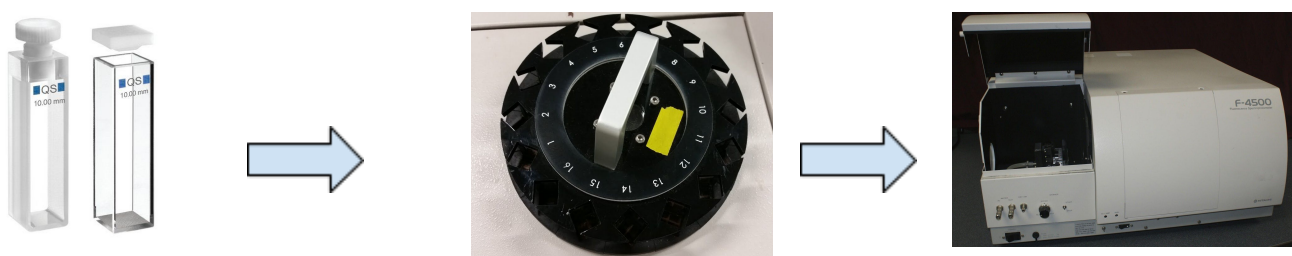


**Figure II.14** : Pictures showing the quartz cuvettes, the “tourelle” and the F-4500 spectrofluorometer. The arrows shows the sequence of measurement.

#### II.2.10.2.1 First EEM data acquisition : “Elnahhal” method

Three dimensional excitation emission matrices EEMs of fluorescence measurements were performed using a spectrofluorometer (F-4500, Hitachi, Japan) at a PMT voltage of 700 V for the method of data acquisition “Elnahhal”. “Elnahhal” method has shorter wavelengths for both excitation and emission range which are to have a closer look on the protein-like fluorescence. Emission spectra were collected at 5-nm intervals between 220 and 420 nm, while excitation spectra were measured between 200 and 400 nm at 5-nm intervals. The scan speed was set 2400 nm/mn. The slit widths for both excitation and emission wavelengths were set at 5 nm. The method focuses on the protein like fluorophores with a smaller Ex/Em step increment in the way to detect more accurately the proteins. Results from this method were be annotated \_EN. All fluorescence intensity data were presented in arbitrary units.

#### II.2.10.2.2 Second EEM data acquisition: “Croatie” method

Three dimensional excitation emission matrices EEMs of fluorescence measurements were performed using a spectrofluorometer (F-4500, Hitachi, Japan) at a PMT voltage of 700 V for the method of data acquisition Croatie. This croatie method has longer wavelengths on both the excitation and the emission in order to have a comprehensive view on the fluorescence of



the fluorescent dissolved organic matter and its corresponding fluorophores. The emission spectra were collected at 5-nm intervals between 200 and 800 nm for the “Croatie” method, while excitation spectra were measured between 200 and 600 nm at 5-nm intervals for the 2<sup>nd</sup> method of acquisition and the scan speed was 2400 nm/mn. The slit widths for both excitation and emission wavelengths were set at 10 nm. This method focuses on a larger domain of  $\lambda_{\text{Ex}}/\lambda_{\text{Em}}$ , using a high step increment. Results from this method were annotated \_CR. All fluorescence intensity data were presented in arbitrary units. “Elnahhal” method and “Croatie” method are shown visually in the following figure (**Figure II.15**)

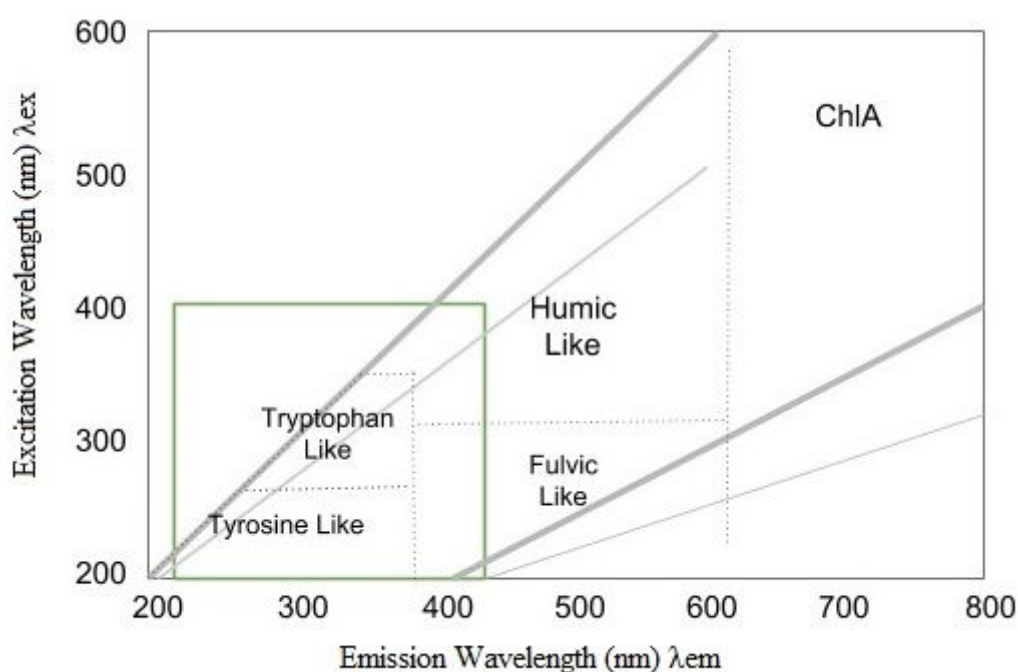


**Figure II.15:** The fluorescence landscape with the square inside showing the region of focus for the method of data acquisition named “Elnahhal” ( $\lambda_{\text{EX}}=200\text{-}400$  nm), ( $\lambda_{\text{EM}}=220\text{-}420$  nm) in green. The whole square shows the region of focus for the data acquisition named “Croatie” ( $\lambda_{\text{EX}}=200\text{-}600$  nm), ( $\lambda_{\text{EM}}=200\text{-}800$  nm) the whole picture. Vertical axis represents excitation wavelengths  $\lambda_{\text{EX}}$  and horizontal axis represents emission wavelengths  $\lambda_{\text{EM}}$

### II.2.10.2.3 Third data acquisition method : two dimensional fluorescence

Two dimensional fluorescence measurements were performed using a spectrofluorometer (F-4500, Hitachi, Japan) at a PMT voltage of 700 V. This method has one excitation wavelength and a range of emission wavelengths. The excitation wavelength was set at 250

nm for the whole range of the emission wavelengths. The emission spectra were collected at 1-nm intervals between 250 and 500 nm and the scan speed was 2400 nm/mn. The slit widths for both excitation and emission wavelengths were set at 5 nm. This method was used throughout the whole works of the present PhD Thesis; however, the results acquired using this method were not exploited due to the time factor although so many useful data could be derived from them.

The following figure (**Figure II.16**) summarizes the protocol of the irradiation experiments in short

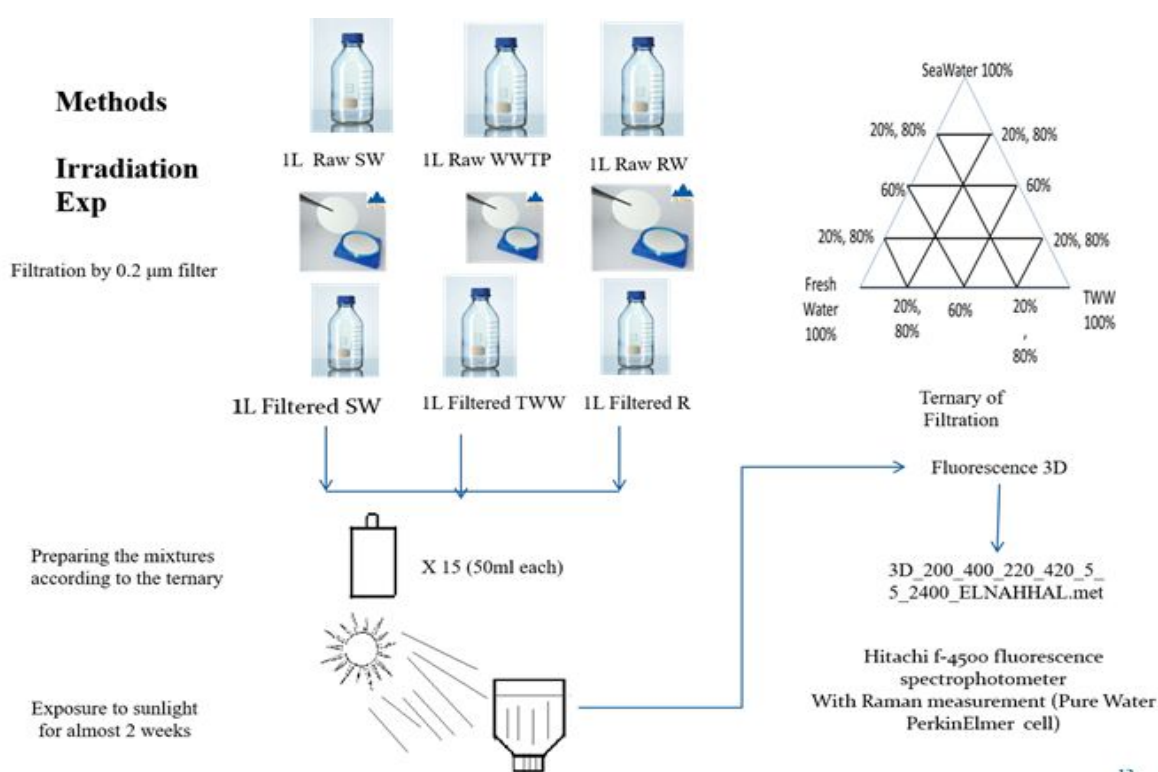


**Figure II.16** : The sunlight irradiation experiments protocol for all the experiments, in addition that another method of fluorescence data acquisition is used which is croatie which has a broader windows on both the excitation and the emission wavelengths.

## II.2.11 PARAFAC modelling of the data

The spectral contribution of fluorescent components to the total excitation emission matrix fluorescence was determined using the algorithm called CP/PARAFAC. More details about

CP/PARAFAC algorithm could be found in a tutorial in the literature ([Bro, 1997](#); [Colin A. Stedmon & Markager, 2005a](#)). The EEMs data sets were managed by Graphical User Interface (GUI) PROGMEEF software developed in MIO laboratory by Dr. Roland Redon (<http://protee.univ-tln.fr/PROGMEEF.html>) on the platform Matlab 2013a software and the N-way toolbox. As CP/PARAFAC deal only with trilinear model, the first step is to eliminate the dispersion signals. A cut-off filter was taken as 25 nm to eliminate the Raman and Rayleigh scattering according to the Zepp method ([Richard G. Zepp et al., 2004](#)) to avoid any effect on the CP/PARAFAC components number and in doing so, all of our EEMs were cleaned from the scattering and dispersion signals and got ready for further analysis. No inner filter correction was done because the samples has enough low absorbance value even though it was not measured by the UV-vis absorption spectroscopy. The PROGMEEF software was ordered to begin the decomposition starting from two and stopping at five components as a maximum number of CP/PARAFAC components, with 50 iterations. Nonnegativity constraints were applied for excitation and emission loadings. The accepted correct number of CP/PARAFAC components was the greatest number of CP/PARAFAC which fulfill the following criterion : the CONCORDIA score should be greater than or equal to 60%. No outliers were found or present in our dataset and three CP/PARAFAC components were found, chosen. This procedure of CP/PARAFAC modelling was used throughout the whole works of the present PhD thesis for the decomposition of the whole EEM datasets of all solar irradiation experiments. In addition, CP/PARAFAC modelling was done also for the purpose of decomposition of the temporal field experiment of the water sources (Wastewater treatment plant effluent , Seawater, Gapeau River water, and CONFLUENCE of Gapeau and Le Real Martin) in addition to the decompositions of EEM datasets of the part of the geographical field experiment. Table II.8 summarizes the results of the CP/PARAFAC analysis and modelling for the excitation emission matrices of all the works of the present PhD thesis.

**Table II.8** : Table showing the number of the EEM text files in each dataset of Elnahhal and Croatie for all the irradiation experiments and the temporal field experiment and the geographical field experiment. In addition their CP/PARAFAC analysis and modelling

Method of EEM acquisition	Experiment	Number of EEM text files in the dataset	Concordia score	Number of CP/PARAFAC components chosen
---------------------------	------------	---	-----------------	--

Elnahhal	Irradiation	963	80.75 %	3
Croatie	Irradiation	961	86.04 %	3
Elnahhal	Temporal field experiment	186	72.82 %	2
Croatie	Temporal field experiment	188	63.93 %	2
Elnahhal	Geographical field experiment	45	99.75 %	2
Croatie	Geographical field experiment	45	99.99 %	2

## II.2.12 Normalization of Contribution of CP/PARAFAC components of irradiation experiments

Once the CP/PARAFAC decomposition is done, the contributions of each CP/PARAFAC component were normalised to its maximum value of each irradiation experiment Ixyz separately, generally the initial one before the start of the photochemical irradiation experiments (time zero=not irradiated), to allow for the comparison of the evolution of the multilinear regression coefficients with irradiation time (see the following sections for more details). The normalization of each contribution of each CP/PARAFAC component was done according to the following equation :

$$c_i^{Ixyz, \%P, Tn} = C_i^{Ixyz, \%P(a,b,c), Tn} / [\max(C_i^{Ixyz, \%P(a,b,c), Tn}) \forall (n,a,b,c)] \quad (\text{eq.1})$$

Where :

$C_i^{Ixyz, \%P(a,b,c), Tn}$  is the value of the contribution of a given CP/PARAFAC component, i, which corresponds to a given photochemical solar irradiation experiment Ixyz and corresponds to a specific sample/mixture  $\%P(a,b,c)$  of endmember in corresponding day/time of irradiation, Tn, in that specific Ixyz photochemical sunlight irradiation experiment.

$\max(C_i^{Ixyz, \%P(a,b,c), Tn}) \forall (n,a,b,c)$  corresponds to the maximum contribution of a given CP/PARAFAC component in a known photochemical sunlight irradiation experiment Ixyz

for all the irradiation days,  $T_n$ , and for all the mixtures,  $\%P(a,b,c)$ , and the last phrase is expressed mathematically by the following expression  $\forall (n,a,b,c)$ .

The normalization of the contribution of any CP/PARAFAC component normalize the values to a percent value. However, it doesn't have any effect on the actual variation of the data. Figure II.17 shows the first CP/PARAFAC component contribution in the mixtures samples for day zero (Normalized and non-normalized contributions) as an example from the irradiation experiment I000 as an example for the effect of normalization on the CP/PARAFAC components. Moreover, the same variation of the data in our example could be clearly seen and observed in the next figure (figure II.18) where the normalized CP/PARAFAC component was put onto the secondary axis.

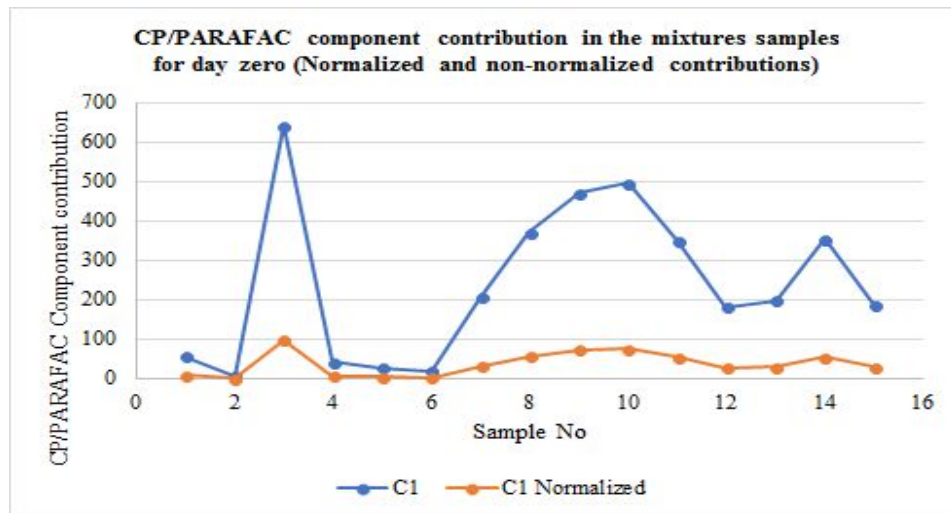


**Figure II.17** : Figure showing the first CP/PARAFAC component C1 contribution in the mixtures samples for day zero (Normalized and non-normalized contributions) as an example from the irradiation experiment I000

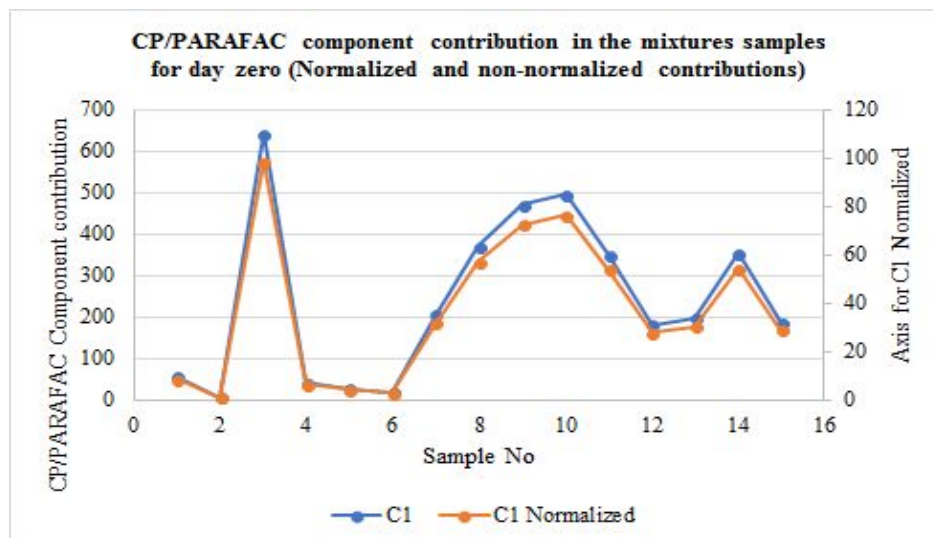


**Figure II.18** : Figure showing the first CP/PARAFAC component C1 contribution in the mixtures samples for day zero (Normalized and non-normalized contributions) as an example from the irradiation experiment I000 with the Contribution of C1 Normalized put onto the secondary axis.

### II.2.13 Multi-linear regression modelling of the CP/PARAFAC Components with two endmember mixing composition.

Multi-linear regression modelling of the CP/PARAFAC analysis results of each irradiation experiment was done using Microsoft Excel 2013 software and the Analysis toolPak add-in and the regression tool which enable the excel users to do simple linear regression as well as multi-linear regression modelling of data. The multilinear regression was done/conducted to calculate the coefficients in the general mathematical regression formula given here

$$Y = a_0 + a_1 * X_1 + a_2 * X_2 + \dots + a_n X_n \quad (\text{eq. 2})$$

In this work, this formula was reduced to  $n=2$ , in order that  $Y$  represents the contribution of each normalized CP/PARAFAC component in the results of each photochemical solar irradiation experiment and  $X_1$  and  $X_2$  were the two endmember mixing composition, seawater ( $f_{sw}$ ) and fresh/river water ( $f_{rw}$ ) in the sample, whereas, the impact of the mixing composition of the wastewater treatment plants (WWTP) endmember on the contribution of

each normalized CP/PARAFAC component was assumed to be taken into account in the constant (intercept) of the regression formula. The number of the independent variables in the multilinear regression equation is n, which in our case,  $n = 2$  which are the  $f_{SW}$  and  $f_{RW}$ .

The modification (changing the terms ) of the above multilinear regression equation (eq.1) was done to have the multilinear coefficients of the normalized contribution of the CP/PARAFAC component number i as follows:

$$c_i^{Ixyz,Tn} = A^{WW,Ixyz,Tn}_{i,0} + A^{WW,Ixyz,Tn}_{i,1} * f_{SW} + A^{WW,Ixyz,Tn}_{i,2} * f_{RW} \quad (\text{eq.3})$$

With  $i = 1, 2$  or  $3$  corresponds to the studied CP/PARAFAC component (e.g. C1, C2,.. etc ), Ixyz is the codified photochemical sunlight irradiation experiment, and Tn is the corresponding day number in that given sunlight irradiation experiment.

The explanation how did we get this expression  $A^{WW,Ixyz,Tn}$ , and why the superscript “WW” is their for all of the multilinear regression coefficients is found in the following paragraphs of this section.

Indeed, in the multilinear regression modelling of three endmember mixing model of freshwater/river water, RW, seawater, SW, and wastewater treatment plant, WW, endmember mixing components, content percentage of the third term is constrained by the two others because the total sum of the three content percentages should equal 100 by the following equation :

$$f_{SW} + f_{RW} + f_{WW} = 100 \quad (0 < f_i < 100) \quad (\text{eq.4})$$

Where  $f_{SW}$ ,  $f_{RW}$ ,  $f_{WW}$  are the percent fraction (content fraction) of seawater, river water (freshwater) and wastewater treatment plant endmember mixing components respectively. All the percent fraction obviously positive and less than or equal to 100.

Then :

$$f_{WW} = 100 - f_{SW} - f_{RW} \quad (\text{eq.5})$$

By substituting in the regression eq. 1 for  $f_{WW}$  where  $n=2$ , the different terms we obtain :

$$C_i = a_{i,0} + a_{i,1} * f_{SW} + a_{i,2} * f_{RW} + a_{i,3} * f_{WW} \quad (\text{eq.6})$$

Where  $C_i$  is the total contribution of the CP/PARAFAC component number  $i$ , and  $a_{i,1}$ ,  $a_{i,2}$ ,  $a_{i,3}$  the respective partial contribution to the value of contribution of  $C_i$  of the three endmember mixing components SW, RW and WW coefficients. By substituting for  $f_{WW}$  by its expression in the equation (eq.4) we obtain :

$$C_i = a_{i,0} + a_{i,1} * f_{SW} + a_{i,2} * f_{RW} + a_{i,3} * (100 - f_{SW} - f_{RW}) \quad (\text{eq.7})$$

$$C_i = a_{i,0} + a_{i,1} * f_{SW} + a_{i,2} * f_{RW} + a_{i,3} * 100 - a_{i,3} * f_{SW} - a_{i,3} * f_{RW} \quad (\text{eq.8})$$

By arranging the similar terms together and taking the common factor , we obtain :

$$C_i = (a_{i,0} + a_{i,3} * 100) + (a_{i,1} - a_{i,3}) * f_{SW} + (a_{i,2} - a_{i,3}) * f_{RW} \quad (\text{eq.9})$$

By giving a proper name/term for the constant and the new coefficients to account for the substituted for term which is  $f_{WW}$  as follows :

$$A_{i,0}^{WW} = (a_{i,0} + a_{i,3} * 100) \quad A_{i,1}^{WW} = (a_{i,1} - a_{i,3}) \quad A_{i,2}^{WW} = (a_{i,2} - a_{i,3})$$

We obtain the final multilinear regression equation as a function of two content fraction of two endmember mixing components :

$$C_i = A_{i,0}^{WW} + A_{i,1}^{WW} * f_{SW} + A_{i,2}^{WW} * f_{RW} \quad (\text{eq.10})$$

Where  $A_{i,0}^{WW}$  ,  $A_{i,1}^{WW}$  and  $A_{i,2}^{WW}$  represent the multilinear regression coefficients related to mixing equation when the  $f_{WW}$  (anthropogenic organic matter endmember) is expressed in terms of the content fraction of the other two endmembers ( $f_{RW}$  and  $f_{SW}$ ). The values of  $A_{i,0}^{WW}$  ,  $A_{i,1}^{WW}$  and  $A_{i,2}^{WW}$  for each day of irradiation for each solar irradiation experiment for the two methods of EEM data acquisition (Elnahhal and Croatie) were calculated and the results are put in Annex I.

One can remarks that by circular permutation we can obtain two other relations/formula, but none give the  $a_{i,0}$  coefficient independently which is the constant in the multilinear regression



equation of the mixing equation with the three endmembers used. If it could be calculated independently, the coefficients of all the three endmembers could be found and calculated.

$$C_i = (a_{i,0} + a_{i,2} * 100) + (a_{i,1} - a_{i,2}) * f_{SW} + (a_{i,3} - a_{i,2}) * f_{WW} \quad \text{or} \quad C_i = A_{i,0}^{RW} + A_{i,1}^{RW} * f_{SW} + A_{i,2}^{RW} * f_{WW} \quad (\text{eq.11})$$

With  $A_{i,0}^{RW} = (a_{i,0} + a_{i,2} * 100)$ ,  $A_{i,1}^{RW} = (a_{i,1} - a_{i,2})$  and  $A_{i,2}^{RW} = (a_{i,3} - a_{i,2})$  which represent the multilinear regression coefficients related to mixing equation when the  $f_{RW}$  (freshwater or river water endmember content fraction) is expressed in terms of the content fraction of the other two endmembers ( $f_{WW}$  and  $f_{SW}$ ). The values of  $A_{i,0}^{RW}$ ,  $A_{i,1}^{RW}$  and  $A_{i,2}^{RW}$  for each day of irradiation for each solar irradiation experiment for the two methods of EEM data acquisition (Elnahhal and Croatie) were calculated and the results are put in Annex II.

The last permutation is

$$C_i = (a_{i,0} + a_{i,1} * 100) + (a_{i,3} - a_{i,1}) * f_{WW} + (a_{i,2} - a_{i,1}) * f_{RW} \quad \text{or} \quad C_i = A_{i,0}^{SW} + A_{i,1}^{SW} * f_{WW} + A_{i,2}^{SW} * f_{RW} \quad (\text{eq.12})$$

With  $A_{i,0}^{SW} = (a_{i,0} + a_{i,1} * 100)$ ,  $A_{i,1}^{SW} = (a_{i,3} - a_{i,1})$  and  $A_{i,2}^{SW} = (a_{i,2} - a_{i,1})$  which represent the multilinear regression coefficients related to mixing equation when the  $f_{SW}$  (freshwater or river water endmember content fraction) is expressed in terms of the content fraction of the other two endmembers ( $f_{WW}$  and  $f_{RW}$ ). The values of  $A_{i,0}^{SW}$ ,  $A_{i,1}^{SW}$  and  $A_{i,2}^{SW}$  for each day of irradiation for each solar irradiation experiment for the two methods of EEM data acquisition (Elnahhal and Croatie) were calculated and the results are put in Annex III.

In the rest of this work, we decided to use the expression using  $f_{RW}$  and  $f_{SW}$ .

## II.2.14 Kinetics or Pseudo-Kinetics order determinations

Once the decomposition done, we have to observe the variation on the multilinear coefficient with the irradiation energy (insolation or irradiance) or in other words as a function of the solar irradiance, meaning :

$$A_{i,0}^{WW, Ixyz} (V)$$

$$A_{i,1}^{WW, Ixyz} (V)$$

$$A_{i,2}^{WW, Ixyz} (V)$$

Where  $V$  is the received irradiation energy (insolation/irradiance) in Volts (V), detected by our physical actinometer (solar cell sensor) or calculated from the linear regression equation developed in this study between our data of the physical actinometer and the data from MeteoFrance (Marignane Station). Hence it is possible to reconstruct the CP/PARAFAC contribution during irradiation experiment as a function of the mixing composition of two endmember :

$$c_i^{I_{xyz}}(V) = A^{WW, I_{xyz}}_{i,0}(V) + A^{WW, I_{xyz}}_{i,1}(V) * f_{SW} + A^{WW, I_{xyz}}_{i,2}(V) * f_{RW}$$

This equation enables us to predict and calculate the contribution of a given CP/PARAFAC component in a known mixture (two endmembers) at a known irradiation time (substituted for here in our case by the data in volts corresponding to the insolation data) .

By using this parameter, it is then possible to predict the EEM response of a given mixture  $P\%$ , during received irradiation,  $V$  as :

$$EEM^{I_{xyz}, \%P}(V) = c_1^{I_{xyz}, \%P}(V) * EEM_{C1} + c_2^{I_{xyz}, \%P}(V) * EEM_{C2} + c_3^{I_{xyz}, \%P}(V) * EEM_{C3} \quad (\text{eq. 14})$$

## II.3 Geographical field experiment

Three field trip were conducted on the flowpath of the Gapeau River starting from a distance of 500m before the wastewater treatment plant La Crau till the leisure harbor “marina” of the river Gapeau at the sea in the coastal zone of the city of Hyeres to follow the path of the fluorescence signal and its development through its way till the sea and what it undergoes such as photodegradation and biodegradation.

### **Geographical variations of the fluorescence of the anthropogenic dissolved organic matter**

#### **II.3.1 Choosing the sampling sites**

The sample sites were chosen roughly using google maps site on the internet. Four sites were chosen on the estuary mixing zone (we chose the word “estuary” to describe the area of

interaction between the freshwater river and the seawater even though the Gapeau river doesn't have an estuary nor a delta and it just has a river mouth directly into the sea), then another site was chosen after the confluence of the river gapeau and the tributary Réal Martin and a sampling site was chosen before the wastewater treatment plant. List of the sampling sites on the path of the Gapeau river are shown in table II.10. A reconnaissance cruise was done before to get sure of the chosen sites on google maps (figure II.19), the fourteen samples sites coordinates are shown in table II.10. A first sampling cruise was done to get acquainted with the sampling sites which were previously chosen on a maps. The fourteen samples were taken in the path of the river gapeau till the estuary (Hyères harbour) and the sea (Figure II.19). In between point 9 and 10, there is a salt barrier (anti-salt dam = Barrage anti-sel in french) which is used to stop the advancement of the sea water into the river (resisting the sea water intrusion). The sampling cruises were done twice in different days during the month of August, 2016. The exact dates and corresponding day of week of the sampling campaigns of the two geographical field experiments are shown in details in table II.9. The sampling was done in 60 mL bottles which were rinsed with deionized water (18.2 M $\Omega$  Milli-Q at 25 °C, millipore water rinse) a day before each cruise to get rid of any particulate matter. Then, the bottles were rinsed with the river water along its path three times to ensure a high signal over noise ratio and to be sure that this sampled water represents completely the river water. The first sample was taken using a one liter bottle and handle stick in order that a homogeneous and representative sample is taken. Samples were annotated depending on their location using GAxx and GBxx respectively for the sample of the geographical field experiments sampling campaign, with xx the location number mentioned in table II.10. Some photos of the sampling campaigns of the geographical field experiment could be seen in figure II.20.

**Table II.9 :** Dates and day of the week of the three sampling campaigns of the geographical field campaigns

<b>Geographical field experiment</b>	<b>Date and day of week of the sampling campaign of the geographical field experiments</b>
1 <sup>st</sup>	19-08-2016 Friday

**Table II.10:** Coordinates of the sampled sites during the river path of the river Gapeau in the city of Hyeres ( southeastern of France , PACA region).

N°	Sampling site name	latitude	longitude
01	Gapeau - La Crau (RW)	43.151325	6.081343
02	WWTP (WW)	43.145467	6.093158
03	Château les Mesclans avant confluence avec Le Réal Martin	43.152044	6.120395
04	camping vert gapeau confluence Réal Martin	43.15220	6.127978
05	la Clapiere	43.149764	6.147565
06	barrage la Clapiere	43.146901	6.149686
07	Abords terrain militaire	43.131293	6.164386
08	Pierre Pêche	43.125625	6.171226
09	amont du barrage anti-sel	43.121489	6.177349
10	aval du barrage anti-sel debut du gradient de salinité	43.120367	6.179271
11	Estuaire 1	43.118376	6.181620
12	Embarquadaire	43.114503	6.187077
13	Port Plaisance	43.111305	6.192815
14	Marché de l'Ayguade mer	43.103346	6.177326

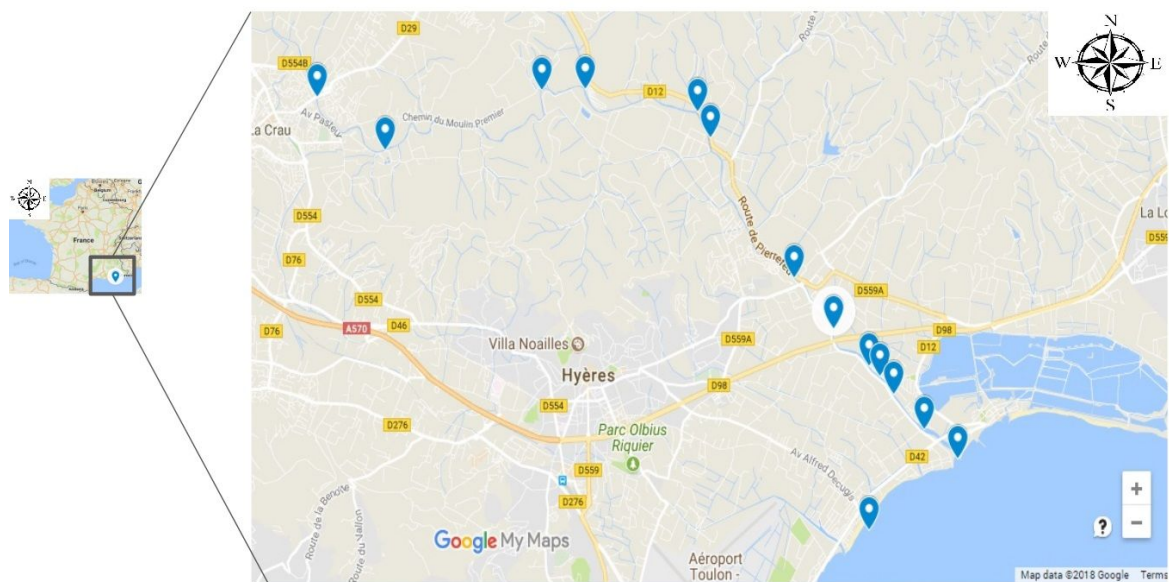


**Figure II.19:** Map showing the sampling sites for the geographical field experiment along the pathway of the river Gapeau till its river mouth at the city of Hyeres. The map shows also the relative site of the sampling sites with respect to France. Sampling sites were at the southeastern part of France in Region PACA



**Figure II.20** : Figure showing the pictures of the sampling campaign for the geographical field experiment .

### **II.3.2 Electrical Conductivity and pH of Geographical field experiment**

Electrical conductivity (EC) and pH were measured in situ using a multiparameter sonde. The measurements of the pH and EC were done on raw samples. Calibration of pH meter was done before the sampling experiment using a solution of KCl and HANNA pH standard respectively. Measurement were automatically temperature corrected.

### **II.3.3 3D excitation emission matrix of fluorescence spectroscopy of Geographical field experiment**

After each sampling campaign of the sampling points along the pathway of Gapeau river, we conducted measurements of the excitation emission matrix spectra of 3D fluorescence spectroscopy for the sample of the geographical field experiment. Filtration of these same

samples in the second sampling campaign (22-august-2016) was done in order to investigate the effect of particles of the sample solution on the fluorescence signal. Samples corresponding to the sampling sites of geographical field experiment (table II.10) were sampled without applying any filtration by taking 3 mL and transferring them to 1 cm quartz cell in a 16 cuvette sample holder to measure excitation emission matrix of fluorescence spectroscopy 3D EEMs according to the previously described in details methods of data acquisition in section (II.2.10.2) of the present chapter. EEM data analysis was also conducted using CP/PARAFAC algorithm described earlier in this methodology chapter. Each cuvette were previously washed by 10% nitric acid (10% HNO<sub>3</sub>) one time and then rinsed with with 18.2 MΩ·cm at 25 °C Milli-Q-water two times.

## **II.4 Temporal variations Field experiment**

Temporal variations of the three endmember mixing components were investigated to understand how the fluorescence signal of the dissolved organic matter of each one of the three endmember mixing components varies. These three endmember mixing components are the Gapeau river (RW), wastewater treatment plant of La Crau city (WW), the seawater at the site l'Ayguade (SW) at the Hyeres commune. In addition, the confluence of the river Gapeau with the tributary Réal Martin was also studied. The sampling were done automatically using an autosampler machine which is a container containing twenty four 1 L plastic bottle and provided with a processor.

### **II.4.1 Preparing bottles of the autosampler :**

Each bottle of the 24 bottles in the carousel of the autosampler (figure II.21) was filled with nitric acid (10%, Analytical Grade) then transferred to the agitation system and left for 24 hour to get rid of any type of bacteria or any other biofilms or microorganisms. Or <sup>3</sup>/<sub>4</sub> filled with nitric acid (10%, Analytical Grade), shaken manually 5 min, and rested during 15 min just to economize the chemical resources. Then the bottle is rinsed with 18.2 MΩ·cm at 25 °C MilliQ-water to get rid of any remains of the nitric acid. The nitric acid (10 % HNO<sub>3</sub>) is transferred to the next bottle. After that, the bottles were filled with 18.2 MΩ·cm at 25 °C MilliQ-water for 24 h, two time in addition to get rid of any contamination if any.

## II.4.2 Sampling of three Endmembers during a 48 hour cycle

The River Gapeau (43°09'07.2"N 6°04'52.4"E) was sampled on 19<sup>th</sup> sept 2016 to 21<sup>th</sup> September 2016. The confluence (43°09'00.3"N 6°07'46.1"E) of the Gapeau river with the Réal Martin tributary was sampled on 4<sup>th</sup> October 2016 – 6<sup>th</sup> October 2016. The WWTP (43°08'43.1"N 6°05'35.4"E ) was sampled on ( 15<sup>th</sup>, 16<sup>th</sup> and 17<sup>th</sup> November 2016) whereas the seawater was sampled on 17<sup>th</sup> and 18<sup>th</sup> and 19<sup>th</sup> october 2016 during 48 hour at a site which is called l'Ayguade at the city of Hyères (43°06'14.5"N 6°10'42.9"E). For the wastewater treatment plant (WW), twenty two Samples were taken from the outlet of the plant. Two samples were not sampled for technical reasons. The autosampler was then taken from the sampling site after two days (assuming we have 24 samples for 48 hours ), as it is described before. Samples were given proper names corresponding to the number of the sample from 01 to 24. Figure II.22 shows some pictures of the sampling campaigns of the temporal variation field experiment.

**Table II.11 :** The sampling dates and time of 1st and last sample of the temporal sampling campaigns for the Gapeau river (RW), the waste water treatment plant of La Crau (WW), the confluence (Gapeau-Réal Martin) and the seawater (SW) at L'Ayguade-Hyeres.

	<b>Gapeau river</b>	<b>WWTP of La Crau</b>	<b>Confluence (Gapeau-Réal Martin)</b>	<b>Seawater (L'ayguade)</b>
<b>Sampling Dates</b>	19 to 21-09-16	15 to 17-11-16	04 to 06-10-16	17 to 19-10-16
<b>Time of starting sampling</b>	11:53 am	11:05 am	01:27 pm	03:13 pm
<b>Time of end of sampling</b>	09:53 am	09:05 am	07:27 am	01:13 pm





**Figure II.21:** Picture of the autosampler used for sampling . It has the capacity of 24 plastic bottles of 1L. It was programmed to take one sample every two hour to cover a range of 24 bottles which corresponds to 48 hours sampling campaign.

**Gapeau River**



**WWTP of La Crau**



**Confluence of Gapeau and Le Real Martin**



**Sea at Hyeres city**



**Figure II.22** : Photos of the temporal variation field experiments of the waters of the Gapeau river and wastewater treatment plant of La Crau city and the confluence of the Gapeau river and its tributary Le Real Martin, and the seawater at the city of Hyeres .

### **II.4.3 Filtration/Non filtration of the samples of the temporal variations of the sources (Endmember mixing components)**

The twenty four samples were measured on raw and filtered states to investigate the effect of the particles

### **II.4.3.1 Measurement of non-filtered (NF) samples**

After 48h sampling, each one liter gallon of the 24 gallons in the autosampler was shaken to make a homogeneous solution and sampled by taking 3 mL and transferring them to a one cm quartz cell in a 16 cuvette sample holder to measure EEMs, according to the previously described in details methods of data acquisition in section (II.2.10.2) of the present chapter. EEM data analysis was also conducted using CP/PARAFAC algorithm. Each cuvette were previously washed by nitric acid one time and then rinsed with with 18.2 MΩ·cm at 25 °C Milli-Q-water two times. Sixty milliliters (60 mL) were taken from each 1L gallon in the autosampler and transferred to a (60 mL Nalgene ) vials. Then the vials were put in the refrigerator at a 4 °C to make the filtration of them. The sample holder (toureille) only contains sixteen cuvette and we have twenty four gallon in the autosampler so in the first working day where we got back the autosampler from in situ, we measured sixteen samples and eight other samples remained unmeasured by fluorescence spectrophotometer therefore we took 60 mL and put them in the refrigerator at a temperature degree of 4 °C to continue the measurement in the next day and to keep the samples for the filtration process which would occur some days after and be sure that the filtered samples represents the original samples.

### **II.4.3.2 Measurement of the filtered (F) samples**

The samples which were in the refrigerator were taken out and left for 20 to 30 minutes in order that they gain the surrounding temperature of the room and to have accurate and representative measurements. The samples were then filtered using a microfilter (Sartorius 0.45 micrometer). And a plastic syringe (LDPE) and a small tube of (5 mm diameter). The filtrate were then passed into a 1cm Quartz cell in a 16 cuvette holder to obtain EEM using the methods EN and CR (II.2.10.2 ) in addition to the EEM data analysis using CP/PARAFAC algorithm was done. The syringe was washed at each time the sampled water was changed and rinsed at least one time by the next sample water to insure that the signal over noise ratio of the new sample is high and not to confuse it with the water from the previous samples.

#### **II.4.4 Electrical Conductivity and pH measurement**

Electrical conductivity (EC) was measured using the conductivity meter (WJW) LF 330 Bioblock Scientific. pH was measured using WTW pocket pH meter kits. Calibration of pH meter was done before the sampling experiment using a solution of KCl and HANNA pH standard respectively. Measurement were automatically temperature-corrected. The measurements of pH and EC were done on raw samples after collecting the autosampler to our MIO laboratory.

---

## **Chapter 3 : Photodegradation of DOM from three endmembers and multilinear regression**

---

## **Photodegradation of Fluorescent Organic Matter in River Systems : endmember mixing and multilinear regression.**

El Nahhal Ibrahim<sup>a\*</sup>, Redon Roland<sup>a</sup>, Raynaud Michel<sup>a</sup> and Mounier Stephane<sup>a</sup>

<sup>a</sup> Université de Toulon, Aix Marseille Univ, CNRS, IRD, MIO - CS 60584, 83041 TOULON CEDEX 9 , France

\*Corresponding author : [elnahhal.i@gmail.com](mailto:elnahhal.i@gmail.com) (I.Y.EL-Nahhal)

### **ABSTRACT :**

Human activity puts pressures on coastal zone (agriculture, industry, urbanization) altering dissolved organic matter quality. Solar irradiation were conducted on mixed samples of River water, sea water, wastewater treatment plant effluent. Excitation Emission Matrices of Fluorescence were used to monitor the fate of wastewater treatment plant effluent. Multilinear regression of CP/PARAFAC components contribution depending on mixing composition were done and was excellent. Kinetics of decreasing contribution versus irradiation time were investigated. Second order Kinetics were found for C1 and C2. Distinction between fluorescence signal of endmembers was undoable. Wastewater treatment plant endmember after photodegradation was highly predominant.

Keywords : fluorescent organic matter, PARAFAC , multilinear regression, photodegradation, Coastal zone

### **III.1 Introduction**

Coastal zone is a gradual transitional zone between the terrestrial and oceanic zones (Huguet et al. 2009) and mixing zone between marine/oceanic waters inputs and the freshwater riverine inputs (Parlanti et al. 2000a). The riverine inputs are continental endmember (Bouloubassi et al. 1997) and an important source of terrestrial organic matter (Raymond and Spencer 2015) in coastal zone. Dissolved organic matter (DOM) play an important role in physical, chemical functioning of aquatic ecosystems (D. A. Hansell 2009) and biogeochemical processes (D. A. Hansell and Carlson 2014) and is a heterogenous mixture of organic compounds of both aromatic and aliphatic nature (D. A. Hansell and Carlson 2014). Chromophoric Dissolved Organic Matter (CDOM) is a fraction of DOM which can interact with light (Lei, Pan, and Devlin 2018)(Coble 1996, [a] 2007) and is ubiquitous in aquatic environmental media (Nelson and Siegel 2013) with a subgroup fluorescing FDOM (Coble 1996; Mostofa et al. 2012). DOM plays a key role in global carbon cycle (D. Hansell 2001) and is highly influenced by continental inputs (Fichot and Benner 2012; Yamashita, Boyer, and Jaffé 2013) and by autochthonous sources (Romera-Castillo et al. 2011). Most of organic matter in the coastal zone is of terrestrial origin (Parlanti et al. 2000a; Hedges, Keil, and Benner 1997).

Human activity has contributed to increased inputs of terrestrial CDOM in aquatic ecosystems (Massicotte et al. 2017). Urbanization is increasing and expected to triple between 2000 and 2030 (Seto, Güneralp, and Hutyrá 2012) with higher population density and migration to the coastal zone (Hugo 2011). In turn it changes land cover, hence quality and quantity of DOM in rivers (Seto, Güneralp, and Hutyrá 2012). Anthropogenic sources of organic matter vary from industrial (Carvalho et al. 2008), agricultural (Manninen et al. 2018), wastewater treatment plants effluents (Maizel and Remucal 2017) , landfill leachates (Oloibiri et al. 2017). Moreover, it has been found (Williams et al. 2016) that anthropogenic influence on urban watersheds caused distinct DOM composition. However, contribution of anthropogenic inputs to FDOM in coastal zone is not yet well defined and evaluated. Biogeochemistry of natural waters is impacted significantly by photo-reactivity of CDOM (Andrew et al. 2013; Lønborg et al. 2016) since photochemistry affects bioavailability of DOM (Moran and Zepp 1997; Oleinikova et al. 2017), microbial

activity (Piccini et al. 2009) and production of DOM of different character (W.-Z. Zhu, Yang, and Zhang 2017).

Partial information can be extracted from global analytical techniques (DOC, TOC, BOD, etc...) due to complex composition of DOM. And these techniques are time consuming and require elaborated sample preparation. Optical properties of CDOM and FDOM provides a valuable tool in delineating DOM sources (Osburn, Boyd, et al. 2016) and tracking DOM fluxes of terrigenous origin into ocean (Osburn, Boyd, et al. 2016) enables online or real-time monitoring in various media (Cohen et al. 2014; Helms et al. 2013). There are so many advantages of fluorescence spectroscopy which is useful, less time-consuming, inexpensive, precise qualitative and quantitative technique (Fellman, Hood, and Spencer 2010; G. Zhu et al. 2014) used among varying scientific fields (Gao et al. 2017). Excitation Emission Matrix fluorescence spectroscopy (EEM) has furthered scientific research in aquatic systems (Kim and Kim 2015; Cheng et al. 2018; Sgroi et al. 2017; Dainard et al. 2015). It enables characterization of optical properties of FDOM due to its high sensitivity, good selectivity and non-destruction of samples (Coble 1996). Coupled with Canonical Polyadic / Parallel Factor Analysis (CP/PARAFAC) it enables deconvolution of overlapping independent EEM spectra into distinct components (Stedmon and Bro 2008).

To the best of our knowledge, there is no evaluation of the specific contribution of anthropogenic organic matter to FDOM of the coastal zone. The present study is focussing on the wastewater treatment plants effluent discharge in urban river systems. It was conducted in laboratory three endmember mixing experiments, river, sea and wastewater treatment plant, to define contributions after mixing and solar irradiation. In addition, we investigated the influence of biological factor by using previous filtration. Multivariate linear regression was proposed for the prediction of FDOM signal and its photodegradation kinetic as a function of the mixing percentages and exposure.

## **III.2. Material and methods**


### **III.2.1 Sampling Sites**



Gapeau river birth at Signes city (43° 17' 24" N, 5° 52' 59" E) and run till the sea at city of Hyères (43°06'42" N, 6°11'33" E) in southeastern part of France (figure 1). Gapeau river has a length of 34.4 km (Ollier 1972) and watershed of 544 km<sup>2</sup> (Ducros et al. 2018) with a pluvial regime. River water endmember (RW) was sampled along Gapeau river roughly 500 m before wastewater treatment plant which is located at ( 43°08'38.6"N 6°05'36.1"E) whereas wastewater treatment plant endmember (WW) was sampled at its output. Wastewater treatment plant of La Crau city has a daily volume of 14,500 m<sup>3</sup>/day and serves 80,000 population equivalents. It inputs a treated wastewater effluent directly to Gapeau river of the following characteristics : BOD<sub>5</sub>= 15 mg/L, COD<sub>5</sub>=50 mg/L, suspended solids= 20 mg/L (private report from WWTP of La Crau). Sea water (SW) endmember was sampled at the coastal area of Hyères city at roughly seven meters far from beach ( 43°06'10.4"N 6°10'38.3"E ). Plastic bottle of one liter (cleaned with ethanol 100% and three times rinsed with 18.2 MΩ at 25 °C MilliQ water was used to sample 1 liter of each endmember. Eight sampling cruises were conducted for solar irradiation experiments, sampling dates corresponding to each irradiation experiment are shown in table 2.

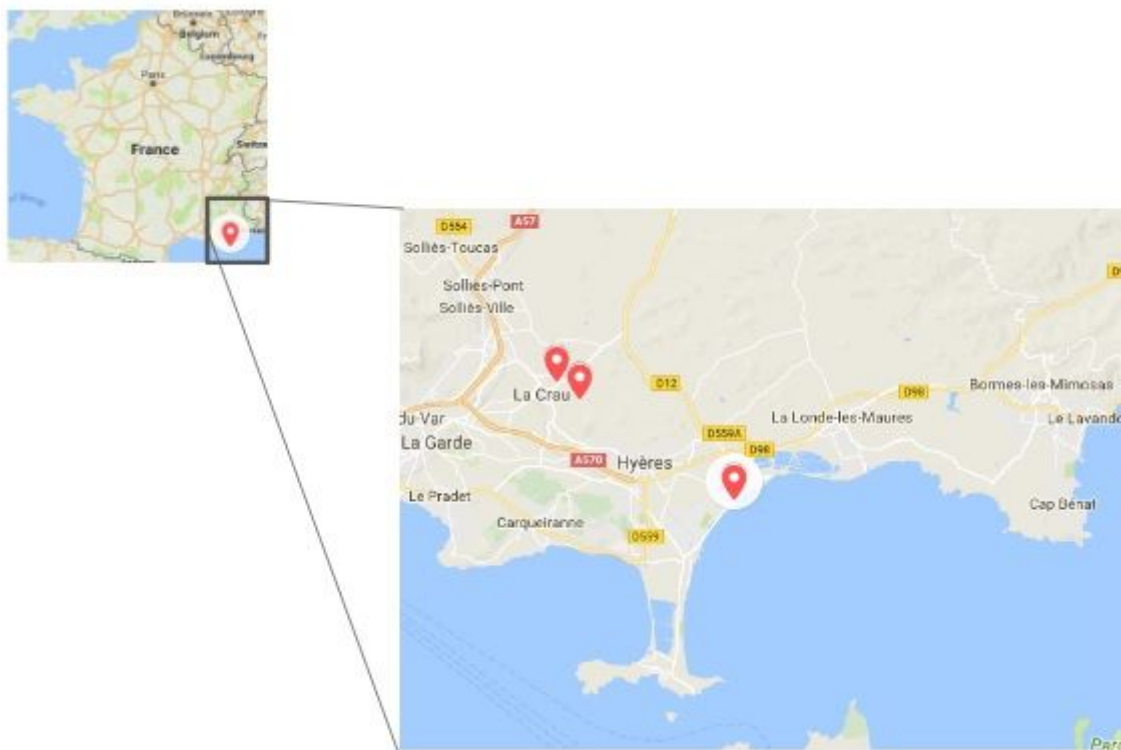


**Figure III.1 :** Map showing approximate locations of sampling sites of three endmember from upward to downward , Gapeau river, wastewater treatment plant of la Crau city and Sea water

at Hyères city (Rade d'Hyères) .() shows where samples were collected. Map made by using Google Maps

### **III.2.2 Materials of irradiation experiment**

#### **III.2.2.1 Filtration**

Depending on experiment, all or part of endmember sample was filtered using MilliPore filters (Type GNWP 0.20  $\mu\text{m}$ , 47 mm diameter) and filtration kit was previously cleaned by acidified water (10%  $\text{HNO}_3$ ). Filtered waters of each endmember were put in a novel 1 liter glass bottle (pre-rinsed with 10 %  $\text{HNO}_3$  and 3 times with 18.2  $\text{M}\Omega\cdot\text{cm}$  at 25 °C MilliQ-water) and transferred to refrigerator at 4 °C in the dark. Filtrates were used for preparation of mixtures in the following day.

#### **III.2.2.1 Preparation of mixtures**

Sixteen 50 mL quartz vials were washed with reverse osmosis water then transferred to 10 %  $\text{HNO}_3$  bath for 24 hours then rinsed three times with 18.2  $\text{M}\Omega\cdot\text{cm}$  at 25 °C Milli Q-water. Then burnt in oven at 450 °C for 24 hours to insure no remaining traces of organic carbon. Fifteen mixtures were fabricated based on three endmember. The exact mixing percentages are summarized in table 1. Percentage of three endmember was taken by weight, assuming a density of 1.00, 1.00 and 1.025 for WW, RW and SW respectively. A number was given to the vial according to its corresponding mixture (table 1). Each vial was shaken gently by hand after preparation of mixtures to insure homogeneity of mixtures.

#### **III.2.2.3. Experiment notation/codification**

Each solar irradiation experiment concern 15 mixed samples with no, total or partial filtration of endmember. The following notation Ixyz was used to codify them, where x, y z correspond to RW, SW and WW endmember respectively and indicate that endmember is filtered with a value of 1. As an example, the experiment code I101 corresponds to the solar irradiation experiment of 15 mixed samples in which RW and WW filtered while SW is not (table 2).

**Table III.1**-Content fraction of each endmember mixing components of fifteen samples used in this study

Endmember	Sample Number														
	1	2	3	4	5	6	7	8	9	10	11	12	13	14	15
RW	100	0	0	75	50	25	75	50	25	0	0	0	50	25	25
SW	0	100	0	25	50	75	0	0	0	25	50	75	25	25	50
WW	0	0	100	0	0	0	25	50	75	75	50	25	25	50	25

### III.2.2.4. Irradiation experiments

Eight photochemical experiments were conducted at different periods ([table 2](#)). Quartz vials were put on roof of laboratory MIO (43° 08' 11.2" N 6° 01' 16.7" E) in wooden plank at sufficient distances to insure receiving same solar irradiation. Control samples were prepared and filled in dark vials and put in empty icebox. This icebox was placed beside the wooden plank. For solar irradiation experiment (I111), no control samples were prepared because we repeated this experiment several time for reproducibility reason and it was the first solar irradiation experiment conducted in which all three endmember were filtered and no biological activity was assumed.

**Table III.2**-Solar Irradiation Experiment dates and types.

Experiment	Sampling date	Beginning of irradiation Date	End of irradiation Date	Experiment code
1 <sup>st</sup>	26-May-2015	27-May-2015	5-June-2015	I111
2 <sup>nd</sup>	19-Jun-2015	22-Jun-2015	4-July-2015	I111
3 <sup>rd</sup>	7-Jul-2015	10-Jul-2015	17-July-2015	I111

4 <sup>th</sup>	26-Aug-2015	28-Aug-2015	11-Sept-2015	I111
5 <sup>th</sup>	9-Nov-2015	10-Nov-2015	20-Nov-2015	I110
6 <sup>th</sup>	30-Nov-2015	3-Dec-2015	17-Dec-2015	I011
7 <sup>th</sup>	12-Feb-2016	15-Feb-2016	4-March-2016	I101
8 <sup>th</sup>	9-May-2016	11-May-2016	27-May-2016	I000

---

### III.2.2.5. Solar irradiance measurement

Electric physical actinometer sensor was setup to measure solar irradiation in volts (Solar Cell 9V/109 mA). Measured data were saved on a small data logger connected to (Solar Cell 9V/109 mA). On the same time, daily insolation data were asked to Météo-France ([www.meteofrance.com](http://www.meteofrance.com)). Data required were from the measuring stations at two cities near La Garde city (Nice and Marignane). Linear regression analysis was conducted to have the relationship between data from electric physical actinometer sensor and Météo-France data to use this relationship to find missing data from our electric physical actinometer sensor and have local irradiation estimation (SI-1).

### III.2.3. Excitation Emission Matrix EEM fluorescence spectroscopy

#### III.2.3.1. Sampling

Three mL aliquots from each 50 mL quartz vial was sampled and transferred into 10x10 mm quartz cell. Sodium azide was added to stop microbial activity (100  $\mu$ L of 1M NaN<sub>3</sub>). EEM of solar irradiation experiments samples were performed using fluorescence spectrophotometer (F4500, Hitachi) with PMT voltage of 700 V, at 25 °C. F4500 is also equipped by 16 cuvette cells holder (homemade mirrored turret) enabling automatic measurement mode. Ultrapure Perkin Elmer deionized water was measured to check spectrofluorimeter stability. Scan speed was set at 2,400 nm.min<sup>-1</sup>. Emission spectra were collected at 5 nm intervals between 220 and 420 nm, while excitation spectra were measured between 200 and 400 nm at 5 nm intervals. Slit widths for both excitation and emission wavelengths were set at 5 nm. EEM datasets of solar

irradiation experiments were processed using Matlab 2013a (Math Works Inc., USA). All fluorescence intensity were in arbitrary units.

### III.2.3.2. Data processing

Spectral contribution of each CP/PARAFAC components to total EEM fluorescence was determined using CP/PARAFAC algorithm (Bro 1997; Stedmon and Markager 2005a). Finally, 965 EEMs were modelled using PROGMEEF software (<http://protee.univ-tln.fr/PROGMEEF.html>). Numerical filter was taken as 25 nm to eliminate Raman and Rayleigh scattering according to Zepp method (Zepp, Sheldon, and Moran 2004) to avoid any effect on CP/PARAFAC components number. No inner filter correction was done because samples had too low absorbance value. CP/PARAFAC decomposition started from two component and stopped at five components with 50 iterations. Nonnegativity constraints were applied for CP/PARAFAC components for excitation and emission loadings. Accepted correct number of CP/PARAFAC components was taken according to evaluation of CONCORDIA score (threshold value 60%) with the higher component number. No outliers were found or present in our dataset and three CP/PARAFAC components model was found. CP/PARAFAC decomposition is done globally for all EEMs corresponding to all solar irradiation experiments and all mixtures therein. Once decomposition is done, contributions of each CP/PARAFAC components were normalised to the maximum value of its irradiation experiment separately, generally the initial one before the start of solar irradiation experiments, to allow for comparison of evolution of multilinear regression coefficients with irradiation time according to the following equation :

$$C_i^{Ixyzf_{SW}f_{RW},T_n} = \frac{c_i^{Ixyzf_{SW}f_{RW},T_n}}{\max(c_i^{Ixyzf_{SW}f_{RW},T_n}) \forall (nf_{SW}f_{RW})} \quad (\text{eq.1})$$

Where :

Ixyz is solar irradiation experiment,  $f_{RW}$  and  $f_{SW}$  are percent endmembers composition of the sample of RW and SW,  $T_n$  is the  $n^{th}$  day of irradiation.  $c_i^{Ixyz, f_{RW}, f_{SW}, T_n}$  is value of contribution of CP/PARAFAC component  $i$  and  $C_i^{Ixyz, f_{RW}, f_{SW}, T_n}$  the normalised to the maximum contribution of CP/PARAFAC component  $i$

### III.2.4. Multi-linear regression

Multi-linear regression was done for all  $f_{RW}$ ,  $f_{SW}$  of a fixed component  $i$ ; a specific irradiation day  $T_n$  and irradiation experiment Ixyz. Multilinear regression was done to calculate coefficients in the general mathematical regression formula given here

$$Y = a_0 + a_1 \cdot X_1 + a_2 \cdot X_2 + \dots + a_n \cdot X_n \quad (\text{eq. 2})$$

#### III.2.4.1. Multilinear regression of three endmember

River water RW, Sea water SW and Wastewater treatment plant WW is constrained by mass total sum of three content fraction that should be equal to 100 according to the following equation :

$$f_{SW} + f_{RW} + f_{WW} = 100 \quad (0 < f_i < 100) \quad (\text{eq.4})$$

Where  $f_{SW}$ ,  $f_{RW}$ ,  $f_{WW}$  are content fraction of SW, RW and WW respectively. All percent fractions obviously positive and less than or equal to 100.

Then

$$f_{WW} = 100 - f_{SW} - f_{RW} \quad (\text{eq. 5})$$

By substituting in regression eq. 2 for  $f_{WW}$  where  $n=3$ , the different terms we obtain :

$$C_i^{Ixyz, f_{SW}, f_{RW}, T_n} = a_{i,0} + a_{i,1} \cdot f_{SW} + a_{i,2} \cdot f_{RW} + a_{i,3} \cdot f_{WW} \quad (\text{eq.6})$$

Where  $C_i^{I_{xyz},f_{RW},f_{SW},T_n}$  is total contribution of CP/PARAFAC component number  $i$ , and  $a_{i,1}$ ,  $a_{i,2}$ ,  $a_{i,3}$  the respective partial contribution to this contribution by three endmember SW, RW and WW. To simplify,  $C_i^{I_{xyz},f_{RW},f_{SW},T_n}$  is replaced by  $C_i^*$  in the next equations

By substituting for  $f_{WW}$  by its expression in (eq.5) we obtain :

$$C_i^* = a_{i,0} + a_{i,1} \cdot f_{SW} + a_{i,2} \cdot f_{RW} + a_{i,3} \cdot (100 - f_{SW} - f_{RW}) \quad (\text{eq.7})$$

$$C_i^* = a_{i,0} + a_{i,1} \cdot f_{SW} + a_{i,2} \cdot f_{RW} + a_{i,3} \cdot 100 - a_{i,3} \cdot f_{SW} - a_{i,3} \cdot f_{RW} \quad (\text{eq.8})$$

By arranging similar terms together and taking the common factor, we obtain :

$$C_i^* = (a_{i,0} + a_{i,3} \cdot 100) + (a_{i,1} - a_{i,3}) \cdot f_{SW} + (a_{i,2} - a_{i,3}) \cdot f_{RW} \quad (\text{eq.9})$$

By giving a proper term for the constant and newly modified coefficients to account for  $f_{WW}$  term, we get:

$$A_{i,0}^{WW} = (a_{i,0} + a_{i,3} \cdot 100) \quad A_{i,1}^{WW} = (a_{i,1} - a_{i,3}) \quad A_{i,2}^{WW} = (a_{i,2} - a_{i,3})$$

We obtain the final multilinear regression equation as a function of two content fractions of two endmembers :

$$C_i^* = A_{i,0}^{WW} + A_{i,1}^{WW} \cdot f_{SW} + A_{i,2}^{WW} \cdot f_{RW} \quad (\text{eq.10})$$

Where  $A_{i,0}^{WW}$ ,  $A_{i,1}^{WW}$  and  $A_{i,2}^{WW}$  represent multilinear regression coefficients related to mixing equation when  $f_{WW}$  is expressed in terms of content fraction of the other two endmembers ( $f_{RW}$  and  $f_{SW}$ ). One can remarks that by circular permutation we can obtain two other formulae, but

none give  $a_{*,*}$  coefficients independently. If it could be calculated independently, independent coefficients of all the three endmembers could be found and calculated.

### III.2.5. Kinetics

Observation of variation of multilinear regression coefficients with irradiation energy has been conducted once multilinear regression is done for all  $T_n$  as expressed mathematically :

$$\begin{aligned} A^{WW, Ixyz}_{i,0}(V) \\ A^{WW, Ixyz}_{i,1}(V) \\ A^{WW, Ixyz}_{i,2}(V) \end{aligned} \quad (eq.11)$$

Where  $V$  is received solar irradiation in Volts (V). CP/PARAFAC contribution during irradiation experiment can be expressed as a function of content fraction of two endmember depending on  $V$ , allowing kinetic study:

$$C^*_i(V) = A^{WW}_{i,0}(V) + A^{WW}_{i,1}(V) \cdot f_{SW} + A^{WW}_{i,2}(V) \cdot f_{RW} \quad (ep.12)$$

## III.3. Results and Discussion

### III.3.1. EEMs Results

CORCONDIA analysis showed drop between four components and five, from near 70 % to less than or around 30 % which surpasses acceptable threshold of 60% where as it showed a value of 80.75 % for three components, indicating that a three-factor model was more appropriate. Spectral contour plots of EEM of three CP/PARAFAC components and their corresponding loadings for both the excitation and the emission wavelengths are shown in figure 2.

C1

C2

C3



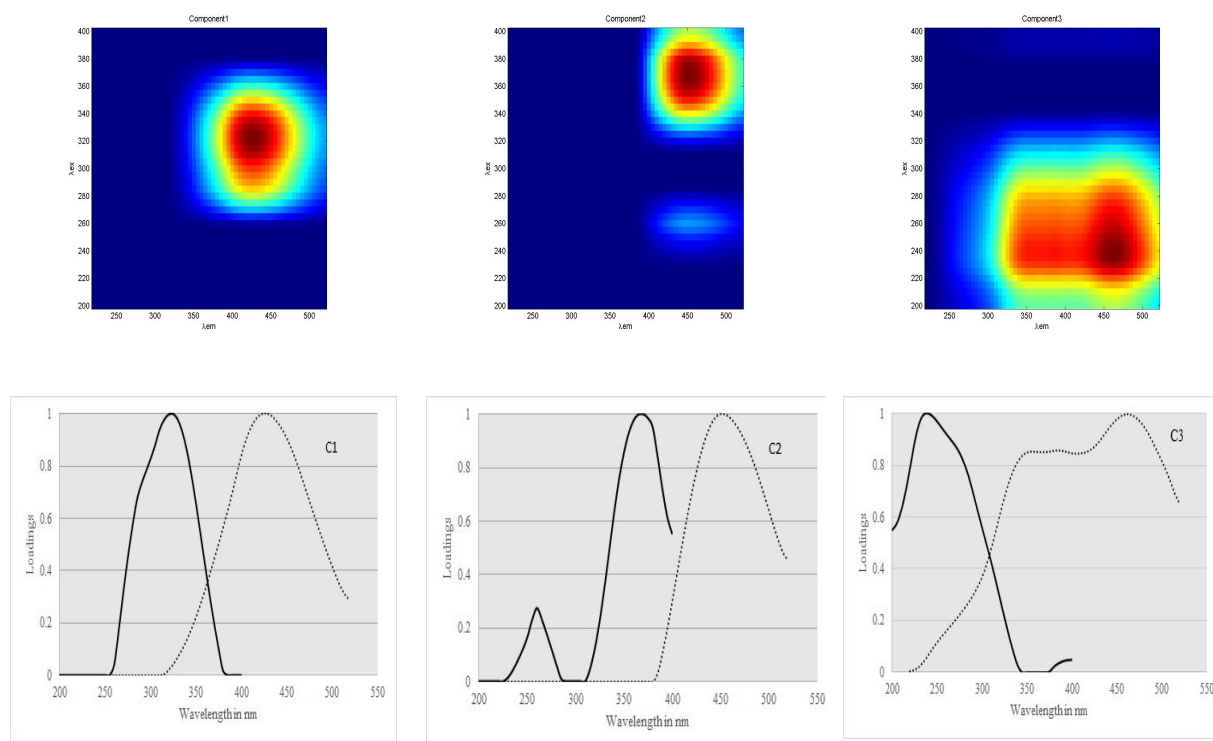


**Figure III.2.** Contour plots of CP/PARAFAC components identified from the decomposition of all EEM datasets. Spectral loadings of excitation and emission wavelengths of the three identified CP/PARAFAC in the present study. Excitation loading for CP/PARAC component are solid lines whereas emission loadings are shown in dotted lines.

Description of excitation and emission pairs of main peak positions for CP/PARAFAC components are summarized in Table 3 and compared to literature.

**Table III.3-**Descriptions of CP/PARAFAC components and comparison with literature

Component	$\lambda_{EX}/\lambda_{EM}$ (nm)	Description and references in literature
Component C1	325/425	Component 4 (Stedmon, Markager, and Bro 2003a) : terrestrially derived organic matter Peak C (Coble 1996; Coble, Del Castillo, and Avril 1998) : visible humic-like Component 2 (Yamashita et al. 2008) : terrestrial humic-like

---

		Component 4 (Stedmon and Markager 2005a)
Component C2	(260) 370/450	Component 3 (Stedmon, Markager, and Bro 2003a) Component G3 (Murphy et al. 2011a) Component 3 (Li et al. 2014a) Component 7 (Osburn, Handsel, et al. 2016) Component 5 (Baghoth, Sharma, and Amy 2011) Component 1 (W.-Z. Zhu, Zhang, and Yang 2017) Humic-Like
Component C3	240/460	Component 1 (Yamashita et al. 2008) Peak A (Coble 1996) Q2 (Cory and McKnight 2005) Component 1 (Yang et al. 2014)

---

These three CP/PARAFAC components have been previously identified (Table 3). Nature of these CP/PARAFAC components seems not to be affected by the filtration mode or mixing process and they are found in every sample in the global EEMs dataset. C1, showed an excitation maximum at 325 nm and an emission maximum at 425 nm and a range of excitation emission wavelengths (Ex=300-340 nm , Em=400-450 nm). Previous studies have associated this component to UVA humic-like fluorescent CP/PARAFAC component and Peak C (Coble 2007b) and peak “∞” (Parlanti et al. 2000b; Sierra et al. 2005). It has been also cited to represent terrestrial, anthropogenic, agricultural sources (Stedmon, Markager, and Bro 2003b; Stedmon and Markager 2005b). C2 component showed an excitation maximum at 370 nm and an emission maximum at 450 nm and a range of excitation emission wavelengths (Ex=340-400 nm, Em=400-500 nm). In addition, spectra of C2 resembles spectra of component “G3” which has Ex<sub>max</sub>=350 nm, Em<sub>max</sub>=428 nm in (Murphy et al. 2011b) who have attributed it to wastewater or nutrient enrichment tracer. This component has also been identified as humic-like component, similar to “C3” in the study conducted by (Li et al. 2014b) which had two excitation maxima (at 250, 350 nm) corresponding to the same emission maxima (at 440 nm). Furthermore, C2 has

very similar spectra to “C7” from recycled water studies, which included samples of wastewater, treated water, gray water (Osburn, Handsel, et al. 2016). C3, showed an excitation maximum at 240 nm and an emission maximum at 460 nm. It’s range of excitation emission wavelengths is  $E_x=220-280$  nm,  $E_m=325-500$  nm. In review article, Carstea et al. (2016) attributed this region to potential fluorophores like humic acids. C3 exhibited fluorescence similar to fluorescence normally found from humic-like fluorophores in UV region which is previously identified to be Peak A (Coble 1996; Coble, Del Castillo, and Avril 1998). In the decomposition process, no specific protein-like component was detected which could be due to a greater contribution of organic matter fluorescence in all the mixing endmember signal hiding the protein signal.

### III.3.2 Multivariate Linear Regression Parameters

Numerical values of multilinear regression coefficients for each CP/PARAFAC component are shown in table 4 for time zero, i.e. before the start of irradiation experiments, for all the irradiation/mixing experiments.

**Table III.4-**Multilinear regression parameters of CP/PARAFAC components found in the present study

Ixyz	Coefficient C1 à T0				Coefficient C2 à T0				Coefficient C3 à T0			
	$A_{1,0}^{ww}$ intercept	$A_{1,1}^{ww}$ ( $f_{sw}$ )	$A_{1,2}^{ww}$ ( $f_{rw}$ )	$r^2$	$A_{2,0}^{ww}$ intercept	$A_{2,1}^{ww}$ ( $f_{sw}$ )	$A_{2,2}^{ww}$ ( $f_{rw}$ )	$r^2$	$A_{3,0}^{ww}$ intercept	$A_{3,1}^{ww}$ ( $f_{sw}$ )	$A_{3,2}^{ww}$ ( $f_{rw}$ )	$r^2$
I111	100.34	-0.99	-0.93	0.99	98.42	-0.97	-0.92	0.99	112.35	-1.08	-1.03	0.97
I110	68.91	-0.66	-0.60	0.99	80.73	-0.75	-0.68	0.98	43.76	0.15	0.13	0.34
I011	49.73	-0.46	-0.40	0.98	63.33	-0.55	-0.48	0.98	49.57	-0.02	-0.08	0.33
I101	60.45	-0.58	-0.52	0.97	73.18	-0.70	-0.63	0.96	32.40	-0.05	-0.11	0.14
I000	100.13	-0.97	-0.91	0.99	96.14	-0.93	-0.89	0.99	83.32	-0.38	-0.38	0.59

From table 4, it can be seen that values the correlation coefficient is over 0.95 for C1 and C2 indicating multilinear regression is excellent. While it occurs only for I111 for C3. Values of the intercept are always greater than values of coefficients of  $f_{sw}$  and  $f_{rw}$ . Knowing that values of the intercept account for effect of the fraction of wastewater treatment plants on contribution of

CP/PARAFAC component these results show that contribution of CP/PARAFAC component decreases with increasing sea or river water. Indeed, all of coefficients  $f_{SW}$ ,  $f_{RW}$  have negative sign suggesting that for a unit increase in content fraction of  $f_{SW}$ ,  $f_{RW}$  there is a decrease equal in amount to the corresponding coefficient. Furthermore, one can observe that for  $f_{SW}=100$  or  $f_{RW}=100$ , residual contributions are weak compared to the  $f_{WW}=100$ , i.e.  $f_{SW}=f_{RW}=0$ . These indicated that most of fluorescence contributions are due to WWTP endmember considering the residual fluorescence  $a_{i,0}$  as neglectable. Additionally, it seems that there is no specific end members response as this behavior is similar for C1 and C2.

Regardless of mode of filtration, the contribution of fluorescence of mixing process is predominated by wastewater treatment plant endmember for the three CP/PARAFAC components and filtration has a measurable effect on multilinear regression parameters. When only one endmember is filtered and the other two endmembers are not, there is a diminution of values of the intercept parameter which suggest that there is an effect on fluorophores of filtered particles. When RW endmember is not filtered, values of the intercept parameter is less, 49.73, than that when SW endmember is not filtered, 60.45, suggesting that removal of fluorophores of river water plays a negative role on values of intercept parameter. In general, there is an influence of filtration on the initial contribution of multilinear regression parameters. Coefficients of  $f_{SW}$  and  $f_{RW}$  are around 1% of the initial contribution of the mixing process.

### III.3.3. Determination of coefficient kinetic decay and order

All irradiation experiment showed continuous decrease of fluorescence signal with irradiation time. No stable signal or significant fluorescence increase was observed like in other works ([Zhu et al. 2017](#); [Song et al. 2015](#)). Integrated rate law linear equations of zero<sup>th</sup>, 1<sup>st</sup>, 2<sup>nd</sup>, and 3<sup>rd</sup> kinetic order were investigated for each coefficient  $A^{WW,xyz}_{i,0}$ ,  $A^{WW,xyz}_{i,1}$  and  $A^{WW,xyz}_{i,3}$  to determine kinetics of photodegradation for each multilinear regression parameter. Kinetic order choice was done by choosing the best linearisation according to kinetic order law, selecting linear correlation coefficient which must be greater than the threshold 0.75 after eliminating outliers. Results are presented in table 5 for kinetic order, and kinetic constant,  $k$ , are presented in table 6. We found that all kinetics are 2<sup>nd</sup> order in agreement with previous works (Yang et al. 2014). Long term photodegradation of fluorescent organic matter is a bimolecular reaction probably involving excited organic matter and organic matter itself. Other work assumed first order kinetic under

solar simulated irradiation (Wu et al. 2016) but experiment were done during 12h and under 2.80 mW/cm<sup>2</sup> (visible) and 70.00 mW/cm<sup>2</sup>, corresponding to the starting point of present irradiation experiment that could be assumed as first order kinetic.

**Table III.5**-Kinetic order of coefficients of multilinear regression for each CP/PARAFAC . “NA” means that correlation coefficient for 2<sup>nd</sup> order rate was less than 0.75, and was dismissed.

	C1			C2			C3		
	$A_{1,0}^{ww}$ intercept	$A_{1,1}^{ww}$ (f <sub>sw</sub> )	$A_{1,2}^{ww}$ (f <sub>rw</sub> )	$A_{2,1}^{ww}$ intercept	$A_{2,1}^{ww}$ (f <sub>sw</sub> )	$A_{2,2}^{ww}$ (f <sub>rw</sub> )	$A_{3,1}^{ww}$ intercept	$A_{3,2}^{ww}$ (f <sub>sw</sub> )	$A_{3,3}^{ww}$ (f <sub>rw</sub> )
I111	2	2	2	2	2	2	2	2	2
I110	2	2	2	2	2	2	NA	NA	NA
I011	2	2	2	2	2	2	NA	NA	NA
I101	2	2	2	2	2	2	NA	NA	NA
I000	2	2	2	2	2	2	NA	NA	NA

**Table III.6**-Kinetic constant for coefficients of multilinear regression for each CP/PARAFAC component. Values in parenthesis are relative standard deviation for kinetic constant

	C1			C2			C3		
k*1e6	$A_{1,0}^{ww}$ intercept	$A_{1,1}^{ww}$ (f <sub>sw</sub> )	$A_{1,2}^{ww}$ (f <sub>rw</sub> )	$A_{2,0}^{ww}$ intercept	$A_{2,1}^{ww}$ (f <sub>sw</sub> )	$A_{2,2}^{ww}$ (f <sub>rw</sub> )	$A_{3,1}^{ww}$ intercept	$A_{3,2}^{ww}$ (f <sub>sw</sub> )	$A_{3,3}^{ww}$ (f <sub>rw</sub> )
I111	7.13(9.82)	721.1(10.82)	720.94(7.63)	4.57(8.75)	498.14(8.21)	507.39(8.86)	0.419(23.86)	56.51(19.64)	61.46(5.53)
I110	4.83(8.28)	515.33(20.74)	645.77(12.14)	4.85(14.43)	674.14(28.34)	770.01(17.02)	-	-	-
I011	7.85(6.37)	805.34(13.73)	949.56(13.71)	8.10(8.64)	911.58(10.65)	977.34(10.72)	-	-	-
I101	7.60(14.47)	857.10(14.11)	1057.22(20.44)	6.13(16.31)	877.75(13.92)	943.41(12.84)	-	-	-

It can be seen from table 6 that values of kinetic constant for intercept for both C1 and C2 are smaller than those values of kinetic constant for  $A_{1,1}^{WW}$  which is coefficient of  $f_{SW}$  and  $A_{1,2}^{WW}$  which is coefficient of  $f_{RW}$ . This finding could be interpreted as follows: C1 and C2 contribution of RW and SW are more sensitive to photodegradation than WW which decay 100 time slower under irradiation. Hence even if there is no specific endmember CP/PARAFAC contribution, it exist a photosensitivity difference between WW and RW or SW. Under long irradiation, WW contribution is more resilient. This difference of behavior depending on endmember mixing was already observed between terrestrial and autochthonous organic matter (W.-Z. Zhu, Zhang, and Yang 2017). Small differences were also observed on reclaimed water using fluorescence matrix regional integration between humic-like and protein-like under high irradiation (Wu et al. 2016). Therefore, we could say that wastewater treatment plant fluorophores are somehow more refractory to photodegradation. Anthropogenic dissolved organic matter, in the present study, remains the greatest contribution of CP/PARAFAC components along irradiation process and fluorescence signal going to the coastal zone should mainly come from WW endmember.

Concerning effect of filtration, kinetic constants are lower when WW is not filtered (I110) meaning that particles from WW delay photodegradation of C1 and C2. For C2, the lower constants are found for I111 meaning that particles from RW and SW increase or enhance C2 photodegradation process. When there is WW particles, C1 photodegradation is slower (case of I110 and I000) while for C2, presence of RW or SW particles enhance photodegradation kinetic (I011, I101 and I000). Effect of WW and RW or SW particles differ depending on the fluorescence component. More investigation on the nature of the particles should be done to understand their role in photodegradation.

Comparing C1 versus C2 degradation kinetic, it was observed that humic-like FDOM is more reactive than protein-like FDOM (Yang et al. 2014). However, results above demonstrated that it's not so simple. CP/PARAFAC components are constituted by several types of FDOM that behave differently depending on their origin and their photosensitivity.

For control non irradiated samples, due to biological activity (Yang et al. 2014) no clear behaviour was found except the mean contributions relative deviation standard (RSD). It can be seen in table 7, that for I000 values RSD values are the smallest compared to all other irradiation

experiments. RSD values for C3 coefficients of multilinear regression are higher for all irradiation experiments compared to those of C1 and C2. C3 component was suggested in this study to exhibit noise. The greater RSD value of C3 for all coefficients can be interpreted as having chaotic variations. Another observation is that RSD values for C1 and C2 have an order of  $I110 > I011 > I101 > I000$ . Particles from WW seems to be responsible for the variation with a greater degree compared to SW and RW particles in the samples. Compared to irradiation experiment ( I000 ), the synergistic effect of all of particles makes RSD values to be the smallest possible. This observation could be attributed to the fact that particles from each endmember and microorganisms are competing which therefore stabilise fluorescence signal in non sterile dark control.

**Table III.7-**Relative standard deviation RSD for multilinear regression parameters for CP/PARAFAC components for control samples of irradiation experiments

RSD of	C1			C2			C3		
	$A_{1,0}^{ww}$ intercept	$A_{1,1}^{ww}$ ( $f_{SW}$ )	$A_{1,2}^{ww}$ ( $f_{RW}$ )	$A_{2,1}^{ww}$ intercept	$A_{2,1}^{ww}$ ( $f_{SW}$ )	$A_{2,2}^{ww}$ ( $f_{RW}$ )	$A_{3,1}^{ww}$ intercept	$A_{3,2}^{ww}$ ( $f_{SW}$ )	$A_{3,3}^{ww}$ ( $f_{RW}$ )
I111	-	-	-	-	-	-	-	-	-
I110	26.08	23.84	25.78	14.80	12.95	15.10	81.87	111.29	71.52
I011	21.09	23.10	22.83	13.40	15.01	14.68	50.91	75.18	76.46
I101	16.57	21.10	19.46	14.22	18.15	19.67	39.08	76.12	94.22
I000	3.02	4.25	3.30	2.42	2.74	3.49	14.72	53.34	43.74

### III.4. Conclusions

In this study, natural solar changes on three endmember mixing laboratory experiments were investigated leading to the following conclusions :

- (1) Multilinear regression model for contribution of CP/PARAFAC components is excellent and could be done for the three endmembers,
- (2) Photodegradation of C1 and C2 multilinear regression coefficient followed second order kinetics except C3,
- (3) Search for specific fluorescence signal or signature for river water , wastewater treatment plants and sea water couldn't be done in this work,
- (4) Major endmember contributing to fluorescence signal in human impacted system is wastewater treatment plant contribution. After irradiation, resulting photobleached fluorescence is coming from wastewater treatment, according to results of kinetic constant which favour anthropic organic matter contribution (100 less sensitive to photobleaching),
- (5) In human impacted coastal zone, residual fluorescent organic matter come from wastewater treatment plant, and no specific signal from sea water could be detected near the coast.

## **Acknowledgements**

The authors would like to thank Erasmus Mundus/Hermes program for financial support of present work which was part of a PhD thesis. Météo-France is also acknowledged for providing datasets of insolation. Christian Martino and Gael Durrieu are thanked for participating in sampling campaigns. Christian Martino is also acknowledged for preparation of wooden plank used in this study. Nicolas Layglon is thanked for preparing the map of Sampling sites

## **Conflict of interest**

The authors declare no conflict of interest by any means whatsoever.

## **References**

- Andrew, Andrea A., Rossana Del Vecchio, Ajit Subramaniam, and Neil V. Blough. 2013. "Chromophoric Dissolved Organic Matter (CDOM) in the Equatorial Atlantic Ocean: Optical Properties and Their Relation to CDOM Structure and Source." *Marine Chemistry* 148: 33–43. <https://doi.org/10.1016/j.marchem.2012.11.001>.



- Baghoth, S. A., S. K. Sharma, and G. L. Amy. 2011. "Tracking Natural Organic Matter (NOM) in a Drinking Water Treatment Plant Using Fluorescence Excitation–emission Matrices and PARAFAC." *Water Research* 45 (2): 797–809. <https://doi.org/10.1016/j.watres.2010.09.005>.
- Bouloubassi, I., E. Lipiatou, A. Saliot, I. Tolosa, J. M. Bayona, and J. Albaigés. 1997. "Carbon Sources and Cycle in the Western Mediterranean—the Use of Molecular Markers to Determine the Origin of Organic Matter." *Deep-Sea Research. Part II, Topical Studies in Oceanography* 44 (3-4): 781–99. [https://doi.org/10.1016/s0967-0645\(96\)00094-x](https://doi.org/10.1016/s0967-0645(96)00094-x).
- Bro, Rasmus. 1997. "PARAFAC. Tutorial and Applications." *Chemometrics and Intelligent Laboratory Systems* 38 (2): 149–71. [https://doi.org/10.1016/s0169-7439\(97\)00032-4](https://doi.org/10.1016/s0169-7439(97)00032-4).
- Carstea, Elfrida M., John Bridgeman, Andy Baker, and Darren M. Reynolds. 2016. "Fluorescence Spectroscopy for Wastewater Monitoring: A Review." *Water Research* 95 (May): 205–19. <https://doi.org/10.1016/j.watres.2016.03.021>.
- Carvalho, Sandra I. M., Marta Otero, Armando C. Duarte, and Eduarda B. H. Santos. 2008. "Effects of Solar Radiation on the Fluorescence Properties and Molecular Weight of Fulvic Acids from Pulp Mill Effluents." *Chemosphere* 71 (8): 1539–46. <https://doi.org/10.1016/j.chemosphere.2007.11.046>.
- Cheng, Cheng, Jing Wu, Luodan You, Jiukai Tang, Yidi Chai, Bo Liu, and Muhammad Farooq Saleem Khan. 2018. "Novel Insights into Variation of Dissolved Organic Matter during Textile Wastewater Treatment by Fluorescence Excitation Emission Matrix." *Chemical Engineering Journal* 335: 13–21. <https://doi.org/10.1016/j.cej.2017.10.059>.
- Coble, Paula G. 1996. "Characterization of Marine and Terrestrial DOM in Seawater Using Excitation-Emission Matrix Spectroscopy." *Marine Chemistry* 51 (4): 325–46. [https://doi.org/10.1016/0304-4203\(95\)00062-3](https://doi.org/10.1016/0304-4203(95)00062-3).
- . 2007a. "Marine Optical Biogeochemistry: The Chemistry of Ocean Color." *Chemical Reviews* 107 (2): 402–18. <https://doi.org/10.1021/cr050350+>.
- . 2007b. "Marine Optical Biogeochemistry: The Chemistry of Ocean Color." *Chemical Reviews* 107 (2): 402–18. <https://doi.org/10.1021/cr050350+>.
- Coble, Paula G., Carlos E. Del Castillo, and Bernard Avril. 1998. "Distribution and Optical Properties of CDOM in the Arabian Sea during the 1995 Southwest Monsoon." *Deep-Sea Research. Part II, Topical Studies in Oceanography* 45 (10-11): 2195–2223. [https://doi.org/10.1016/s0967-0645\(98\)00068-x](https://doi.org/10.1016/s0967-0645(98)00068-x).

- Cohen, Elinatan, Guy J. Levy, and Mikhail Borisover. 2014. "Fluorescent Components of Organic Matter in Wastewater: Efficacy and Selectivity of the Water Treatment." *Water Research* 55 (May): 323–34. <https://doi.org/10.1016/j.watres.2014.02.040>.
- Cory, Rose M., and Diane M. McKnight. 2005. "Fluorescence Spectroscopy Reveals Ubiquitous Presence of Oxidized and Reduced Quinones in Dissolved Organic Matter." *Environmental Science & Technology* 39 (21): 8142–49. <https://doi.org/10.1021/es0506962>.
- Dainard, Paul G., Céline Guéguen, Natasha McDonald, and William J. Williams. 2015. "Photobleaching of Fluorescent Dissolved Organic Matter in Beaufort Sea and North Atlantic Subtropical Gyre." *Marine Chemistry* 177: 630–37. <https://doi.org/10.1016/j.marchem.2015.10.004>.
- Ducros, Loïc, Frédérique Eyrolle, Claire Della Vedova, Sabine Charmasson, Marc Leblanc, Adriano Mayer, Milanka Babic, Christelle Antonelli, David Mourier, and Franck Giner. 2018. "Tritium in River Waters from French Mediterranean Catchments: Background Levels and Variability." *The Science of the Total Environment* 612 (January): 672–82. <https://doi.org/10.1016/j.scitotenv.2017.08.026>.
- Fellman, Jason B., Eran Hood, and Robert G. M. Spencer. 2010. "Fluorescence Spectroscopy Opens New Windows into Dissolved Organic Matter Dynamics in Freshwater Ecosystems: A Review." *Limnology and Oceanography* 55 (6): 2452–62. <https://doi.org/10.4319/lo.2010.55.6.2452>.
- Fichot, Cédric G., and Ronald Benner. 2012. "The Spectral Slope Coefficient of Chromophoric Dissolved Organic Matter (S<sub>275-295</sub>) as a Tracer of Terrigenous Dissolved Organic Carbon in River-Influenced Ocean Margins." *Limnology and Oceanography* 57 (5): 1453–66. <https://doi.org/10.4319/lo.2012.57.5.1453>.
- Gao, Jiakai, Chenglong Liang, Guangzhu Shen, Jialong Lv, and Haiming Wu. 2017. "Spectral Characteristics of Dissolved Organic Matter in Various Agricultural Soils throughout China." *Chemosphere* 176 (June): 108–16. <https://doi.org/10.1016/j.chemosphere.2017.02.104>.
- Hansell, Dennis. 2001. "Marine Dissolved Organic Matter and the Carbon Cycle." *Oceanography* 14 (4): 41–49. <https://doi.org/10.5670/oceanog.2001.05>.
- Hansell, Dennis A. 2009. "Dissolved Organic Carbon in the Carbon Cycle of the Indian Ocean." In *Geophysical Monograph Series*, 217–30. <https://doi.org/10.1029/2007gm000684>.
- Hansell, Dennis A., and Craig A. Carlson. 2014. *Biogeochemistry of Marine Dissolved Organic*

- Matter*. Academic Press. <https://market.android.com/details?id=book-7iKOAwAAQBAJ>.
- Hedges, J. I., R. G. Keil, and R. Benner. 1997. "What Happens to Terrestrial Organic Matter in the Ocean?" *Organic Geochemistry* 27 (5-6): 195–212. [https://doi.org/10.1016/s0146-6380\(97\)00066-1](https://doi.org/10.1016/s0146-6380(97)00066-1).
- Helms, John R., Aron Stubbins, E. Michael Perdue, Nelson W. Green, Hongmei Chen, and Kenneth Mopper. 2013. "Photochemical Bleaching of Oceanic Dissolved Organic Matter and Its Effect on Absorption Spectral Slope and Fluorescence." *Marine Chemistry* 155: 81–91. <https://doi.org/10.1016/j.marchem.2013.05.015>.
- Hugo, Graeme. 2011. "Future Demographic Change and Its Interactions with Migration and Climate Change." *Global Environmental Change: Human and Policy Dimensions* 21: S21–33. <https://doi.org/10.1016/j.gloenvcha.2011.09.008>.
- Huguet, A., L. Vacher, S. Relexans, S. Saubusse, J. M. Froidefond, and E. Parlanti. 2009. "Properties of Fluorescent Dissolved Organic Matter in the Gironde Estuary." *Organic Geochemistry* 40 (6): 706–19. <https://doi.org/10.1016/j.orggeochem.2009.03.002>.
- Kim, Jeonghyun, and Guebuem Kim. 2015. "Importance of Colored Dissolved Organic Matter (CDOM) Inputs from the Deep Sea to the Euphotic Zone: Results from the East (Japan) Sea." *Marine Chemistry* 169: 33–40. <https://doi.org/10.1016/j.marchem.2014.12.010>.
- Lei, Xia, Jiayi Pan, and Adam T. Devlin. 2018. "Mixing Behavior of Chromophoric Dissolved Organic Matter in the Pearl River Estuary in Spring." *Continental Shelf Research* 154: 46–54. <https://doi.org/10.1016/j.csr.2018.01.004>.
- Li, Wen-Tao, Shi-Yu Chen, Zi-Xiao Xu, Yan Li, Chen-Dong Shuang, and Ai-Min Li. 2014a. "Characterization of Dissolved Organic Matter in Municipal Wastewater Using Fluorescence PARAFAC Analysis and Chromatography Multi-Excitation/emission Scan: A Comparative Study." *Environmental Science & Technology* 48 (5): 2603–9. <https://doi.org/10.1021/es404624q>.
- . 2014b. "Characterization of Dissolved Organic Matter in Municipal Wastewater Using Fluorescence PARAFAC Analysis and Chromatography Multi-Excitation/emission Scan: A Comparative Study." *Environmental Science & Technology* 48 (5): 2603–9. <https://doi.org/10.1021/es404624q>.
- Lønborg, Christian, Mar Nieto-Cid, Victor Hernando-Morales, Marta Hernández-Ruiz, Eva Teira, and Xosé Antón Álvarez-Salgado. 2016. "Photochemical Alteration of Dissolved Organic Matter and the Subsequent Effects on Bacterial Carbon Cycling and Diversity."

*FEMS Microbiology Ecology* 92 (5): fiw048. <https://doi.org/10.1093/femsec/fiw048>.

- Maizel, Andrew C., and Christina K. Remucal. 2017. "The Effect of Advanced Secondary Municipal Wastewater Treatment on the Molecular Composition of Dissolved Organic Matter." *Water Research* 122 (October): 42–52. <https://doi.org/10.1016/j.watres.2017.05.055>.
- Manninen, Noora, Helena Soinne, Riitta Lemola, Laura Hoikkala, and Eila Turtola. 2018. "Effects of Agricultural Land Use on Dissolved Organic Carbon and Nitrogen in Surface Runoff and Subsurface Drainage." *The Science of the Total Environment* 618 (March): 1519–28. <https://doi.org/10.1016/j.scitotenv.2017.09.319>.
- Massicotte, Philippe, Eero Asmala, Colin Stedmon, and Stiig Markager. 2017. "Global Distribution of Dissolved Organic Matter along the Aquatic Continuum: Across Rivers, Lakes and Oceans." *The Science of the Total Environment* 609 (December): 180–91. <https://doi.org/10.1016/j.scitotenv.2017.07.076>.
- Moran, Mary Ann, and Richard G. Zepp. 1997. "Role of Photoreactions in the Formation of Biologically Labile Compounds from Dissolved Organic Matter." *Limnology and Oceanography* 42 (6): 1307–16. <https://doi.org/10.4319/lo.1997.42.6.1307>.
- Mostofa, Khan M. G., Cong-Qiang Liu, Takahito Yoshioka, Davide Vione, Yunlin Zhang, and Hiroshi Sakugawa. 2012. "Fluorescent Dissolved Organic Matter in Natural Waters." In *Environmental Science and Engineering*, 429–559. [https://doi.org/10.1007/978-3-642-32223-5\\_6](https://doi.org/10.1007/978-3-642-32223-5_6).
- Murphy, Kathleen R., Adam Hambly, Sachin Singh, Rita K. Henderson, Andy Baker, Richard Stuetz, and Stuart J. Khan. 2011a. "Organic Matter Fluorescence in Municipal Water Recycling Schemes: Toward a Unified PARAFAC Model." *Environmental Science & Technology* 45 (7): 2909–16. <https://doi.org/10.1021/es103015e>.
- . 2011b. "Organic Matter Fluorescence in Municipal Water Recycling Schemes: Toward a Unified PARAFAC Model." *Environmental Science & Technology* 45 (7): 2909–16. <https://doi.org/10.1021/es103015e>.
- Nelson, Norman B., and David A. Siegel. 2013. "The Global Distribution and Dynamics of Chromophoric Dissolved Organic Matter." *Annual Review of Marine Science* 5: 447–76. <https://doi.org/10.1146/annurev-marine-120710-100751>.
- Oleinikova, Olga V., Olga Yu Drozdova, Sergey A. Lapitskiy, Vladimir V. Demin, Andrey Yu Bychkov, and Oleg S. Pokrovsky. 2017. "Dissolved Organic Matter Degradation by

- Sunlight Coagulates Organo-Mineral Colloids and Produces Low-Molecular Weight Fraction of Metals in Boreal Humic Waters.” *Geochimica et Cosmochimica Acta* 211: 97–114. <https://doi.org/10.1016/j.gca.2017.05.023>.
- Ollier, Joseph. 1972. “Contribution à L’étude Physico-Chimique de Quelques Sources Du Bassin Versant Du Gapeau (Var).” *Bulletin Mensuel de La Societe Linneenne de Lyon* 41 (3): 41–48. <https://doi.org/10.3406/linly.1972.9979>.
- Oloibiri, Violet, Sam De Coninck, Michael Chys, Kristof Demeestere, and Stijn W. H. Van Hulle. 2017. “Characterisation of Landfill Leachate by EEM-PARAFAC-SOM during Physical-Chemical Treatment by Coagulation-Flocculation, Activated Carbon Adsorption and Ion Exchange.” *Chemosphere* 186 (November): 873–83. <https://doi.org/10.1016/j.chemosphere.2017.08.035>.
- Osburn, Christopher L., Thomas J. Boyd, Michael T. Montgomery, Thomas S. Bianchi, Richard B. Coffin, and Hans W. Paerl. 2016. “Optical Proxies for Terrestrial Dissolved Organic Matter in Estuaries and Coastal Waters.” *Frontiers in Marine Science* 2. <https://doi.org/10.3389/fmars.2015.00127>.
- Osburn, Christopher L., Lauren T. Handsel, Benjamin L. Peierls, and Hans W. Paerl. 2016. “Predicting Sources of Dissolved Organic Nitrogen to an Estuary from an Agro-Urban Coastal Watershed.” *Environmental Science & Technology* 50 (16): 8473–84. <https://doi.org/10.1021/acs.est.6b00053>.
- Parlanti, E., K. Wörz, L. Geoffroy, and M. Lamotte. 2000a. “Dissolved Organic Matter Fluorescence Spectroscopy as a Tool to Estimate Biological Activity in a Coastal Zone Submitted to Anthropogenic Inputs.” *Organic Geochemistry* 31 (12): 1765–81. [https://doi.org/10.1016/s0146-6380\(00\)00124-8](https://doi.org/10.1016/s0146-6380(00)00124-8).
- . 2000b. “Dissolved Organic Matter Fluorescence Spectroscopy as a Tool to Estimate Biological Activity in a Coastal Zone Submitted to Anthropogenic Inputs.” *Organic Geochemistry* 31 (12): 1765–81. [https://doi.org/10.1016/s0146-6380\(00\)00124-8](https://doi.org/10.1016/s0146-6380(00)00124-8).
- Piccini, Claudia, Daniel Conde, Jakob Pernthaler, and Ruben Sommaruga. 2009. “Alteration of Chromophoric Dissolved Organic Matter by Solar UV Radiation Causes Rapid Changes in Bacterial Community Composition.” *Photochemical & Photobiological Sciences: Official Journal of the European Photochemistry Association and the European Society for Photobiology* 8 (9): 1321–28. <https://doi.org/10.1039/b905040j>.
- Raymond, Peter A., and Robert G. M. Spencer. 2015. “Riverine DOM.” In *Biogeochemistry of*

<https://doi.org/10.1016/b978-0-12-405940-5.00011-x>.

- Romera-Castillo, Cristina, Hugo Sarmiento, Xosé Antón Alvarez-Salgado, Josep M. Gasol, and Celia Marrasé. 2011. “Net Production and Consumption of Fluorescent Colored Dissolved Organic Matter by Natural Bacterial Assemblages Growing on Marine Phytoplankton Exudates.” *Applied and Environmental Microbiology* 77 (21): 7490–98. <https://doi.org/10.1128/AEM.00200-11>.
- Seto, Karen C., Burak Güneralp, and Lucy R. Hutyra. 2012. “Global Forecasts of Urban Expansion to 2030 and Direct Impacts on Biodiversity and Carbon Pools.” *Proceedings of the National Academy of Sciences of the United States of America* 109 (40): 16083–88. <https://doi.org/10.1073/pnas.1211658109>.
- Sgroi, Massimiliano, Paolo Roccaro, Gregory V. Korshin, and Federico G. A. Vagliasindi. 2017. “Monitoring the Behavior of Emerging Contaminants in Wastewater-Impacted Rivers Based on the Use of Fluorescence Excitation Emission Matrixes (EEM).” *Environmental Science & Technology* 51 (8): 4306–16. <https://doi.org/10.1021/acs.est.6b05785>.
- Sierra, M. M. D., M. Giovanela, E. Parlanti, and E. J. Soriano-Sierra. 2005. “Fluorescence Fingerprint of Fulvic and Humic Acids from Varied Origins as Viewed by Single-Scan and Excitation/emission Matrix Techniques.” *Chemosphere* 58 (6): 715–33. <https://doi.org/10.1016/j.chemosphere.2004.09.038>.
- Song, Wenjuan, Chenxi Zhao, Shuyong Mu, Xiangliang Pan, Daoyong Zhang, Fahad A. Al-Misned, and M. Golam Mortuza. 2015. “Effects of Irradiation and pH on Fluorescence Properties and Flocculation of Extracellular Polymeric Substances from the Cyanobacterium *Chroococcus Minutus*.” *Colloids and Surfaces. B, Biointerfaces* 128 (April): 115–18. <https://doi.org/10.1016/j.colsurfb.2015.02.017>.
- Stedmon, Colin A., and Rasmus Bro. 2008. “Characterizing Dissolved Organic Matter Fluorescence with Parallel Factor Analysis: A Tutorial.” *Limnology and Oceanography, Methods / ASLO* 6 (11): 572–79. <https://doi.org/10.4319/lom.2008.6.572b>.
- Stedmon, Colin A., and Stiig Markager. 2005a. “Resolving the Variability in Dissolved Organic Matter Fluorescence in a Temperate Estuary and Its Catchment Using PARAFAC Analysis.” *Limnology and Oceanography* 50 (2): 686–97. <https://doi.org/10.4319/lo.2005.50.2.0686>.
- . 2005b. “Resolving the Variability in Dissolved Organic Matter Fluorescence in a

- Temperate Estuary and Its Catchment Using PARAFAC Analysis.” *Limnology and Oceanography* 50 (2): 686–97. <https://doi.org/10.4319/lo.2005.50.2.0686>.
- Stedmon, Colin A., Stiig Markager, and Rasmus Bro. 2003a. “Tracing Dissolved Organic Matter in Aquatic Environments Using a New Approach to Fluorescence Spectroscopy.” *Marine Chemistry* 82 (3-4): 239–54. [https://doi.org/10.1016/s0304-4203\(03\)00072-0](https://doi.org/10.1016/s0304-4203(03)00072-0).
- . 2003b. “Tracing Dissolved Organic Matter in Aquatic Environments Using a New Approach to Fluorescence Spectroscopy.” *Marine Chemistry* 82 (3-4): 239–54. [https://doi.org/10.1016/s0304-4203\(03\)00072-0](https://doi.org/10.1016/s0304-4203(03)00072-0).
- Williams, Clayton J., Paul C. Frost, Ana M. Morales-Williams, James H. Larson, William B. Richardson, Aisha S. Chiandet, and Marguerite A. Xenopoulos. 2016. “Human Activities Cause Distinct Dissolved Organic Matter Composition across Freshwater Ecosystems.” *Global Change Biology* 22 (2): 613–26. <https://doi.org/10.1111/gcb.13094>.
- Wu, Qianyuan, Chao Li, Wenlong Wang, Tao He, Hongying Hu, Ye Du, and Ting Wang. 2016. “Removal of Fluorescence and Ultraviolet Absorbance of Dissolved Organic Matter in Reclaimed Water by Solar Light.” *Journal of Environmental Sciences* 43 (May): 118–27. <https://doi.org/10.1016/j.jes.2015.08.021>.
- Yamashita, Youhei, Joseph N. Boyer, and Rudolf Jaffé. 2013. “Evaluating the Distribution of Terrestrial Dissolved Organic Matter in a Complex Coastal Ecosystem Using Fluorescence Spectroscopy.” *Continental Shelf Research* 66: 136–44. <https://doi.org/10.1016/j.csr.2013.06.010>.
- Yamashita, Youhei, Rudolf Jaffé, Nagamitsu Maie, and Eiichiro Tanoue. 2008. “Assessing the Dynamics of Dissolved Organic Matter (DOM) in Coastal Environments by Excitation Emission Matrix Fluorescence and Parallel Factor Analysis (EEM-PARAFAC).” *Limnology and Oceanography* 53 (5): 1900–1908. <https://doi.org/10.4319/lo.2008.53.5.1900>.
- Yang, Xiaofang, Fangang Meng, Guocheng Huang, Li Sun, and Zheng Lin. 2014. “Sunlight-Induced Changes in Chromophores and Fluorophores of Wastewater-Derived Organic Matter in Receiving Waters--the Role of Salinity.” *Water Research* 62 (October): 281–92. <https://doi.org/10.1016/j.watres.2014.05.050>.
- Zepp, Richard G., Wade M. Sheldon, and Mary Ann Moran. 2004. “Dissolved Organic Fluorophores in Southeastern US Coastal Waters: Correction Method for Eliminating Rayleigh and Raman Scattering Peaks in Excitation–emission Matrices.” *Marine Chemistry* 89 (1-4): 15–36. <https://doi.org/10.1016/j.marchem.2004.02.006>.

- Zhu, Guocheng, Jun Yin, Peng Zhang, Xiaofeng Wang, Gongduan Fan, Bin Hua, Bozhi Ren, Huaili Zheng, and Baolin Deng. 2014. "DOM Removal by Flocculation Process: Fluorescence Excitation–emission Matrix Spectroscopy (EEMs) Characterization." *Desalination* 346: 38–45. <https://doi.org/10.1016/j.desal.2014.04.031>.
- Zhu, Wen-Zhuo, Gui-Peng Yang, and Hong-Hai Zhang. 2017. "Photochemical Behavior of Dissolved and Colloidal Organic Matter in Estuarine and Oceanic Waters." *The Science of the Total Environment* 607-608 (December): 214–24. <https://doi.org/10.1016/j.scitotenv.2017.06.163>.
- Zhu, Wen-Zhuo, Jing Zhang, and Gui-Peng Yang. 2017. "Mixing Behavior and Photobleaching of Chromophoric Dissolved Organic Matter in the Changjiang River Estuary and the Adjacent East China Sea." *Estuarine, Coastal and Shelf Science*, July. <https://doi.org/10.1016/j.ecss.2017.07.019>.



---

## **Chapter 4 - Temporal and Spatial investigations on the river Gapeau**

---

The results of the geographical field experiment and the temporal variation of the 48 hours of the three endmember mixing components are presented in the present chapter. First the temporal results are exposed to explore the short temporal variation. Secondly an exploration of the geographical behavior is studied to understand how the mixing process occurs and if it could be explained by the end members mixing model.

## IV.1 Temporal Field experiment

Temporal variations of the three endmember mixing components were investigated to understand how the fluorescence signal of the dissolved organic matter of each one of the three endmember mixing components varies. In order to understand how the fluorescence signal of the anthropogenic dissolved organic matter varies during the day, and is it could be resumed in an average contribution instead taking in account a day to night variation.

### Time table and different sampling

**Table IV.1** : The exact sampling dates of both the Temporal and Spatial "Geographical" field experiments of the endmembers (WW, RW, Confluence and SW). S : Spatial ; T : Temporal.

2016, month	1	2	3	4	5	6	7	8	9	10	11	12
WWTP								S			T	
Gapeau								S	T			
Confluence								S		T		
Sea								S		T		

The above table (table IV.1) summarizes the campaigns of temporal (T) and geographical (S) investigation of the Gapeau river, the confluence of Gapeau River, the Réal Martin tributary in addition to the wastewater treatment plant of La Crau city (WW) and the seawater (SW) at the coastal zone of Hyères

city. The geographical “spatial” investigative field experiments for all the above mentioned water sources “endmembers” were conducted in the month of August 2016 “19<sup>th</sup>, 22<sup>th</sup>, 23<sup>th</sup>” and are shown in “S” with a lighter gray color. Whereas, the temporal investigative field experiments were conducted in different months but close together. The twenty four samples of the temporal field experiment of the WWTP were done in the month of november 2016 and the temporal field experiment of the Gapeau river was in the month of September whereas for the Confluence (Gapeau-Réal Martin) and the seawater at (place St. Louis at Hyères city) were sampled for temporal investigation in the same month of October 2016. The exact dates for both the temporal and the geographical field experiment could be consulted in section (II.4.2) of the methodology chapter . Some photos of the four sampling sites for the temporal field experiments are shown in figure IV.1.

(a): Gapeau River



(b): WWTP of La Crau City



(c) : Confluence (Gapeau-Le Réal Martin)



(d): Sea (L’Aygade at Hyeres city)



**Figure IV.1** : Figures showing photos of the sampling campaigns for the temporal field experiment of the four water sources on the gapeau river (a): Gapeau River, (b): WWTP of La Crau City, (c) : Confluence (Gapeau-Le Réal Martin), (d): Sea (L’Aygade at Hyeres city).

---

**Table IV.2** : Weather conditions for the temporal field experiments of the four sampling sites.

Gapeau River	<b>19/09/2016</b>	<b>20/09/2016</b>	<b>21/09/2016</b>
	Temperatures : 23°C/29°C Precipitations : 0 mm	Temperatures : 21°C/27°C Precipitations : 0 mm	Temperatures : 21°C/25°C Precipitations : 0.3 mm
Confluence (Gapeau-Réal Martin)	<b>04/10/2016</b>	<b>05/10/2016</b>	<b>06/10/2016</b>
	Temperatures : 19°C/24°C Precipitations : 0 mm	Temperatures : 18°C/23°C Precipitations : 0 mm	Temperatures : 19°C/21°C Precipitations : 1.8 mm
WWTP of La CRAU	<b>15/11/2016</b>	<b>16/11/2016</b>	<b>17/11/2016</b>
	Temperatures : 13°C/16°C Precipitations : 0 mm	Temperatures : 11°C/18°C Precipitations : 0 mm	Temperatures : 11°C/17°C Precipitations : 0 mm
Sea at Hyères	<b>17/10/2016</b>	<b>18/10/2016</b>	<b>19/10/2016</b>
	Temperatures : 17°C/22°C Precipitations : 0.5 mm	Temperatures : 18°C/24°C Precipitations : 0.2 mm	Temperatures : 15°C/22°C Precipitations : 0 mm

Data were recovered in retrograde from  
<https://www.historique-meteo.net/france/provence-alpes-c-te-d-azur/hyeres/2016/>

The temperatures and the precipitation in mm are shown in table IV.2 for all of the sampled sites for the temporal field experiment. For the sampling site of the confluence of the Gapeau river and the Real Martin, the sampling was finished at 08:41 am of 06/10/2016 as it is clearly mentioned in Table II.9 in section II.4.2 of the methodology chapter. However, it is mentioned in this same table that the precipitation was 1.8 mm which was recovered meteoFrance<sup>1</sup>. The rain event happened after recovering and finishing the sampling of the confluence site (Gapeau River - Réal Martin tributary). Therefore, there was no expected effect of the rainfall event on the samples taken from this site. For the sampling campaign of the seawater at St. Louis at Hyères city, there was a rain event occurred at night. The precipitations which are shown in the above table (table IV.2) were collected from meteoFrance<sup>1</sup> which are smaller than the exact precipitation data in mm for the exact hours of this rainfall event which are

---

<sup>1</sup> <https://www.historique-meteo.net/france/provence-alpes-c-te-d-azur/hyeres/2016/>

presented in the next table (table IV.3) which were collected and recovered from meteociel<sup>2</sup> website. We collected and recovered the weather condition data from the web. The exact data of precipitation in mm of the rainfall event on the seawater at Hyeres city are shown in the following table (table IV.3) with the exact hours of the rainfall event. The more intense rainfall event for the sampling campaign of the sampling site of seawater at St.Louis occurred at the first day of sampling at 5 pm and continued till 8 pm.

**Table IV.3** : Rain event occurred for the temporal field experiments of the sea water at St.louis -Hyerres city . For the non-mentioned hours , there was no rain event with 0 mm precipitation.

17 - october -2016					19 - October -2016
Hour	5 PM	6 PM	7 PM	8 PM	5 AM
Precipitation in mm	7 mm	2 mm	7 mm	2 mm	0.2 mm

Data were recovered and collected in retrograde from the following website

<https://www.meteociel.fr>

#### IV.1.1 Variation of the conductivity during temporal field experiment

The conductivity allow the monitoring of the seawater mixing for coastal zone, and it is also a good tracer for the urban input in river water. Even if it not the same scale between seawater and continental or anthropic waters, one can see on figure IV.2 that conductivity is constant along the day for WW and the confluence. For this figure (figure IV.2), the average value is calculated and expressed versus hour of the day. The electrical conductivity of the sea water was in the range of  $54.82 \pm 1.09 \text{ mS.cm}^{-1}$  which is normal mediterranean sea conductivity as it was found by (Abbassi et al., 2017) in the coastal waters of the city of Sidi Ifni (Morocco) in which they found the electrical conductivity of these coastal waters to range from  $40.14 \text{ mS.cm}^{-1} (\pm 0.05)$  to  $53.23 \text{ mS.cm}^{-1} (\pm 0.1)$ .

For the sea there was a rainy day which started at ( 5 pm = 0.75 day) and one can observe that there is fluctuation in the conductivity meaning that there is freshwater input at 0.75 day which contributed to the slight decrease of the electrical conductivity of the sea water. However the variation is small compared to the to the salinity meaning that the salinity remained in the usual range despite the rainfall event.

<sup>2</sup> <https://www.meteociel.fr>

Concerning the electrical conductivity of the Gapeau river, it is clear that there is no diurnal variation and is around  $833.88 \pm 116.51 \mu\text{S}\cdot\text{cm}^{-1}$ . It is the same trend for the WW which is around  $951.82 \pm 20.05 \mu\text{S}\cdot\text{cm}^{-1}$  which is in the range of  $29\text{--}1,015 \mu\text{S}\cdot\text{cm}^{-1}$ , which is found in an urban municipal wastewater treatment plant effluent in south africa (Odjadjare and Okoh 2010). The electrical conductivity of the confluence of Gapeau river with the Réal Martin tributary is consequently an intermediate value ( $898.22 \pm 18.03 \mu\text{S}\cdot\text{cm}^{-1}$ ) results of the river and WW discharge mixing. By using the mixing formula it is possible to estimate the discharge ratio between the Gapeau river and the WW considering that the electrical conductivity EC is conservative and the Réal Martin contribution could be negligible.

In our case the calculus for a river water at  $833.88 \pm 116.51 \mu\text{S}\cdot\text{cm}^{-1}$ , a WWTP at  $951.82 \pm 20.05 \mu\text{S}\cdot\text{cm}^{-1}$  and a confluence at  $898.22 \pm 18.03 \mu\text{S}\cdot\text{cm}^{-1}$  give a discharge ratio of about  $0.8 \pm 1.86$

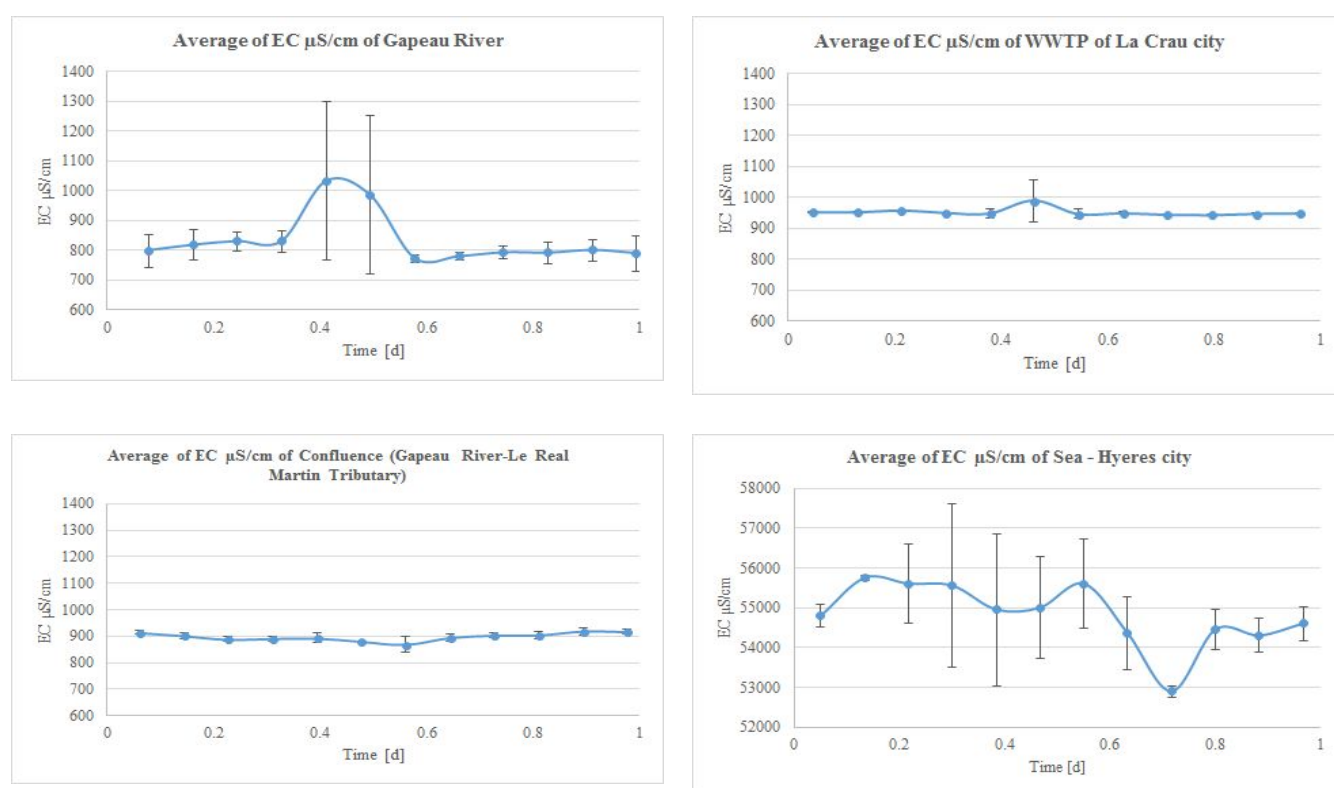


**Figure IV.2** : Diurnal (48 h cycle) variation of the conductivity values in  $\mu\text{S}/\text{cm}$  of the four water sources (endmembers) sampled for the temporal field experiment

## IV.1.2 Variation of the pH values during temporal field experiment

Concerning pH, sea and confluence present a constant value. Compared to the conductivity, there is no pH change due to the rain for sea water. It seems that there is a tendency for the pH to decrease during the day and increasing during the night. This could be explained by the buffer role of the carbonate system.

For the Gapeau, one can see that there is a higher variability and a slight decrease during the night, pH is around 8. The WWTP at the contrary, is more often under the value of 8 during the 48H of sampling.

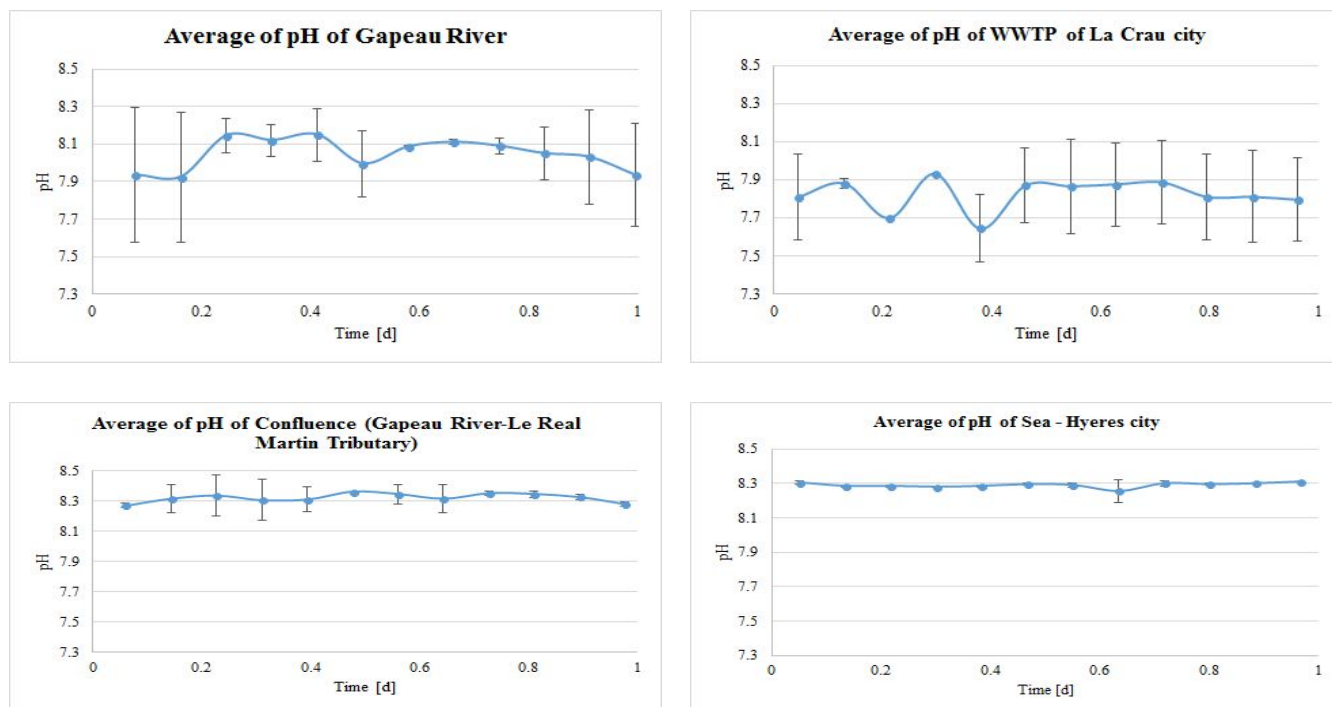


**Figure IV.3** : Diurnal (48 h cycle) variation of pH values of the four water sources (endmembers) sampled for the temporal field experiment

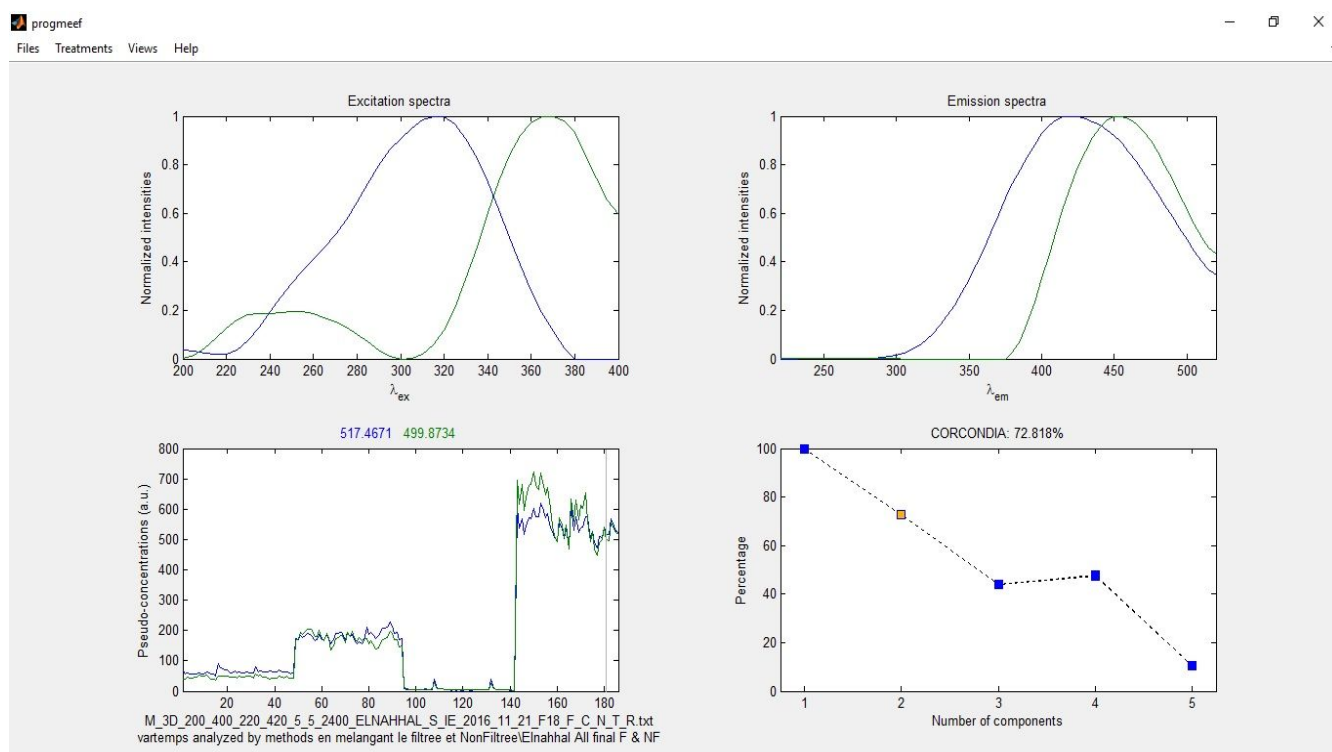
The pH of the Gapeau river showed an average  $8.05 \pm 0.17$ . The pH of the SW is quite constant and around  $8.29 \pm 0.02$ . The confluence shows an average pH of  $8.32 \pm 0.06$ . For the WW, the pH is the lower one as expected  $7.82 \pm 0.16$  which is more acidic compared to others. In addition, the range of pH of wastewater treatment plant effluent is in the normal range which is consistent with the results of [\(Odjadjare and Okoh 2010\)](#) who found that the pH values ranged between 6.8 and 8.3 in an urban municipal wastewater effluent. For the Gapeau river the first day shows a maximum at 01 pm, and a minimum at 04 am. After this time, there is an increase to pH=8 and no more detectable variation. During night, the pH of Gapeau river is constant and started to increase in the beginning of the morning (0.25 day) because there are other wastewater treatment plant effluent upstream the Gapeau river in different commune which impact and could contribute to this slight increase of pH of Gapeau river and it remain a little bit constant (around 8.1) till noon where there is a slight decrease then it returns back to its higher constant value in the night till midnight. The pH of the wastewater treatment plant effluent shows the highest variability starting from morning till noon because the wastewater treatment plant has its higher load during the morning which influence its pH value by decreasing it. The variability of pH values for



the confluence between Gapeau river and Le Réal Martin showed little variability which is the same as the variability of pH of the sea water. The slight decrease of pH value of the sea water at (0.7 day  $\approx$  17 hours  $\approx$  5pm) could be attributed to the rainfall event the day of sampling. One can keep in mind that the sampling experiments were not made on the same couple of days. The spatial variation of pH is as following  $WW < RW < Confluence < SW$ .

### IV.1.3 EEMs temporal determination

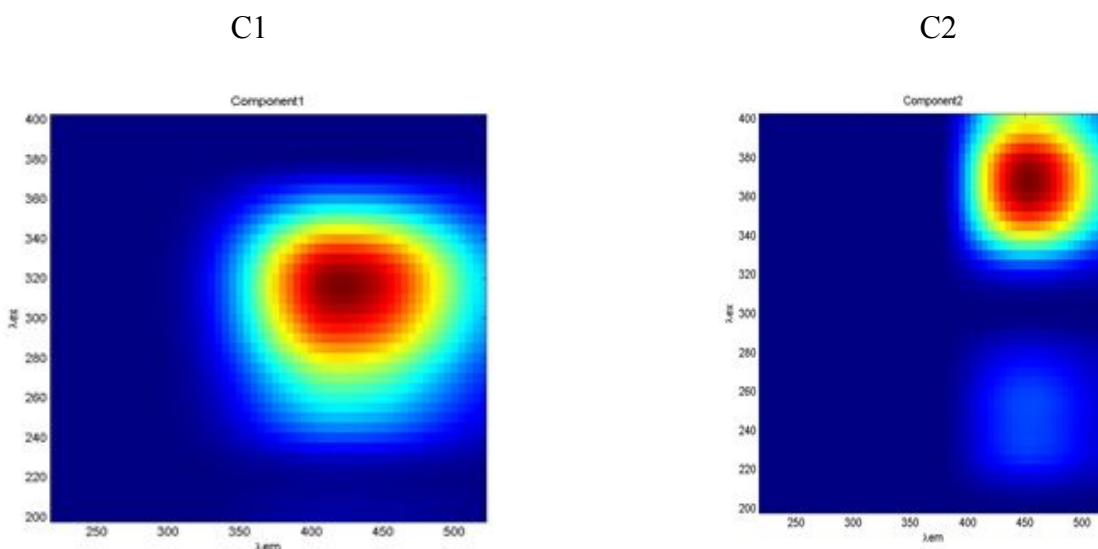
The CP/PARAFAC algorithm was applied using Progmeeff software, on the datasets of EEM of the 48 hours sampling campaigns. This CP/PARAFAC decomposition was carried out on the global datasets which contained the sub datasets corresponding to each sampling site : the Gapeau river, wastewater treatment plant of La Crau city, the confluence of Gapeau and Le Réal Martin tributary and the sea water sampled at l'Aiguade at Hyères city in the PACA REGION of France. These subsets or sub-datasets contained also the EEMs of the filtered samples of each sampling site in this temporal field experiment. And the following figures summarized the results of the process of CP/PARAFAC decomposition.

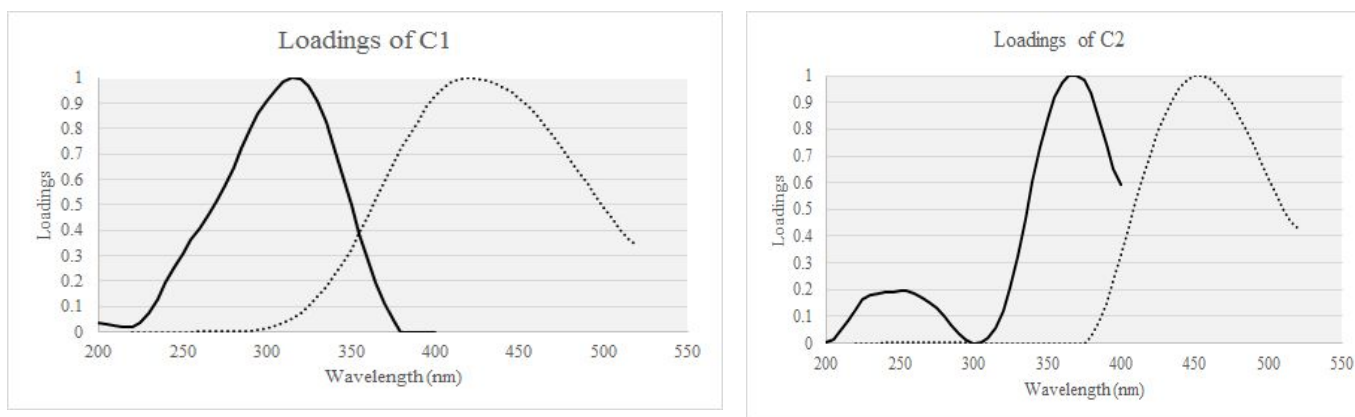


**Figure IV.4** : CP/PARAFAC results by the PROGMEEF software showing the loading for the two parafac components and the concordia results (72.82% for two components)



The CORCONDIA analysis showed a drop in core consistency between three elements and five, from below 60 % to less than or around 20 % which surpasses the acceptable threshold of 60% where as it showed a value of 72.82 % for two CP/PARAFAC components, indicating that a two-factor model was appropriate as it is shown in the lower right hand graph of figure IV.4. In addition, the lower left hand graph of figure IV.4 shows the pseudo-concentrations (or relative contribution) of these CP/PARAFAC components in the EEMs text files of the datasets of the temporal field experiments of the four water sources (Gapeau River, Wastewater treatment plant of La Crau WWTP, Confluence of Gapeau and Le Réal Martin tributary, and the sea water at L'Aiguade at Hyeres city southeastern of France ). The higher values of pseudo-concentrations of CP/PARAFAC components (extreme right of the lower left hand side graph of figure IV.4) are clearly found in the EEMs (excitation emission matrix) of the wastewater treatment plant temporal field experiment which highly agrees with the results of the photodegradation (solar irradiation) experiments which are presented in the previous chapter (chapter 3) in which it was found the remaining fluorescence signal, in the developed multilinear regression model, after the irradiation process takes place comes mainly from the wastewater treatment plant endmember mixing component which is consistent.





Fulvic Like Component

Humic Like Component

**Figure IV.5.** Contour plots of CP/PARAFAC components identified from the decomposition of all EEM datasets of the Temporal field experiments of the Gapeau river , Confluence (Gapeau river, Le Réal Martin), wastewater treatment plant of La Crau city, Sea water at Hyères city. Spectral loadings of excitation and emission wavelengths of the two identified CP/PARAFAC in the temporal field experiment are also shown. Excitation loading for CP/PARAFAC component are solid lines whereas emission loadings are shown in dotted lines.

**Table IV.4-**Descriptions of CP/PARAFAC components and comparison with literature

Component	$\lambda_{EX}/\lambda_{EM}$ (nm)	Description and references in literature
Component C1	315/420	Component 4 (Stedmon, Markager, and Bro 2003a) : terrestrially derived organic matter Peak C (Coble 1996; Coble, Del Castillo, and Avril 1998) : visible humic-like Component 2 (Yamashita et al. 2008) : terrestrial humic-like Component 4 (Stedmon and Markager 2005a)
Component C2	(250) 370/455	Component 3 (Stedmon, Markager, and Bro 2003a) Component G3 (Murphy et al. 2011a) Component 3 (Li et al. 2014a) Component 7 (Osburn, Handsel, et al. 2016) Component 5 (Baghoth, Sharma, and Amy 2011) Terrestrial humic substances Component 1 (W.-Z. Zhu, Zhang, and Yang 2017) Humic-Like

Two components were successfully decomposed by CP/PARAFAC modeling on the EEM datasets of the temporal field experiment of four water sources (Gapeau river , Wastewater treatment plant of La Crau, Confluence Gapeau and Le Real Martin tributary, sea water at L'ayguade at Hyeres city) after the removal of the 1<sup>st</sup> and 2<sup>nd</sup> order Rayleigh and Raman Scattering. The above table shows the contour plots of the three CP/PARAFAC components which were found from the analysis conducted in the matlab

software and progmeef in all of the excitation emission matrices as well as their corresponding loadings for both the excitation and the emission wavelengths. These two fluorescent CP/PARAFAC components have been previously identified (Table IV.4). The 1<sup>st</sup> CP/PARAFAC component, found in this study, C1 component showed an excitation maximum at 315 nm and an emission maximum at 420 nm and a range of excitation emission wavelengths (Ex=250-350 nm, Em=350-500 nm). Previous studies have associated this component to UVA humic-like fluorescent CP/PARAFAC component and Peak C (Coble, 2007b). In addition this C1 component (Ex=250-350 nm, Em=350-500 nm) has been cited to have terrestrial, anthropogenic, agricultural sources by the studies conducted by (Colin A. Stedmon & Markager, 2005b; Colin A. Stedmon, Markager, & Bro, 2003b). The 2<sup>nd</sup> CP/PARAFAC component, found in this study, C2 component showed an excitation maximum at 370 nm with a minor peak at 250 nm and an emission maximum at 455 nm and a range of excitation emission wavelengths (Ex=330-400 nm, Em=400-500 nm). These two CP/PARAFAC components C1 and C2 greatly resembles the CP/PARAFAC components C1 and C2 found in the global decomposition of the EEMs datasets of the all irradiation experiments which were found by the CP/PARAFAC decomposition in the previous chapter (chapter 3). In addition, the spectra of this CP/PARAFAC C2 component resembles the spectra of the CP/PARAFAC component G3 which has excitation emission maxima at 350 nm/428 nm and found in the study conducted by (Murphy et al., 2011b) who have attributed this CP/PARAFAC component to be wastewater/nutrient enrichment tracer. This CP/PARAFAC C2 component has also been observed in previously reported literature and has been identified as the humic-like component and it is similar to C3 in the study conducted by (Li et al., 2014b) which had two excitation maxima (at 250, 350 nm) corresponding to the same emission maxima (at 440 nm). Furthermore, this CP/PARAFAC C2 component has very similar spectra as C7 in the study done by (Osburn, Handsel, et al., 2016) in which they compared their CP/PARAFAC components with the published literature using the OpenFluor database (<http://www.openfluor.org>) and found that their CP/PARAFAC component C7 matched with 6 models, all from recycled water studies, which included samples of wastewater, treated water, gray water. This CP/PARAFAC component has the peak C and peak A as in the study conducted by (Coble, 1996b) and is considered to be humic substances of terrestrial origin or vascular plant origin.

#### IV.1.4 EEMs temporal variation

After the global CP/PARAFAC decomposition of the global dataset which consists of the sub-datasets of EEMs of the temporal variation of the Gapeau river, wastewater treatment plant of La Crau, Confluence of Gapeau river and Le Real Martin Tributary and the seawater at l'Aiguade at Hyères city has been

done; the results of the two CP/PARAFAC components were isolated for each water source (Gapeau, WWTP, Confluence, Sea) in a separate excel file then a normalization step were applied to each dataset in a separate manner. The normalization was done by dividing the values of the contribution of C1 and C2 by the maximum value of C1 or C2 contribution in the dataset in order to enable the relative comparison.

$$C_i^{\text{Temporal Endmember}} = C_i^{\text{Temporal Endmember}} / [\max(C_i^{\text{Temporal Endmember}})] * 100$$

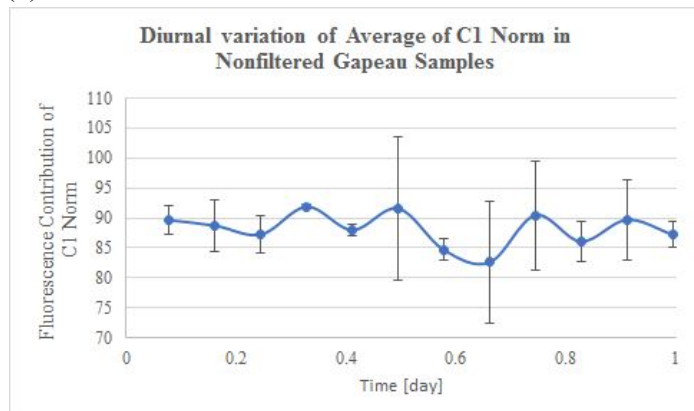
Where :

$C_i$  : is the CP/PARAFAC Component C1 and C2 previously described in table IV.4. Temporal Endmember : is Temporal field experiment for the Gapeau River , Wastewater treatment plant , Confluence of Gapeau and Le Real Martin or Sea dataset

#### IV1.4.1 Gapeau River

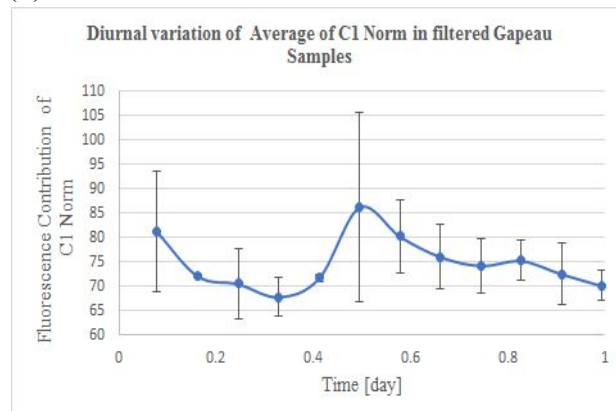
The temporal variation of the CP/PARAFAC components C1 and C2 (terrestrial humic-like fluorescence) ; found from the CP/PARAFAC decomposition of the global dataset of the temporal field experiment ; for the Gapeau river for both the filtered samples and the nonfiltered samples are shown in the following figure (figure IV.6) .

(a)



(c)

(b)



(d)

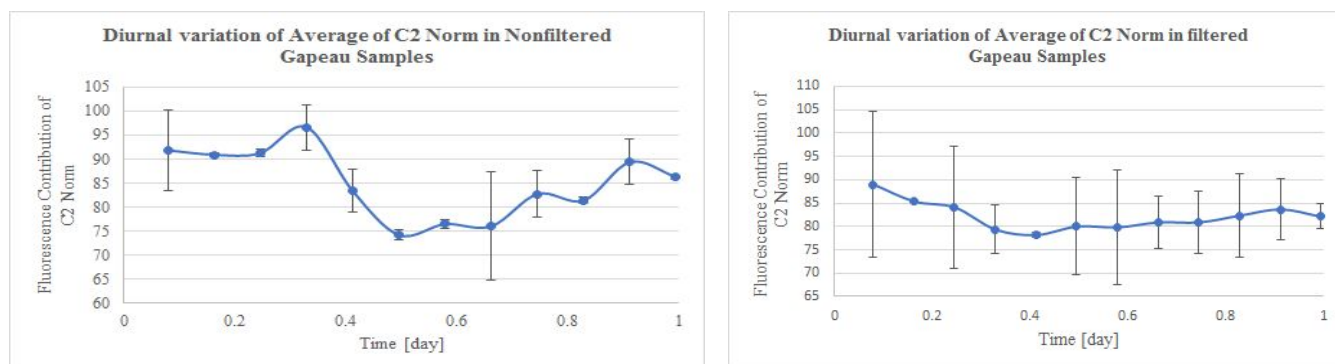


**Figure IV.6 :** Four figures of the normalized contribution of CP/PARAFAC components C1 and C2 for the temporal field experiment of the Gapeau River . Figures on the left hand side shows the variations of C1 and C2 for the nonfiltered Gapeau Samples whereas the right hand side shows the variations of C1 and C2 for the filtered Gapeau Samples. Units of Fluorescence contributions of C1 and C2 are arbitrary units

It can be seen from figure IV.6 that for the non filtered samples, the contribution of the CP/PARAFAC component C1 fluctuates around a mean value of about  $88.15 \pm 5.08$  and shows a fluctuation with a constant trend. The values of the contribution of CP/PARAC C1 component in the filtered samples (graph (b)) are less than those in the nonfiltered samples. The effect of filtration of the samples on the first CP/PARAFAC component can be seen in graph (b) which shows a diminution of the contribution of this CP/PARAFAC component and there is a diminution and decline of the contribution of this C1 during night [0-0.25 day] and [0.75-1 day] while during the day there is an increase of the contribution of C1 from morning till noon and then a decrease can be seen from afternoon till the end of the day. For the second CP/PARAFAC component C2, its contribution is constant during the first hours of the day [0-0.25 day] then it started to decrease till noon and after that it increased till night in the nonfiltered samples . The effect of filtration on the contribution of this C2 could be noticed as a slight diminution of its variations . Component C2 is related to vascular plant or terrestrial origin, and this variation could be interpreted as “morning” effect.

#### IV.1.4.2 Wastewater Treatment plant

The temporal variation of the CP/PARAFAC components C1 and C2 (terrestrial humic-like fluorescence) ; found from the CP/PARAFAC decomposition of the global dataset of the temporal field experiment ; for the wastewater treatment plant discharge for both the filtered samples and the nonfiltered samples are shown in the following figure (figure IV.7) .

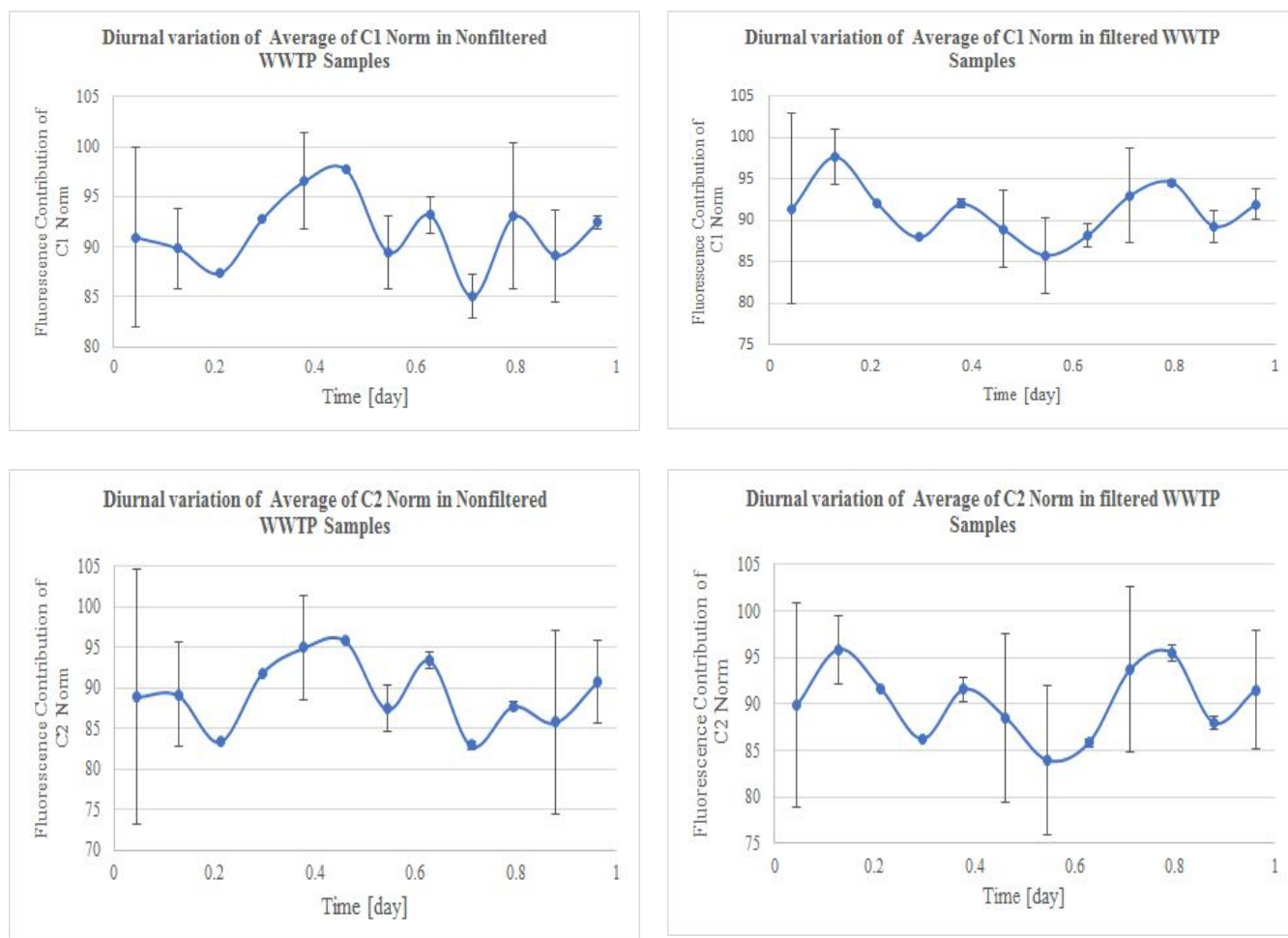


**Figure IV.7 :** Four figures of the normalized contribution of CP/PARAFAC components C1 and C2 for the temporal field experiment of the wastewater treatment plant WWTP of La Crau city . Figures on the left hand side shows the variations of C1 and C2 for the nonfiltered Gapeau Samples whereas the right hand side shows the variations of C1 and C2 for the filtered Gapeau Samples. Units of Fluorescence contributions of C1 and C2 are arbitrary units

It can be seen from figure IV.7 that for both of the CP/PARAFAC components C1 and C2, they have the big variations when compared to the variations of C1 and C2 in the other endmembers (Gapeau river, Confluence Gapeau & Le Réal Martin, seawater). This variation corresponds to the effluents and the times of peak flow of the wastewater treatment plant and the quality of the fluorophores in the effluent dissolved organic matter. There is no measurable effect of the filtration of the samples on the variability of C1 or C2 which suggests that the fluorophores have strong concentrations and the particulate matter has negligible contribution on the fluorescence of the CP/PARAFAC components C1 and C2 which are approximately of the same type (humic-like fluorescence). One can consider the mean WW variation is about 90 % of the total contribution.

#### IV.1.4.3 Confluence Gapeau River & Le Réal Martin

The temporal variation of the CP/PARAFAC components C1 and C2 (terrestrial humic-like fluorescence) ; found from the CP/PARAFAC decomposition of the global dataset of the temporal field experiment ; for the confluence of the Gapeau river and wastewater treatment plant discharge and the Le Réal Martin tributary for both the filtered samples and the nonfiltered samples are shown in the following figure (figure IV.8) .

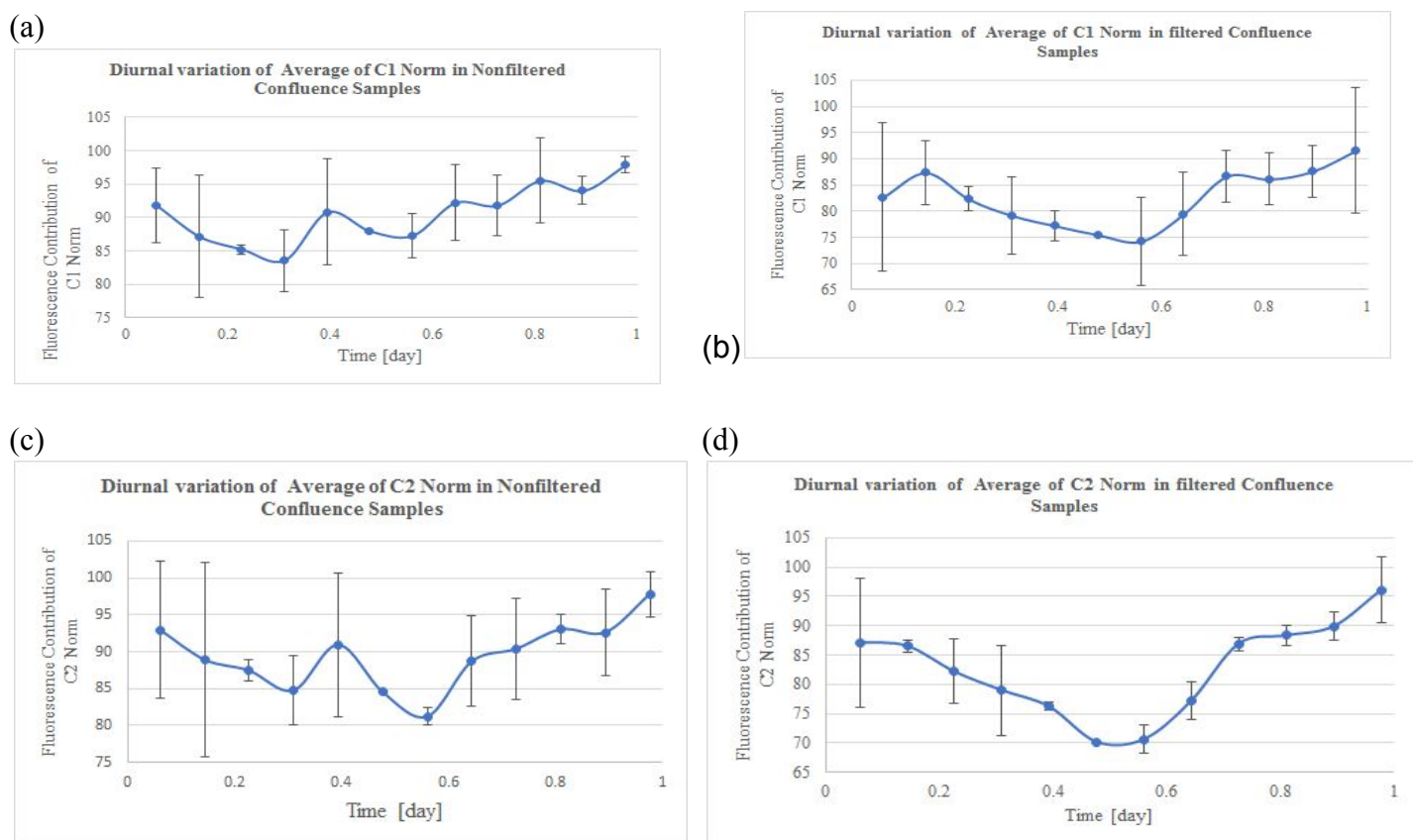


**Figure IV.8 :** Four figures of the normalized contribution of CP/PARAFAC components C1 and C2 for the temporal field experiment of the Confluence of Gapeau River and Le Real Martin tributary . Figures on the left hand side shows the variations of C1 and C2 for the nonfiltered Gapeau Samples whereas the right hand side shows the variations of C1 and C2 for the filtered Gapeau Samples. Units of Fluorescence contributions of C1 and C2 are arbitrary units

It can be seen from the above figure (figure IV.8) that for the graph (a) that contribution of CP/PARAFAC component C1 for the confluence samples (Gapeau river, Le Réal Martin) decrease during the night (0-0.25 day) from midnight till the beginning of morning then it starts to fluctuate in an increasing trend till it reaches the next midnight. For graph (b) in this same figure (figure IV.8) which shows the effect of the filtration on the contribution of CP/PARAFAC component C1, it is shown that the contribution of C1 started to decrease from midnight and continued to decrease till afternoon (0.55 day) which suggests that the particulate matter has a measurable effect of the variation of this CP/PARAFAC component and shows that some of the fluorophores undergoes photodegradation process. Afterwards, it started to increase to attain a value less than that of the non filtered samples in graph (a) of the same figure (figure IV.8) . Moreover, for the diurnal variation of the CP/PARAFAC component C2 in the non filtered samples of the confluence Gapeau river and Le Réal Martin which are shown in the graph (c) of this same figure (figure IV.8), the variation of the contribution of C2 approximately resembles the variations of C1 in graph (a) in the same figure (figure IV.8) and there is an increase of the contribution of C2 which starts at noon and continued till next midnight . One can consider that at the confluence with



the Réal Martin there is a diurnal trend for the component C2, terrestrial, with a minimum at noon. No further investigation were done to understand why this trend exist as it is out of this work focus.

#### IV.1.4.4 Sea Water

The temporal variation of the CP/PARAFAC components C1 and C2 (terrestrial humic-like fluorescence) ; found from the CP/PARAFAC decomposition of the global dataset of the temporal field experiment ; for the seawater at the site of l'Aiguade at the city of Hyères in Region PACA in the southeastern part of France for both the filtered samples and the nonfiltered samples are shown in the following figure (figure IV.9) :

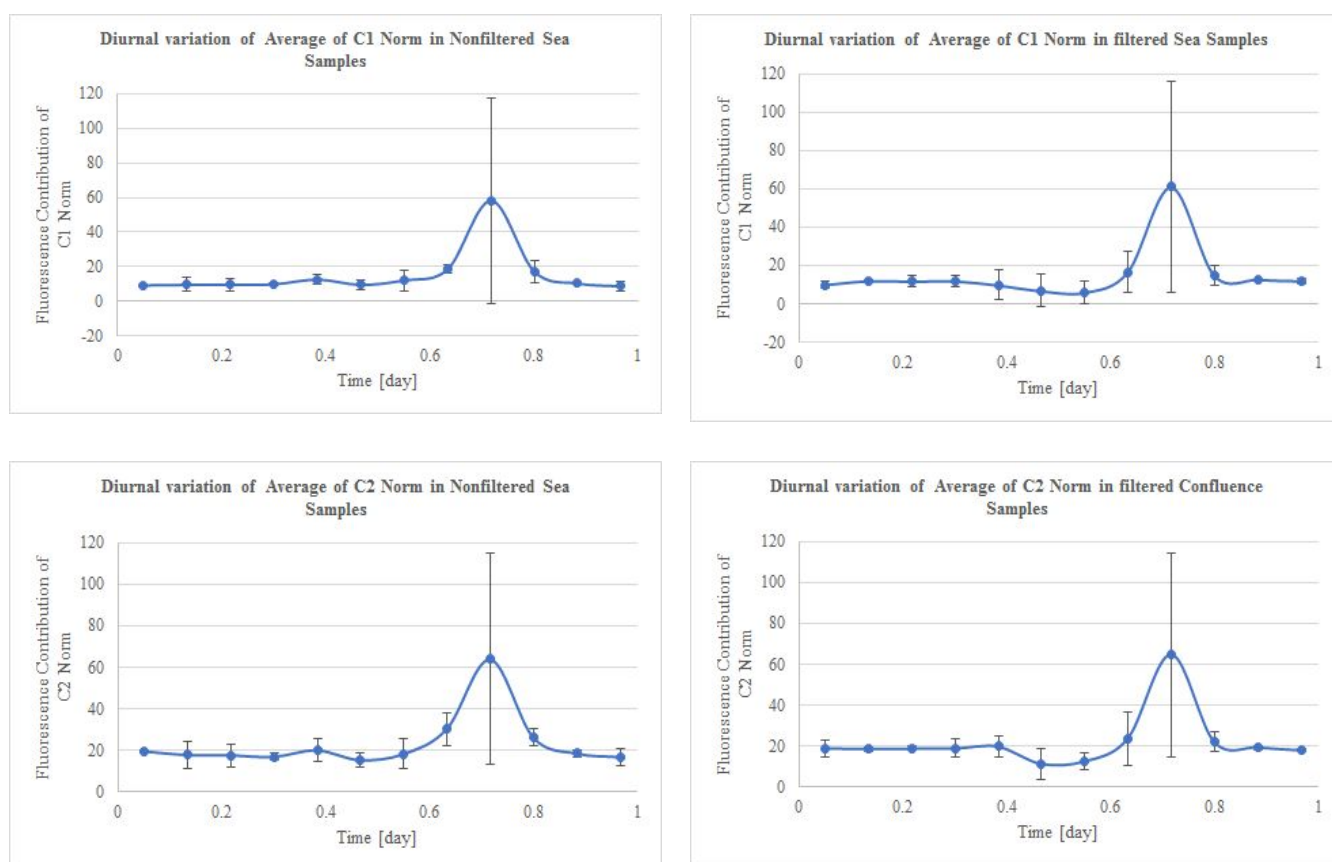


**Figure IV.9 :** Four figures of the normalized contribution of CP/PARAFAC components C1 and C2 for the temporal field experiment of the sea water samples at St.Louis, Hyeres city . Figures on the left hand side shows the variations of C1 and C2 for the nonfiltered Gapeau Samples whereas the right hand side shows the variations of C1 and C2 for the filtered Gapeau Samples. Units of Fluorescence contributions of C1 and C2 are arbitrary units

It can be seen from this figure (figure IV.9) that there is a peak at approximately (0.75 day  $\approx$  5 pm) which corresponds to the rainfall event which started to occur at 5 pm at it is clearly indicated in **Table IV.3** at stopped at 8 pm. This suggests that the rainfall event inputs some of terrestrial humic-like

fluorescence at indicated by this fluorescence peak of both the CP/PARAFAC components C1 and C2. In addition, it can also be seen that there is approximately constant variations before and after this peak in C1 and C2. Moreover, there are no measurable effect could be seen due to the filtration of the samples taken from the temporal field experiment of the sea water. This suggests that the particulate matter has no influence of the temporal variation of the fluorescence contribution of both of the CP/PARAFAC components C1 and C2. This temporal variability of the fluorescence signal of the sea water is constant except for one point which represents the rainfall event and is somehow comparable with spatial variability of the fluorescence signal in the Lazaret bay , a part of the Toulon bay which were conducted in another work within the framework of the present PhD thesis which are presented in annex IV which was a poster in a conference 2015 of the european geosciences union EGU.

### **Conclusion on this Temporal field experiment :**

At a first glance, we could make the hypothesis that the variations of the pH , EC , C1 and (filtered and non-filtered) could be as summarized in the following table (table IV.5) for diurnal variations for a day in autumn for the four water sources (endmembers), Gapeau river, Confluence “Gapeau River & Le Réal Martin”, Wastewater treatment plant of La Crau city and for the sea water at St.Louis at Hyères city. More research studies are needed to have a 48 hour cycle of these water sources (endmembers) in several seasons. Or several 48 hour cycle with higher resolution in each season, in order to have a global idea about the diurnal variations of these water sources (endmembers) and the effects of the photodegradation in presence or absence of particles.

Anyway, theses average values could be used as entry parameters in a first step approach model of end members mixing particularly for fluorescence contribution. In a second way, diurnal variation of C1/C2 could be introduced to have a more detailed model.

**Table IV.5** : Mean and standard deviation of pH, EC , C1, C2 for the four water sources “endmembers” for the temporal field experiment . C1 and C2 units are arbitrary units.

	<b>Gapeau River (RW)</b>	<b>SeaWater at Hyeres (SW)</b>	<b>Wastewater treatment plant WWTP (WW)</b>	<b>Confluence “Gapeau-Real Martin” (Conf)</b>
pH	8.05 ± 0.17	8.29 ± 0.02	7.82 ± 0.16	8.32 ± 0.06
EC ( $\mu\text{S.cm}^{-1}$ )	833.8 ± 116.5	54,8 ± 1,1	951.8 ± 20.0	898.2 ± 18.0
C1_Norm_NonFilt	88.15 ± 5.08	15.36 ± 18.47	91.58 ± 4.81	90.55 ± 5.67
C2_Norm_NonFilt	85.04 ± 7.86	23.35 ± 17.28	89.50 ± 6.31	89.65 ± 6.55
C1_Norm_Filt	74.90 ± 7.87	15.44 ± 18.77	91.19 ± 4.62	82.79 ± 7.57
C2_Norm_Filt	82.14 ± 6.92	22.17 ± 17.49	90.28 ± 5.81	83.05 ± 8.30

## IV.2 Geographical field experiment results

The geographical field sampling campaigns were conducted to follow the mixing process or our proposed endmember mixing process developed in the previous chapter (chapter 3) and to be able to infer the mixing composition from the excitation emission matrices of fluorescence spectroscopy if it is possible to be explained by the endmember mixing model.

### IV.2.1 Description of the weather during the sampling for the spatial “geographical” field experiment .

The two sampling campaigns of the geographical field experiment were two days during the month of august in the year 2016 which were august 19<sup>th</sup> and 22<sup>nd</sup> -2016. The weather conditions are summarized in table IV.6 which clearly show that there was no rainfall event during the month of august in the Hyères city since the precipitation values were 0 mm. Whereas the temperatures were around 25 °C which is an average temperature degree during the month of august in this French city Hyères according to meteo-france <http://www.meteofrance.com>. Figure IV.10 shows some photos during the two sampling campaigns for the geographical field experiment.

**Table IV.6 :** Weather conditions for the temporal field experiments of the four sampling sites.

19-08-2016 Friday	22-08-2016 Monday
Temperatures : 25°C/29°C Precipitations : 0 mm	Temperatures : 26°C/28°C Precipitations : 0 mm

Data were recovered in retrograde from  
<https://www.historique-meteo.net/france/provence-alpes-c-te-d-azur/hyeres/2016/>



Downstream of the Anti-salt Dam (Barrage)

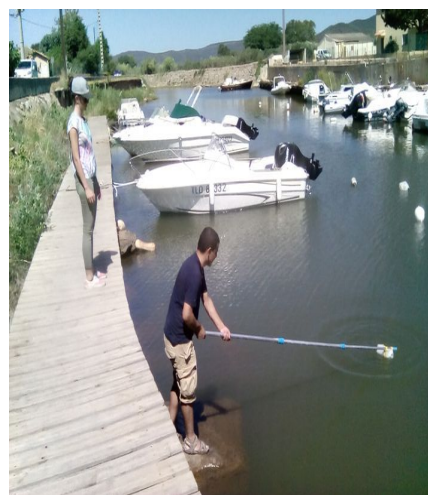
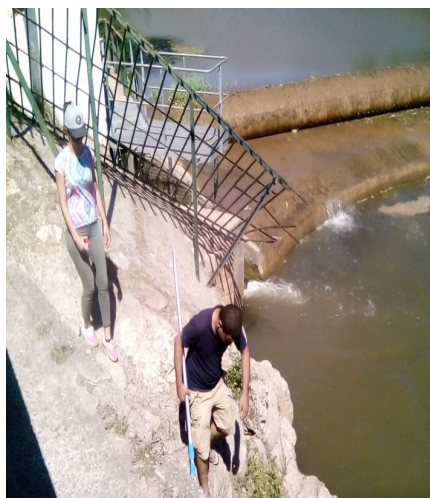


**Figure IV.10 :** Some photos of the geographical field experiment during the two sampling campaigns of 19-august-2016 and 22-august-2016. In addition, the left hand corner pictures shows the downstream of the anti-salt dam(barrage) on the Gapeau river estuary. Moreover, photos shows also the sampling rod “stick” used.

## IV.2.2 pH results of the Geographical field experiment

The pH was measured in each sampling site through the Gapeau river from before the wastewater treatment plant of La Crau till the sea water at the market which is named l'Ayguade at the city of Hyères. The results of the pH as a function of the distance in kilometers are shown in figure IV.11 .

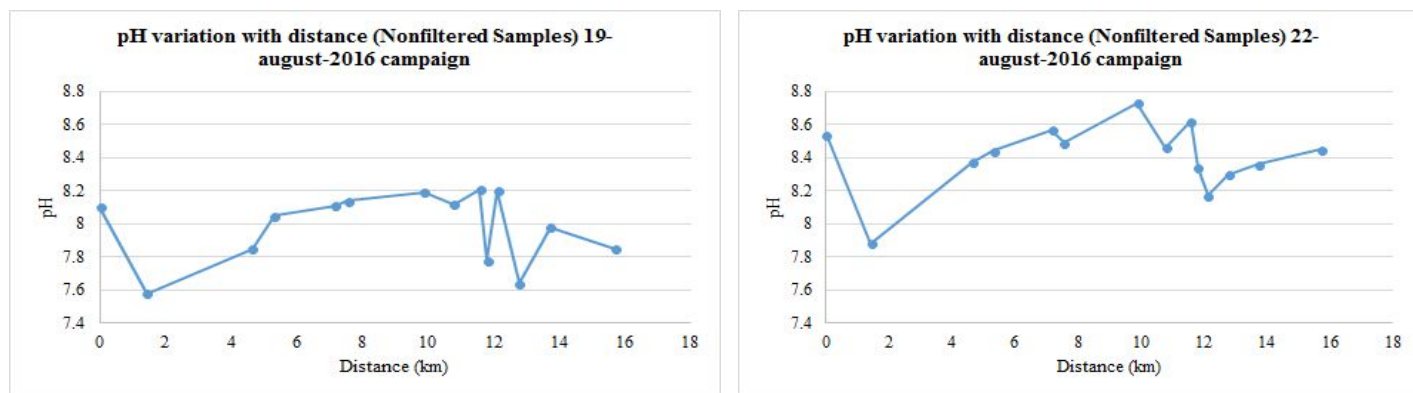


**Figure IV.11** : Figure showing the variation of the pH with distance in kilometers for the first (19-august-2016) and the second (22-august-2016) geographical field sampling experiment

It can be seen from figure IV.11 that the pH values for the first sampling campaign of the geographical field experiment which was conducted on 19-august-2016 varied in the range of 7.5 and 8.25 which indicated acidic conditions and are lower than the values of pH for the second sampling campaign of the geographical field experiment which was on 22-august-2016 which were a little bit basic conditions. This result that the pH values of the second sampling campaign were a bit basic could be attributed to a basic water input but it is not clear from where it comes. In addition, the second point in both of the graphs in figure IV.11 were lower values which is attributed to the wastewater treatment plant discharge input into the Gapeau river water and it varies between 7.6 for the 19-august sampling campaign and 7.85 for the second sampling campaign of 22-august-2016 and this result is consistent with the results of the pH measurement of the wastewater treatment plant discharge for the temporal field experiment which be clearly seen in figure (Figure IV.3). After this input of the wastewater treatment plant of La Crau city, the mixing process is the reason that there is an increase of the pH values for both of the sampling campaigns after the point of the wastewater treatment plant. Then at approximately around 12 km which represent the anti-salt dam (barrage anti-sel), there are slight fluctuations in the pH values which could be attributed to the sea water intrusion and the mixing between freshwater and the sea water .

### IV.2.3 Electrical Conductivity for Geographical field experiment

The electrical conductivity in  $\mu\text{S}/\text{cm}$  was measured in each sampling site through the gapeau river from before the wastewater treatment plant of La Crau till the sea water. The results of the electrical conductivity as a function of the distance in kilometers are shown in figure IV.12 .

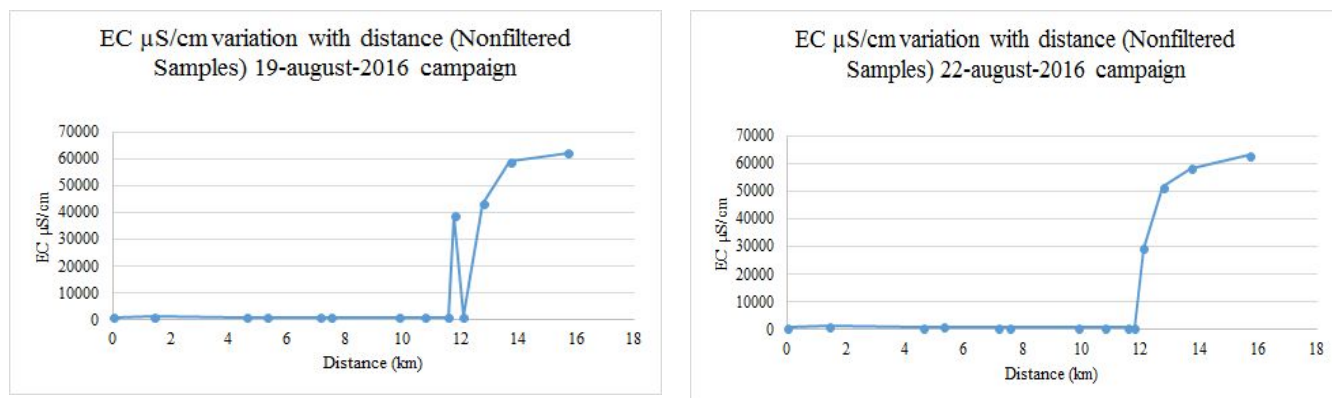


**Figure IV.12** : Figure showing the variation of the electrical conductivity EC  $\mu\text{S}/\text{cm}$  with distance in kilometers for the first (19-august-2016) and the second (22-august-2016) geographical field sampling experiment

The electrical conductivity of the water sampled in situ through the pathway of the gapeau river till the sea water are shown in figure IV.12 for the two sampling campaigns of the geographical field experiment (19-august-2016 and 22-august-2016). The variation in the electrical conductivity shows an apparently constant trend from 0 to 12 km except for the second point which has a value of EC equal to 1,177  $\mu\text{S}\cdot\text{cm}^{-1}$  and 1,090  $\mu\text{S}\cdot\text{cm}^{-1}$  which are the values of the electrical conductivity of the wastewater treatment plant discharge which is very small compared to the electrical conductivity values found after the anti-salt dam (barrage anti-sel) starting from 12 km from the beginning point of sampling which was the first point sampled for the two sampling campaigns of the geographical field experiment which was approximately about 500 m to 1 km before the wastewater treatment plant of La Crau and represent the river endmember. Starting from approximately 12 km, the electrical conductivity started to increase from (30,000, 40,000  $\mu\text{S}\cdot\text{cm}^{-1}$ ) to attain the electrical conductivity of more or less 60,000  $\mu\text{S}\cdot\text{cm}^{-1}$  which represent the electrical conductivity of the sea water at l'Ayguade. The increase of the electrical conductivity  $\mu\text{S}\cdot\text{cm}^{-1}$  after the anti-salt dam (barrage antisel) is because of the fact that it is the Gapeau river mouth meaning that the sea water enter the land and this anti-salt dam was constructed to prevent the sea water intrusion and to limit the advancement of brackish water (which is called in french "biseau salé") into the river water.



#### IV.2.4 Geographical variation of temperature

The temperature °C of water of the water course of the gapeau river till the seawater at l'Ayguade at Hyères city using the same multi-parameter sonde which was used to measure the pH and electrical conductivity of the sampled water in situ.

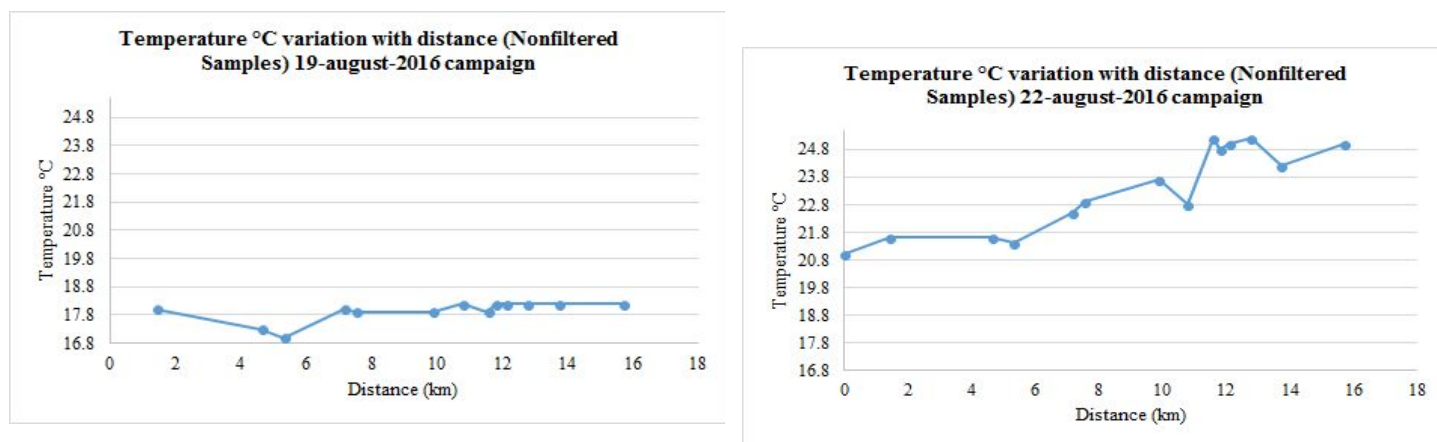


**Figure IV.13** : Figure showing the variation of the temperature °C with distance in kilometers for the first (19-august-2016) and the second (22-august-2016) geographical field sampling experiment

The variation of temperature in °C with the distance are shown in figure IV.13 for the two sampling campaigns of the geographical field experiment. The temperature variation for the first sampling campaign 19-august-2016 show a very little variation which is a decrease in only one degree celsius and returned back to its constant value and it has a mean value of  $17.94 \pm 0.38$  where we started this sampling campaign of the geographical field experiment (19-august-2016) on 11:07 am and finished sampling at 03:30 pm. Whereas for the 2nd sampling campaign of the geographical field experiment which was conducted on 22-august-2016, the temperature geographical distribution increased with distance in kilometers and showed an increase of approximately 4 °C. This temperature increase in this sampling campaign (22-august-2016) are consistent with the temperature range 26°C/28°C retrieved from <https://www.historique-meteo.net/france/provence-alpes-c-te-d-azur/hyeres/2016/> which is the temperature of the weather not the temperature of the water course of Gapeau River whereas the temperature for the 1st sampling campaign (19-august-2016) was lower compared to the 2<sup>nd</sup> sampling campaign (22-august-2016) which we couldn't attribute it to a clear reason.

## IV.2.5 CP/PARAFAC Components results of the decomposition of the geographical field experiment

The results of the decomposition of CP/PARAFAC algorithm by the Progmeef software on Matlab platform are shown in the following figures .

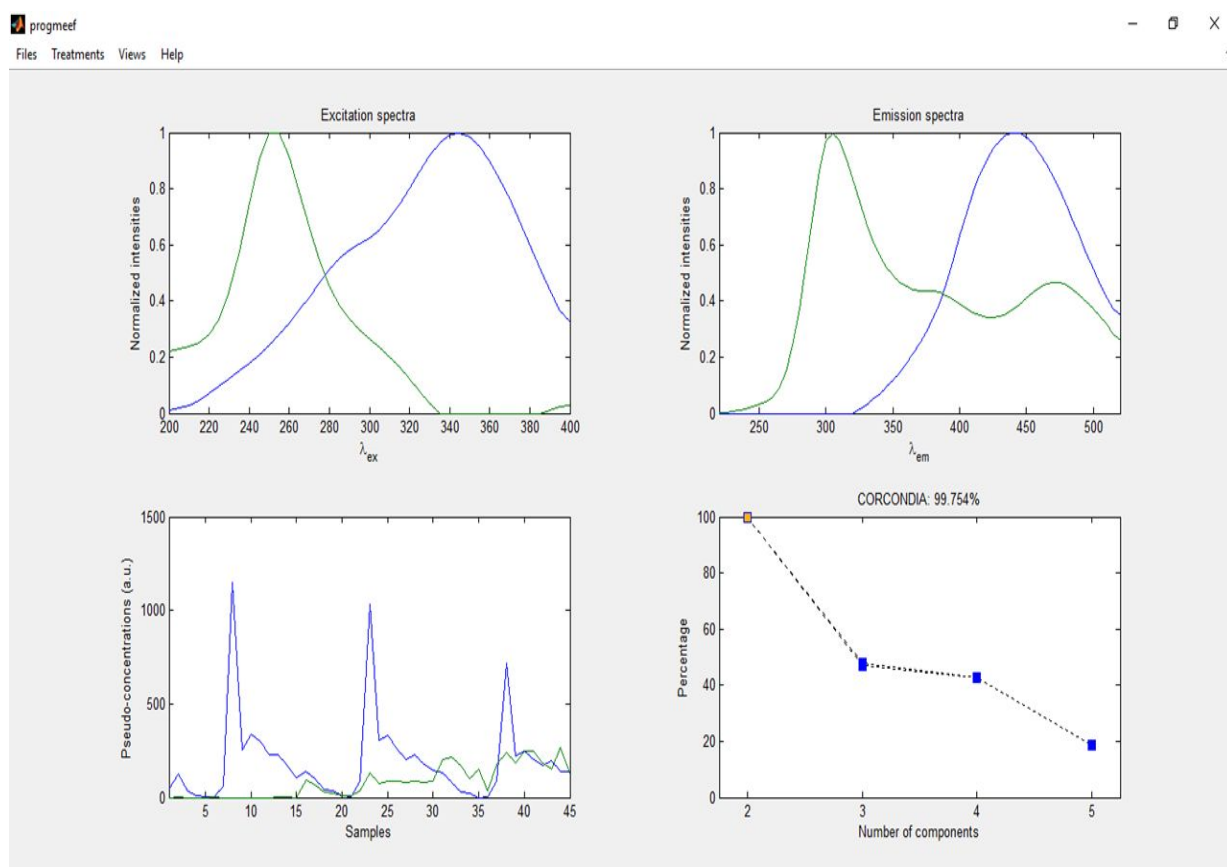


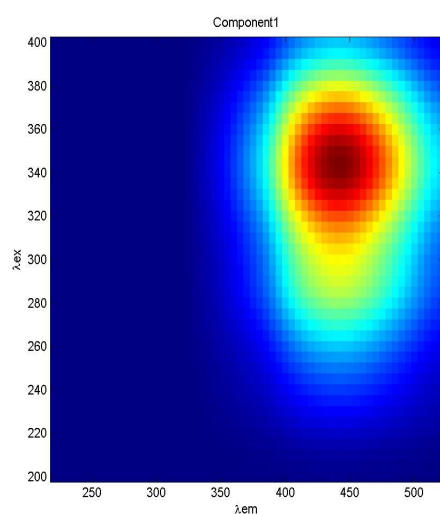
**Figure IV.14** : Progmeef results windows showing the concordia graph on the lower right hand corner and the value of the concordia test for two CP/PARAFAC components is shown above this graph (99.75%). Loadings of the two CP/PARAFAC components are also shown.

The CORCONDIA analysis showed a drop in core consistency between two core elements and five core elements, from near 100 % to less than or around 20 % which surpasses the acceptable threshold of 60% where as it showed a value of 99.75 % for two components, indicating that a two-factor model was appropriate, as it is shown in the lower right hand graph of figure IV.14. In addition, the lower left hand graph of figure IV.14 shows the pseudo-concentrations (or relative contribution) of these CP/PARAFAC Components in the EEMs text files of the datasets of the Geographical field experiments along the Gapeau River pathway till the sea water at L'Aiguade at Hyères city southeastern of France which were three datasets (the first dataset was the EEMs files of the 19-august-2016 geographical field experiment or mission, the second datasets was those EEMs files of the 22-august-2016 mission and the last and third



dataset was those of the EEMs files of filtered samples of the 22-august-2016 geographical field experiment). It is clearly shown in the graph in the lower left hand side of figure IV.14 that there is a peak which is attributed to the pseudo-concentrations of CP/PARAFAC components in the wastewater treatment plant sample EEMs in this geographical field experiment. In addition, this peak is lower in comparison to the first and second peaks in the same graph which indicated that this peak is related to the filtered samples EEMs of the 22-august-2016 geographical field sampling experiment. This result is consistent with the results in the geographical variation of CP/PARAFAC C1 component shown in figure IV.16.

C1



C2

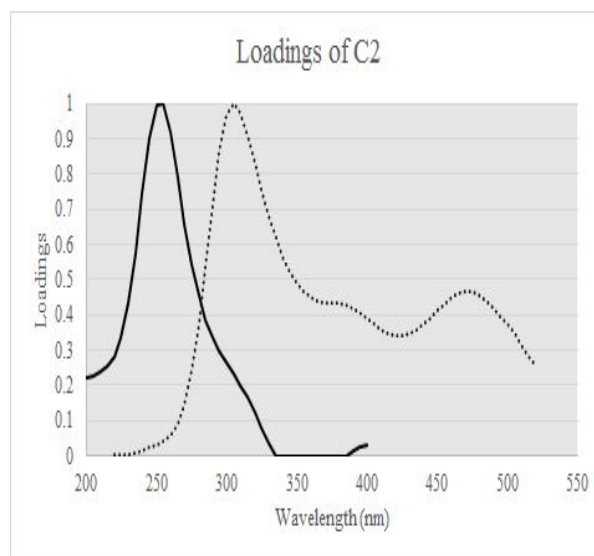
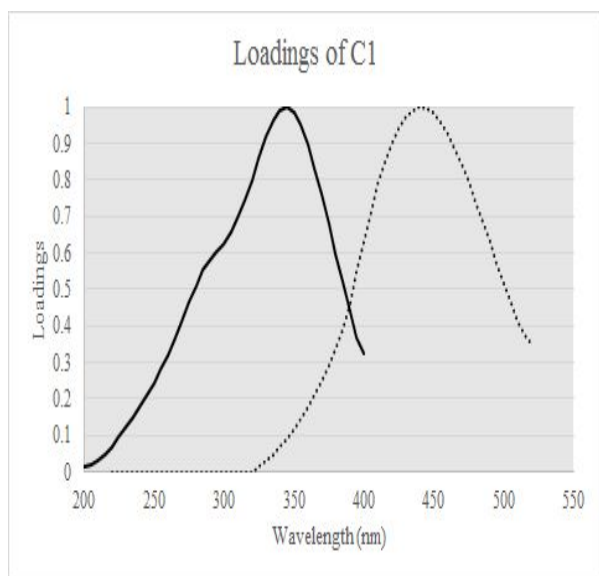
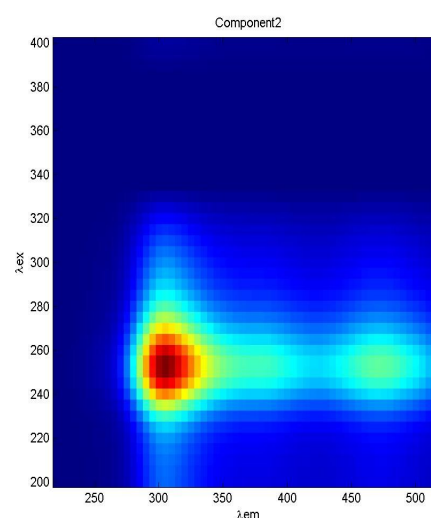


**Figure IV.15.** Contour plots of CP/PARAFAC components identified from the decomposition of all EEM datasets of the Spatial (geographical) field experiments. Spectral loadings of excitation and emission wavelengths of the two identified CP/PARAFAC in the spatial “geographical” field experiment are also shown. Excitation loading for CP/PARAC component are solid lines whereas emission loadings are shown in dotted lines.

**Table IV.7-**Descriptions of CP/PARAFAC components and comparison with literature

Component	$\lambda_{EX}/\lambda_{EM}$ (nm)	Description and references in literature
Component C1	345/440	-Peak C (Coble 1996; Coble, Del Castillo, and Avril 1998) : Terrestrial origin - degradation of plant and animal debris (humic substances)  -Component 4 (Stedmon, Markager, and Bro 2003a) : terrestrially derived organic matter
Component C2	255/305 (470)	-Peak B (Coble 1996) Tyrosine-like component -Component 5 ( <a href="#">Osburn et al. 2016</a> ) Component 7 ( <a href="#">Yamashita et al. 2008</a> )

Two components were successfully decomposed by CP/PARAFAC modeling on the EEM datasets of the two geographical field experiment along Gapeau river till sea (19-august-2016 and 22-august-2016) after the removal of the 1<sup>st</sup> and 2<sup>nd</sup> order Rayleigh and Raman Scattering. The above figure (figure IV.15) shows the contour plots of the two CP/PARAFAC components which were found from the analysis conducted in the matlab software and progmeef in all of the excitation emission matrices as well as their corresponding loadings for both the excitation and the emission wavelengths. These two fluorescent CP/PARAFAC components have been previously identified (Table IV.7). The 1<sup>st</sup> CP/PARAFAC component, found in this study from the CP/PARAFAC decomposition of geographical field experiment EEMs of samples, C1 component showed an excitation maximum at 345 nm and an emission maximum at 440 nm and a range of excitation emission wavelengths (Ex=280-400 nm , Em=400-480 nm). Previous studies have associated this component to UVA humic-like fluorescent CP/PARAFAC component and Peak C (Coble, 2007b) and peak  $\infty$  (Parlanti, Wörz, Geoffroy, & Lamotte, 2000b; Sierra, Giovanela, Parlanti, & Soriano-Sierra, 2005). In addition this C1 component (Ex=280-400 nm , Em=400-480 nm) has been cited to have terrestrial, anthropogenic, agricultural sources by the studies conducted by (Colin A. Stedmon & Markager, 2005b; Colin A. Stedmon, Markager, & Bro, 2003b). The 2<sup>nd</sup> CP/PARAFAC component, found in this study from the CP/PARAFAC decomposition of geographical field experiment EEMs of samples, C2 component showed an excitation maximum at 255 nm and an emission maximum at 305 nm with a minor emission peak at 470 nm and a range of excitation emission wavelengths (Ex=230-290 nm , Em=290-500 nm). Previous studies have associated this component to resemble tyrosine-like fluorescent component ([Osburn et al. 2016](#); [Yamashita et al. 2008](#)). In addition to that this

protein like fluorescent component contains -Peak B found in the study conducted by [\(Coble 1996; Coble et al. 1998\)](#).

## IV.2.6 Variation with Geographical Distance of CP/PARAFAC Components

### IV.2.6.1 The 1<sup>st</sup> CP/PARAFAC component

The results of the variation with distance in kilometers (km) of the first CP/PARAFAC component (humic-like fluorescence) for the first (19-august-2016) and the second (22-august-2016) sampling campaigns of the geographical field experiment are shown in the following figure (figure IV.16) keeping in mind that the second sampling campaigns samples were filtered and other EEM-PARAFAC were applied.

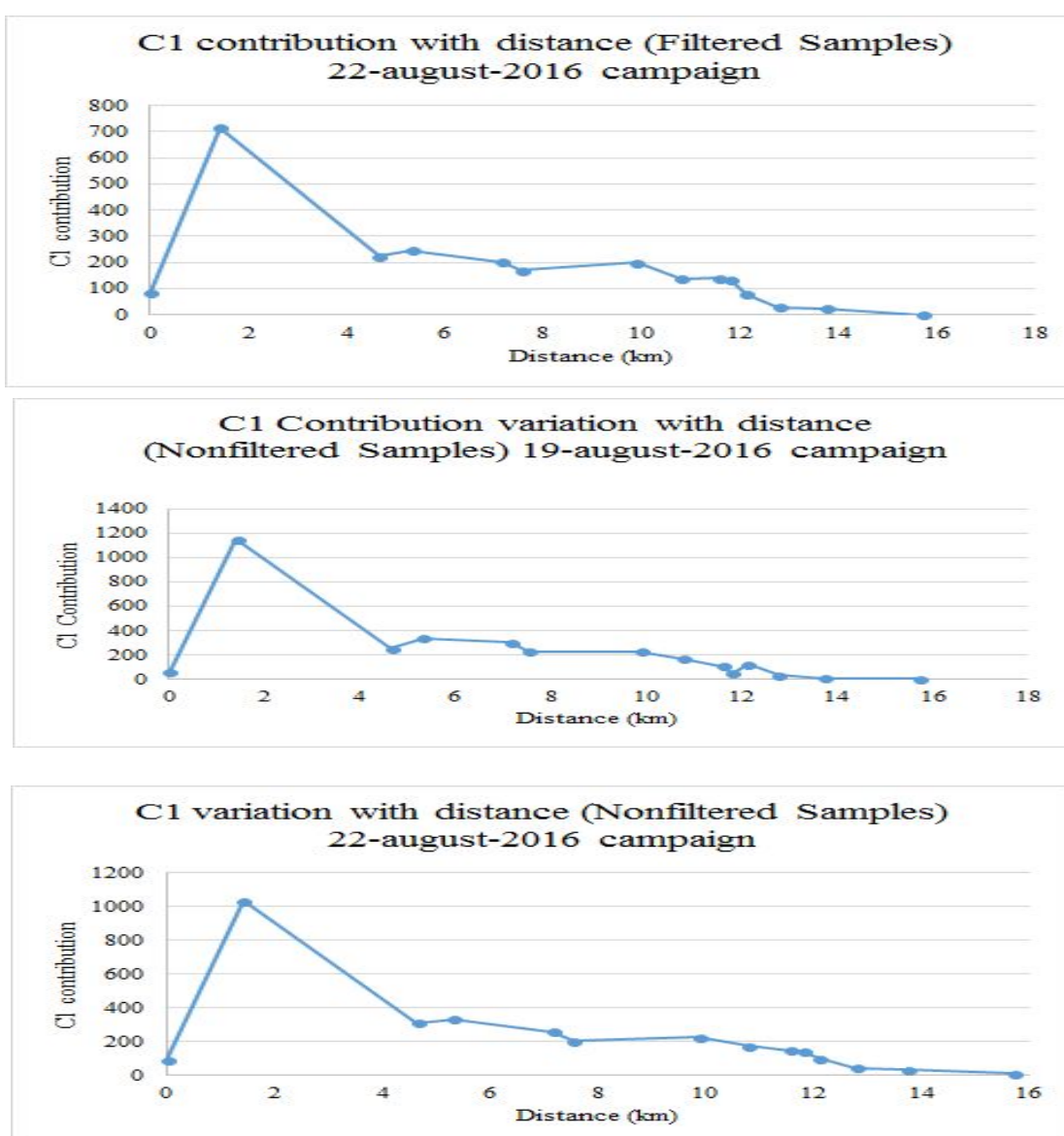


**Figure IV.16 :** Figure showing graphs of the geographical variation of the contribution of CP/PARAFAC component C1 with distance in kilometers along the pathway of Gapeau river till the sea at l'ayguade at Hyeres city. The geographical field experiment of 19-august-2016 doesn't have a filtration dataset.

It can be seen from this figure (figure IV.16) the first CP/PARAFAC component C1 found from the CP/PARAFAC analysis of the global dataset of the geographical field experiment shows a peak at approximately less about 2 km. This point corresponds to the wastewater treatment plant discharge in the Gapeau river. This leads to the fact that there is a significant input of humic-like fluorescence ( the 1<sup>st</sup> CP/PARAFAC component C1) by the wastewater treatment plant to the already existing background fluorescence of the Gapeau river. After that, it is shown in this figure (figure IV.16) that the contribution of this 1<sup>st</sup> CP/PARAFAC component decreases as the distance increase in the three graphs in this figure (figure IV.16) which corresponds to the first and second (Nonfiltered , filtered dataset) sampling campaigns for the geographical field experiment. This decrease of the contribution of C1 could be attributed to the photodegradation process occurring during these sampling days ( 19-august-2016 and 22-august-2016) and also the biodegradation process plays another role in addition to the mixing process which leads to dilution also. Moreover, the pattern of graphs of the second sampling campaign (22-august-2016) is approximately the same except the contribution of C1 is lower in the case of the filtered samples (dataset) which clearly shows the effect of the filtration process on the fluorescence contribution of the first CP/PARAFAC component C1 (humic-like fluorescence) which is that it decreased its contribution which suggests that part of the contribution of C1 (1st CP/PARAFAC component) is due to the particulate matter. Also the evolution of the C1 contribution is robust from a day to another meaning that process altering the C1 contribution are stable and that finally there is and equilibrium in term of fluorescence.

#### **IV.2.6.2 The 2<sup>nd</sup> CP/PARAFAC component**

The results of the variation with distance in kilometers (km) of the second CP/PARAFAC component (Protein “tyrosine) -like fluorescence) for the first (19-august-2016) and the second (22-august-2016) sampling campaigns of the geographical field experiment are shown in the following figure (figure IV.17) keeping in mind that the second sampling campaigns samples were filtered and other EEM-PARAFAC were applied.

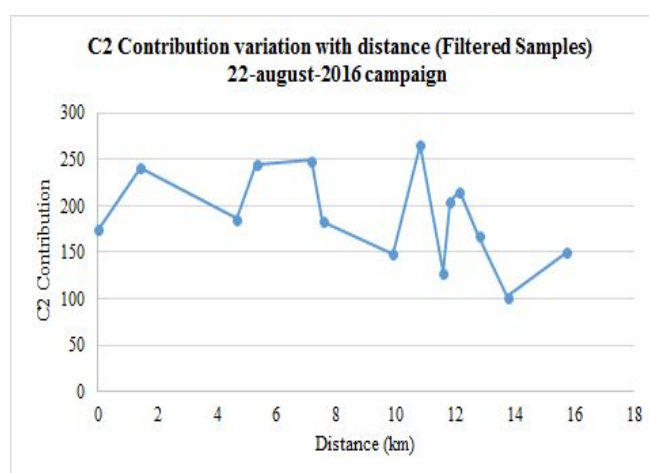
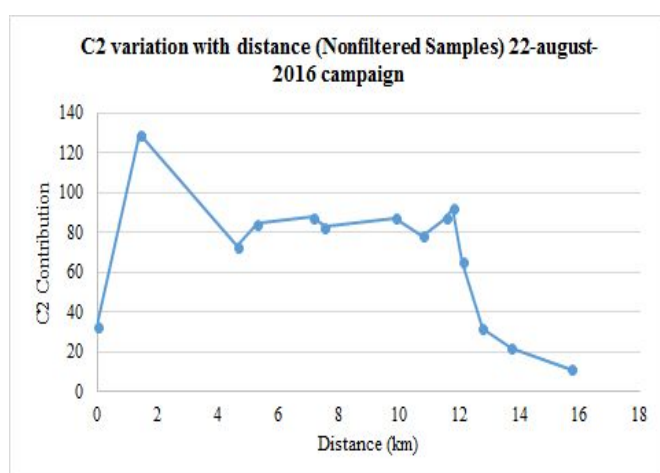
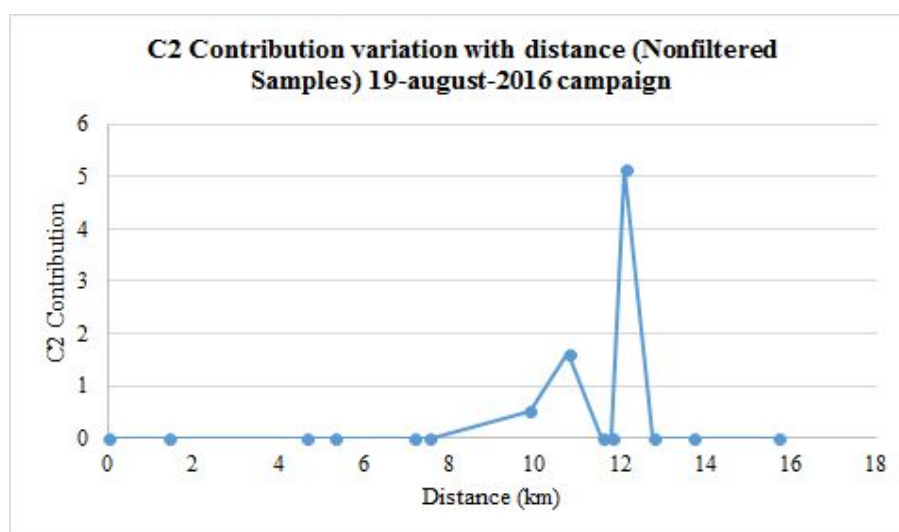


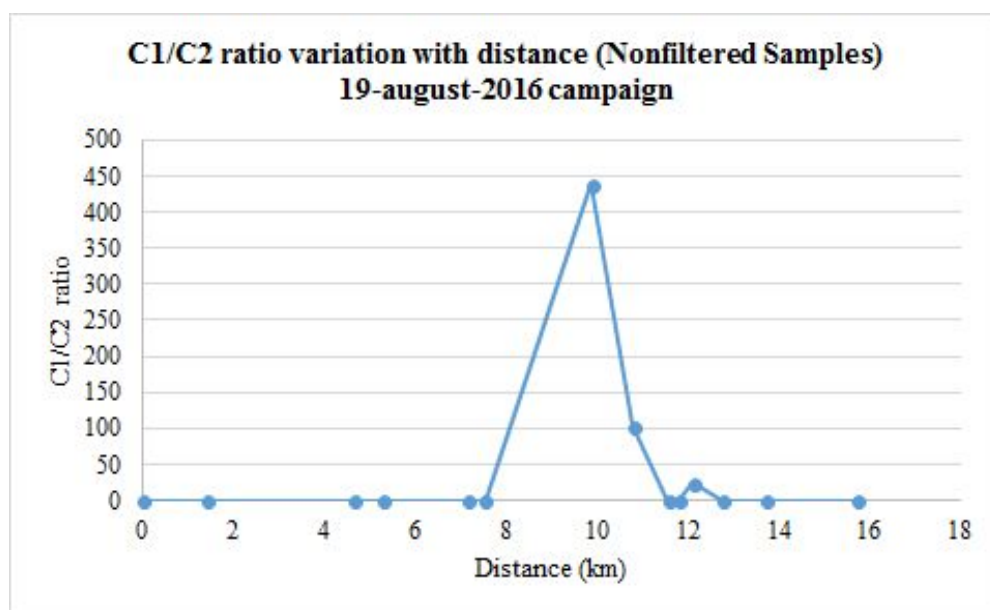
**Figure IV.17** : Figure showing graphs of the geographical variation of the contribution of CP/PARAFAC component C2 with distance in kilometers along the pathway of Gapeau river till the sea at l'ayguade at Hyeres city. The geographical field experiment of 19-august-2016 doesn't have a filtration dataset.

It can be seen that the values of the contribution of the second CP/PARAFAC component for the first sampling campaign, the contribution is zero except for (8-13 km) which suggests that there is an input of protein-like fluorescence around the before the salt dam (barrage antisel) which could be attributed to the microbial or biological activity. It is interesting to see that for this campaign no protein-like signal was observed at the WW point (2 km). For the first glance at the variation of the contribution of C2 (protein "tyrosine"-like fluorescence) for the 1st sampling campaign appear to be chaotic. For the second sampling campaign (22-august-2016), the filtration process lead to increased values of the contribution of the 2<sup>nd</sup> CP/PARAFAC component with distance in km which suggest that there was an inner filter effect due to the particulate matter. The variation of contribution of C2 for the filtered dataset in (22-august-2016) showed a decreasing trend with distance after the anti-salt dam (barrage anti-sel). However, for the non filtered dataset of the second sampling campaign, there was an increase in the contribution of C2 (protein-like fluorescence) in the second point which corresponds to the sampling

point of the wastewater treatment plant then it decreased and had an approximately constant fluctuation till it reaches 12 km which is the antisalt dam then it decreases rapidly till the sea water at l'Ayguade at Hyères city.

#### IV.2.6.3 The ratio of the 1<sup>st</sup> and 2<sup>nd</sup> CP/PARAFAC Components

The results of the variation with distance in kilometers (km) of the ratio between the first and the second CP/PARAFAC components (C1/C2) for the first (19-august-2016) and the second (22-august-2016) sampling campaigns of the geographical field experiment are shown in the following figure (figure IV.18) keeping in mind that the second sampling campaigns samples were filtered and other EEM-PARAFAC were applied.



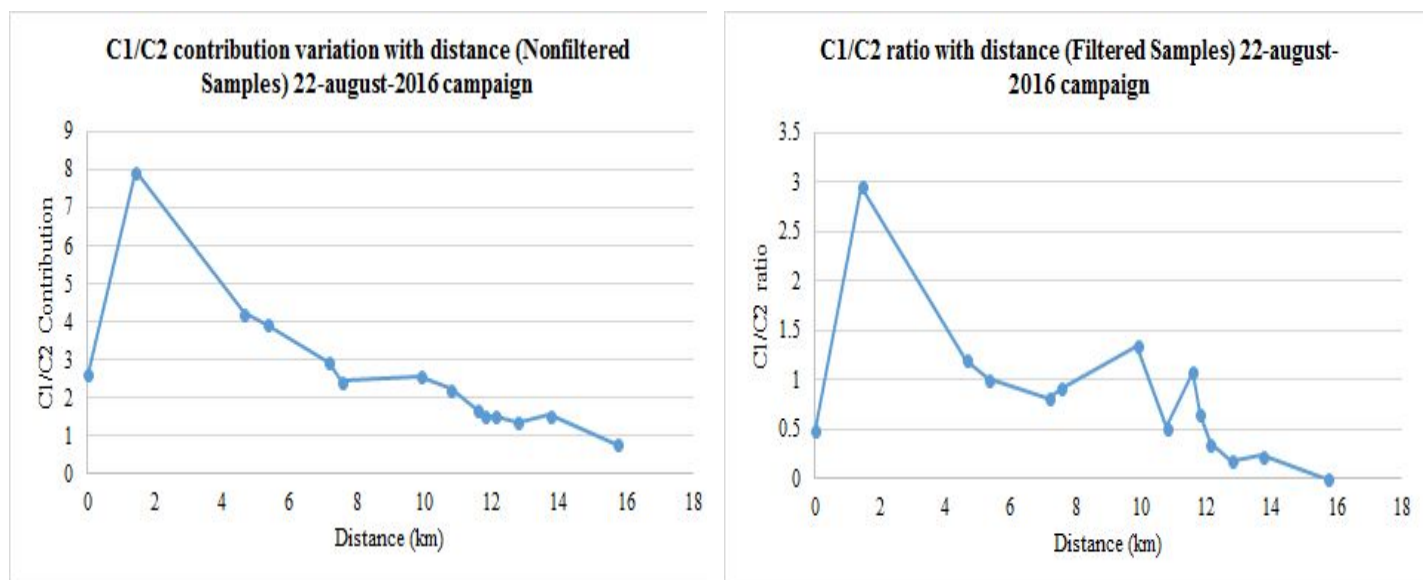


**Figure IV.18** : Figure showing graphs of the geographical variation of the ratio of CP/PARAFAC component C1/C2 with distance in kilometers along the pathway of Gapeau river till the sea at l'ayguade at Hyeres city. The geographical field experiment of 19-august-2016 doesn't have a filtration dataset

It can be seen that for the first sampling campaign (19-august-2016), the ratio C1/C2 has zero values before 8 km and after ~13km. There is a peak at 10 km then rapid decrease to zero value at 12 km. This C1/C2 peak at 10 km indicate that there is more C1 (humic-like fluorescence) and less C2 (protein-like fluorescence). For the second sampling campaign of the geographical field experiment which was on 22-august-2016, the variation of the ratio of C1/C2 follow similar trend as the variation of the contribution of C1 (Nonfiltered and filtered dataset) with distance indicating that the first CP/PARAFAC component C1 (humic-like fluorescence) is higher than C2 (Protein "tyrosine" -like fluorescence). If we had a dilution effect , the ratio C1/C2 should have been constant with distance (in km) which is not the case here. The ratio C1/C2 decreases with the distance which means that there is an increase in C2 which is the cause of this decrease in the raio C1/C2 which is the case as it is shown in figure IV.17. The 2nd CP/PARAFAC component C2 here from the decomposition of the geographical field experiment has been identified to be protein-like fluorescence, this suggests that there is a bacteriological production of this protein like fluorescence with the distance (in km) and there is predominance of fluorescence signal of biological origin (from the biological activity) with the distance.It is also consistent with the fact that C1 decreases with the distance as it is shown in figure IV.16

---

## **Chapter 5 - Estimation of annual inputs**

---



In this chapter we used the multivariate linear regression model between the content fractions and the irradiation to predict the evolution of the fluorescence as a function of the distance or as a function of the seasons to investigate the applicability of our multilinear regression model that we developed throughout the whole works of the present PhD thesis .

### V.1 The multilinear regression model used here :

The model that we used here is the model that we developed in Chapter 3 between the contribution of CP/PARAFAC components and the content fraction of sea water and river water in the solution with the general mathematical formula :

$$c_i^{Ixyz} = A^{WW,Ixyz}_{i,0}(V) + A^{WW,Ixyz}_{i,1}(V)*f_{SW} + A^{WW,Ixyz}_{i,2}(V)*f_{RW}$$

Where :

$c_i^{Ixyz}$  : is the contribution of a given CP/PARAFAC component previously identified in chapter 3 which could be either C1 or C2 whereas for C3 we decided to neglect it because of its chaotic behaviour

$A^{WW,Ixyz}_{i,0}(V)$  : is the constant in the multilinear regression model for a given irradiation experiment however it depends on irradiation in volts which was found to have a second order kinetics and its value could be calculated from the following equation

$$A^{WW,Ixyz}_{i,0}(V) = A^{WW,Ixyz}_{i,0}(0)/(1+A^{WW,Ixyz}_{i,0}(0))*kA^{WW,Ixyz}_{i,0}(V) * V$$

$V$  : represents the irradiation in volts

$kA^{WW,Ixyz}_{i,0}(V)$  : is the decay constant for the  $A^{WW,Ixyz}_{i,0}(V)$  coefficient which has been calculated in chapter 3

$A^{WW,Ixyz}_{i,1}(V)$  : is the coefficient of the content fraction of sea water in the solution in the multilinear regression model for a given irradiation experiment however it depends on irradiation in volts which was found to have a second order kinetics and its value could be calculated from the following equation

$$A^{WW,Ixyz}_{i,1}(V) = A^{WW,Ixyz}_{i,1}(V)/(1 + A^{WW,Ixyz}_{i,1}(0)) * k A^{WW,Ixyz}_{i,1}(V) * V$$

$V$  : represents the irradiation in volts

$kA^{WW,Ixyz}_{i,1}(V)$  : is the decay constant for the  $A^{WW,Ixyz}_{i,1}(V)$  coefficient which has been also calculated in chapter 3

$A^{WW,Ixyz}_{i,2}(V)$  : is the coefficient of the content fraction of river water in the solution in the multilinear regression model for a given irradiation experiment however it depends on irradiation in volts which was found to have a second order kinetics and its value could be calculated from the following equation

$$A^{WW,Ixyz}_{i,2}(V) = A^{WW,Ixyz}_{i,2}(V)/(1 + A^{WW,Ixyz}_{i,2}(0)) * kA^{WW,Ixyz}_{i,2}(V) * V$$

$V$  : represents the irradiation in volts

$kA^{WW,Ixyz}_{i,2}(V)$  : is the decay constant for the  $A^{WW,Ixyz}_{i,2}(V)$  coefficient which has been also calculated in chapter 3

The other parameters of the multilinear regression model for the other two circular permutations could also be used for the application of the multilinear regression model , however for stucked to the permutation that we used in chapter 3 which is the permutation of ( $f_{SW}$  and  $f_{RW}$ ) and the contribution of each CP/PARAFAC model. The parameters of the multilinear regression model for the other two permutation are found in Annex II , Annex III and Annex VI .

For the case of ( $f_{SW}$  and  $f_{RW}$ ) permutation , the exact values for the parameters of the multilinear regression model which are  $A^{WW,Ixyz}_{i,0}(V)$  ,  $A^{WW,Ixyz}_{i,1}(V)$  and  $A^{WW,Ixyz}_{i,2}(V)$  could be found in chapter 3 in table III.4 which is the following table

**Table V.1**-Multilinear regression parameters of each CP/PARAFAC components at time zero with their corresponding coefficients of correlation found in the present study from the Elnahhal method of data acquisition

Ixyz	Coefficient C1 à T0				Coefficient C2 à T0				Coefficient C3 à T0			
	$A^{WW}_{1,0}$	$A^{WW}_{1,1}$	$A^{WW}_{1,2}$	$r^2$	$A^{WW}_0$	$A^{WW}_{2,1}$	$A^{WW}_{2,2}$	$r^2$	$A^{WW}_{3,0}$	$A^{WW}_{3,1}$	$A^{WW}_{3,2}$	$r^2$
	intercept	( $f_{SW}$ )	( $f_{RW}$ )		intercept	( $f_{SW}$ )	( $f_{RW}$ )		intercept	( $f_{SW}$ )	( $f_{RW}$ )	
I111	100.34	-0.99	-0.93	<b>0.99</b>	98.42	-0.97	-0.92	<b>0.99</b>	112.35	-1.08	-1.03	<b>0.97</b>
I110	68.91	-0.66	-0.60	<b>0.99</b>	80.73	-0.75	-0.68	<b>0.98</b>	43.76	0.15	0.13	0.34
I011	49.73	-0.46	-0.40	<b>0.98</b>	63.33	-0.55	-0.48	<b>0.98</b>	49.57	-0.02	-0.08	0.33
I101	60.45	-0.58	-0.52	<b>0.97</b>	73.18	-0.70	-0.63	<b>0.96</b>	32.40	-0.05	-0.11	0.14
I000	100.13	-0.97	-0.91	<b>0.99</b>	96.14	-0.93	-0.89	<b>0.99</b>	83.32	-0.38	-0.38	0.59

In addition, the values of the decay constant for a second order kinetics for each parameter  $A^{WW,Ixyz}_{i,0}(V)$  ,  $A^{WW,Ixyz}_{i,1}(V)$  and  $A^{WW,Ixyz}_{i,2}(V)$  which are  $kA^{WW,Ixyz}_{i,0}(V)$  ,  $kA^{WW,Ixyz}_{i,1}(V)$  and  $kA^{WW,Ixyz}_{i,2}(V)$  could be consulted in table III.6 in chapter 3 which is the following table :

**Table V.2**-Kinetic constant for coefficients of multilinear regression for each CP/PARAFAC component from the Elnahhal method of EEM data acquisition .

	C1			C2			C3		
k*1e6	$A_{1,0}^{ww}$	$A_{1,1}^{ww}$	$A_{1,2}^{ww}$	$A_{2,0}^{ww}$	$A_{2,1}^{ww}$	$A_{2,2}^{ww}$	$A_{3,1}^{ww}$	$A_{3,2}^{ww}$	$A_{3,3}^{ww}$
	intercept	(f <sub>sw</sub> )	(f <sub>rw</sub> )	intercept	(f <sub>sw</sub> )	(f <sub>rw</sub> )	intercept	(f <sub>sw</sub> )	(f <sub>rw</sub> )
I111	7.13	721.1	720.94	4.57	498.14	507.39	0.419	56.51	61.46
I110	4.83	515.33	645.77	4.85	674.14	770.01	-	-	-
I011	7.85	805.34	949.56	8.10	911.58	977.34	-	-	-
I101	7.60	857.10	1057.22	6.13	877.75	943.41	-	-	-
I000	6.1	604	715	6.45	842.33	907.81	-	-	-

## V.2 Annual variation modeling

### V.2.1 Variation in the presence of UV irradiation

Based on the previous équation and values we tried use the meteoFrance irradiation data in V to estimate the contribution of the C1 and C2 during an average year. However, we couldn't find a published data of irradiation per month in volts in the internet , and it was needed time to request it from the part of the meteoFrance. Therefore for the purpose of speed, we used the following data for irradiation to be substituted for in the equation of each coefficient in the multilinear regression model

**Table V.3** : irradiation in volts used the modelling

Month	Irradiation Volts per day
1	400
2	600
3	734
4	1569
5	2404
6	2733
7	2830
8	2343
9	2343
10	1722
11	1722
12	599

Each irradiation value in the above table (table V.3) is mean value of irradiation in volts received per day which were calculated based on the irradiation data from the irradiation experiments conducted in the works of the present PhD thesis . The values of irradiation in table V.3 could be visualized in the following figure (figure V.1)



**Figure V.1** : figure showing histogram of the irradiation in volts for each month of the year

Discharge of the Gapeau river in each month of the year was taken for the chapter 2 at point Rivère Gapeau from Figure II.2, WWTP also estimated in chapter 2 to be and considered as constant along the year with a mean value of mean  $0.17 \text{ m}^3/\text{s}$ . SW content was estimated as constant enough to give a final salinity of 35. The discharge for each source are mentioned in the following table (table V.4) :

**Table V.4** : Discharges of the Seawater SW , River water RW , wastewater treatment plant WWTP , units are  $\text{m}^3/\text{s}$  .

Month	SW	RW	WWTP
1	100000	9.15	0.17
2	100000	8.72	0.17
3	100000	6.23	0.17
4	100000	4.26	0.17
5	100000	3.37	0.17
6	100000	1.52	0.17
7	100000	0.451	0.17
8	100000	0.408	0.17
9	100000	0.826	0.17
10	100000	2.89	0.17

11	100000	5.658	0.17
12	100000	6.32	0.17

We evaluated the fluorescence response of the contribution of CP/PARAFAC components C1 and C2 in two case : the first one was after the mixing of the Gapeau river and the wastewater treatment plant and the second case was after the final mixing of the three water sources ( Gapeau river water , wastewater treatment plant effluent , seawater ).

The multilinear regression model is applicable on content fraction or percentages of  $f_{SW}$  and  $f_{RW}$  not on discharge values in  $m^3/s$  , therefore we did the mixing and calculated percentages based on the above mentioned table (table V.4)

The exact mixed percentages are summarized in the following table (table V.5) for the first case of mixing (RW+ WWTP)

**Table V.5** : table showing the exact percentage or content fractions of Seawater SW , River water RW , wastewater treatment plant effluent for the first case of mixing mentioned above in the text of this chapter 5 which were used in the application of the multilinear regression model.

Month	$f_{SW}$	$f_{RW}$	$f_{WWTP}$
1	0.00	98.20	1.80
2	0.00	98.11	1.89
3	0.00	97.38	2.62
4	0.00	96.21	3.79
5	0.00	95.26	4.74
6	0.00	90.06	9.94
7	0.00	72.88	27.12
8	0.00	70.85	29.15
9	0.00	83.11	16.89
10	0.00	94.51	5.49
11	0.00	97.12	2.88
12	0.00	97.41	2.59

These values of content fraction for each water source could be visualized using a line chart as a function of month of the year in the following figure (figure V.2) :

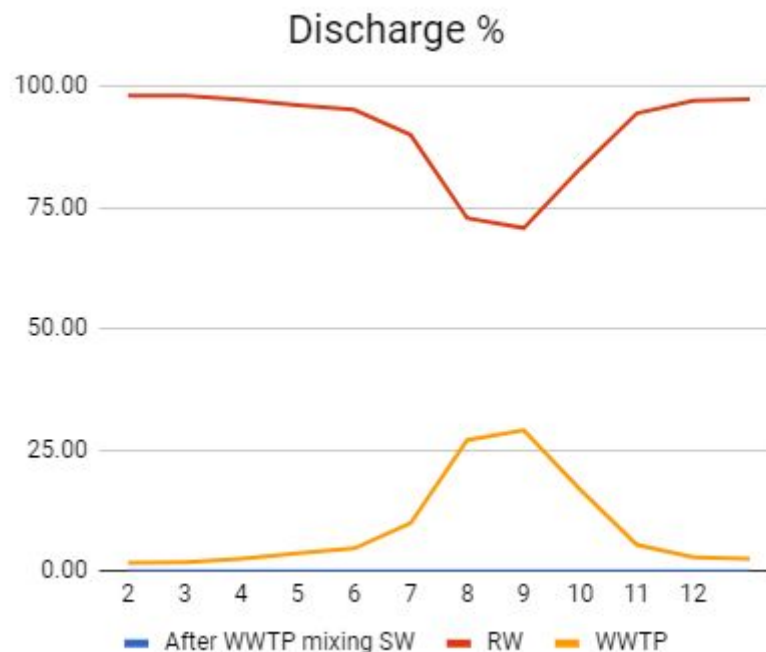


**Figure V.2** : figure showing the variation of the content fraction or discharges of the wastewater treatment plant WWTP , seawater SW and river water RW as a function of month of the year

It can be seen from figure V.2 that the relative discharge percentages of River water RW and wastewater treatment plant WWTP vary in an inverse manner through the months of the year. For example for a month between July and October , it is clear that the content fraction of the wastewater treatment plant increases while the content fraction of river water decreases . This is due to the fact that the Gapeau river has a pluvial hydric regime meaning that it has the least flow during the month of the summer season and this decrease leads to the decrease in its mixing percentage (or content fraction) whereas the wastewater treatment plant discharge is assumed to be constant ( $0.17 \text{ m}^3/\text{s}$ ) throughout the year , its mixing percentage (or content fraction) increase not because of that its discharge increased but because of the relative decrease of the discharge of the river water.



For the second case of mixing we had the following mixing percentages or content fraction of fSW and fRW to be substituted for in the multilinear regression model which are summarized in the following table (Table V.6)

**Table V.6:** table showing the mixing percentages or content fraction of the seawater fSW and river water fRW using in the application of the multilinear regression model for the second case of mixing mentioned above in the text of this chapter (chapter V)

Month	$f_{SW}$	$f_{RW}$	$f_{WWTP}$
1	99.99	0.01	0.00
2	99.99	0.01	0.00
3	99.99	0.01	0.00
4	100.00	0.00	0.00
5	100.00	0.00	0.00
6	100.00	0.00	0.00
7	100.00	0.00	0.00
8	100.00	0.00	0.00
9	100.00	0.00	0.00
10	100.00	0.00	0.00
11	99.99	0.01	0.00
12	99.99	0.01	0.00

Output of the model give for the after confluence RW/WW the following results :

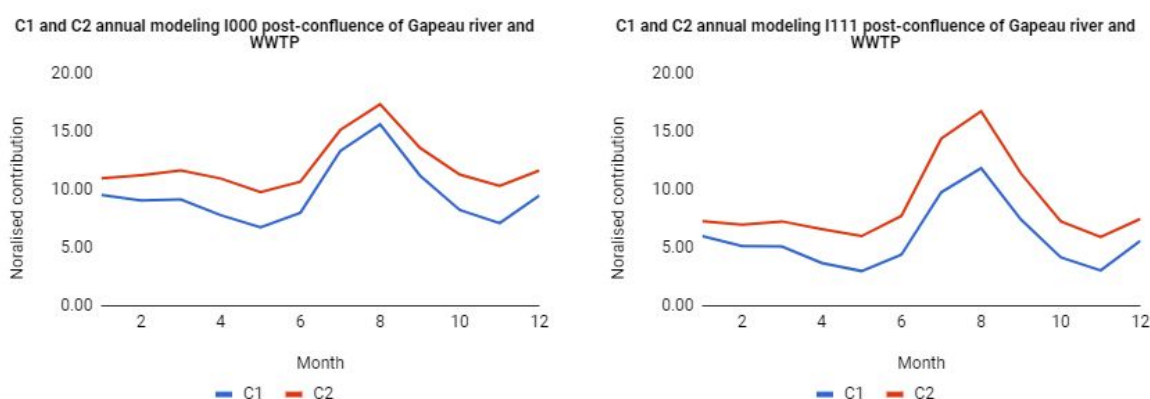


**Figure V.3** : figure showing the variation of the contribution of CP/PARAFAC C1 and C2 as a function of month of the year for two irradiation experiments I000 and I111 for the first case of mixing (mixing of only river water and wastewater treatment plant) . These variation are produced from the multilinear regression model.

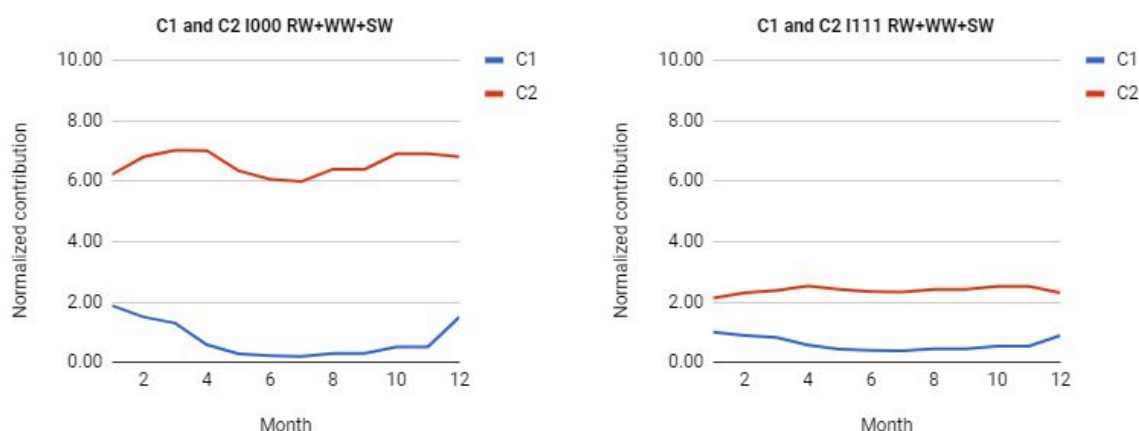


**Figure V.4** : figure showing the variation of the contribution of CP/PARAFAC C1 and C2 as a function of month of the year for two irradiation experiments I000 and I111 for the second case of mixing (mixing of river water and wastewater treatment plant and sea water ). These variation are produced from the multilinear regression model.

It can be seen that for the first case of mixing (in figure V.3) which is the mixing of only the river water and the wastewater treatment plant effluent that the filtration (in the case of I111 experiment) decreases the normalized contribution of CP/PARAFAC components C1 and C2 . And the contribution of the second CP/PARAFAC component C2 is greater than the contribution of C1 for both the I111 and I000 experiments regardless of the filtration state . In addition there is a peak for both the contribution of C1 and C2 which could be due to the increase of the content fraction of the wastewater treatment plant . For the second case of mixing which is the mixing of river water , wastewater treatment plant and sea water , it can be seen from figure V.4 that the contribution of C1 decreases and approaches low or near zero values . With the presence of particulate matter (I000 experiment) , the difference between the contribution of C1 and C2 is more pronounced than that in absence of particulate matter . This could be due to the difference in the photodegradation potential between these CP/PARAFAC components C1 and C2 .

### **V.2.2 Importance of the irradiation in the model**

Without the irradiation , the coefficients of the multilinear regression stays constant and don't change depending on the decay constant based on second order kinetics .

If we draw the relation between the ratio  $C1/C2$  (with irradiation +UV , without irradiation -UV) as a function of month of the year , we get the following graph

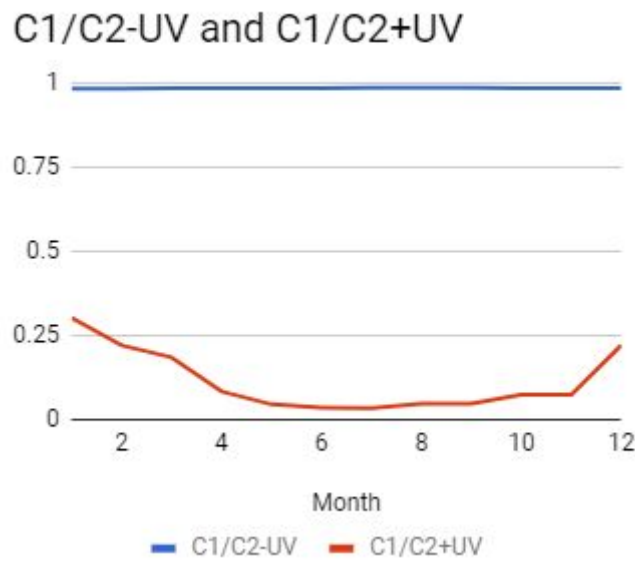


**Figure V.5** : figure showing the ratio between C1 and C2 which is  $C1/C2$  for two cases of irradiation ( with irradiation= $C1/C2+UV$ ; without irradiation= $C1/C2-UV$ ) as a function of month of the year. The ratio varies from zero and one.

It can be seen from figure V.5 that the irradiation has a measurable effect on the ratio  $C1/C2$ . With the absence of irradiation , the ratio  $C1/C2$  remains somehow constant and have a value near one 1 during the months of the year whereas in the presence of irradiation, this  $C1/C2$  ratio decreases greatly to attain a value of 0.25 and continues to decrease during the months of summer where there is higher irradiation values.

### **V.3 Geographical field experiment : modelling based on the multilinear regression model**

The distance of the modeled sampling points were the same as the distances between the sampling points in the actual geographical field experiment. The distance which is equal to zero = 0 km represents the point of the Gapeau river before the wastewater treatment plant . The discharge or flow of the Gapeau river depends on the month of the year as previously indicated in this chapter in Table V.4. We chose to modelize only the case of the month of august where the discharge of the Gapeau river is equal to 0.41 m<sup>3</sup>/s and it increase with the distance and we chose to model this increase of discharge as a function of distance in km with the following equation

$$\text{Discharge} = \text{Discharge (km=0)} + fD * \text{distance}$$

Where :

Discharge : is the discharge in  $\text{m}^3/\text{s}$  at a given distance starting from point zero distance which represents the Gapeau river.

Discharge (km=0) : is the discharge value in  $\text{m}^3/\text{s}$  at distance = 0 km which is the starting point of sampling which is the Gapeau river

$fD$  : is the factor of distance or the factor multiplied to the distance in km we chose arbitrary values which are equal to 0.025 of the monthly discharge of the Gapeau river

**Table V.7** : table showing the factor multiplied by the distance to take into account the increase of discharge of the river a function of distance in km .

Month	1	2	3	4	5	6	7	8	9	10	11	12
$fD$	0.23	0.22	0.16	0.11	0.08	0.04	0.01	0.01	0.02	0.07	0.14	0.16

In addition, the irradiation increases with the increase in distance (in km), we assumed that the increase in irradiation is a factor of 200 multiplied to the distance in km , these values affect the values of the coefficients of the multilinear regression model.

For the mixing of the Gapeau river water and the wastewater treatment plant discharge and the seawater discharge , we assumed 0 % of seawater before the anti-salt dam (barrage anti-sel) , and after the anti-salt dam (barrage anti-sel) , the content fraction of sea water is estimated according to the measured salinity or electrical conductivity and the wastewater treatment plant discharge assumed to be constant all the way along the Gapeau river

The exact values of discharges for the Gapeau river water and the wastewater treatment plant and the seawater are summarized in the following table (table V.8)

**Table V.8** : Table showing the exact discharge values in m<sup>3</sup>/s used in the application of the multilinear regression model , irradiation is in volts

<b>Distance ( in km)</b>	<b>SW</b>	<b>RW</b>	<b>WWTP</b>	<b>Irradiation</b>
0	0	0.451	0	0
1.42	0	0	0.17	284
4.64	0	0.503	0.17	928
5.32	0	0.511	0.17	1064
7.16	0	0.532	0.17	1432
7.55	0	0.536	0.17	1510
9.88	0	0.562	0.17	1976
10.79	0	0.573	0.17	2158
11.58	0	0.582	0.17	2316
11.8	0	0.584	0.17	2360
12.11	1.6	0.572	0.17	2422
12.78	7	0.582	0.17	2556
13.73	16	0.582	0.17	2746
15.71	1000000	0.582	0.17	3142

The values in the above table (table V.8) were used to calculate the mixing percentages or content fractions of fSW and fRW which are used in the modelling of the evolution of the fluorescence signal using the multilinear regression model. Therefore , the mixing percentages or the content fraction for the Gapeau river water and the wastewater treatment plant and the sea water are summarized in the following table (table V.9)

**Table V.9** ; Table showing the content fractions  $f_{SW}$  and  $f_{RW}$  based on values from table V.x . These content fraction were used in the application of the multilinear regression model for the modelling of the geographical field of the Gapeau river.

Distance (km)	$f_{SW}$	$f_{RW}$	$f_{WWTP}$
0	0.00	100.00	0.00
1.42	0.00	0.00	100.00
4.64	0.00	74.99	25.01
5.32	0.00	75.28	24.72
7.16	0.00	76.01	23.99
7.55	0.00	76.16	23.84
9.88	0.00	77.02	22.98
10.79	0.00	77.34	22.66
11.58	0.00	77.61	22.39
11.8	0.00	77.68	22.32
12.11	68.36	24.47	7.17
12.78	90.33	7.50	2.17
13.73	95.53	3.47	1.00
15.71	100.0	0.00	0.00

The output results of the modelling are the following :

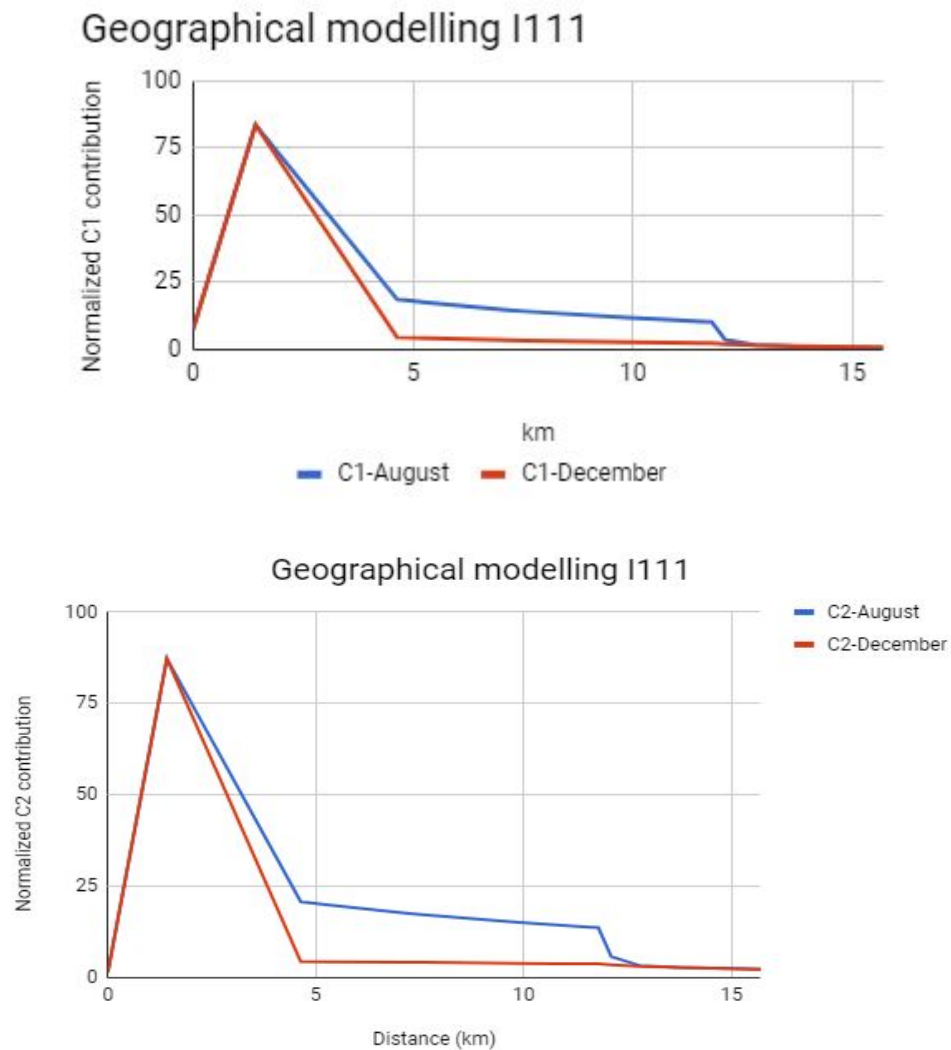


**Figure V.6** : Figure showing the variation with distance of the normalized C1 contribution for the irradiation experiment I111 based upon the multilinear regression model. Blue curve shows the variation of normalized C1 in the month of august in the summer whereas the red curve shows the variation of normalized C1 in the month of december



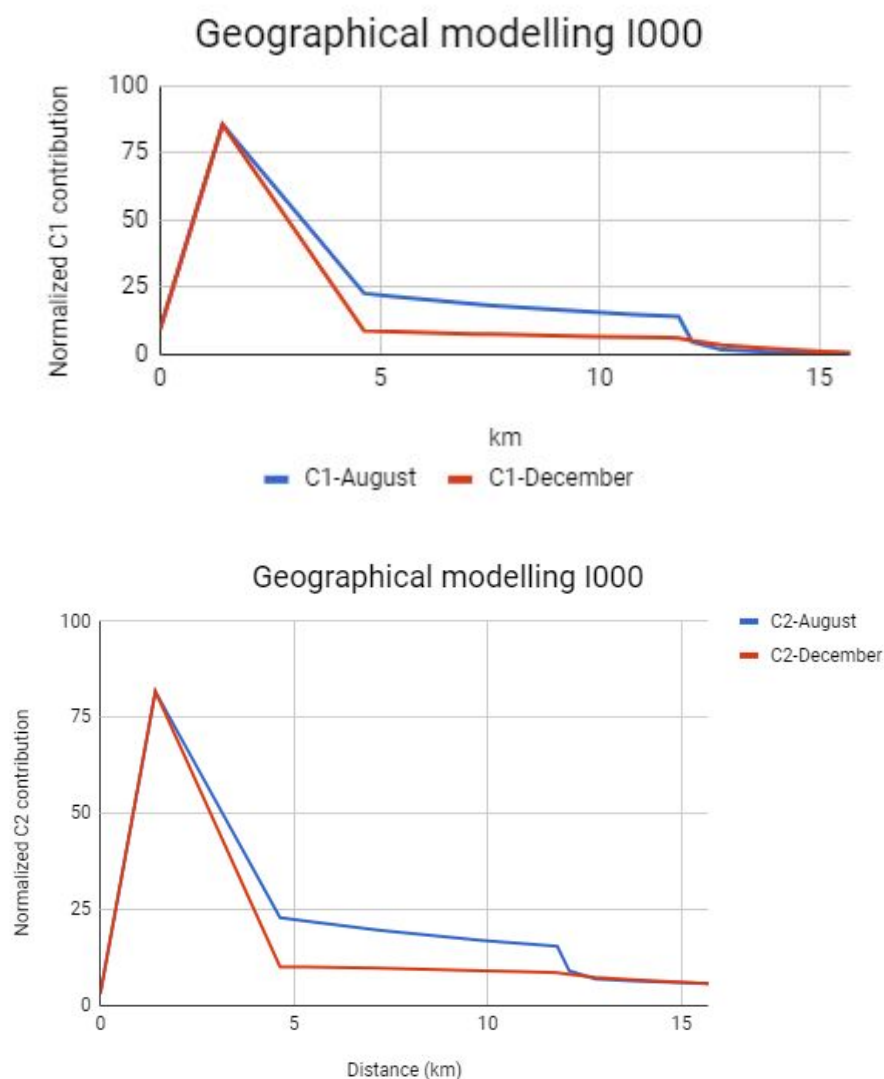


**Figure V.7 :** Figure showing the variation with distance of the normalized C1 contribution for the irradiation experiment I000 based upon the multilinear regression model. Blue curve shows the variation of normalized C1 in the month of august in the summer whereas the red curve shows the variation of normalized C1 in the month of december

It can be seen from the above two figures (figure V.6 and figure V.7) that for both the contributions of CP/PARAFAC C1 and C2 for both the experiments I000 and I111 , the variation is more pronounced in august and it decreases rapidly with the seawater after the antisalt-dam (barrage anti-sel) whereas for the month of december , there are little variation due to the higher flow rate or discharge ( $\text{m}^3/\text{s}$ ) of the Gapeau river in this month of the year.

Moreover, for the second CP/PARAFAC component C2 modelled here was modelled based on the CP/PARAFAC component C2 developed from chapter 3 in the present PhD thesis and it gave approximately similar results to that found in chapter 4 (Figure IV.17). However the second CP/PARAFAC component found from the geographical field experiment was considered to be a protein-like fluorescence. Therefore, more work should be done and conducted to investigate the applicability of the developed model of the evolution of the fluorescence signal.

#### **V.4 Conclusion on the model :**

- We have been able to make approximate estimation of the annual fluorescence for the two CP/PARAFAC components however, the exact irradiation data in volts should be demanded from the part of meteoFrance to verify the results of the present model.
- We have been able to reproduce the geographical variation with distance in the month of August in which we had geographical field experiment in very good manner. However, we hadn't been able to model the small variations along the Gapeau river due to the lack of data and therefore, more work or sampling campaigns to confirm the variations in the month of December or any other chosen month.
- The model needs still work to be ameliorated in order to take into account the intermediary inputs in the pathway of the Gapeau river and also the time of irradiation as a function of the water course of the Gapeau river and also the not irradiated zones due to the trees on the pathway of the Gapeau river which obstructs the entrance of light to the water.

---

## **Conclusions and Perspectives**

---

## Conclusion

In this work, the natural sunlight-induced changes and the effect of the filtration mode (which could represent the particulate matter effect) of three end member mixing model (freshwater, i.e. River Water” end-member, Wastewater Treatment Plants discharge end-member, and the Sea Water end-member) on the fluorescent organic matter were investigated using the technique of the excitation emission matrices of fluorescence (EEM) coupled with the multivariate statistical analysis tool parallel factor analysis CP/PARAFAC with the main objective of quantifying the contribution of the anthropogenic organic matter endmember (represented by the wastewater treatment plant discharge) on the fluorescence in the coastal zone. Multilinear regression model was developed between the contribution of CP/PARAFAC components and the content fraction of two endmembers.

The major findings of this study could be summarized as follows :

1- The CP/PARAFAC decomposition of the several mixing samples gave only 3 components C1, C2 and C3. C1 was visible terrestrial humic-like fluorescence , C2 was Humic-Like fluorescence and C3 was UV humic-like fluorescence contained Peak A; surprisingly no protein like component was predominant along the water discharge.

2-The multilinear regression model for the prediction of the contribution of CP/PARAFAC components and thus the total fluorescence excitation emission matrices turns out to be good and could be done for the three end-member mixing model ( River Water, Wastewater Treatment Plant , Sea Water)

3- The photochemically-induced degradation of the coefficients of the multi-linear regression model of the CP/PARAFAC components followed a second order kinetics except of the third CP/PARAFAC component. In addition, the mixing process of the three endmember mixing components and the effect of solar irradiation on it could be modeled using the percentage in solution of just two endmembers.

3- The search for a specific signal or signature of fluorescence for each end-member of the three end-member mixing components ( River Water , Wastewater Treatment Plants, Sea Water) turned out to be impossible from the perspective of the present study using the CP/PARAFAC modelling of the Excitation Emission matrices EEMs of the fluorescence of the dissolved organic matter coming from each endmember.

4 - The major end-member contributing to the fluorescence signal remaining after the irradiation experiments by sunlight and the resulting photobleaching of the fluorescent organic matter is that of terrestrial sources and from the continental end-member flux and if there is a wastewater treatment discharge in the river ; this fluorescence signal could be attributed to the anthropogenic organic matter (represented by the Wastewater Treatment Plant discharge end-member) according to the results of the kinetic constant for each coefficient of the percentage in solution of just two end-member of the three end-member mixing components since we found slower kinetic constant for the anthropogenic dissolved organic matter contribution to the fluorescence of the CP/PARAFAC modelled using the multilinear regression model.

5- The normal solar irradiation has a measurable effect on the photodegradation of the fluorescence signal coming from organic matter in the coastal zone under normal conditions since a known or a given percentage of the fluorescence signal will be destructed and destroyed by the work of the sunlight only according to the results of the present study.

6- It is possible to make approximate estimation of the annual fluorescence for the two CP/PARAFAC components and it is possible to reproduce the geographical variation with distance in the month of august in which we had geographical field experiment in very good

manner. However, we hadn't been able to model the small variations along the Gapeau river due to lack of data and therefore, more work or sampling campaigns to confirm the variations in the month of december or any other chosen month.

7- The model needs still work to be ameliorated in order to take into account the intermediary inputs in the pathway of the Gapeau river and also the time of irradiation as a function of the water course of the Gapeau river and also the not irradiated zones due to the trees on the pathway of the Gapeau river which obstructs the entrance of light to the water.

### **Recommendations and Perspectives :**

In addition, if we have used other chemical analytical methods like the GC-MS maybe we could have found a specific signal that comes from the anthropogenic sources of organic matter. Therefore, the used technique in this study did not allow the determination or the finding of a specific signal in the coastal zones that comes from the anthropogenic organic matter which is mainly from the wastewater treatment plant in the La Crau city in the southern east of france in la region PACA.

We didn't find a characteristic fluorescence signal of Sea Water from the conducted photochemical irradiation experiments and in our mixing experiments the anthropic end-member was predominant. In addition, we couldn't discriminate the fluorescence signals from the three endmember mixing components in this study, in other words, we couldn't find something fluorescent that would enable us to separate the three water sources.

From these conclusions, it is clear that further studies are warranted in order to discriminate the fluorescence signals in the coastal zone. Three endmember mixing components and experiments would be needed by making fractionation of our three endmembers with the same filtration/nonfiltration we used in the present study. In more details, this could be elaborated as : the freshwater end-member could be fractionated into hydrophobic - hydrophilic - transphilic fraction,

The same goes for the seawater end-member could be fractionated into hydrophobic - hydrophilic - transphilic fraction,

The same goes for the wastewater treatment plants effluent endmember : fractionated into hydrophobic - hydrophilic - transphilic fraction,

Permutations should also be made as shown in the following table :

**Table** : Permutation of the choosing the water fraction and its mixing with the two remaining endmember mixing components

<b>Freshwater</b>	<b>Wastewater treatment plant effluent</b>	<b>Seawater</b>
HPhi	HPhi	HPhi
HPhi	HPhi	HPho
HPhi	HPho	HPhi
HPho	HPhi	HPhi
HPho	HPho	HPho
HPho	HPho	HPhi
HPho	HPhi	HPho
HPhi	HPho	HPho
TPhi	TPhi	TPhi
TPhi	TPhi	HPhi
TPhi	HPhi	TPhi
HPhi	TPhi	TPhi
TPhi	TPhi	TPhi
TPhi	TPhi	HPho
TPhi	HPho	TPhi
HPho	TPhi	TPhi

The results of the above mentioned experiments will certainly yield something new and it will further our knowledge and our capabilities to search for a distinguishing fluorescence

signals of the three end-member mixing components and especially the anthropogenic organic matter endmember.

Moreover, the fluorescence signal of the Wastewater Treatment Plant end-member could be monitored by sampling the outlet every month of the year to follow-up the development of its fluorescence signal and to see if it yields a specific fluorescence signal or not. UV-Visible spectroscopy measuring the absorbance and total organic carbon measurements could have provided more useful information in the present works of this PhD thesis therefore, it is recommended to add the UV-VIS spectroscopy and total organic carbon measurements to the methods for future research.



---

## REFERENCES

---

## References:

- Abbassi, M., Banaoui, A., Charioui, I., Kaaya, A., Elkhoul, A., Nadir, M., Agnaou, M., Lefrere, L., El Hamidi, F. (2017). Physico-chemical characterization of the coastal waters of the city of Sidi Ifni (Morocco). *Journal of Materials and Environmental Sciences JMES*, 8(9), 3112-3120.
- A Global Analysis of Human Settlement in Coastal Zones on JSTOR. (n.d.). Retrieved April 9, 2018, from <http://www.jstor.org/stable/4299200>
- Aiken, G. R. (1985). *Humic Substances in Soil, Sediment, and Water: Geochemistry, Isolation, and Characterization*. Wiley-Interscience.
- Alam, M. J., Jahangir Alam, M., Nagao, S., & Emran Quayum, M. (2015). Transport of Particulate Organic Matter and Dissolved Organic Matter from Land to Ocean in Hokkaido, Japan. *Dhaka University Journal of Science*, 63(1). <https://doi.org/10.3329/dujs.v63i1.21768>
- Albani, J. R. (2008). *Principles and Applications of Fluorescence Spectroscopy*. John Wiley & Sons.
- Amon, R. M. W. (2004). The Role of Dissolved Organic Matter for the Organic Carbon Cycle in the Arctic Ocean. In *The Organic Carbon Cycle in the Arctic Ocean* (pp. 83–99).
- Andersen, C. M., & Bro, R. (2003). Practical aspects of PARAFAC modeling of fluorescence excitation-emission data. *Journal of Chemometrics*, 17(4), 200–215.
- Baghoth, S. A., Sharma, S. K., & Amy, G. L. (2011). Tracking natural organic matter (NOM) in a drinking water treatment plant using fluorescence excitation–emission matrices and

PARAFAC. *Water Research*, 45(2), 797–809.

- Bahram, Morteza, Rasmus Bro, Colin Stedmon, and Abbas Afkhami. 2006. “Handling of Rayleigh and Raman Scatter for PARAFAC Modeling of Fluorescence Data Using Interpolation.” *Journal of Chemometrics* 20 (3-4): 99–105.
- Baker, A., Inverarity, R., Charlton, M., & Richmond, S. (2003). Detecting river pollution using fluorescence spectrophotometry: case studies from the Ouseburn, NE England. *Environmental Pollution*, 124(1), 57–70.
- Beatley, T., Brower, D., & Schwab, A. K. (2002). *An Introduction to Coastal Zone Management: Second Edition*. Island Press.
- Bertilsson, S., Carlsson, P., & Granéli, W. (2004). Influence of solar radiation on the availability of dissolved organic matter to bacteria in the Southern Ocean. *Deep-Sea Research. Part II, Topical Studies in Oceanography*, 51(22-24), 2557–2568.
- Bieroza, M., Baker, A., & Bridgeman, J. (2012). Exploratory analysis of excitation–emission matrix fluorescence spectra with self-organizing maps—A tutorial. *Education for Chemical Engineers*, 7(1), e22–e31.
- Blough, N. V., & Del Vecchio, R. (2002). Chromophoric DOM in the Coastal Environment. In *Biogeochemistry of Marine Dissolved Organic Matter* (pp. 509–546).
- Boehme, J., & Wells, M. (2006). Fluorescence variability of marine and terrestrial colloids: Examining size fractions of chromophoric dissolved organic matter in the Damariscotta River estuary. *Marine Chemistry*, 101(1-2), 95–103.
- Boehme, J., Coble, P., Conmy, R., & Stovall-Leonard, A. (2004). Examining CDOM

- fluorescence variability using principal component analysis: seasonal and regional modeling of three-dimensional fluorescence in the Gulf of Mexico. *Marine Chemistry*, 89(1-4), 3–14.
- Bro, Rasmus. 1997. “PARAFAC. Tutorial and Applications.” *Chemometrics and Intelligent Laboratory Systems* 38 (2): 149–71.
- Carroll, J. D., Douglas Carroll, J., & Chang, J.-J. (1970). Analysis of individual differences in multidimensional scaling via an n-way generalization of “Eckart-Young” decomposition. *Psychometrika*, 35(3), 283–319.
- Chen, M., & Jaffé, R. (2014). Photo- and bio-reactivity patterns of dissolved organic matter from biomass and soil leachates and surface waters in a subtropical wetland. *Water Research*, 61, 181–190.
- Chen, W., Westerhoff, P., Leenheer, J. A., & Booksh, K. (2003). Fluorescence Excitation–Emission Matrix Regional Integration to Quantify Spectra for Dissolved Organic Matter. *Environmental Science & Technology*, 37(24), 5701–5710.
- Clayton, K. (1992). Book reviews : Hinrichsen, D. 1990: Our common seas: coasts in crisis. London: Earthscan. viii 184 pp. £6.95 paper. ISBN: 1 85383 030 5. *Progress in Human Geography*, 16(2), 299–300.
- Coble, P., Hu, C., Gould, R., Chang, G., & Wood, M. (2004). Colored Dissolved Organic Matter in the Coastal Ocean: An Optical Tool for Coastal Zone Environmental Assessment and Management. *Oceanography*, 17(2), 50–59.
- Coble, P., Lead, J., Baker, A., Reynolds, D., & Spencer, R. G. M. (2014). *Aquatic Organic Matter Fluorescence*. Cambridge University Press.
- Coble, P. G. (1996). Characterization of marine and terrestrial DOM in seawater using

- excitation-emission matrix spectroscopy. *Marine Chemistry*, 51(4), 325–346.
- Coble, P. G. (2007). Marine optical biogeochemistry: the chemistry of ocean color. *Chemical Reviews*, 107(2), 402–418.
- Cohen, E., Levy, G. J., & Borisover, M. (2014). Fluorescent components of organic matter in wastewater: efficacy and selectivity of the water treatment. *Water Research*, 55, 323–334.
- Cory, R. M., & McKnight, D. M. (2005). Fluorescence Spectroscopy Reveals Ubiquitous Presence of Oxidized and Reduced Quinones in Dissolved Organic Matter. *Environmental Science & Technology*, 39(21), 8142–8149.
- Crossland, C. J., Baird, D., Ducrotoy, J.-P., Lindeboom, H., Buddemeier, R. W., Dennison, W. C., ... Swaney, D. P. (2005). The Coastal Zone — a Domain of Global Interactions. In *Global Change — The IGBP Series* (pp. 1–37).
- Dainard, P. G., & Guéguen, C. (2013). Distribution of PARAFAC modeled CDOM components in the North Pacific Ocean, Bering, Chukchi and Beaufort Seas. *Marine Chemistry*, 157, 216–223.
- de Andrés, M., Barragán, J. M., & Scherer, M. (2018). Urban centres and coastal zone definition: Which area should we manage? *Land Use Policy*, 71, 121–128.
- Del Vecchio, R., & Blough, N. V. (2002). Photobleaching of chromophoric dissolved organic matter in natural waters: kinetics and modeling. *Marine Chemistry*, 78(4), 231–253.
- Del Vecchio, R., & Blough, N. V. (2004). Spatial and seasonal distribution of chromophoric dissolved organic matter and dissolved organic carbon in the Middle Atlantic Bight. *Marine Chemistry*, 89(1-4), 169–187.
- De Souza Sierra, M. M., Donard, O. F. X., Lamotte, M., Belin, C., & Ewald, M. (1994).

- Fluorescence spectroscopy of coastal and marine waters. *Marine Chemistry*, 47(2), 127–144.
- Du, Y., Zhang, Y., Chen, F., Chang, Y., & Liu, Z. (2016). Photochemical reactivities of dissolved organic matter (DOM) in a sub-alpine lake revealed by EEM-PARAFAC: An insight into the fate of allochthonous DOM in alpine lakes affected by climate change. *The Science of the Total Environment*, 568, 216–225.
- Ferrari, G. M., Dowell, M. D., Grossi, S., & Targa, C. (1996). Relationship between the optical properties of chromophoric dissolved organic matter and total concentration of dissolved organic carbon in the southern Baltic Sea region. *Marine Chemistry*, 55(3-4), 299–316.
- Ferretto, N. (2014). Nicolas FERRETTO. Étude de la matière organique dissoute fluorescente et évaluation de la pression anthropique en Méditerranée. [Http://www.theses.fr](http://www.theses.fr), 1–158. Retrieved from <http://www.theses.fr/2014AIXM4024>
- Filella, M. (2008). Freshwaters: which NOM matters? *Environmental Chemistry Letters*, 7(1), 21–35.
- Fluorescence - An Introduction to Biotechnology - Chapter 8. (n.d.-a). Retrieved November 13, 2017, from <https://doi.org/10.1016/B978-1-907568-28-2.00008-3>
- Fluorescence - An Introduction to Biotechnology - Chapter 8. (n.d.-b). Retrieved November 14, 2017, from <https://doi.org/10.1016/B978-1-907568-28-2.00008-3>
- Frackowiak, D. (1988). The Jablonski diagram. *Journal of Photochemistry and Photobiology. B, Biology*, 2(3), 399.
- Gao, H., & Zepp, R. G. (1998). Factors Influencing Photoreactions of Dissolved Organic Matter in a Coastal River of the Southeastern United States. *Environmental Science & Technology*, 32(19), 2940–2946.

- Gardner, G. B., Bernard Gardner, G., Chen, R. F., & Berry, A. (2005). High-resolution measurements of chromophoric dissolved organic matter (CDOM) in the Neponset River Estuary, Boston Harbor, MA. *Marine Chemistry*, 96(1-2), 137–154.
- Giacomin, M., Gillis, P. L., Bianchini, A., & Wood, C. M. (2013). Interactive effects of copper and dissolved organic matter on sodium uptake, copper bioaccumulation, and oxidative stress in juvenile freshwater mussels (*Lampsilis siliquoidea*). *Aquatic Toxicology*, 144-145, 105–115.
- Glusac, K. (2016). What has light ever done for chemistry? *Nature Chemistry*, 8(8), 734–735.
- Gouldson, & Gouldson. (1996). EUROPE’S ENVIRONMENT: THE DOBRIS ASSESSMENT. *European Environment*, 6(1), 30–30.
- Gregorich, E. G., Beare, M. H., McKim, U. F., & Skjemstad, J. O. (2006). Chemical and Biological Characteristics of Physically Uncomplexed Organic Matter. *Soil Science Society of America Journal*. *Soil Science Society of America*, 70(3), 975.
- Grzybowski, W. (2016). Dark recovery of photodegraded chromophoric dissolved organic matter. *Journal of Photochemistry and Photobiology. A, Chemistry*, 330, 175–180.
- Hall, G. J., & Kenny, J. E. (2007). Estuarine water classification using EEM spectroscopy and PARAFAC–SIMCA. *Analytica Chimica Acta*, 581(1), 118–124.
- Hansell, D., Carlson, C., Repeta, D., & Schlitzer, R. (2009). Dissolved Organic Matter in the Ocean: A Controversy Stimulates New Insights. *Oceanography*, 22(4), 202–211.
- Harshman, R. A., & Lundy, M. E. (1994). PARAFAC: Parallel factor analysis. *Computational Statistics & Data Analysis*, 18(1), 39–72.
- Hayase, K., & Tsubota, H. (1985). Sedimentary humic acid and fulvic acid as fluorescent organic

- materials. *Geochimica et Cosmochimica Acta*, 49(1), 159–163.
- Heibati, M., Stedmon, C. A., Stenroth, K., Rauch, S., Toljander, J., S  ve-S  derbergh, M., & Murphy, K. R. (2017). Assessment of drinking water quality at the tap using fluorescence spectroscopy. *Water Research*, 125, 1–10.
- Helms, J. R., Stubbins, A., Michael Perdue, E., Green, N. W., Chen, H., & Mopper, K. (2013). Photochemical bleaching of oceanic dissolved organic matter and its effect on absorption spectral slope and fluorescence. *Marine Chemistry*, 155, 81–91.
- Henderson, R. K., Baker, A., Murphy, K. R., Hambly, A., Stuetz, R. M., & Khan, S. J. (2009). Fluorescence as a potential monitoring tool for recycled water systems: a review. *Water Research*, 43(4), 863–881.
- Herrmann, R., & Onkelinx, C. (1984). Quantities and units in clinical chemistry: nebulizer and flame properties in flame emission and absorption spectrometry (Provisional). *Journal of Macromolecular Science, Part A: Pure and Applied Chemistry*, 56(10).  
<https://doi.org/10.1351/pac198456101499>
- Hinrichsen, D. (2016). *Our Common Seas: Coasts in Crisis*. Routledge.
- Houghton, R. A. (2003). The Contemporary Carbon Cycle. In *Treatise on Geochemistry* (pp. 473–513).
- Hudson, N., Baker, A., & Reynolds, D. (2007). Fluorescence analysis of dissolved organic matter in natural, waste and polluted waters—a review. *River Research and Applications*, 23(6), 631–649.
- Hugo, G. (2011). Future demographic change and its interactions with migration and climate change. *Global Environmental Change: Human and Policy Dimensions*, 21, S21–S33.



- Hur, J., & Cho, J. (2012). Prediction of BOD, COD, and Total Nitrogen Concentrations in a Typical Urban River Using a Fluorescence Excitation-Emission Matrix with PARAFAC and UV Absorption Indices. *Sensors*, 12(12), 972–986.
- Iqbal, M. (2012). *An Introduction To Solar Radiation*. Elsevier.
- [IUPAC](#), *Compendium of Chemical Terminology*, 2nd ed. (the "Gold Book") (1997). Online corrected version: (2006–) "[photochemistry](#)".
- Jablonski, A. (1933). Efficiency of Anti-Stokes Fluorescence in Dyes. *Nature*, 131(3319), 839–840.
- Jaffe, H. H., & Miller, A. L. (1966). The fates of electronic excitation energy. *Journal of Chemical Education*, 43(9), 469.
- Kalle, K. (1963). Über das Verhalten und die Herkunft der in den Gewässern und in der Atmosphäre vorhandenen himmelblauen Fluoreszenz. *Deutsche Hydrographische Zeitschrift*, 16(4), 153–166.
- Kieber, R. J., Hydro, L. H., & Seaton, P. J. (1997). Photooxidation of triglycerides and fatty acids in seawater: Implication toward the formation of marine humic substances. *Limnology and Oceanography*, 42(6), 1454–1462.
- Kim, Y. C. (2016). *Handbook of Coastal and Ocean Engineering*.
- Krupa, M. (2010). *Controls on Dissolved Organic Carbon Composition and Export from Rice-dominated Systems*.
- Laird, L. M. (1991). D. Hinrichsen 1990. Our common seas: coasts in crisis. Earthscan Publications Ltd London in Association with the United Nations Environmental Programme, Nairobi. 184 pages. ISBN 1 85383-030-5. Price: £6.95 (paperback). *Journal of*

*Tropical Ecology*, 7(02), 286.

Lakowicz, J. R. (1983). *Principles of Fluorescence Spectroscopy*.

Li, S., Zhang, J., Guo, E., Zhang, F., Ma, Q., & Mu, G. (2017). Dynamics and ecological risk assessment of chromophoric dissolved organic matter in the Yinma River Watershed: Rivers, reservoirs, and urban waters. *Environmental Research*, 158, 245–254.

Li, S., Zhang, J., Mu, G., Ju, H., Wang, R., & Li, D. (2016). Spatiotemporal Characterization of Chromophoric Dissolved Organic Matter (CDOM) and CDOM-DOC Relationships for Highly-Polluted River. <https://doi.org/10.20944/preprints201608.0193.v1>

Li, W.-T., Chen, S.-Y., Xu, Z.-X., Li, Y., Shuang, C.-D., & Li, A.-M. (2014). Characterization of dissolved organic matter in municipal wastewater using fluorescence PARAFAC analysis and chromatography multi-excitation/emission scan: a comparative study. *Environmental Science & Technology*, 48(5), 2603–2609.

Masalu, D. C. P. (2008). Coastal data and information management for integrated coastal management: The role of IODE. *Marine Policy*, 32(4), 544–550.

McGranahan, G., Balk, D., & Anderson, B. (2007). The rising tide: assessing the risks of climate change and human settlements in low elevation coastal zones. *Environment and Urbanization*, 19(1), 17–37.

McNaught, A. D., & Wilkinson, A. (1997). *Compendium of Chemical Terminology: IUPAC Recommendations*. Wiley-Blackwell.

Meng, F., Huang, G., Yang, X., Li, Z., Li, J., Cao, J., ... Sun, L. (2013). Identifying the sources and fate of anthropogenically impacted dissolved organic matter (DOM) in urbanized rivers. *Water Research*, 47(14), 5027–5039.

- Miller, W. L., Moran, M., Sheldon, W. M., Zepp, R. G., & Opsahl, S. (2002). Determination of apparent quantum yield spectra for the formation of biologically labile photoproducts. *Limnology and Oceanography*, 47(2), 343–352.
- Moran, M. A., Sheldon, W. M., & Zepp, R. G. (2000). Carbon loss and optical property changes during long-term photochemical and biological degradation of estuarine dissolved organic matter. *Limnology and Oceanography*, 45(6), 1254–1264.
- Mostofa, K. M. G., Liu, C.-Q., Yoshioka, T., Vione, D., Zhang, Y., & Sakugawa, H. (2012). Fluorescent Dissolved Organic Matter in Natural Waters. In *Environmental Science and Engineering* (pp. 429–559).
- Mostofa, K. M. G., Wu, F., Liu, C.-Q., Fang, W. L., Yuan, J., Ying, W. L., ... Yi, M. (2009). Characterization of Nanming River (southwestern China) sewerage-impacted pollution using an excitation-emission matrix and PARAFAC. *Limnology / The Japanese Society of Limnology*, 11(3), 217–231.
- Mostofa, K. M. G., Yoshioka, T., Mottaleb, A., & Vione, D. (2012). *Photobiogeochemistry of Organic Matter: Principles and Practices in Water Environments*. Springer Science & Business Media.
- Mostofa KMG, Wu FC, Yoshioka T, Sakugawa H, Tanoue E (2009a) Dissolved organic matter in the aquatic environments. In: Wu FC, Xing B (eds) Natural organic matter and its significance in the environment. Science Press, Beijing, pp 3–66
- Mounier, Stéphane, Huiyu Zhao, Cédric Garnier, and Roland Redon. 2011. “Copper Complexing Properties of Dissolved Organic Matter: PARAFAC Treatment of Fluorescence Quenching.” *Biogeochemistry* 106 (1): 107–16.
- Murphy, K. R., Stedmon, C. A., Graeber, D., & Bro, R. (2013). Fluorescence spectroscopy and

- multi-way techniques. PARAFAC. *Analytical Methods*, 5(23), 6557.
- Nelson, N. B., & Siegel, D. A. (2002). Chromophoric DOM in the Open Ocean. In *Biogeochemistry of Marine Dissolved Organic Matter* (pp. 547–578).
- Neumann, B., Vafeidis, A. T., Zimmermann, J., & Nicholls, R. J. (2015). Future coastal population growth and exposure to sea-level rise and coastal flooding--a global assessment. *PloS One*, 10(3), e0118571.
- Pagano, T., Bida, M., & Kenny, J. (2014). Trends in Levels of Allochthonous Dissolved Organic Carbon in Natural Water: A Review of Potential Mechanisms under a Changing Climate. *WATER*, 6(12), 2862–2897.
- Patel-Sorrentino, N., Mounier, S., Lucas, Y., & Benaim, J. Y. (2004). Effects of UV-visible irradiation on natural organic matter from the Amazon basin. *The Science of the Total Environment*, 321(1-3), 231–239.
- Peña-Cortés, F., Rozas-Vásquez, D., Rebolledo, G., Pincheira-Ulbrich, J., Escalona, M., Hauenstein, E., ... Cisternas, M. (2013). Territorial Planning for Coastal Zones in Chile: The Need for Geographical-Environmental and Natural Risk Indicators for Spatial Decision Support Systems. *International Journal of Geosciences*, 04(06), 17–29.
- Perminova, I. V., Frimmel, F. H., Kudryavtsev, A. V., Kulikova, N. A., Abbt-Braun, G., Hesse, S., & Petrosyant, V. S. (2003). Molecular weight characteristics of humic substances from different environments as determined by size exclusion chromatography and their statistical evaluation. *Environmental Science & Technology*, 37(11), 2477–2485.
- Qian, C., Chen, W., Li, W.-H., & Yu, H.-Q. (2017). A chemometric analysis on the fluorescent dissolved organic matter in a full-scale sequencing batch reactor for municipal wastewater

- treatment. *Frontiers of Environmental Science & Engineering in China*, 11(4).  
<https://doi.org/10.1007/s11783-017-0962-2>
- Research Watch: Dissolved organic matter in the ocean. (1998). *Environmental Science & Technology*, 32(13), 333A – 333A.
- Rodríguez-Zúñiga, U. F., Milori, D. M. B. P., da Silva, W. T. L., Martin-Neto, L., Oliveira, L. C., & Rocha, J. C. (2008). Changes in optical properties caused by UV-irradiation of aquatic humic substances from the amazon river basin: seasonal variability evaluation. *Environmental Science & Technology*, 42(6), 1948–1953.
- Romankevich, E. A. (1984). Carbon of Dissolved Organic Matter in the Ocean. In *Geochemistry of Organic Matter in the Ocean* (pp. 27–55).
- Schlesinger, W. H., & Bernhardt, E. S. (2013). *Biogeochemistry: An Analysis of Global Change*. Academic Press.
- Senesi, N. (1990). Molecular and quantitative aspects of the chemistry of fulvic acid and its interactions with metal ions and organic chemicals. *Analytica Chimica Acta*, 232, 77–106.
- Shi, W., Jin, Z., Hu, S., Fang, X., & Li, F. (2017). Dissolved organic matter affects the bioaccumulation of copper and lead in *Chlorella pyrenoidosa*: A case of long-term exposure. *Chemosphere*, 174, 447–455.
- Shutova, Y., Baker, A., Bridgeman, J., & Henderson, R. K. (2014). Spectroscopic characterisation of dissolved organic matter changes in drinking water treatment: From PARAFAC analysis to online monitoring wavelengths. *Water Research*, 54, 159–169.
- Skoog, A., Wedborg, M., & Fogelqvist, E. (1996). Photobleaching of fluorescence and the organic carbon concentration in a coastal environment. *Marine Chemistry*, 55(3-4),

333–345.

Smith, K. (2011). We are seven billion. *Nature Climate Change*, 1(7), 331–335.

Song, G., Li, Y., Hu, S., Li, G., Zhao, R., Sun, X., & Xie, H. (2017). Photobleaching of chromophoric dissolved organic matter (CDOM) in the Yangtze River estuary: kinetics and effects of temperature, pH, and salinity. *Environmental Science. Processes & Impacts*, 19(6), 861–873.

Stedmon, C. A., & Bro, R. (2008). Characterizing dissolved organic matter fluorescence with parallel factor analysis: a tutorial. *Limnology and Oceanography, Methods / ASLO*, 6(11), 572–579.

Stedmon, C. A., & Markager, S. (2005). Resolving the variability in dissolved organic matter fluorescence in a temperate estuary and its catchment using PARAFAC analysis. *Limnology and Oceanography*, 50(2), 686–697.

Stedmon, C. A., Markager, S., & Bro, R. (2003). Tracing dissolved organic matter in aquatic environments using a new approach to fluorescence spectroscopy. *Marine Chemistry*, 82(3-4), 239–254.

Stedmon, Colin A., and Rasmus Bro. 2008. “Characterizing Dissolved Organic Matter Fluorescence with Parallel Factor Analysis: A Tutorial.” *Limnology and Oceanography, Methods / ASLO* 6 (11): 572–79.

Søndergaard, M., Stedmon, C. A., & Borch, N. H. (2003). Fate of terrigenous dissolved organic matter (DOM) in estuaries: Aggregation and bioavailability. *Ophelia*, 57(3), 161–176.

Tedetti, M., Longhitano, R., Garcia, N., Guigue, C., Ferretto, N., & Goutx, M. (2012). Fluorescence properties of dissolved organic matter in coastal Mediterranean waters

- influenced by a municipal sewage effluent (Bay of Marseilles, France). *Huan Jing Hua Xue* = *Environmental Chemistry*, 9(5), 438.
- Thurman, E. M. (1985). *Organic Geochemistry of Natural Waters*.
- Vera, M., Cruz, S., Boleda, M. R., Mesa, J., Martín-Alonso, J., Casas, S., ... Cortina, J. L. (2017). Fluorescence spectroscopy and parallel factor analysis as a dissolved organic monitoring tool to assess treatment performance in drinking water trains. *The Science of the Total Environment*, 584-585, 1212–1220.
- Vidali, R., Remoundaki, E., & Tsezos, M. (2009). Humic Acids Copper Binding Following Their Photochemical Alteration by Simulated Solar Light. *Aquatic Geochemistry*, 16(1), 207–218.
- Wagner, S., Riedel, T., Niggemann, J., Vähätalo, A. V., Dittmar, T., & Jaffé, R. (2015). Linking the Molecular Signature of Heteroatomic Dissolved Organic Matter to Watershed Characteristics in World Rivers. *Environmental Science & Technology*, 49(23), 13798–13806.
- Waiser, M. J., & Robarts, R. D. (2005). Photodegradation of DOC in a shallow prairie wetland: evidence from seasonal changes in DOC optical properties and chemical characteristics. *Biogeochemistry*, 75(3), 529–552.
- Wang, M., & Chen, Y. (2018). Generation and characterization of DOM in wastewater treatment processes. *Chemosphere*, 201, 96–109.
- Wang, Y., Zhang, D., Shen, Z., Chen, J., & Feng, C. (2014). Characterization and spacial distribution variability of chromophoric dissolved organic matter (CDOM) in the Yangtze Estuary. *Chemosphere*, 95, 353–362.
- Website. (n.d.). Retrieved April 9, 2018, from

<https://doi.org/10.1002/9781118786352.wbieg0972>

- White, E. M., Vaughan, P. P., & Zepp, R. G. (2003). Role of the photo-Fenton reaction in the production of hydroxyl radicals and photobleaching of colored dissolved organic matter in a coastal river of the southeastern United States. *Aquatic Sciences - Research Across Boundaries*, 65(4), 402–414.
- Whitehead, R. F., & de Mora, S. J. (2004). Modeling the effect of ozone loss on photobleaching of chromophoric dissolved organic matter in the St. Lawrence estuary. *Global Biogeochemical Cycles*, 18(1). <https://doi.org/10.1029/2003gb002101>
- Wigley, T. M. L., & Schimel, D. S. (2005). *The Carbon Cycle*. Cambridge University Press.
- Williams, P. M., & Druffel, E. (1988). Dissolved Organic Matter in the Ocean: Comments on a Controversy. *Oceanography*, 1(1), 14–17.
- Wu, Jun, Hua Zhang, Pin-Jing He, and Li-Ming Shao. 2011. “Insight into the Heavy Metal Binding Potential of Dissolved Organic Matter in MSW Leachate Using EEM Quenching Combined with PARAFAC Analysis.” *Water Research* 45 (4): 1711–19.
- Yan, M., Ma, J., Zhang, C., Zhou, Y., Liu, F., Han, X., ... Ni, J. (2017). Optical property of dissolved organic matters (DOMs) and its link to the presence of metal ions in surface freshwaters in China. *Chemosphere*, 188, 502–509.
- Yang, L., Han, D. H., Lee, B.-M., & Hur, J. (2015). Characterizing treated wastewaters of different industries using clustered fluorescence EEM–PARAFAC and FT-IR spectroscopy: Implications for downstream impact and source identification. *Chemosphere*, 127, 222–228.
- Yang, L., Hur, J., & Zhuang, W. (2015). Occurrence and behaviors of fluorescence EEM-PARAFAC components in drinking water and wastewater treatment systems and their



- applications: a review. *Environmental Science and Pollution Research*, 22(9), 6500–6510.
- Yang, L., Shin, H.-S., & Hur, J. (2014). Estimating the concentration and biodegradability of organic matter in 22 wastewater treatment plants using fluorescence excitation emission matrices and parallel factor analysis. *Sensors*, 14(1), 1771–1786.
- Yang, X., Meng, F., Huang, G., Sun, L., & Lin, Z. (2014). Sunlight-induced changes in chromophores and fluorophores of wastewater-derived organic matter in receiving waters – The role of salinity. *Water Research*, 62, 281–292.
- Yu, H., Song, Y., Du, E., Yang, N., Peng, J., & Liu, R. (2016). Comparison of PARAFAC components of fluorescent dissolved and particular organic matter from two urbanized rivers. *Environmental Science and Pollution Research International*, 23(11), 10644–10655.
- Zanardi-Lamardo, E., Moore, C. A., & Zika, R. G. (2004). Seasonal variation in molecular mass and optical properties of chromophoric dissolved organic material in coastal waters of southwest Florida. *Marine Chemistry*, 89(1-4), 37–54.
- Zepp, R. G., Sheldon, W. M., & Moran, M. A. (2004). Dissolved organic fluorophores in southeastern US coastal waters: correction method for eliminating Rayleigh and Raman scattering peaks in excitation–emission matrices. *Marine Chemistry*, 89(1-4), 15–36.
- Zhang, Y., Liang, X., Wang, Z., & Xu, L. (2015). A novel approach combining self-organizing map and parallel factor analysis for monitoring water quality of watersheds under non-point source pollution. *Scientific Reports*, 5, 16079.
- Zhao, Huiyu. 2011. “Analyse de la matière organique et ses propriétés dans l’environnement naturel en spectroscopie de fluorescence 3D traitée par PARAFAC.” Université du Sud Toulon Var. <https://tel.archives-ouvertes.fr/tel-00626538/document>.

- Zhou, J., Wang, J.-J., Baudon, A., & Chow, A. T. (2013). Improved fluorescence excitation-emission matrix regional integration to quantify spectra for fluorescent dissolved organic matter. *Journal of Environmental Quality*, 42(3), 925–930.
- Zhou, Z., Guo, L., & Minor, E. C. (2016). Characterization of bulk and chromophoric dissolved organic matter in the Laurentian Great Lakes during summer 2013. *Journal of Great Lakes Research*, 42(4), 789–801.

---

# ANNEXES

---

# ANNEX I

## $f_{RW}$ and $f_{SW}$ Permutation

**Table Annex I.1 :** the evolution of the coefficients of multilinear regression for the first CP/PARAFAC component for the irradiation experiment I111 ( river water filtered , sea water filtered , wwtp water filtered .(aug-sept 2015 experiment)

Coefficient C1 à I111	Voltage (Volts)	$A^{WW,EN}_0$	$A^{WW,EN}_2(f_{RW})$	$A^{WW,EN}_1(f_{SW})$	$r_{EN}^2$	$A^{WW,CR}_0$	$A^{WW,CR}_2(f_{RW})$	$A^{WW,CR}_1(f_{SW})$	$r_{CR}^2$
T0	0	100.34	-0.93	-0.99	0.99	100.13	-0.93	-0.99	0.99
T3	11140.81	11.56	-0.11	-0.11	0.99	9.32	-0.08	-0.09	0.98
T4	12470.48	11.50	-0.10	-0.11	0.99	8.6	-0.07	-0.08	0.9
T5	14821.40	9.17	-0.08	-0.08	0.98	6.51	-0.0	-0.064	0.99
T6	16363.55	8.24	-0.07	-0.07	0.97	5.67	-0.05	-0.05	0.99
T7	17521.88	5.80	-0.06	-0.05	0.97	4.9	-0.0494	-0.05	0.99
T11	27011.24	5.36	-0.0	-0.05	0.78	3.00	-0.02	-0.03	0.77
T12	28944.07	2.06	-0.01	-0.02	0.55	1.51	-0.01	-0.01	0.79
T13	30410.83	4.01	-0.03	-0.03	0.89	2.52	-0.02	-0.02	0.92
T14	32806.30	4.38	-0.04	-0.04	0.96	1.90	-0.01	-0.02	0.84

**Table Annex I.2:** the evolution of the coefficients of multilinear regression for the second CP/PARAFAC component for the irradiation experiment I111 ( river water filtered , sea water filtered , wwtp water filtered .(aug-sept 2015 experiment)

Coefficient C2 à I111	Voltage (Volts)	$A^{WW,EN}_0$	$A^{WW,EN}_2(f_{RW})$	$A^{WW,EN}_1(f_{SW})$	$r_{EN}^2$	$A^{WW,CR}_0$	$A^{WW,CR}_2(f_{RW})$	$A^{WW,CR}_1(f_{SW})$	$r_{CR}^2$
T0	0	98.42	-0.92	-0.97	<b>0.99</b>	111.15	-0.94	-1.03	<b>0.96</b>
T3	11140.81	16.73	-0.14	-0.15	<b>0.97</b>	63.21	-0.53	-0.54	<b>0.95</b>
T4	12470.48	16.04	-0.15	-0.14	<b>0.98</b>	55.60	-0.49	-0.48	<b>0.97</b>
T5	14821.40	14.39	-0.13	-0.14	<b>0.98</b>	51.90	-0.45	-0.46	<b>0.97</b>
T6	16363.55	12.98	-0.12	-0.12	<b>0.98</b>	50.71	-0.45	-0.43	<b>0.96</b>
T7	17521.88	13.07	-0.11	-0.12	<b>0.98</b>	51.1	-0.43	-0.42	<b>0.96</b>
T11	27011.24	6.47	-0.059	-0.06	<b>0.95</b>	35.58	-0.29	-0.32	<b>0.92</b>
T12	28944.07	8.56	-0.07	-0.08	<b>0.96</b>	50.12	-0.41	-0.39	<b>0.90</b>
T13	30410.83	7.01	-0.06	-0.06	<b>0.93</b>	39.13	-0.32	-0.30	<b>0.88</b>
T14	32806.30	6.14	-0.05	-0.05	<b>0.95</b>	41.17	-0.35	-0.31	<b>0.87</b>

**Table Annex I.3:** the evolution of the coefficients of multilinear regression for the third CP/PARAFAC component for the irradiation experiment I111 ( river water filtered , sea water filtered , wwtp water filtered .(aug-sept 2015 experiment)

Coefficient C3 à I111	Voltage (Volts)	$A^{WW,EN}_0$	$A^{WW,EN}_2$ ( $f_{RW}$ )	$A^{WW,EN}_1$ ( $f_{SW}$ )	$r_{EN}^2$	$A^{WW,CR}_0$	$A^{WWTP,CR}_2$ ( $f_{RW}$ )	$A^{WW,CR}_1$ ( $f_{SW}$ )	$r_{CR}^2$
T0	0	112.35	-1.03	-1.08	<b>0.97</b>	101.65	-0.93	-0.98	<b>0.99</b>
T3	11140.81	85.79	-0.67	-0.69	<b>0.97</b>	21.98	-0.19	-0.20	<b>0.96</b>
T4	12470.48	66.59	-0.58	-0.58	<b>0.96</b>	22.02	-0.20	-0.20	<b>0.98</b>
T5	14821.40	61.21	-0.53	-0.55	<b>0.98</b>	20.40	-0.18	-0.19	<b>0.98</b>
T6	16363.55	58.16	-0.52	-0.50	<b>0.97</b>	18.97	-0.17	-0.17	<b>0.99</b>
T7	17521.88	78.87	-0.54	-0.55	<b>0.97</b>	17.99	-0.16	-0.16	<b>0.98</b>
T11	27011.24	30.94	-0.26	-0.29	<b>0.67</b>	10.35	-0.09	-0.10	<b>0.96</b>
T12	28944.07	75.03	-0.55	-0.53	<b>0.89</b>	11.68	-0.10	-0.10	<b>0.96</b>
T13	30410.83	50.22	-0.36	-0.37	<b>0.64</b>	10.14	-0.09	-0.08	<b>0.95</b>
T14	32806.30	41.63	-0.33	-0.30	<b>0.92</b>	9.78	-0.08	-0.08	<b>0.95</b>

**Table Annex I.4:** the evolution of the coefficients of multilinear regression for the first CP/PARAFAC component for the irradiation experiment I110( river water filtered , seawater filtered , wwtp water non-filtered . (November 10-20th 2015 experiment)

Coefficient C1 à I110	Voltage (Volts)	$A^{WW,EN}_0$	$A^{WW,EN}_2$ ( $f_{RW}$ )	$A^{WW,EN}_1$ ( $f_{SW}$ )	$r_{EN}^2$	$A^{WW,CR}_0$	$A^{WW,CR}_2$ ( $f_{RW}$ )	$A^{WW,CR}_1$ ( $f_{SW}$ )	$r_{CR}^2$
D0	1.7	68.91	-0.60	-0.66	0.99	65.53	-0.59	-0.64	0.99
D2_EXP	3295.15	3.84	-0.04	-0.04	0.83	24.79	-0.22	-0.22	0.97
D3_EXP	4704.05	27.89	-0.23	-0.28	0.98	27.75	-0.23	-0.26	0.98
D6_EXP	10211.45	15.47	-0.12	-0.14	0.99	12.52	-0.10	-0.11	0.99
D7_EXP	11961.6	9.75	-0.07	-0.09	0.95	14.25	-0.11	-0.13	0.98
D8_EXP	13725.15	12.28	-0.09	-0.13	0.97	10.38	-0.08	-0.10	0.98
D9_EXP	15569.15	10.12	-0.07	-0.08	0.98	8.28	-0.06	-0.07	0.99
D10_EXP	17221.55	11.19	-0.08	-0.11	0.99	11.28	-0.09	-0.10	0.99

**Table Annex I.5 :** the temporal evolution of the coefficients of multilinear regression for the first CP/PARAFAC component for the irradiation experiment I110( river water filtered , seawater filtered ,wwtp water non-filtered . (November 10-20th 2015 experiment) . The 1st CP/PARAFAC Component Regression parameters or the control samples (dark incubations) .

Coefficient C1 à I110	Voltage (Volts)	$A^{WW,EN}_0$	$A^{WW,EN}_2$ ( $f_{RW}$ )	$A^{WW,EN}_1$ ( $f_{SW}$ )	$r_{EN}^2$	$A^{WW,CR}_0$	$A^{WW,CR}_2$ ( $f_{RW}$ )	$A^{WW,CR}_1$ ( $f_{SW}$ )	$r_{CR}^2$
D0	1.7	68.91	-0.60	-0.66	0.99	65.53	-0.59	-0.64	0.99
D2_NEXP	3295.15	41.09	-0.39	-0.42	0.96	103.99	-0.97	-1.03	0.99
D3_NEXP	4704.05	109.84	-0.97	-1.03	0.97	106.02	-0.95	-1.06	0.98
D6_NEXP	10211.45	76.40	-0.66	-0.73	0.99	70.37	-0.63	-0.68	0.99
D7_NEXP	11961.6	81.75	-0.75	-0.78	0.98	83.36	-0.75	-0.80	0.99
D8_NEXP	13725.15	69.97	-0.58	-0.70	0.92	66.09	-0.57	-0.66	0.94
D9_NEXP	15569.15	64.94	-0.55	-0.64	0.99	64.22	-0.57	-0.67	0.99
D10_NEXP	17221.55	83.69	-0.71	-0.83	0.95	78.08	-0.68	-0.77	0.97

**Table Annex I.6:** the evolution of the coefficients of multilinear regression for the second CP/PARAFAC component for the irradiation experiment I110( river water filtered , seawater filtered , wwtp water non-filtered . (November 10-20th 2015 experiment)

<b>Coefficient C2 à I110</b>	<b>Voltage (Volts)</b>	$A^{WW,EN}_0$	$A^{WW,EN}_2(f_{RW})$	$A^{WW,EN}_1(f_{SW})$	$r_{EN}^2$	$A^{WW,CR}_0$	$A^{WW,CR}_2(f_{RW})$	$A^{WW,CR}_1(f_{SW})$	$r_{CR}^2$
D0	1.7	80.73	-0.68	-0.75	<b>0.98</b>	0.20	0.18	0.17	<b>0.57</b>
D2_EXP	3295.15	5.84	-0.05	-0.07	<b>0.93</b>	45.99	-0.45	-0.43	<b>0.93</b>
D3_EXP	4704.05	19.93	-0.15	-0.17	<b>0.98</b>	137.00	-1.04	-1.19	<b>0.98</b>
D6_EXP	10211.45	14.16	-0.10	-0.12	<b>0.98</b>	45.82	-0.28	-0.32	<b>0.96</b>
D7_EXP	11961.6	7.96	-0.05	-0.06	<b>0.92</b>	51.63	-0.40	-0.47	<b>0.97</b>
D8_EXP	13725.15	10.618	-0.07	-0.09	<b>0.96</b>	41.14	-0.24	-0.30	<b>0.98</b>
D9_EXP	15569.15	9.84	-0.06	-0.05	<b>0.96</b>	38.25	-0.21	-0.24	<b>0.94</b>
D10_EXP	17221.55	11.148	-0.07	-0.09	<b>0.97</b>	54.67	-0.34	-0.36	<b>0.96</b>

**Table Annex I.7:** the temporal evolution of the coefficients of multilinear regression for the second CP/PARAFAC component for the irradiation experiment I110( river water filtered , seawater filtered , wwtp water non-filtered . (November 10-20th 2015 experiment) . The 2nd CP/PARAFAC Component Regression parameters or the control samples (dark incubations) .

<b>Coefficient C2 à I110</b>	<b>Voltage (Volts)</b>	$A^{WW,EN}_0$	$A^{WW,EN}_2(f_{RW})$	$A^{WW,EN}_1(f_{SW})$	$r_{EN}^2$	$A^{WW,CR}_0$	$A^{WW,CR}_1(f_{SW})$	$A^{WW,CR}_2(f_{RW})$	$r_{CR}^2$
D0	1.7	80.73	-0.68	-0.75	<b>0.98</b>	0.20	0.18	0.17	<b>0.57</b>
D2_NEXP	3295.15	65.42	-0.61	-0.68	<b>0.97</b>	8.97	-0.10	-0.03	0.10
D3_NEXP	4704.05	106.83	-0.93	-1.02	<b>0.98</b>	18.31	0.32	0.77	0.31
D6_NEXP	10211.45	83.57	-0.72	-0.80	<b>0.98</b>	0.56	0.13	0.17	0.40
D7_NEXP	11961.6	90.14	-0.82	-0.87	<b>0.99</b>	3.027	0.15	0.298	0.40
D8_NEXP	13725.15	75.37	-0.62	-0.75	<b>0.911</b>	3.98	0.13	0.12	0.20
D9_NEXP	15569.15	76.25	-0.65	-0.75	<b>0.99</b>	0.93	0.20	0.29	<b>0.70</b>
D10_NEXP	17221.55	88.30	-0.74	-0.86	<b>0.96</b>	27.06	0.00	-0.05	0.05

**Table Annex I.8:** the evolution of the coefficients of multilinear regression for the third CP/PARAFAC component for the irradiation experiment I110( river water filtered , seawater filtered , wwtp water non-filtered . (November 10-20th 2015 experiment)

<b>Coefficient C3 à I110</b>	<b>Voltage (Volts)</b>	$A^{WW,EN}_0$	$A^{WW,EN}_2(f_{RW})$	$A^{WW,EN}_1(f_{SW})$	$r_{EN}^2$	$A^{WW,CR}_0$	$A^{WW,CR}_2(f_{RW})$	$A^{WW,CR}_1(f_{SW})$	$r_{CR}^2$
D0	1.7	43.76	0.13	0.15	0.34	73.57	-0.65	-0.72	<b>0.98</b>
D2_EXP	3295.15	6.73	-0.02	-0.08	0.12	45.99	-0.45	-0.43	<b>0.98</b>
D3_EXP	4704.05	110.36	-0.36	-0.39	<b>0.88</b>	24.46	-0.20	-0.23	<b>0.98</b>
D6_EXP	10211.45	57.59	-0.09	-0.21	<b>0.821</b>	14.01	-0.11	-0.13	<b>0.99</b>
D7_EXP	11961.6	23.02	0.025	0.00	0.04	13.93	-0.11	-0.13	<b>0.96</b>
D8_EXP	13725.15	53.12	-0.03	-0.24	<b>0.65</b>	10.64	-0.08	-0.10	<b>0.98</b>
D9_EXP	15569.15	57.77	-0.00	0.00	0.03	9.56	-0.08	-0.08	<b>0.97</b>
D10_EXP	17221.55	70.63	-0.11	-0.21	<b>0.70</b>	12.73	-0.11	-0.12	<b>0.99</b>

**Table Annex I.9** : the temporal evolution of the coefficients of multilinear regression for the third CP/PARAFAC component for the irradiation experiment I110( river water filtered , seawater filtered , wwtp water non-filtered . (November 10-20th 2015 experiment) The 3rd CP/PARAFAC Component Regression parameters or the control samples (dark incubations) .

<b>Coefficient C3 à I110</b>	<b>Voltage (Volts)</b>	$A^{WW,EN}_0$	$A^{WW,EN}_2$ (f <sub>rw</sub> )	$A^{WW,EN}_1$ (f <sub>sw</sub> )	$r_{EN}^2$	$A^{WW,CR}_0$	$A^{WW,CR}_2$ (f <sub>rw</sub> )	$A^{WW,CR}_1$ (f <sub>sw</sub> )	$r_{CR}^2$
D0	1.7	43.76	0.13	0.15	0.34	73.57	-0.65	-0.72	<b>0.98</b>
D2_NEXP	3295.15	-1.85	0.04	0.04	0.73	105.45	-0.98	-1.06	<b>0.99</b>
D3_NEXP	4704.05	82.08	0.06	-0.11	0.20	105.86	-0.95	-1.07	<b>0.98</b>
D6_NEXP	10211.45	31.71	0.12	0.13	0.73	76.40	-0.67	-0.75	<b>0.99</b>
D7_NEXP	11961.6	-2.92	0.36	0.10	0.66	91.03	-0.84	-0.90	<b>0.99</b>
D8_NEXP	13725.15	25.89	0.17	0.17	<b>0.85</b>	69.40	-0.59	-0.69	<b>0.92</b>
D9_NEXP	15569.15	49.61	0.07	0.04	0.35	71.66	-0.64	-0.75	<b>0.99</b>
D10_NEXP	17221.55	46.02	0.12	0.12	0.72	81.00	-0.69	-0.80	<b>0.96</b>

**Table Annex I.10** : the evolution of the coefficients of multilinear regression for the first CP/PARAFAC component for the irradiation experiment I101 ( river water filtered , seawater non-filtered , wwtp water filtered ” RIV F MER NF STEP F” ) . (Feb 15th -Mars 4th 2016 experiment)

<b>Coefficient C1 à I101</b>	<b>Voltage (Volts)</b>	$A^{WW,EN}_0$	$A^{WW,EN}_2$ (f <sub>rw</sub> )	$A^{WW,EN}_1$ (f <sub>sw</sub> )	$r_{EN}^2$	$A^{WW,CR}_0$	$A^{WW,CR}_2$ (f <sub>rw</sub> )	$A^{WW,CR}_1$ (f <sub>sw</sub> )	$r_{CR}^2$
D0	0	60.45	-0.52	-0.58	<b>0.97</b>	65.27	-0.57	-0.64	<b>0.94</b>
D1_EXP	486.95	39.24	-0.33	-0.42	<b>0.99</b>	39.42	-0.31	-0.37	<b>0.98</b>
D2_EXP	1034.15	27.69	-0.22	-0.26	<b>0.84</b>	33.21	-0.27	-0.31	<b>0.93</b>
D3_EXP	1520.9	31.67	-0.26	-0.40	<b>0.92</b>	32.25	-0.26	-0.36	<b>0.94</b>
D4_EXP	2089.1	15.02	-0.08	-0.15	0.69	20.20	-0.13	-0.19	<b>0.80</b>
D7_EXP	3600.15	19.86	-0.16	-0.19	<b>0.97</b>	21.25	-0.17	-0.20	<b>0.99</b>
D8_EXP	4285.85	9.59	-0.06	-0.07	<b>0.95</b>	15.31	-0.11	-0.13	<b>0.98</b>
D10_EXP	5499.2	6.73	-0.04	-0.05	<b>0.97</b>	12.35	-0.09	-0.11	<b>0.98</b>
D11_EXP	6111.35	11.80	-0.08	-0.11	<b>0.96</b>	14.73	-0.11	-0.13	<b>0.98</b>
D14_EXP	7246.55	8.32	-0.05	-0.07	<b>0.96</b>	12.71	-0.09	-0.11	<b>0.98</b>
D15_EXP	7894.95	10.39	-0.08	-0.12	<b>0.88</b>	12.95	-0.10	-0.15	<b>0.93</b>
D16_EXP	9618.75	8.24	-0.05	-0.06	<b>0.97</b>	11.51	-0.08	-0.09	<b>0.98</b>
D17_EXP	11688	7.95	-0.06	-0.08	<b>0.91</b>	12.25	-0.09	-0.11	<b>0.97</b>
D18_EXP	13283.85	9.73	-0.06	-0.08	<b>0.92</b>	11.60	-0.08	-0.09	<b>0.95</b>

**Table Annex I.11** : the evolution of the coefficients of multilinear regression for the first CP/PARAFAC component for the irradiation experiment I101 ( river water filtered , seawater non-filtered , wwtp water filtered ” RIV F MER NF STEP F” ) . (Feb 15th -Mars 4th 2016 experiment) for the non irradiated control samples. The 1st CP/PARAFAC Component Regression parameters or the control samples (dark incubations) .

Coefficient C1 à I101	Voltage (Volts)	$A^{WW,EN}_0$	$A^{WW,EN}_2(f_{RW})$	$A^{WW,EN}_1(f_{SW})$	$r_{EN}^2$	$A^{WW,CR}_0$	$A^{WW,CR}_2(f_{RW})$	$A^{WW,CR}_1(f_{SW})$	$r_{CR}^2$
D0	0	60.45	-0.52	-0.58	0.97	65.27	-0.57	-0.64	0.94
D1_NEXP	486.95	74.21	-0.62	-0.72	0.98	71.20	-0.59	-0.66	0.97
D2_NEXP	1034.15	97.36	-0.85	-1.08	0.97	87.93	-0.73	-0.91	0.97
D3_NEXP	1520.9	67.02	-0.49	-0.68	0.79	65.17	-0.48	-0.62	0.90
D4_NEXP	2089.1	88.39	-0.75	-1.13	0.92	83.83	-0.70	-0.98	0.92
D7_NEXP	3600.15	81.93	-0.65	-0.80	0.96	74.10	-0.59	-0.70	0.96
D8_NEXP	4285.85	58.38	-0.50	-0.56	0.98	79.43	-0.68	-0.77	0.96
D10_NEXP	5499.2	75.79	-0.69	-0.81	0.96	80.05	-0.69	-0.79	0.95
D11_NEXP	6111.35	74.83	-0.63	-0.72	0.99	73.10	-0.61	-0.68	0.97
D14_NEXP	7246.55	88.94	-0.79	-0.90	0.99	87.42	-0.74	-0.85	0.97
D15_NEXP	7894.95	63.12	-0.49	-0.64	0.78	62.91	-0.49	-0.60	0.86
D16_NEXP	9618.75	87.59	-0.77	-0.85	0.99	83.48	-0.70	-0.77	0.98
D17_NEXP	11688	84.44	-0.72	-0.83	0.98	80.67	-0.67	-0.75	0.97
D18_NEXP	13283.85	97.86	-0.87	-0.95	0.98	97.12	-0.84	-0.96	0.99

**Table Annex I.12** : the evolution of the coefficients of multilinear regression for the second CP/PARAFAC component for the irradiation experiment I101 ( river water filtered , seawater non-filtered , wwtp water filtered ” RIV F MER NF STEP F” ) . (Feb 15th -Mars 4th 2016 experiment)

Coefficient C2 à I101	Voltage (Volts)	$A^{WW,EN}_0$	$A^{WW,EN}_2(f_{RW})$	$A^{WW,EN}_1(f_{SW})$	$r_{EN}^2$	$A^{WW,CR}_0$	$A^{WW,CR}_2(f_{RW})$	$A^{WW,CR}_1(f_{SW})$	$r_{CR}^2$
D0	0	73.18	-0.63	-0.70	0.96	20.75	-0.08	-0.06	0.08
D1_EXP	486.95	37.36	-0.31	-0.40	0.98	61.67	-0.44	-0.53	0.97
D2_EXP	1034.15	22.34	-0.15	-0.17	0.84	80.85	-0.55	-0.59	0.92
D3_EXP	1520.9	29.13	-0.23	-0.33	0.90	80.34	-0.53	-0.77	0.93
D4_EXP	2089.1	16.66	-0.08	-0.12	0.68	59.94	-0.29	-0.39	0.72
D7_EXP	3600.15	20.872	-0.12	-0.16	0.98	71.17	-0.38	-0.48	0.98
D8_EXP	4285.85	12.16	-0.05	-0.07	0.97	52.12	-0.23	-0.29	0.97
D10_EXP	5499.2	7.83	-0.04	-0.05	0.87	29.58	-0.15	-0.18	0.94
D11_EXP	6111.35	13.17	-0.09	-0.10	0.97	41.92	-0.24	-0.28	0.95
D14_EXP	7246.55	9.37	-0.05	-0.06	0.94	37.14	-0.22	-0.24	0.97
D15_EXP	7894.95	11.55	-0.07	-0.11	0.90	37.67	-0.21	-0.33	0.90
D16_EXP	9618.75	8.96	-0.043	-0.04	0.88	39.57	-0.22	-0.20	0.88
D17_EXP	11688	9.53	-0.064	-0.081	0.90	37.81	-0.23	-0.26	0.9
D18_EXP	13283.85	11.20	-0.06	-0.06	0.94	43.31	-0.28	-0.227	0.80



**Table Annex I.13** : the evolution of the coefficients of multilinear regression for the second CP/PARAFAC component for the irradiation experiment I101 ( river water filtered , seawater non-filtered , wwtp water filtered ” RIV F MER NF STEP F” ) . (Feb 15th -Mars 4th 2016 experiment) for the non irradiated control samples. The 2nd CP/PARAFAC Component Regression parameters or the control samples (dark incubations) .

Coefficient C2 à I101	Voltage (Volts)	$A^{WW, EN}_0$	$A^{WW, EN}_2(f_{RW})$	$A^{WW, EN}_1(f_{SW})$	$r_{EN}^2$	$A^{WW, CR}_0$	$A^{WW, CR}_2(f_{RW})$	$A^{WW, CR}_1(f_{SW})$	$r_{CR}^2$
D0	0	73.18	-0.63	-0.70	<b>0.96</b>	20.75	-0.08	-0.06	0.085
D1_NEXP	486.95	74.18	-0.60	-0.71	<b>0.98</b>	78.44	-0.61	-0.66	<b>0.98</b>
D2_NEXP	1034.15	87.01	-0.74	-0.95	<b>0.97</b>	89.64	-0.52	-0.54	0.48
D3_NEXP	1520.9	59.00	-0.38	-0.58	<b>0.78</b>	113.77	-0.76	-0.96	0.82
D4_NEXP	2089.1	84.38	-0.69	-1.05	<b>0.91</b>	83.89	-0.40	-0.66	0.58
D7_NEXP	3600.15	78.55	-0.57	-0.72	<b>0.95</b>	125.42	-0.78	-0.97	<b>0.96</b>
D8_NEXP	4285.85	68.51	-0.57	-0.68	<b>0.97</b>	61.359	-0.23	-0.17	0.24
D10_NEXP	5499.2	79.30	-0.71	-0.84	<b>0.95</b>	51.22	-0.26	-0.28	0.42
D11_NEXP	6111.35	74.24	-0.59	-0.70	<b>0.98</b>	103.03	-0.76	-0.8	<b>0.97</b>
D14_NEXP	7246.55	91.06	-0.80	-0.94	<b>0.98</b>	54.85	-0.26	-0.21	0.26
D15_NEXP	7894.95	63.25	-0.48	-0.62	<b>0.77</b>	82.60	-0.56	-0.70	<b>0.79</b>
D16_NEXP	9618.75	88.98	-0.76	-0.88	<b>0.99</b>	61.92	-0.29	-0.19	0.274
D17_NEXP	11688	81.66	-0.68	-0.79	<b>0.98</b>	112.33	-0.89	-0.98	<b>0.97</b>
D18_NEXP	13283.85	100.28	-0.87	-0.97	<b>0.98</b>	54.51	-0.21	-0.08	0.15

**Table Annex I.14** : the evolution of the coefficients of multilinear regression for the third CP/PARAFAC component for the irradiation experiment I101 ( river water filtered , seawater non-filtered , wwtp water filtered ” RIV F MER NF STEP F” ) . (Feb 15th -Mars 4th 2016 experiment)

Coefficient C3 à I101	Voltage (Volts)	$A^{WW, EN}_0$	$A^{WW, EN}_2(f_{RW})$	$A^{WW, EN}_1(f_{SW})$	$r_{EN}^2$	$A^{WW, CR}_0$	$A^{WW, CR}_2(f_{RW})$	$A^{WW, CR}_1(f_{SW})$	$r_{CR}^2$
D0	0	32.40	-0.10	-0.05	0.14	68.52	-0.61	-0.68	<b>0.94</b>
D1_EXP	486.95	37.36	-0.10	-0.15	<b>0.79</b>	33.57	-0.28	-0.34	<b>0.99</b>
D2_EXP	1034.15	57.44	0.02	-0.02	0.07	23.98	-0.20	-0.22	<b>0.95</b>
D3_EXP	1520.9	67.57	-0.10	-0.32	0.47	26.63	-0.23	-0.30	<b>0.95</b>
D4_EXP	2089.1	67.73	0.05	-0.01	0.05	16.54	-0.12	-0.16	<b>0.8</b>
D7_EXP	3600.15	95.56	-0.06	-0.35	0.57	17.52	-0.14	-0.16	<b>0.98</b>
D8_EXP	4285.85	36.89	0.07	0.00	0.66	13.98	-0.10	-0.12	<b>0.96</b>
D10_EXP	5499.2	25.70	0.06	0.06	0.21	10.42	-0.08	-0.09	<b>0.96</b>
D11_EXP	6111.35	44.77	-0.06	-0.10	<b>0.72</b>	13.08	-0.11	-0.12	<b>0.98</b>
D14_EXP	7246.55	32.38	0.03	0.00	0.07	11.30	-0.09	-0.10	<b>0.97</b>
D15_EXP	7894.95	41.79	-0.01	-0.14	0.47	11.22	-0.09	-0.12	<b>0.96</b>
D16_EXP	9618.75	37.42	0.08	0.10	0.37	10.07	-0.08	-0.08	<b>0.96</b>
D17_EXP	11688	38.17	-0.00791	-0.16	0.42	10.73	-0.09	-0.09	<b>0.96</b>
D18_EXP	13283.85	48.08	-0.00	0.01	0.08	11.18	-0.10	-0.09	<b>0.95</b>

**Table Annex I.15** : the evolution of the coefficients of multilinear regression for the third CP/PARAFAC component for the irradiation experiment I101 ( river water filtered , seawater non-filtered , wwtp water filtered ” RIV F MER NF STEP F” ) . (Feb 15th -Mars 4th 2016 experiment) for the non irradiated control samples

The 3rd CP/PARAFAC Component Regression parameters of the control samples (dark incubations) .

<b>Coefficient C3 à I101</b>	<b>Voltage (Volts)</b>	$A^{WW,EN}_0$	$A^{WW,EN}_2$ (f <sub>RW</sub> )	$A^{WW,EN}_1$ (f <sub>SW</sub> )	$r_{EN}^2$	$A^{WW,CR}_0$	$A^{WW,CR}_2$ (f <sub>RW</sub> )	$A^{WW,CR}_1$ (f <sub>SW</sub> )	$r_{CR}^2$
D0	0	32.40	-0.10	-0.05	0.14	68.52	-0.61	-0.68	<b>0.94</b>
D1_NEXP	486.95	30.05	-0.02	-0.02	0.17	66.51	-0.55	-0.63	<b>0.98</b>
D2_NEXP	1034.15	82.81	-0.21	-0.46	<b>0.75</b>	76.35	-0.66	-0.81	<b>0.98</b>
D3_NEXP	1520.9	65.63	-0.01	-0.13	0.24	56.71	-0.42	-0.56	<b>0.87</b>
D4_NEXP	2089.1	91.46	-0.12	-0.50	0.60	78.55	-0.68	-0.95	<b>0.92</b>
D7_NEXP	3600.15	96.52	-0.05	-0.15	0.36	68.80	-0.54	-0.66	<b>0.96</b>
D8_NEXP	4285.85	40.77	-0.01	-0.10	0.36	79.12	-0.69	-0.81	<b>0.95</b>
D10_NEXP	5499.2	37.18	0.00	-0.17	0.39	78.66	-0.70	-0.82	<b>0.94</b>
D11_NEXP	6111.35	56.38	-0.11	-0.20	0.65	68.33	-0.57	-0.65	<b>0.98</b>
D14_NEXP	7246.55	46.90	-0.03	-0.28	0.55	86.18	-0.76	-0.90	<b>0.97</b>
D15_NEXP	7894.95	40.93	-0.00	-0.02	0.02	59.20	-0.48	-0.58	<b>0.85</b>
D16_NEXP	9618.75	59.83	-0.09	-0.30	<b>0.68</b>	82.41	-0.72	-0.83	<b>0.98</b>
D17_NEXP	11688	39.30	-0.03	-0.08	0.34	74.94	-0.64	-0.72	<b>0.99</b>
D18_NEXP	13283.85	70.22	-0.18	-0.28	<b>0.83</b>	96.28	-0.86	-0.99	<b>0.99</b>

**Table Annex I.16** : the evolution of the coefficients of multilinear regression for the first CP/PARAFAC component for the irradiation experiment I011 ( river water non-filtered , seawater filtered , wwtp water filtered ” RIV NF MER F STEP F” ) . (December 3rd -17th 2015 experiment)

<b>Coefficient C1 à I011</b>	<b>Voltage (Volts)</b>	$A^{WW,EN}_0$	$A^{WW,EN}_2$ (f <sub>RW</sub> )	$A^{WW,EN}_1$ (f <sub>SW</sub> )	$r_{EN}^2$	$A^{WW,CR}_0$	$A^{WW,CR}_2$ (f <sub>RW</sub> )	$A^{WW,CR}_1$ (f <sub>SW</sub> )	$r_{CR}^2$
D0	0	49.73	-0.40	-0.46	<b>0.98</b>	49.63	-0.42	-0.48	<b>0.98</b>
D1_EXP	752.9	49.90	-0.45	-0.54	<b>0.98</b>	48.23	-0.38	-0.40	<b>0.94</b>
D2_EXP	1514.1	38.36	-0.33	-0.40	<b>0.97</b>	45.80	-0.38	-0.45	<b>0.98</b>
D5_EXP	2565.05	29.98	-0.26	-0.30	<b>0.99</b>	30.63	-0.24	-0.31	<b>0.98</b>
D6_EXP	3317.65	20.96	-0.17	-0.20	<b>0.98</b>	25.58	-0.21	-0.24	<b>0.99</b>
D7_EXP	4036.45	19.10	-0.16	-0.19	<b>0.99</b>	21.84	-0.17	-0.20	<b>0.97</b>
D8_EXP	4800	17.16	-0.13	-0.16	<b>0.98</b>	22.80	-0.19	-0.21	<b>0.99</b>
D9_EXP	5539	18.28	-0.15	-0.18	<b>0.96</b>	35.49	-0.27	-0.32	<b>0.86</b>
D12_EXP	7029.95	23.77	-0.21	-0.23	<b>0.98</b>	27.59	-0.23	-0.26	<b>0.99</b>
D13_EXP	7678.65	21.78	-0.19	-0.21	<b>0.99</b>	22.62	-0.18	-0.20	<b>0.98</b>
D14_EXP	8400.05	20.06	-0.16	-0.20	<b>0.99</b>	22.04	-0.18	-0.21	<b>0.99</b>
D15_EXP	8984.85	20.36	-0.17	-0.20	<b>0.99</b>	21.31	-0.17	-0.20	<b>0.99</b>

**Table Annex I.17** : the evolution of the coefficients of multilinear regression for the first CP/PARAFAC component for the irradiation experiment I011 ( river water non-filtered , seawater filtered , wwtp water filtered ” RIV NF MER F STEP F” ) . (December 3rd -17th 2015 experiment) The 1st CP/PARAFAC Component Regression parameters or the control samples (dark incubations) .

<b>Coefficient C1 à I011</b>	<b>Voltage (Volts)</b>	$A^{WW,EN}_0$	$A^{WW,EN}_2(f_{RW})$	$A^{WW,EN}_1(f_{SW})$	$r_{EN}^2$	$A^{WW,CR}_0$	$A^{WW,CR}_2(f_{RW})$	$A^{WW,CR}_1(f_{SW})$	$r_{CR}^2$
D0	0	49.73	-0.40	-0.46	<b>0.98</b>	49.63	-0.42	-0.48	<b>0.98</b>
D1_NEXP	752.9	104.88	-0.99	-1.05	<b>0.99</b>	88.54	-0.77	-0.83	<b>0.98</b>
D2_NEXP	1514.1	101.28	-0.92	-1.00	<b>0.98</b>	93.50	-0.78	-0.88	<b>0.99</b>
D5_NEXP	2565.05	105.35	-0.97	-1.04	<b>0.99</b>	12.55	0	-0.10	<b>0.99</b>
D6_NEXP	3317.65	70.20	-0.66	-0.64	<b>0.97</b>	71.97	-0.64	-0.66	<b>0.98</b>
D7_NEXP	4036.45	71.25	-0.62	-0.70	<b>0.99</b>	67.27	-0.57	-0.64	<b>0.98</b>
D8_NEXP	4800	71.14	-0.62	-0.64	<b>0.98</b>	73.12	-0.61	-0.67	<b>0.99</b>
D9_NEXP	5539	87.44	-0.77	-0.86	<b>0.99</b>	115.41	-1.00	-1.10	<b>0.98</b>
D12_NEXP	7029.95	106.49	-0.94	-0.99	<b>0.98</b>	97.88	-0.83	-0.94	<b>0.99</b>
D13_NEXP	7678.65	103.54	-0.91	-1.02	<b>0.98</b>	83.40	-0.70	-0.78	<b>0.98</b>
D14_NEXP	8400.05	91.79	-0.79	-0.84	<b>0.98</b>	84.60	-0.71	-0.83	<b>0.99</b>
D15_NEXP	8984.85	99.67	-0.8	-0.98	<b>0.99</b>	82.32	-0.72	-0.77	<b>0.9</b>

**Table Annex I.18** : the evolution of the coefficients of multilinear regression for the second CP/PARAFAC component for the irradiation experiment I011 ( river water non-filtered , seawater filtered , wwtp water filtered ” RIV NF MER F STEP F” ) . (December 3rd -17th 2015 experiment)

<b>Coefficient C2 à I011</b>	<b>Voltage (Volts)</b>	$A^{WW,EN}_0$	$A^{WW,EN}_2(f_{RW})$	$A^{WW,EN}_1(f_{SW})$	$r_{EN}^2$	$A^{WW,CR}_0$	$A^{WW,CR}_2(f_{RW})$	$A^{WW,CR}_1(f_{SW})$	$r_{CR}^2$
D0	0	63.33	-0.48	-0.55	<b>0.98</b>	7.23	-0.00	-0.01	0.06
D1_EXP	752.9	43.72	-0.37	-0.41	<b>0.99</b>	30.81	-0.19	-0.26	<b>0.69</b>
D2_EXP	1514.1	35.38	-0.27	-0.33	<b>0.97</b>	42.95	-0.33	-0.38	<b>0.96</b>
D5_EXP	2565.05	27.80	-0.23	-0.25	<b>0.99</b>	23.00	-0.16	-0.20	0.97
D6_EXP	3317.65	19.95	-0.16	-0.17	<b>0.98</b>	17.47	-0.14	-0.14	<b>0.99</b>
D7_EXP	4036.45	18.98	-0.15	-0.18	<b>0.99</b>	13.67	-0.10	-0.09	<b>0.97</b>
D8_EXP	4800	17.5	-0.13	-0.15	<b>0.99</b>	16.13	-0.13	-0.13	<b>0.97</b>
D9_EXP	5539	17.75	-0.14	-0.16	<b>0.97</b>	61.20	-0.42	-0.35	0.52
D12_EXP	7029.95	21.00	-0.15	-0.16	<b>0.98</b>	30.86	-0.23	-0.23	<b>0.97</b>
D13_EXP	7678.65	20.87	-0.14	-0.16	<b>0.99</b>	24.17	-0.16	-0.13	<b>0.96</b>
D14_EXP	8400.05	18.60	-0.11	-0.13	<b>0.98</b>	25.21	-0.17	-0.18	<b>0.99</b>
D15_EXP	8984.85	23.41	-0.16	-0.18	<b>0.97</b>	26.10	-0.16	-0.16	<b>0.97</b>

**Table Annex I.19:** the evolution of the coefficients of multilinear regression for the second CP/PARAFAC component for the irradiation experiment I011 ( river water non-filtered , seawater filtered , wwtp water filtered ” RIV NF MER F STEP F” ) . (December 3rd -17th 2015 experiment) The 2nd CP/PARAFAC Component Regression parameters or the control samples (dark incubations) .

Coefficient C2 à I011	Voltage (Volts)	$A^{WW,EN}_0$	$A^{WW,EN}_2(f_{RW})$	$A^{WW,EN}_1(f_{SW})$	$r_{EN}^2$	$A^{WW,CR}_0$	$A^{WW,CR}_2(f_{RW})$	$A^{WW,CR}_1(f_{SW})$	$r_{CR}^2$
D0	0	63.33	-0.48	-0.55	<b>0.98</b>	7.23	-0.00	-0.01	0.06
D1_NEXP	752.9	87.89	-0.76	-0.85	<b>0.99</b>	51.98	-0.48	-0.44	<b>0.98</b>
D2_NEXP	1514.1	97.00	-0.81	-0.93	<b>0.99</b>	31.44	-0.19	-0.08	0.35
D5_NEXP	2565.05	100.94	-0.90	-0.98	<b>0.99</b>	5.18	0	-0.01	<b>0.99</b>
D6_NEXP	3317.65	76.63	-0.70	-0.71	<b>0.97</b>	9.10	-0.06	0.03	0.36
D7_NEXP	4036.45	76.63	-0.64	-0.74	<b>0.99</b>	20.36	-0.16	-0.17	<b>0.95</b>
D8_NEXP	4800	78.63	-0.66	-0.73	<b>0.99</b>	11.14	-0.06	0.02	0.25
D9_NEXP	5539	90.69	-0.77	-0.88	<b>0.99</b>	141.59	-1.15	-1.26	<b>0.88</b>
D12_NEXP	7029.95	101.74	-0.85	-0.98	<b>0.99</b>	26.82	-0.14	-0.02	0.27
D13_NEXP	7678.65	95.80	-0.76	-0.90	<b>0.99</b>	42.78	-0.33	-0.34	<b>0.94</b>
D14_NEXP	8400.05	91.56	-0.75	-0.83	<b>0.99</b>	25.76	-0.14	-0.05	0.38
D15_NEXP	8984.85	95.58	-0.74	-0.88	<b>0.99</b>	44.38	-0.36	-0.33	<b>0.93</b>

**Table Annex I.20:** the evolution of the coefficients of multilinear regression for the third CP/PARAFAC component for the irradiation experiment I011 ( river water non-filtered , seawater filtered , wwtp water filtered ” RIV NF MER F STEP F” ) . (December 3rd -17th 2015 experiment)

Coefficient C3 à I011	Voltage (Volts)	$A^{WW,EN}_0$	$A^{WW,EN}_2(f_{RW})$	$A^{WW,EN}_1(f_{SW})$	$r_{EN}^2$	$A^{WW,CR}_0$	$A^{WW,CR}_2(f_{RW})$	$A^{WW,CR}_1(f_{SW})$	$r_{CR}^2$
D0	0	49.57	-0.08	-0.02	0.33	52.26	-0.43	-0.50	<b>0.97</b>
D1_EXP	752.9	58.24	-0.10	-0.14	0.38	36.55	-0.30	-0.33	<b>0.97</b>
D2_EXP	1514.1	74.88	-0.33	-0.34	<b>0.95</b>	36.29	-0.30	-0.35	<b>0.97</b>
D5_EXP	2565.05	39.86	-0.13	-0.14	<b>0.99</b>	25.32	-0.21	-0.25	0.99
D6_EXP	3317.65	21.03	-0.05	0.00	0.20	21.64	-0.19	-0.20	<b>0.99</b>
D7_EXP	4036.45	23.74	-0.04	-0.10	0.54	18.56	-0.16	-0.16	<b>0.97</b>
D8_EXP	4800	31.49	-0.12	-0.12	<b>0.75</b>	18.93	-0.16	-0.17	<b>0.98</b>
D9_EXP	5539	19.32	-0.04	-0.04	0.18	28.35	-0.23	-0.23	<b>0.86</b>
D12_EXP	7029.95	60.88	-0.07	-0.11	0.49	21.88	-0.19	-0.20	<b>0.99</b>
D13_EXP	7678.65	65.34	-0.10	-0.22	<b>0.75</b>	18.95	-0.16	-0.16	<b>0.98</b>
D14_EXP	8400.05	59.52	-0.01	-0.01	0.01	18.57	-0.15	-0.17	<b>0.99</b>
D15_EXP	8984.85	92.29	-0.22	-0.31	0.53	19.69	-0.16	-0.18	<b>0.98</b>

**Table Annex I.21** : the evolution of the coefficients of multilinear regression for the third CP/PARAFAC component for the irradiation experiment I011 ( river water non-filtered , seawater filtered , wwtp water filtered ” RIV NF MER F STEP F” ) . (December 3rd -17th 2015 experiment) The 3rd CP/PARAFAC Component Regression parameters or the control samples (dark incubations) .

Coefficient C3 à I011	Voltage (Volts)	$A^{WW,EN}_0$	$A^{WW,EN}_2(f_{RW})$	$A^{WW,EN}_1(f_{SW})$	$r_{EN}^2$	$A^{WW,CR}_0$	$A^{WW,CR}_2(f_{RW})$	$A^{WW,CR}_1(f_{SW})$	$r_{CR}^2$
D0	0	49.57	-0.08	-0.02	0.33	52.26	-0.43	-0.50	<b>0.97</b>
D1_NEXP	752.9	71.52	-0.29	-0.25	<b>0.88</b>	75.73	-0.69	-0.73	<b>0.99</b>
D2_NEXP	1514.1	72.09	-0.25	-0.17	0.66	92.53	-0.79	-0.93	<b>0.99</b>
D5_NEXP	2565.05	45.29	-0.20	-0.21	<b>0.99</b>	10.53	0	-0.09	<b>0.99</b>
D6_NEXP	3317.65	22.09	-0.02	-0.06	0.25	72.50	-0.66	-0.70	<b>0.98</b>
D7_NEXP	4036.45	18.93	-0.00	0.00	0.00	67.13	-0.57	-0.65	<b>0.99</b>
D8_NEXP	4800	26.05	-0.05	-0.07	0.51	73.94	-0.64	-0.72	<b>0.99</b>
D9_NEXP	5539	19.28	-0.02	-0.03	0.19	123.83	-1.07	-1.21	<b>0.99</b>
D12_NEXP	7029.95	80.80	-0.27	-0.37	<b>0.89</b>	97.56	-0.86	-1.00	<b>0.99</b>
D13_NEXP	7678.65	76.42	-0.16	-0.20	0.71	82.88	-0.70	-0.80	<b>0.99</b>
D14_NEXP	8400.05	83.08	-0.24	-0.29	<b>0.87</b>	82.46	-0.70	-0.82	<b>0.99</b>
D15_NEXP	8984.85	93.64	-0.06	-0.18	0.65	81.50	-0.71	-0.78	<b>0.99</b>

**Table Annex I.22** : the evolution of the coefficients of multilinear regression for the first CP/PARAFAC component for the irradiation experiment I000 ( river water non-filtered , seawater filtered , wwtp water filtered ” RIV NF MER NF STEP NF” ) . (May 11th -27th 2016 experiment)

Coefficient C1 à I000	Voltage (Volts)	$A^{WW,EN}_0$	$A^{WW,EN}_2(f_{RW})$	$A^{WW,EN}_1(f_{SW})$	$r_{EN}^2$	$A^{WW,CR}_0$	$A^{WW,CR}_2(f_{RW})$	$A^{WW,CR}_1(f_{SW})$	$r_{CR}^2$
D0	0	100.13	-0.91	-0.97	<b>0.99</b>	101.66	-0.92	-0.99	<b>0.99</b>
D1_EXP	2311.15	21.03	-0.17	-0.19	<b>0.99</b>	19.99	-0.16	-0.19	<b>0.99</b>
D2_EXP	4060	16.81	-0.14	-0.16	<b>0.99</b>	16.47	-0.13	-0.15	<b>0.99</b>
D6_EXP	13534.8	8.08	-0.06	-0.07	<b>0.96</b>	8.01	-0.06	-0.07	<b>0.99</b>
D7_EXP	15961.15	7.36	-0.07	-0.07	<b>0.99</b>	7.25	-0.06	-0.06	<b>0.99</b>
D8_EXP	18580.4	6.03	-0.05	-0.04	<b>0.97</b>	6.16	-0.04	-0.05	<b>0.98</b>
D12_EXP	28400.1	4.88	-0.04	-0.04	<b>0.99</b>	4.95	-0.03	-0.04	<b>0.99</b>
D13_EXP	31048.8	3.56	-0.03	-0.03	<b>0.99</b>	3.97	-0.02	-0.03	<b>0.99</b>
D14_EXP	33491	5.30	-0.04	-0.04	<b>0.96</b>	4.58	-0.03	-0.03	<b>0.98</b>
D15_EXP	36000.35	3.64	-0.03	-0.04	<b>0.99</b>	3.75	-0.02	-0.03	0.97
D16_EXP	38469.2	4.21	-0.03	-0.03	<b>0.97</b>	3.91	-0.02	-0.03	<b>0.95</b>

**Table Annex I.23** : the evolution of the coefficients of multilinear regression for the first CP/PARAFAC component for the irradiation experiment I000 ( river water non-filtered , seawater filtered , wwtp water filtered ”RIV NF MER NF STEP NF” ) . (May 11th -27th 2016 experiment) . The 1st CP/PARAFAC Component Regression parameters or the control samples (dark incubations)

Coefficient C1 à I000	Voltage (Volts)	$A^{WW,EN}_0$	$A^{WW,EN}_2(f_{RW})$	$A^{WW,EN}_1(f_{SW})$	$r_{EN}^2$	$A^{WW,CR}_0$	$A^{WW,CR}_2(f_{RW})$	$A^{WW,CR}_1(f_{SW})$	$r_{CR}^2$
D0	0	100.13	-0.91	-0.97	<b>0.99</b>	101.66	-0.92	-0.99	<b>0.99</b>
D1_NEXP	2311.15	100.52	-0.89	-0.99	<b>0.99</b>	103.39	-0.92	-1.03	<b>0.99</b>
D2_NEXP	4060	97.29	-0.90	-0.92	<b>0.99</b>	99.53	-0.91	-0.96	<b>0.99</b>
D6_NEXP	13534.8	99.56	-0.89	-0.98	<b>0.99</b>	101.49	-0.90	-1.00	<b>0.99</b>
D7_NEXP	15961.15	94.71	-0.87	-0.89	<b>0.99</b>	96.83	-0.88	-0.93	<b>0.99</b>
D8_NEXP	18580.4	100.22	-0.90	-0.99	<b>0.99</b>	101.53	-0.90	-1.01	<b>0.99</b>
D12_NEXP	28400.1	92.26	-0.83	-0.92	<b>0.99</b>	95.00	-0.85	-0.95	<b>0.99</b>
D13_NEXP	31048.8	99.87	-0.92	-0.98	<b>0.99</b>	107.44	-0.99	-1.05	<b>0.99</b>
D14_NEXP	33491	99.76	-0.91	-0.93	<b>0.99</b>	100.15	-0.90	-0.96	<b>0.99</b>
D15_NEXP	36000.35	102.60	-0.95	-1.01	<b>0.99</b>	7.50	0	-0.05	0.99
D16_NEXP	38469.2	96.91	-0.90	-0.91	<b>0.99</b>	99.21	-0.92	-0.92	<b>0.98</b>

**Table Annex I.24** : the evolution of the coefficients of multilinear regression for the second CP/PARAFAC component for the irradiation experiment I000 ( river water non-filtered , seawater filtered , wwtp water filtered ”RIV NF MER NF STEP NF” ) . (May 11th -27th 2016 experiment)

Coefficient C2 à I000	Voltage (Volts)	$A^{WW,EN}_0$	$A^{WW,EN}_2(f_{RW})$	$A^{WW,EN}_1(f_{SW})$	$r_{EN}^2$	$A^{WW,CR}_0$	$A^{WW,CR}_2(f_{RW})$	$A^{WW,CR}_1(f_{SW})$	$r_{CR}^2$
D0	0	96.14	-0.89	-0.93	<b>0.99</b>	84.59	-0.58	-0.60	<b>0.83</b>
D1_EXP	2311.15	16.50	-0.14	-0.15	<b>0.98</b>	89.17	-0.65	-0.57	<b>0.97</b>
D2_EXP	4060	13.27	-0.10	-0.12	<b>0.99</b>	64.34	-0.51	-0.52	<b>0.99</b>
D6_EXP	13534.8	8.02	-0.07	-0.07	<b>0.98</b>	41.67	-0.34	-0.18	<b>0.97</b>
D7_EXP	15961.15	6.610	-0.05	-0.05	<b>0.99</b>	42.02	-0.36	-0.28	<b>0.90</b>
D8_EXP	18580.4	6.66	-0.05	-0.05	<b>0.97</b>	41.09	-0.33	-0.11	<b>0.90</b>
D12_EXP	28400.1	4.47	-0.03	-0.03	<b>0.99</b>	33.63	-0.24	-0.25	0.98
D13_EXP	31048.8	3.89	-0.03	-0.02	<b>0.98</b>	30.62	-0.22	-0.18	<b>0.98</b>
D14_EXP	33491	4.03	-0.03	-0.03	<b>0.88</b>	43.01	-0.33	-0.32	<b>0.91</b>
D15_EXP	36000.35	3.44	-0.02	-0.02	0.92	25.93	-0.16	-0.15	0.94
D16_EXP	38469.2	4.00	-0.02	-0.03	<b>0.88</b>	39.32	-0.29	-0.30	<b>0.8</b>

**Table Annex I.25** : the evolution of the coefficients of multilinear regression for the second CP/PARAFAC component for the irradiation experiment I000 ( river water non-filtered , seawater filtered , wwtp water filtered "RIV NF MER NF STEP NF" ) . (May 11th -27th 2016 experiment) . The 2nd CP/PARAFAC Component Regression parameters or the control samples (dark incubations) .

Coefficient C2 à I000	Voltage (Volts)	$A^{WW, EN}_0$	$A^{WW, EN}_2$ ( $f_{RW}$ )	$A^{WW, EN}_1$ ( $f_{SW}$ )	$r_{EN}^2$	$A^{WW, CR}_0$	$A^{WW, CR}_2$ ( $f_{RW}$ )	$A^{WW, CR}_1$ ( $f_{SW}$ )	$r_{CR}^2$
D0	0	96.14	-0.89	-0.93	<b>0.99</b>	84.59	-0.58	-0.60	<b>0.83</b>
D1_NEXP	2311.15	93.77	-0.83	-0.92	<b>0.99</b>	130.13	-0.97	-1.02	<b>0.96</b>
D2_NEXP	4060	96.45	-0.90	-0.93	<b>0.99</b>	59.61	-0.35	-0.31	<b>0.83</b>
D6_NEXP	13534.8	96.94	-0.86	-0.95	<b>0.99</b>	77.15	-0.56	-0.65	<b>0.95</b>
D7_NEXP	15961.15	93.33	-0.87	-0.89	<b>0.99</b>	58.30	-0.36	-0.30	<b>0.76</b>
D8_NEXP	18580.4	95.53	-0.85	-0.94	<b>0.99</b>	81.46	-0.59	-0.70	<b>0.96</b>
D12_NEXP	28400.1	91.04	-0.83	-0.89	<b>0.99</b>	48.19	-0.23	-0.46	0.89
D13_NEXP	31048.8	95.75	-0.88	-0.94	<b>0.99</b>	74.47	-0.52	-0.65	<b>0.99</b>
D14_NEXP	33491	94.08	-0.87	-0.91	<b>0.99</b>	84.35	-0.57	-0.52	<b>0.82</b>
D15_NEXP	36000.35	99.54	-0.92	-0.97	<b>0.99</b>	19.56	0	-0.10	<b>0.99</b>
D16_NEXP	38469.2	97.55	-0.92	-0.90	<b>0.98</b>	59.76	-0.39	-0.32	0.66

**Table Annex I.26** : the evolution of the coefficients of multilinear regression for the third CP/PARAFAC component for the irradiation experiment I000 ( river water non-filtered , seawater filtered , wwtp water filtered "RIV NF MER NF STEP NF" ) . (May 11th -27th 2016 experiment)

Coefficient C3 à I000	Voltage (Volts)	$A^{WW, EN}_0$	$A^{WW, EN}_2$ ( $f_{RW}$ )	$A^{WW, EN}_1$ ( $f_{SW}$ )	$r_{EN}^2$	$A^{WW, CR}_0$	$A^{WW, CR}_2$ ( $f_{RW}$ )	$A^{WW, CR}_1$ ( $f_{SW}$ )	$r_{CR}^2$
D0	0	83.32	-0.38	-0.38	<b>0.59</b>	98.58	-0.87	-0.94	<b>0.99</b>
D1_EXP	2311.15	97.36	-0.60	-0.63	<b>0.95</b>	25.61	-0.21	-0.21	<b>0.97</b>
D2_EXP	4060	112.03	-0.55	-0.59	<b>0.96</b>	21.32	-0.17	-0.19	<b>0.98</b>
D6_EXP	13534.8	87.10	-0.56	-0.09	<b>0.76</b>	13.07	-0.12	-0.11	<b>0.99</b>
D7_EXP	15961.15	89.20	-0.36	-0.30	<b>0.89</b>	10.87	-0.10	-0.09	<b>0.99</b>
D8_EXP	18580.4	92.56	-0.40	-0.18	<b>0.93</b>	11.16	-0.09	-0.08	<b>0.96</b>
D12_EXP	28400.1	76.07	-0.34	-0.36	<b>0.98</b>	8.30	-0.07	-0.07	<b>0.99</b>
D13_EXP	31048.8	77.79	-0.42	-0.13	0.81	6.52	-0.05	-0.05	<b>0.97</b>
D14_EXP	33491	60.69	-0.32	-0.32	<b>0.95</b>	7.71	-0.06	-0.06	<b>0.86</b>
D15_EXP	36000.35	71.74	-0.33	0.04	0.57	5.44	-0.04	-0.04	0.93
D16_EXP	38469.2	83.18	-0.35	-0.40	<b>0.84</b>	7.04	-0.05	-0.06	<b>0.84</b>

**Table Annex I.27** : the evolution of the coefficients of multilinear regression for the third CP/PARAFAC component for the irradiation experiment I000 ( river water non-filtered , seawater filtered , wwtp water filtered ”RIV NF MER NF STEP NF” ) . (May 11th -27th 2016 experiment) . The 3rd CP/PARAFAC Component Regression parameters or the control samples (dark incubations) .

Coefficient C3 à I000	Voltage (Volts)	$A^{WW, EN}_0$	$A^{WW, EN}_2 (f_{RW})$	$A^{WW, EN}_1 (f_{SW})$	$r_{EN}^2$	$A^{WW, CR}_0$	$A^{WW, CR}_2 (f_{RW})$	$A^{WW, CR}_1 (f_{SW})$	$r_{CR}^2$
D0	0	83.32	-0.38	-0.38	<b>0.59</b>	98.58	-0.87	-0.94	<b>0.99</b>
D1_NEXP	2311.15	95.09	-0.53	-0.59	<b>0.92</b>	99.40	-0.85	-0.97	<b>0.99</b>
D2_NEXP	4060	85.65	-0.24	-0.08	0.51	96.68	-0.86	-0.92	<b>0.99</b>
D6_NEXP	13534.8	112.972	-0.528	-0.665	<b>0.76</b>	100.74	-0.87	-0.99	<b>0.99</b>
D7_NEXP	15961.15	89.45	-0.19	-0.17	0.55	93.54	-0.84	-0.89	<b>0.99</b>
D8_NEXP	18580.4	110.94	-0.39	-0.51	<b>0.93</b>	99.68	-0.85	-0.98	<b>0.99</b>
D12_NEXP	28400.1	64.29	-0.05	-0.26	0.33	91.12	-0.80	-0.91	<b>0.99</b>
D13_NEXP	31048.8	91.71	-0.22	-0.47	0.96	105.21	-0.95	-1.03	<b>0.99</b>
D14_NEXP	33491	92.98	-0.34	-0.51	<b>0.70</b>	95.50	-0.85	-0.91	<b>0.99</b>
D15_NEXP	36000.35	99.28	-0.29	-0.51	0.93	9.23	0	-0.07	<b>0.99</b>
D16_NEXP	38469.2	83.51	-0.33	-0.06	0.39	101.07	-0.94	-0.89	<b>0.96</b>



## ANNEX II

### $f_{ww}$ and $f_{sw}$ Permutation

**Table Annex II.1 :** the evolution of the coefficients of multilinear regression for the first CP/PARAFAC component for the irradiation experiment I111 ( river water filtered , sea water filtered , wwtp water filtered .(aug-sept 2015 experiment)

Coefficient C1 à I111	Voltage (Volts)	$A^{RW, EN}_0$	$A^{RW, EN}_1(f_w)$	$A^{RW, EN}_2(f_{ww})$	$r_{EN}^2$	$A^{RW, CR}_0$	$A^{RW, CR}_1(f_{sw})$	$A^{RW, CR}_2(f_{ww})$	$r_{CR}^2$
T0	0	7.03	-0.06	0.93	0.99	6.86	-0.06	0.93	0.99
T3	11140.81	0.33	-0.01	0.11	0.99	0.55	-0.01	0.09	0.99
T4	12470.48	0.76	-0.01	0.11	0.99	0.71	-0.01	0.08	0.99
T5	14821.40	0.64	-0.00	0.09	0.99	0.51	-0.00	0.06	0.99
T6	16363.55	0.29	0.00	0.08	0.97	0.30	-0.00	0.05	0.99
T7	17521.88	-0.23	0.00	0.06	0.98	0.06	-0.00	0.05	0.99
T11	27011.24	0.16	-0.01	0.05	0.79	0.14	-0.00	0.03	0.78
T12	28944.07	0.09	-0.00	0.02	0.55	-0.06	-0.00	0.02	0.80
T13	30410.83	0.07	0.00	0.03942	0.89	0.01	-0.00	0.03	0.93
T14	32806.30	0.08	0.00	0.043048	0.97	-0.10	-0.00	0.02	0.85

**Table Annex II.2 :** the evolution of the coefficients of multilinear regression for the second CP/PARAFAC component for the irradiation experiment I111 ( river water filtered , sea water filtered , wwtp water filtered .(aug-sept 2015 experiment)

Coefficient C2 à I111	Voltage (Volts)	$A^{RW, EN}_0$	$A^{RW, EN}_1(f_{sw})$	$A^{RW, EN}_2(f_{ww})$	$r_{EN}^2$	$A^{RW, CR}_0$	$A^{RW, CR}_1(f_{sw})$	$A^{RW, CR}_2(f_{ww})$	$r_{CR}^2$
T0	0	5.63	-0.04	0.93	0.99	16.87	-0.09	0.94	0.97
T3	11140.81	1.80	-0.01	0.15	0.97	9.47	-0.00	0.54	0.95
T4	12470.48	0.92	0.00	0.15	0.98	6.28	0.01	0.49	0.97
T5	14821.40	1.04	-0.01	0.13	0.99	6.03	-0.00	0.46	0.97
T6	16363.55	0.59	0.00	0.12	0.98	5.07	0.02	0.46	0.96
T7	17521.88	1.25	-0.00	0.12	0.98	8.13	0.00	0.43	0.96
T11	27011.24	0.49	-0.01	0.06	0.95	6.21	-0.03	0.29	0.92
T12	28944.07	0.69	-0.00	0.08	0.97	8.43	0.02	0.42	0.91
T13	30410.83	0.70	-0.00	0.06	0.94	6.37	0.02	0.33	0.89
T14	32806.30	0.64	0.00	0.06	0.96	6.13	0.04	0.35	0.87

**Table Annex II.3 :** the evolution of the coefficients of multilinear regression for the third CP/PARAFAC component for the irradiation experiment I111 ( river water filtered , sea water filtered ,wwtp water filtered .(aug-sept 2015 experiment)

Coefficient C3 à I111	Voltage (Volts)	$A^{RW,EN}_0$	$A^{RW,EN}_1(f_s)$	$A^{RW,EN}_2(f_{ww})$	$r_{EN}^2$	$A^{RW,CR}_0$	$A^{RW,CR}_1(f_{sw})$	$A^{RW,CR}_2(f_{ww})$	$r_{CR}^2$
T0	0	9.36	-0.05	1.03	0.97	7.91	-0.05	0.94	0.99
T3	11140.81	18.75	-0.02	0.67	0.97	2.37	-0.01	0.20	0.97
T4	12470.48	7.76	0.007	0.59	0.96	1.37	0.00	0.21	0.98
T5	14821.40	7.39	-0.01	0.54	0.98	1.53	-0.01	0.19	0.99
T6	16363.55	5.49	0.02	0.53	0.97	1.10	0.00	0.18	0.99
T7	17521.88	24.07	-0.01	0.55	0.97	1.59	-0.01	0.16	0.99
T11	27011.24	4.91	-0.034	0.26	0.68	1.07	-0.01	0.09	0.97
T12	28944.07	19.74	0.02	0.55	0.90	1.19	-0.00	0.10	0.96
T13	30410.83	13.44	-0.01	0.37	0.65	1.05	0.00	0.09	0.96
T14	32806.30	8.54	0.03	0.33	0.92	0.92	0.00	0.09	0.95

**Table Annex II.4 :** the evolution of the coefficients of multilinear regression for the first CP/PARAFAC component for the irradiation experiment I110( river water filtered , seawater filtered , wwtp water non-filtered . (November 10-20th 2015 experiment)

Coefficient C1 à I110	Voltage (Volts)	$A^{RW,EN}_0$	$A^{RW,EN}_1(f_s)$	$A^{RW,EN}_2(f_{ww})$	$r_{EN}^2$	$A^{RW,CR}_0$	$A^{RW,CR}_1(f_{sw})$	$A^{RW,CR}_2(f_{ww})$	$r_{CR}^2$
D0	1.7	8.81	-0.06	0.60	0.99	6.10	-0.05	0.59	0.99
D2_EXP	3295.15	-0.18	-0.01	0.04	0.83	2.37	-0.00	0.22	0.97
D3_EXP	4704.05	4.16	-0.04	0.24	0.99	4.51	-0.03	0.23	0.99
D6_EXP	10211.45	3.23	-0.02	0.12	0.99	2.26	-0.01	0.10	0.99
D7_EXP	11961.6	2.13	-0.02	0.08	0.95	2.47	-0.02	0.12	0.98
D8_EXP	13725.15	2.69	-0.04	0.09	0.97	2.06	-0.02	0.08	0.98
D9_EXP	15569.15	2.64	-0.01	0.07	0.99	1.49	-0.01	0.07	0.99
D10_EXP	17221.55	2.25	-0.03	0.09	0.99	2.23	-0.02	0.09	0.99

**Table Annex II.5 :** the temporal evolution of the coefficients of multilinear regression for the first CP/PARAFAC component for the irradiation experiment I110( river water filtered , seawater filtered ,wwtp water non-filtered . (November 10-20th 2015 experiment) . The 1st CP/PARAFAC Component Regression parameters or the control samples (dark incubations) .

<b>Coefficient C1 à I110</b>	<b>Voltage (Volts)</b>	$A^{RW,EN}_0$	$A^{RW,EN}_1(f_{sw})$	$A^{RW,EN}_2(f_{ww})$	$r_{EN}^2$	$A^{RW,CR}_0$	$A^{RW,CR}_1(f_{sw})$	$A^{RW,CR}_2(f_{ww})$	$r_{CR}^2$
D0	1.7	8.81	-0.06	0.60	0.99	6.10	-0.05	0.59	0.99
D2_NEXP	3295.15	1.40	-0.03	0.39	0.96	6.40	-0.06	0.98	0.99
D3_NEXP	4704.05	12.48	-0.07	0.97	0.97	10.97	-0.12	0.95	0.99
D6_NEXP	10211.45	9.68	-0.07	0.67	0.99	7.18	-0.06	0.63	0.99
D7_NEXP	11961.6	6.10	-0.03	0.76	0.99	7.73	-0.05	0.76	0.99
D8_NEXP	13725.15	11.59	-0.12	0.58	0.92	8.48	-0.09	0.58	0.94
D9_NEXP	15569.15	9.53	-0.09	0.55	0.99	6.75	-0.10	0.57	0.99
D10_NEXP	17221.55	12.28	-0.12	0.71	0.96	9.82	-0.09	0.68	0.97

**Table Annex II.6 :** the evolution of the coefficients of multilinear regression for the second CP/PARAFAC component for the irradiation experiment I110( river water filtered , seawater filtered , wwtp water non-filtered . (November 10-20th 2015 experiment)

<b>Coefficient C2 à I110</b>	<b>Voltage (Volts)</b>	$A^{RW,EN}_0$	$A^{RW,EN}_1(f_{sw})$	$A^{RW,EN}_2(f_{ww})$	$r_{EN}^2$	$A^{RW,CR}_0$	$A^{RW,CR}_1(f_{sw})$	$A^{RW,CR}_2(f_{ww})$	$r_{CR}^2$
D0	1.7	11.73	-0.07	0.69	0.99	18.85	-0.02	-0.19	0.58
D2_EXP	3295.15	-0.02	-0.02	0.06	0.94	0.57	0.02	0.4	0.94
D3_EXP	4704.05	4.63	-0.02	0.15	0.99	32.10	-0.15	1.05	0.98
D6_EXP	10211.45	3.80	-0.02	0.10	0.98	17.01	-0.04	0.29	0.96
D7_EXP	11961.6	2.33	-0.01	0.06	0.92	10.99	-0.06	0.41	0.98
D8_EXP	13725.15	3.42	-0.03	0.07	0.96	16.27	-0.06	0.25	0.98
D9_EXP	15569.15	3.761	0.00	0.06	0.97	16.79	-0.027	0.21	0.95
D10_EXP	17221.55	3.24	-0.01	0.08	0.97	20.08	-0.02	0.35	0.97

**Table Annex II.7 :** the temporal evolution of the coefficients of multilinear regression for the second CP/PARAFAC component for the irradiation experiment I110( river water filtered , seawater filtered , wwtp water non-filtered . (November 10-20th 2015 experiment) . The 2nd CP/PARAFAC Component Regression parameters or the control samples (dark incubations) .

<b>Coefficient C2 à I110</b>	<b>Voltage (Volts)</b>	$A^{RW,EN}_0$	$A^{RW,EN}_1(f_{sw})$	$A^{RW,EN}_2(f_{ww})$	$r_{EN}^2$	$A^{RW,CR}_0$	$A^{RW,CR}_1(f_{sw})$	$A^{RW,CR}_2(f_{ww})$	$r_{CR}^2$
D0	1.7	11.73	-0.07	0.69	0.99	18.85	-0.02	-0.19	0.58
D2_NEXP	3295.15	4.05	-0.07	0.61	0.98	-1.33	0.07	0.10	0.10
D3_NEXP	4704.05	12.93	-0.08	0.94	0.98	50.49	0.45	-0.32	0.31
D6_NEXP	10211.45	11.44	-0.08	0.72	0.99	13.99	0.04	-0.13	0.40
D7_NEXP	11961.6	7.71	-0.05	0.82	0.99	18.99	0.14	-0.16	0.41
D8_NEXP	13725.15	12.84	-0.135	0.63	0.91	17.48	-0.01	-0.13	0.20
D9_NEXP	15569.15	10.62	-0.10	0.66	0.99	21.14	0.09	-0.20	0.71
D10_NEXP	17221.55	14.03	-0.12	0.74	0.96	27.73	-0.06	-0.01	0.06

**Table Annex II.8 :** the evolution of the coefficients of multilinear regression for the third CP/PARAFAC component for the irradiation experiment I110( river water filtered , seawater filtered , tww/wwtp water non-filtered . (November 10-20th 2015 experiment)

Coefficient C3 à I110	Voltage (Volts)	$A^{RW,EN}_0$	$A^{RW,EN}_1(f_{sw})$	$A^{RW,EN}_2(f_{ww})$	$r_{EN}^2$	$A^{RW,CR}_0$	$A^{RW,CR}_1(f_{sw})$	$A^{RW,CR}_2(f_{ww})$	$r_{CR}^2$
D0	1.7	57.07	0.024	-0.13	0.35	7.84	-0.07	0.66	0.99
D2_EXP	3295.15	4.19	-0.06	0.03	0.13	1.07	-0.00	0.19	0.98
D3_EXP	4704.05	74.09	-0.03	0.36	0.89	3.61	-0.03	0.21	0.99
D6_EXP	10211.45	47.98	-0.12	0.096	0.82	2.13	-0.01	0.12	0.99
D7_EXP	11961.6	25.60	-0.02	-0.03	0.04	2.03	-0.02	0.12	0.97
D8_EXP	13725.15	49.97	-0.21	0.03	0.65	1.74	-0.02	0.09	0.99
D9_EXP	15569.15	57.27	0.01	0.01	0.04	1.22	0.00	0.08	0.97
D10_EXP	17221.55	58.81	-0.10	0.12	0.70	1.41	-0.01	0.11	0.99

**Table Annex II.9 :** the temporal evolution of the coefficients of multilinear regression for the third CP/PARAFAC component for the irradiation experiment I110( river water filtered , seawater filtered , wwtp water non-filtered . (November 10-20th 2015 experiment) The 3rd CP/PARAFAC Component Regression parameters or the control samples (dark incubations) .

Coefficient C3 à I110	Voltage (Volts)	$A^{RW,EN}_0$	$A^{RW,EN}_1(f_{sw})$	$A^{RW,EN}_2(f_{ww})$	$r_{EN}^2$	$A^{RW,CR}_0$	$A^{RW,CR}_1(f_{sw})$	$A^{RW,CR}_2(f_{ww})$	$r_{CR}^2$
D0	1.7	57.07	0.02	-0.13	0.35	7.84	-0.07	0.66	0.98
D2_NEXP	3295.15	2.58	-0.00	-0.04	0.74	6.91	-0.08	0.99	0.99
D3_NEXP	4704.05	89.05	-0.18	-0.07	0.00	10.33	-0.12	0.96	0.98
D6_NEXP	10211.45	44.28	0.01	-0.13	0.73	8.93	-0.08	0.67	0.99
D7_NEXP	11961.6	33.27	-0.26	-0.36	0.67	6.59	-0.06	0.84	0.99
D8_NEXP	13725.15	43.45	2.8E-05	-0.18	<b>0.85</b>	10.05	-0.10	0.59	0.93
D9_NEXP	15569.15	57.02	-0.03	-0.07	0.35	7.32	-0.11	0.64	0.99
D10_NEXP	17221.55	58.92	-0.01	-0.13	0.72	11.05	-0.10	0.70	0.96

**Table Annex II.10** : the evolution of the coefficients of multilinear regression for the first CP/PARAFAC component for the irradiation experiment I101 ( river water filtered , seawater non-filtered , tww/wwtp water filtered ” RIV F MER NF STEP F” ) . (Feb 15th -Mars 4th 2016 experiment)

Coefficient C1 à I101	Voltage (Volts)	$A^{RW,EN}_0$	$A^{RW,EN}_1(f_{sw})$	$A^{RW,EN}_2(f_{ww})$	$r_{EN}^2$	$A^{RW,CR}_0$	$A^{RW,CR}_1(f_{sw})$	$A^{RW,CR}_2(f_{ww})$	$r_{CR}^2$
D0	0	7.52	-0.06	0.53	0.97	7.69	-0.07	0.58	0.95
D1_EXP	486.95	5.93	-0.10	0.33	0.99	7.76	-0.06	0.32	0.99
D2_EXP	1034.15	5.52	-0.04	0.22	0.84	5.98	-0.04	0.27	0.93
D3_EXP	1520.9	4.85	-0.13	0.27	0.93	5.88	-0.11	0.26	0.95
D4_EXP	2089.1	6.60	-0.06653	0.08	0.70	6.32	-0.06	0.14	0.80
D7_EXP	3600.15	3.46	-0.03205	0.16	0.98	4.16	-0.03	0.17	0.99
D8_EXP	4285.85	3.54	-0.01041	0.06	0.96	3.45	-0.02	0.12	0.98
D10_EXP	5499.2	2.353	-0.01392	0.04	0.97	2.9	-0.02	0.09	0.98
D11_EXP	6111.35	2.82	-0.02883	0.09	0.97	2.99	-0.02	0.12	0.99
D14_EXP	7246.55	2.41	-0.01157	0.06	0.97	3.08	-0.02	0.10	0.99
D15_EXP	7894.95	2.08	-0.04249	0.08	0.88	2.67	-0.05	0.10	0.94
D16_EXP	9618.75	2.99	-0.0174	0.05	0.97	2.95	-0.01	0.09	0.98
D17_EXP	11688	1.42	-0.01938	0.07	0.91	2.62	-0.02	0.10	0.98
D18_EXP	13283.85	2.91	-0.01531	0.07	0.92	2.66	-0.01	0.09	0.96

**Table Annex II.11** : the evolution of the coefficients of multilinear regression for the first CP/PARAFAC component for the irradiation experiment I101 ( river water filtered , seawater non-filtered , wwtp water filtered ” RIV F MER NF STEP F” ) . (Feb 15th -Mars 4th 2016 experiment) for the non irradiated control samples. The 1st CP/PARAFAC Component Regression parameters or the control samples (dark incubations) .

Coefficient C1 à I101	Voltage (Volts)	$A^{RW,EN}_0$	$A^{RW,EN}_1(f_s)$	$A^{RW,EN}_2(f_{ww})$	$r_{EN}^2$	$A^{RW,CR}_0$	$A^{RW,CR}_1(f_{sw})$	$A^{RW,CR}_2(f_{ww})$	$r_{CR}^2$
D0	0	7.52	-0.06	0.53	0.97	7.69	-0.07	0.57	0.95
D1_NEXP	486.95	11.42	-0.09	0.63	0.98	11.82	-0.08	0.59	0.97
D2_NEXP	1034.15	11.80	-0.23	0.86	0.97	14.15	-0.18	0.74	0.97
D3_NEXP	1520.9	17.56	-0.19	0.49	0.79	16.53	-0.14	0.49	0.90
D4_NEXP	2089.1	12.77	-0.38	0.76	0.93	13.03	-0.28	0.71	0.93
D7_NEXP	3600.15	16.64	-0.15	0.65	0.96	14.90	-0.11	0.59	0.97
D8_NEXP	4285.85	7.81	-0.06	0.51	0.98	10.72	-0.09	0.69	0.96
D10_NEXP	5499.2	6.28	-0.12	0.70	0.97	10.52	-0.10	0.70	0.96
D11_NEXP	6111.35	10.92	-0.09	0.64	0.99	11.98	-0.08	0.61	0.97
D14_NEXP	7246.55	9.23	-0.11	0.80	0.99	12.69	-0.11	0.75	0.98
D15_NEXP	7894.95	13.31	-0.15	0.50	0.79	13.02	-0.10	0.50	0.87
D16_NEXP	9618.75	10.45	-0.09	0.77	0.99	12.70	-0.07	0.71	0.98
D17_NEXP	11688	11.55	-0.11	0.73	0.99	13.06	-0.08	0.68	0.98
D18_NEXP	13283.85	10.70	-0.08	0.87	0.99	12.58	-0.12	0.85	0.99

**Table Annex II.12** : the evolution of the coefficients of multilinear regression for the second CP/PARAFAC component for the irradiation experiment I101 ( river water filtered , seawater non-filtered , tww/wwtp water filtered ” RIV F MER NF STEP F” ) . (Feb 15th -Mars 4th 2016 experiment)

<b>Coefficient C2 à I101</b>	<b>Voltage (Volts)</b>	$A^{RW, EN}_0$	$A^{RW, EN}_1(f_s)$	$A^{RW, EN}_2(f_{ww})$	$r_{EN}^2$	$A^{RW, CR}_0$	$A^{RW, CR}_1(f_{sw})$	$A^{RW, CR}_2(f_{ww})$	$r_{CR}^2$
D0	0	9.40	-0.07	0.64	0.96	12.41	0.02	0.08	0.09
D1_EXP	486.95	5.74	-0.09	0.32	0.99	17.25	-0.09	0.44	0.97
D2_EXP	1034.15	6.81	-0.02	0.16	0.85	25.31	-0.04	0.56	0.93
D3_EXP	1520.9	5.94	-0.10	0.23	0.91	26.63	-0.24	0.54	0.93
D4_EXP	2089.1	8.45	-0.04	0.08	0.68	30.50	-0.10	0.29	0.72
D7_EXP	3600.15	8.55	-0.04	0.12	0.98	32.99	-0.10	0.38	0.98
D8_EXP	4285.85	6.42	-0.02	0.06	0.97	28.21	-0.06	0.24	0.97
D10_EXP	5499.2	3.77	-0.01	0.04	0.87	14.02	-0.03	0.16	0.95
D11_EXP	6111.35	4.04	-0.02	0.09	0.97	17.52	-0.04	0.24	0.96
D14_EXP	7246.55	3.98	-0.01	0.05	0.95	14.73	-0.02	0.22	0.98
D15_EXP	7894.95	3.75	-0.04	0.08	0.91	16.03	-0.11	0.22	0.90
D16_EXP	9618.75	4.67	-0.00	0.04	0.89	16.73	0.02	0.23	0.89
D17_EXP	11688	3.07	-0.02	0.065	0.91	13.93	-0.03	0.24	0.97
D18_EXP	13283.85	4.22	0.00	0.07	0.95	15.25	0.05	0.28	0.81

**Table Annex II.13** : the evolution of the coefficients of multilinear regression for the second CP/PARAFAC component for the irradiation experiment I101 ( river water filtered , seawater non-filtered , wwtp water filtered ” RIV F MER NF STEP F” ) . (Feb 15th -Mars 4th 2016 experiment) for the non irradiated control samples. The 2nd CP/PARAFAC Component Regression parameters of the control samples (dark incubations) .

<b>Coefficient C2 à I101</b>	<b>Voltage (Volts)</b>	$A^{RW, EN}_0$	$A^{RW, EN}_1(f_{sw})$	$A^{RW, EN}_2(f_{ww})$	$r_{EN}^2$	$A^{RW, CR}_0$	$A^{RW, CR}_1(f_{sw})$	$A^{RW, CR}_2(f_{ww})$	$r_{CR}^2$
D0	0	9.40	-0.07	0.64	0.96	12.41	0.02	0.08	0.09
D1_NEXP	486.95	13.60	-0.11	0.61	0.98	16.88	-0.05	0.62	0.98
D2_NEXP	1034.15	12.50	-0.21	0.75	0.97	37.15	-0.02	0.52	0.48
D3_NEXP	1520.9	20.27	-0.19	0.39	0.79	36.79	-0.19	0.77	0.83
D4_NEXP	2089.1	15.17	-0.36	0.69	0.91	43.73	-0.26	0.40	0.58
D7_NEXP	3600.15	21.22	-0.15	0.57	0.95	47.28	-0.20	0.78	0.96
D8_NEXP	4285.85	10.56	-0.10	0.58	0.97	37.87	0.06	0.23	0.24
D10_NEXP	5499.2	8.17	-0.14	0.71	0.96	24.53	-0.01	0.27	0.42
D11_NEXP	6111.35	14.36	-0.11	0.60	0.98	26.40	-0.12	0.77	0.98
D14_NEXP	7246.55	10.98	-0.14	0.80	0.99	28.68	0.05	0.26	0.26
D15_NEXP	7894.95	14.83	-0.14	0.48	0.77	25.63	-0.13	0.57	0.80
D16_NEXP	9618.75	12.78	-0.12	0.76	0.99	32.10	0.10	0.30	0.27
D17_NEXP	11688	13.38	-0.11	0.68	0.99	22.90	-0.09	0.89	0.97
D18_NEXP	13283.85	12.61	-0.10	0.88	0.99	33.39	0.13	0.21	0.16

**Table Annex II.14** : the evolution of the coefficients of multilinear regression for the third CP/PARAFAC component for the irradiation experiment I101 ( river water filtered , seawater non-filtered ,wwtp water filtered ” RIV F MER NF STEP F” ) . (Feb 15th -Mars 4th 2016 experiment)

Coefficient C3 à I101	Voltage (Volts)	$A^{RW, EN}_0$	$A^{RW, EN}_1(f_s)$	$A^{RW, EN}_2(f_{ww})$	$r_{EN}^2$	$A^{RW, CR}_0$	$A^{RW, CR}_1(f_{sw})$	$A^{RW, CR}_2(f_{ww})$	$r_{CR}^2$
D0	0	21.51	0.05	0.11	0.14	7.12	-0.07	0.61	0.95
D1_EXP	486.95	27.12	-0.05	0.10	0.79	5.20	-0.06	0.28	0.99
D2_EXP	1034.15	59.77	-0.05	-0.02	0.07	3.23	-0.01	0.21	0.95
D3_EXP	1520.9	56.80	-0.22	0.11	0.47	3.43	-0.07	0.23	0.95
D4_EXP	2089.1	73.54	-0.07	-0.06	0.05	4.35	-0.04	0.12	0.83
D7_EXP	3600.15	89.43	-0.29	0.06	0.58	3.30	-0.02	0.14	0.99
D8_EXP	4285.85	44.80	-0.08	-0.08	0.66	3.20	-0.02	0.11	0.97
D10_EXP	5499.2	32.02	-0.00	-0.06	0.22	2.02	-0.01	0.08	0.97
D11_EXP	6111.35	38.30	-0.04	0.06	0.73	1.97	-0.01	0.11	0.99
D14_EXP	7246.55	35.69	-0.02	-0.03	0.08	1.75	-0.01	0.09	0.98
D15_EXP	7894.95	39.94	-0.12	0.02	0.47	1.45	-0.03	0.10	0.96
D16_EXP	9618.75	45.54	0.02	-0.08	0.37	1.83	-0.00	0.08	0.97
D17_EXP	11688	37.38	-0.15	0.01	0.43	1.10	-0.00	0.10	0.97
D18_EXP	13283.85	47.99	0.01	0.00	0.08	1.13	0.01	0.10	0.95

**Table Annex II.15** : the evolution of the coefficients of multilinear regression for the third CP/PARAFAC component for the irradiation experiment I101 ( river water filtered , seawater non-filtered , wwtp water filtered ” RIV F MER NF STEP F” ) . (Feb 15th -Mars 4th 2016 experiment) for the non irradiated control samples

The 3rd CP/PARAFAC Component Regression parameters of the control samples (dark incubations)

Coefficient C3 à I101	Voltage (Volts)	$A^{RW, EN}_0$	$A^{RW, EN}_1(f_{sw})$	$A^{RW, EN}_2(f_{ww})$	$r_{EN}^2$	$A^{RW, CR}_0$	$A^{RW, CR}_1(f_{sw})$	$A^{RW, CR}_2(f_{ww})$	$r_{CR}^2$
D0	0	21.51	0.05	0.11	0.14	7.12	-0.07	0.61	0.95
D1_NEXP	486.95	28.04	-0.01	0.02	0.18	11.09	-0.09	0.55	0.98
D2_NEXP	1034.15	61.41	-0.25	0.21	<b>0.75</b>	10.00	-0.16	0.66	0.98
D3_NEXP	1520.9	64.31	-0.12	0.01	0.25	14.39	-0.14	0.42	0.87
D4_NEXP	2089.1	78.55	-0.37	0.13	0.60	10.06	-0.27	0.68	0.92
D7_NEXP	3600.15	90.85	-0.09	0.06	0.37	14.22	-0.12	0.55	0.97
D8_NEXP	4285.85	39.68	-0.09	0.01	0.36	9.20	-0.11	0.70	0.96
D10_NEXP	5499.2	37.40	-0.18	-0.00	0.39	7.73	-0.12	0.71	0.94
D11_NEXP	6111.35	44.58	-0.08	0.12	0.66	10.70	-0.08	0.58	0.99
D14_NEXP	7246.55	43.05	-0.25	0.04	0.56	9.34	-0.13	0.77	0.97
D15_NEXP	7894.95	40.44	-0.02	0.00	0.02	11.15	-0.10	0.48	0.85
D16_NEXP	9618.75	49.99	-0.21	0.10	0.69	10.12	-0.11	0.72	0.99
D17_NEXP	11688	35.60	-0.04	0.04	0.35	10.91	-0.09	0.64	0.99
D18_NEXP	13283.85	51.63	-0.10	0.19	0.84	9.53	-0.13	0.87	0.99

**Table Annex II.16** : the evolution of the coefficients of multilinear regression for the first CP/PARAFAC component for the irradiation experiment I011 ( river water non-filtered , seawater filtered , wwtp water filtered ” RIV NF MER F STEP F” ) . (December 3rd -17th 2015 experiment)

Coefficient C1 à I011	Voltage (Volts)	$A^{RW, EN}_0$	$A^{RW, EN}_1(f_s)$	$A^{RW, EN}_2(f_{ww})$	$r_{EN}^2$	$A^{RW, CR}_0$	$A^{RW, CR}_1(f_{sw})$	$A^{RW, CR}_2(f_{ww})$	$r_{CR}^2$
D0	0	9.36	-0.06	0.40	0.99	4.53	-0.02	0.46	0.97
D1_EXP	752.9	4.45	-0.09	0.45	0.98	9.76	-0.02	0.38	0.94
D2_EXP	1514.1	5.04	-0.07	0.33	0.97	7.15	-0.07	0.39	0.98
D5_EXP	2565.05	3.77	-0.04	0.26	0.99	6.55	-0.08	0.24	0.98
D6_EXP	3317.65	3.66	-0.03	0.17	0.99	4.04	-0.03	0.22	0.99
D7_EXP	4036.45	3.04	-0.04	0.16	0.99	3.95	-0.02	0.18	0.98
D8_EXP	4800	3.19	-0.02	0.14	0.98	3.24	-0.02	0.20	0.99
D9_EXP	5539	2.58	-0.03	0.16	0.97	7.59	-0.04	0.28	0.87
D12_EXP	7029.95	2.52	-0.03	0.21	0.99	4.28	-0.03	0.23	0.99
D13_EXP	7678.65	2.66	-0.02	0.19	0.993	4.15	-0.02	0.18	0.98
D14_EXP	8400.05	3.30	-0.03	0.17	0.99	3.80	-0.03	0.18	0.99
D15_EXP	8984.85	2.39	-0.03	0.18	0.99	3.66	-0.02	0.18	0.99

**Table Annex II.17** : the evolution of the coefficients of multilinear regression for the first CP/PARAFAC component for the irradiation experiment I011 ( river water non-filtered , seawater filtered , wwtp water filtered ” RIV NF MER F STEP F” ) . (December 3rd -17th 2015 experiment) The 1st CP/PARAFAC Component Regression parameters or the control samples (dark incubations) .

Coefficient C1 à I011	Voltage (Volts)	$A^{RW, EN}_0$	$A^{RW, EN}_1(f_{sw})$	$A^{RW, EN}_2(f_{ww})$	$r_{EN}^2$	$A^{RW, CR}_0$	$A^{RW, CR}_1(f_{sw})$	$A^{RW, CR}_2(f_{ww})$	$r_{CR}^2$
D0	0	9.36	-0.06	0.40	0.99	4.53	-0.02	0.46	0.97
D1_NEXP	752.9	5.29	-0.06	0.99	0.99	11.37	-0.07	0.77	0.98
D2_NEXP	1514.1	9.03	-0.08	0.92	0.99	15.02	-0.10	0.78	0.99
D5_NEXP	2565.05	7.99	-0.07	0.97	0.99	NA	NA	NA	NA
D6_NEXP	3317.65	3.95	0.02	0.66	0.98	7.34	-0.02	0.65	0.99
D7_NEXP	4036.45	9.11	-0.08	0.62	0.99	9.70	-0.07	0.58	0.99
D8_NEXP	4800	8.69	-0.02	0.62	0.98	11.14	-0.05	0.62	0.99
D9_NEXP	5539	9.79	-0.09	0.78	0.99	14.94	-0.10	1.00	0.98
D12_NEXP	7029.95	12.29	-0.05	0.94	0.98	14.64	-0.12	0.83	0.99
D13_NEXP	7678.65	12.44	-0.11	0.91	0.99	12.62	-0.08	0.71	0.98
D14_NEXP	8400.05	11.88	-0.05	0.80	0.98	12.86	-0.12	0.71	0.99
D15_NEXP	8984.85	12.38	-0.12	0.87	0.99	10.15	-0.06	0.72	0.99



**Table Annex II.18** : the evolution of the coefficients of multilinear regression for the second CP/PARAFAC component for the irradiation experiment I011 ( river water non-filtered , seawater filtered ,wwtp water filtered ” RIV NF MER F STEP F” ) . (December 3rd -17th 2015 experiment)

Coefficient C2 à I011	Voltage (Volts)	$A^{RW,EN}_0$	$A^{RW,EN}_1(f_{sw})$	$A^{RW,EN}_2(f_{ww})$	$r_{EN}^2$	$A^{RW,CR}_0$	$A^{RW,CR}_1(f_{sw})$	$A^{RW,CR}_2(f_{ww})$	$r_{CR}^2$
D0	0	14.88	-0.07	0.48	0.98	4.06	0.02	0.04	0.19
D1_EXP	752.9	5.99	-0.04	0.377255255	0.99	11.49	-0.07	0.19	0.69
D2_EXP	1514.1	7.80	-0.06	0.27	0.98	9.43	-0.05	0.34	0.97
D5_EXP	2565.05	4.09	-0.02	0.24	0.99	6.30	-0.04	0.17	0.97
D6_EXP	3317.65	3.56	-0.01	0.16	0.99	2.69	0.00	0.15	0.99
D7_EXP	4036.45	3.65	-0.03	0.15	0.99	3.41	0.01	0.10	0.97
D8_EXP	4800	3.61	-0.01	0.14	0.99	2.93	0.00	0.13	0.97
D9_EXP	5539	2.83	-0.01	0.15	0.97	18.55	0.07	0.43	0.52
D12_EXP	7029.95	5.48	-0.01	0.15	0.98	7.19	0.00	0.24	0.98
D13_EXP	7678.65	5.96	-0.02	0.15	0.99	7.73	0.03	0.16	0.96
D14_EXP	8400.05	6.964	-0.02	0.12	0.98	8.16	-0.01	0.17	0.99
D15_EXP	8984.85	7.29	-0.03	0.16	0.97	9.42	0.01	0.17	0.97

**Table Annex II.19** : the evolution of the coefficients of multilinear regression for the second CP/PARAFAC component for the irradiation experiment I011 ( river water non-filtered , seawater filtered , wwtp water filtered ” RIV NF MER F STEP F” ) . (December 3rd -17th 2015 experiment) The 2nd CP/PARAFAC Component Regression parameters or the control samples (dark incubations)

Coefficient C2 à I011	Voltage (Volts)	$A^{RW,EN}_0$	$A^{RW,EN}_1(f_{sw})$	$A^{RW,EN}_2(f_{ww})$	$r_{EN}^2$	$A^{RW,CR}_0$	$A^{RW,CR}_1(f_{sw})$	$A^{RW,CR}_2(f_{ww})$	$r_{CR}^2$
D0	0	14.88	-0.07	0.48	0.98	4.06	0.02	0.04	0.19
D1_NEXP	752.9	11.26	-0.08	0.77	0.99	3.24	0.04	0.49	0.98
D2_NEXP	1514.1	15.10	-0.12	0.82	0.99	11.88	0.11	0.20	0.36
D5_NEXP	2565.05	10.78	-0.08	0.90	0.99	NA	NA	NA	NA
D6_NEXP	3317.65	6.63	-0.01	0.70	0.98	2.69	0.10	0.06	0.37
D7_NEXP	4036.45	12.24	-0.10	0.64	0.99	3.41	-0.00	0.17	0.95
D8_NEXP	4800	11.65	-0.07	0.67	0.99	4.73	0.09	0.06	0.26
D9_NEXP	5539	13.55	-0.12	0.77	0.99	25.98	-0.11	1.16	0.89
D12_NEXP	7029.95	16.07	-0.13	0.86	0.99	12.37	0.12	0.14	0.28
D13_NEXP	7678.65	18.88	-0.13	0.77	0.99	9.77	-0.01	0.33	0.94
D14_NEXP	8400.05	16.49	-0.08	0.75	0.99	11.06	0.09	0.15	0.39
D15_NEXP	8984.85	21.36	-0.14	0.74	0.99	7.90	0.03	0.36	0.93

**Table Annex II.20** : the evolution of the coefficients of multilinear regression for the third CP/PARAFAC component for the irradiation experiment I011 ( river water non-filtered , seawater filtered , wwtp water filtered ” RIV NF MER F STEP F” ) . (December 3rd -17th 2015 experiment)

Coefficient C3 à I011	Voltage (Volts)	$A^{RW, EN}_0$	$A^{RW, EN}_1(f_s)$	$A^{RW, EN}_2(f_{ww})$	$r_{EN}^2$	$A^{RW, CR}_0$	$A^{RW, CR}_1(f_{sw})$	$A^{RW, CR}_2(f_{ww})$	$r_{CR}^2$
D0	0	40.92	0.06	0.09	0.3	5.35	-0.03	0.48	0.96
D1_EXP	752.9	47.92	-0.04	0.10	0.38	5.90	-0.03	0.31	0.98
D2_EXP	1514.1	41.71	-0.01	0.33	0.95	5.73	-0.05	0.31	0.98
D5_EXP	2565.05	25.97	-0.00	0.14	0.99	3.78	-0.04	0.22	0.99
D6_EXP	3317.65	15.33	0.06	0.06	0.21	2.44	-0.01	0.19	0.99
D7_EXP	4036.45	19.19	-0.06	0.05	0.55	2.53	-0.00	0.16	0.98
D8_EXP	4800	19.19	-0.00	0.12	0.76	1.97	-0.01	0.17	0.98
D9_EXP	5539	14.54	0.01	0.05	0.18	4.51	0.01	0.24	0.87
D12_EXP	7029.95	53.26	-0.04	0.08	0.50	2.55	-0.01	0.19	0.99
D13_EXP	7678.65	55.32	-0.12	0.10	0.75	2.74	0.00	0.16	0.98
D14_EXP	8400.05	57.59	0.01	0.02	0.01	2.74	-0.01	0.16	0.99
D15_EXP	8984.85	69.45	-0.09	0.23	0.535013	2.85	-0.01	0.17	0.99

**Table Annex II.21** : the evolution of the coefficients of multilinear regression for the third CP/PARAFAC component for the irradiation experiment I011 ( river water non-filtered , seawater filtered , wwtp water filtered ” RIV NF MER F STEP F” ) . (December 3rd -17th 2015 experiment) The 3rd CP/PARAFAC Component Regression parameters or the control samples (dark incubations) .

Coefficient C3 à I011	Voltage (Volts)	$A^{RW, EN}_0$	$A^{RW, EN}_1(f_{sw})$	$A^{RW, EN}_2(f_{ww})$	$r_{EN}^2$	$A^{RW, CR}_0$	$A^{RW, CR}_1(f_{sw})$	$A^{RW, CR}_2(f_{ww})$	$r_{CR}^2$
D0	0	40.92	0.06	0.09	0.33	5.35	-0.03	0.48	0.96
D1_NEXP	752.9	42.33	0.03	0.29	0.89	5.78	-0.03	0.70	0.99
D2_NEXP	1514.1	46.25	0.08	0.26	0.67	12.78	-0.14	0.80	0.99
D5_NEXP	2565.05	25.246	-0.01	0.20	0.99	NA	NA	NA	NA
D6_NEXP	3317.65	19.36	-0.04	0.03	0.25	5.92	-0.04	0.67	0.98
D7_NEXP	4036.45	18.30	0.01	0.01	0.01	9.16	-0.08	0.58	0.99
D8_NEXP	4800	20.23	-0.02	0.06	0.51	9.76	-0.08	0.64	0.99
D9_NEXP	5539	16.95	-0.01	0.02	0.19	16.16	-0.14	1.08	0.99
D12_NEXP	7029.95	53.08	-0.10	0.28	0.89	11.26	-0.14	0.86	0.99
D13_NEXP	7678.65	59.87	-0.04	0.17	0.71	12.19	-0.09	0.71	0.99
D14_NEXP	8400.05	58.53	-0.05	0.25	0.87	11.51	-0.11	0.71	0.99
D15_NEXP	8984.85	86.9	-0.12	0.07	0.65	10.43	-0.07	0.71	0.99

**Table Annex II.22** : the evolution of the coefficients of multilinear regression for the first CP/PARAFAC component for the irradiation experiment I000 ( river water non-filtered , seawater filtered , wwtp water filtered "RIV NF MER NF STEP NF" ) . (May 11th -27th 2016 experiment)

Coefficient C1 à I000	Voltage (Volts)	$A^{RW, EN}_0$	$A^{RW, EN}_1(f_{sw})$	$A^{RW, EN}_2(f_{ww})$	$r_{EN}^2$	$A^{RW, CR}_0$	$A^{RW, CR}_1(f_{sw})$	$A^{RW, CR}_2(f_{ww})$	$r_{CR}^2$
D0	0	8.73	-0.06	0.91	0.99	9.30	-0.07	0.92	0.99
D1_EXP	2311.15	3.26	-0.02	0.18	0.99	3.30	-0.02	0.17	0.99
D2_EXP	4060	2.31	-0.02	0.15	0.99	3.01	-0.02	0.13	0.99
D6_EXP	13534.8	1.14	-0.01	0.07	0.97	1.51	-0.01	0.07	0.99
D7_EXP	15961.15	0.11	-0.00	0.07	0.99	1.18	-0.01	0.06	0.99
D8_EXP	18580.4	0.23	0.01	0.06	0.98	1.17	-0.00	0.05	0.98
D12_EXP	28400.1	0.49	-0.00	0.04	0.99	0.98	-0.00	0.04	0.99
D13_EXP	31048.8	0.44	-0.01	0.03	0.99	0.99	-0.00	0.03	0.99
D14_EXP	33491	0.92	-0.00	0.04	0.96	1.28	-0.01	0.03	0.99
D15_EXP	36000.35	0.41	-0.01	0.03	0.99	0.90	-0.00	0.03	0.97
D16_EXP	38469.2	0.67	-0.00	0.04	0.97	1.32	-0.01	0.03	0.96

**Table Annex II.23** : the evolution of the coefficients of multilinear regression for the first CP/PARAFAC component for the irradiation experiment I000 ( river water non-filtered , seawater filtered , wwtp water filtered "RIV NF MER NF STEP NF" ) . (May 11th -27th 2016 experiment) . The 1st CP/PARAFAC Component Regression parameters or the control samples (dark incubations) .

Coefficient C1 à I000	Voltage (Volts)	$A^{RW, EN}_0$	$A^{RW, EN}_1(f_s)$	$A^{RW, EN}_2(f_{ww})$	$r_{EN}^2$	$A^{RW, CR}_0$	$A^{RW, CR}_1(f_{sw})$	$A^{RW, CR}_2(f_{ww})$	$r_{CR}^2$
D0	0	8.73	-0.061	0.91	0.99	9.30	-0.07	0.92	0.99
D1_NEXP	2311.15	11.18	-0.09	0.89	0.99	11.06	-0.11	0.92	0.99
D2_NEXP	4060	7.05	-0.02	0.90	0.99	8.49	-0.06	0.91	0.99
D6_NEXP	13534.8	10.41	-0.09	0.89	0.99	11.31	-0.11	0.90	0.99
D7_NEXP	15961.15	6.75	-0.01	0.88	0.99	8.24	-0.05	0.89	0.99
D8_NEXP	18580.4	9.58	-0.09	0.91	0.99	11.08	-0.11	0.90	0.99
D12_NEXP	28400.1	8.60	-0.09	0.84	0.99	9.46	-0.10	0.86	0.99
D13_NEXP	31048.8	7.01	-0.06	0.93	0.99	7.66	-0.06	0.99	0.99
D14_NEXP	33491	7.95	-0.018	0.92	0.99	9.29	-0.06	0.91	0.99
D15_NEXP	36000.35	7.17	-0.06	0.95	0.99	NA	NA	NA	NA
D16_NEXP	38469.2	6.89	-0.01	0.90	0.99	7.11	-0.00	0.92	0.99

**Table Annex II.24** : the evolution of the coefficients of multilinear regression for the second CP/PARAFAC component for the irradiation experiment I000 ( river water non-filtered , seawater filtered , wwtp water filtered ”RIV NF MER NF STEP NF” ) . (May 11th -27th 2016 experiment)

Coefficient C2 à I000	Voltage (Volts)	$A^{RW, EN}_0$	$A^{RW, EN}_1(f_{sw})$	$A^{RW, EN}_2(f_{ww})$	$r_{EN}^2$	$A^{RW, CR}_0$	$A^{RW, CR}_1(f_{sw})$	$A^{RW, CR}_2(f_{ww})$	$r_{CR}^2$
D0	0	7.14	-0.05	0.89	0.99	25.66	-0.01	0.59	0.84
D1_EXP	2311.15	2.19	-0.01	0.14	0.98	24.17	0.07	0.65	0.97
D2_EXP	4060	2.36	-0.01	0.11	0.99	12.84	-0.01	0.51	0.99
D6_EXP	13534.8	0.77	0.00	0.07	0.99	7.62	0.16	0.34	0.98
D7_EXP	15961.15	0.96	-0.00	0.06	0.99	5.45	0.08	0.37	0.90
D8_EXP	18580.4	1.12	0.00	0.06	0.97	7.26	0.23	0.34	0.91
D12_EXP	28400.1	0.90	-0.00	0.04	0.99	9.27	-0.01	0.24	0.98
D13_EXP	31048.8	0.67	0.00	0.03	0.98	8.11	0.04	0.23	0.99
D14_EXP	33491	0.87	-0.002	0.03	0.89	9.40	0.01	0.34	0.91
D15_EXP	36000.35	0.84	0.00	0.03	0.93	9.47	0.01	0.16	0.95
D16_EXP	38469.2	1.42	-0.01	0.03	0.88	9.51	-0.00	0.30	0.89

**Table Annex II.25** : the evolution of the coefficients of multilinear regression for the second CP/PARAFAC component for the irradiation experiment I000 ( river water non-filtered , seawater filtered , wwtp water filtered ”RIV NF MER NF STEP NF” ) . (May 11th -27th 2016 experiment) . The 2nd CP/PARAFAC Component Regression parameters of the control samples (dark incubations) .

Coefficient C2 à I000	Voltage (Volts)	$A^{RW, EN}_0$	$A^{RW, EN}_1(f_{sw})$	$A^{RW, EN}_2(f_{ww})$	$r_{EN}^2$	$A^{RW, CR}_0$	$A^{RW, CR}_1(f_{sw})$	$A^{RW, CR}_2(f_{ww})$	$r_{CR}^2$
D0	0	7.14	-0.05	0.89	0.99	25.66	-0.02	0.59	0.84
D1_NEXP	2311.15	10.01	-0.09	0.84	0.99	32.47	-0.04	0.98	0.97
D2_NEXP	4060	6.40	-0.03	0.90	0.99	23.78	0.04	0.36	0.83
D6_NEXP	13534.8	10.41	-0.09	0.87	0.99	20.38	-0.09	0.57	0.96
D7_NEXP	15961.15	6.15	-0.03	0.871	0.99	21.89	0.06	0.36	0.77
D8_NEXP	18580.4	10.16	-0.09	0.85	0.99	21.78	-0.10	0.60	0.97
D12_NEXP	28400.1	7.17	-0.06	0.84	0.99	24.87	-0.23	0.23	0.89
D13_NEXP	31048.8	7.13	-0.06	0.89	0.99	21.59	-0.13	0.53	0.99
D14_NEXP	33491	6.64	-0.04	0.87	0.99	26.71	0.05	0.58	0.82
D15_NEXP	36000.35	7.05	-0.05	0.92	0.99	NA	NA	NA	NA
D16_NEXP	38469.2	4.70	0.02	0.93	0.98	20.09	0.07	0.40	0.67

**Table Annex II.26** : the evolution of the coefficients of multilinear regression for the third CP/PARAFAC component for the irradiation experiment I000 ( river water non-filtered , seawater filtered , wwtp water filtered ”RIV NF MER NF STEP NF” ) . (May 11th -27th 2016 experiment)

Coefficient C3 à I000	Voltage (Volts)	$A^{RW, EN}_0$	$A^{RW, EN}_1(f_s)$	$A^{RW, EN}_2(f_{ww})$	$r_{EN}^2$	$A^{RW, CR}_0$	$A^{RW, CR}_1(f_{sw})$	$A^{RW, CR}_2(f_{ww})$	$r_{CR}^2$
D0	0	44.72	0.01	0.39	0.59	11.103	-0.07	0.87	0.99
D1_EXP	2311.15	36.81	-0.03	0.61	0.95	4.23	-0.00	0.21	0.98
D2_EXP	4060	56.05	-0.04	0.56	0.96	3.43	-0.02	0.18	0.99
D6_EXP	13534.8	30.26	0.47	0.57	0.77	1.06	0.00	0.12	0.99
D7_EXP	15961.15	52.62	0.06	0.37	0.89	0.61	0.01	0.10	0.99
D8_EXP	18580.4	52.47	0.21	0.40	0.93	1.20	0.01	0.10	0.96
D12_EXP	28400.1	41.17	-0.02	0.35	0.99	0.86	-0.00	0.07	0.99
D13_EXP	31048.8	35.19	0.29	0.43	0.82	0.81	0.00	0.06	0.98
D14_EXP	33491	28.54	-0.00	0.32	0.96	1.46	-0.01	0.06	0.86
D15_EXP	36000.35	38.07	0.38	0.34	0.58	1.16	-0.01	0.04	0.94
D16_EXP	38469.2	47.20	-0.05	0.36	0.85	2.04	-0.01	0.05	0.84

**Table Annex II.27** : the evolution of the coefficients of multilinear regression for the third CP/PARAFAC component for the irradiation experiment I000 ( river water non-filtered , seawater filtered , wwtp water filtered ”RIV NF MER NF STEP NF” ) . (May 11th -27th 2016 experiment) . The 3rd CP/PARAFAC Component Regression parameters or the control samples (dark incubations) .

Coefficient C3 à I000	Voltage (Volts)	$A^{RW, EN}_0$	$A^{RW, EN}_1(f_s)$	$A^{RW, EN}_2(f_{ww})$	$r_{EN}^2$	$A^{RW, CR}_0$	$A^{RW, CR}_1(f_{sw})$	$A^{RW, CR}_2(f_{ww})$	$r_{CR}^2$
D0	0	44.72	0.01	0.39	0.59	11.10	-0.07	0.87	0.99
D1_NEXP	2311.15	42.03	-0.06	0.53	0.93	13.55	-0.11	0.86	0.99
D2_NEXP	4060	60.97	0.16	0.25	0.52	10.53	-0.06	0.86	0.99
D6_NEXP	13534.8	60.54	-0.14	0.52	0.76	13.69	-0.13	0.87	0.99
D7_NEXP	15961.15	69.68	0.02	0.20	0.56	9.39	-0.06	0.84	0.99
D8_NEXP	18580.4	71.24	-0.12	0.40	0.93	1370	-0.13	0.86	0.99
D12_NEXP	28400.1	59.036	-0.21	0.05	0.34	11.01	-0.11	0.80	0.99
D13_NEXP	31048.8	68.97	-0.24	0.23	0.96	9.75	-0.08	0.95	0.99
D14_NEXP	33491	58.15	-0.16	0.35	0.70	10.26	-0.07	0.85	0.99
D15_NEXP	36000.35	69.799	-0.22	0.29	0.93	NA	NA	NA	NA
D16_NEXP	38469.2	49.86	0.27	0.34	0.39	6.86	0.04	0.94	0.97

### ANNEX III

#### $f_{RW}$ and $f_{WW}$ Permutation

**Table Annex III.1** : the evolution of the coefficients of multilinear regression for the first CP/PARAFAC component for the irradiation experiment I111 ( river water filtered , sea water filtered , wwtp water filtered .(aug-sept 2015 experiment)

Coefficient C1 à I111	Voltage (Volts)	$A^{SW,EN}_0$	$A^{SW,EN}_1(f_{RW})$	$A^{RW,EN}_2(f_{WW})$	$r_{EN}^2$	$A^{SW,CR}_0$	$A^{SW,CR}_1(f_{RW})$	$A^{SW,CR}_2(f_{WW})$	$r_{CR}^2$
T0	0	1.23	0.06	0.99	0.99	1.02	0.06	0.99	0.99
T3	11140.81	-0.19	0.01	0.12	0.99	-0.26	0.01	0.10	0.99
T4	12470.48	0.03	0.01	0.11	0.99	-0.05	0.01	0.09	0.99
T5	14821.40	0.33	0.00	0.09	0.99	0.11	0.00	0.06	0.99
T6	16363.55	0.54	-0.00	0.08	0.97	0.20	0.00	0.05	0.99
T7	17521.88	-0.11	-0.00	0.06	0.98	-0.01	0.00	0.05	0.99
T11	27011.24	-0.63	0.01	0.06	0.79	-0.28	0.00	0.03	0.78
T12	28944.07	0.06	0.00	0.02	0.55	-0.13	0.00	0.02	0.80
T13	30410.83	0.16	-0.00	0.04	0.89	-0.11	0.00	0.03	0.93
T14	32806.30	0.17	-0.00	0.04	0.97	-0.26	0.00	0.02	0.85

**Table Annex III.2** : the evolution of the coefficients of multilinear regression for the second CP/PARAFAC component for the irradiation experiment I111 ( river water filtered , sea water filtered , wwtp water filtered .(aug-sept 2015 experiment)

Coefficient C2 à I111	Voltage (Volts)	$A^{SW,EN}_0$	$A^{SW,EN}_1(f_{RW})$	$A^{RW,EN}_2(f_{WW})$	$r_{EN}^2$	$A^{SW,CR}_0$	$A^{SW,CR}_1(f_{RW})$	$A^{SW,CR}_2(f_{WW})$	$r_{CR}^2$
T0	0	1.21	0.04	0.97	0.99	7.95	0.09	1.03	0.97
T3	11140.81	1.06	0.01	0.16	0.97	9.12	0.00	0.54	0.95
T4	12470.48	1.06	-0.00	0.15	0.98	7.23	-0.01	0.48	0.97
T5	14821.40	0.39	0.01	0.14	0.99	5.80	0.00	0.46	0.97
T6	16363.55	0.93	-0.00	0.12	0.98	7.09	-0.02	0.44	0.96
T7	17521.88	0.92	0.00	0.12	0.98	8.38	-0.00	0.43	0.96
T11	27011.24	-0.36	0.01	0.07	0.95	2.72	0.03	0.33	0.92
T12	28944.07	0.56	0.00	0.08	0.97	10.65	-0.02	0.39	0.91
T13	30410.83	0.65	0.00	0.06	0.94	8.69	-0.02	0.30	0.89
T14	32806.30	0.78	-0.00	0.05	0.96	10.07	-0.04	0.31	0.87

**Table Annex III.3 :** the evolution of the coefficients of multilinear regression for the third CP/PARAFAC component for the irradiation experiment I111 ( river water filtered , sea water filtered , wwtp water filtered .(aug-sept 2015 experiment)

Coefficient C3 à I111	Voltage (Volts)	$A^{SW,EN}_0$	$A^{SW,EN}_1(f_Rw)$	$A^{RW,EN}_2(f_{ww})$	$r_{EN}^2$	$A^{SW,CR}_0$	$A^{SW,CR}_1(f_{RW})$	$A^{SW,CR}_2(f_{ww})$	$r_{CR}^2$
T0	0	3.96	0.05	1.08	0.97	2.91	0.05	0.99	0.99
T3	11140.81	16.73	0.02	0.69	0.97	1.42	0.01	0.21	0.97
T4	12470.48	8.48	-0.01	0.58	0.96	1.67	-0.00	0.20	0.98
T5	14821.40	6.06	0.01	0.55	0.99	0.61	0.01	0.20	0.99
T6	16363.55	7.64	-0.02	0.51	0.97	1.29	-0.00	0.18	0.99
T7	17521.88	23.44	0.01	0.55	0.97	1.03	0.01	0.17	0.99
T11	27011.24	1.51	0.03	0.29	0.68	0.05	0.01	0.10	0.97
T12	28944.07	21.93	-0.02	0.53	0.90	1.01	0.00	0.11	0.96
T13	30410.83	12.35	0.01	0.38	0.65	1.16	-0.00	0.09	0.96
T14	32806.30	11.18	-0.03	0.30	0.92	1.24	-0.00	0.09	0.95

**Table Annex III.4 :** the evolution of the coefficients of multilinear regression for the first CP/PARAFAC component for the irradiation experiment I110( river water filtered , seawater filtered , wwtp water non-filtered . (November 10-20th 2015 experiment)

Coefficient C1 à I110	Voltage (Volts)	$A^{SW,EN}_0$	$A^{SW,EN}_1(f_Rw)$	$A^{RW,EN}_2(f_{ww})$	$r_{EN}^2$	$A^{SW,CR}_0$	$A^{SW,CR}_1(f_{RW})$	$A^{SW,CR}_2(f_{ww})$	$r_{CR}^2$
D0	1.7	2.54	0.06	0.66	0.99	1.02	0.05	0.65	0.99
D2_EXP	3295.15	-0.85	0.01	0.05	0.83	2.07	0.00	0.23	0.97
D3_EXP	4704.05	-0.28	0.04	0.28	0.99	1.04	0.03	0.27	0.99
D6_EXP	10211.45	1.26	0.02	0.14	0.99	0.99	0.01	0.12	0.99
D7_EXP	11961.6	0.098	0.02	0.10	0.95	0.48	0.02	0.14	0.98
D8_EXP	13725.15	-0.84	0.04	0.13	0.97	-0.13	0.02	0.11	0.98
D9_EXP	15569.15	1.80	0.01	0.08	0.99	0.73	0.01	0.08	0.99
D10_EXP	17221.55	-0.35	0.03	0.12	0.99	0.38	0.02	0.11	0.99

**Table Annex III.5 :** the temporal evolution of the coefficients of multilinear regression for the first CP/PARAFAC component for the irradiation experiment I110( river water filtered , seawater filtered , wwtp water non-filtered . (November 10-20th 2015 experiment) . The 1st CP/PARAFAC Component Regression parameters or the control samples (dark incubations) .

Coefficient C1 à I110	Voltage (Volts)	$A^{SW,EN}_0$	$A^{SW,EN}_1(f_Rw)$	$A^{RW,EN}_2(f_{ww})$	$r_{EN}^2$	$A^{SW,CR}_0$	$A^{SW,CR}_1(f_{RW})$	$A^{SW,CR}_2(f_{ww})$	$r_{CR}^2$
D0	1.7	2.54	0.06	0.66	0.99	1.02	0.05	0.65	0.99
D2_NEXP	3295.15	-1.86	0.03	0.43	0.96	0.11	0.06	1.04	0.99
D3_NEXP	4704.05	5.89	0.07	1.04	0.97	-0.56	0.12	1.07	0.99
D6_NEXP	10211.45	2.75	0.07	0.74	0.99	1.46	0.06	0.69	0.99
D7_NEXP	11961.6	3.22	0.03	0.79	0.99	2.39	0.05	0.81	0.99
D8_NEXP	13725.15	-0.49	0.12	0.70	0.92	-0.03	0.09	0.66	0.94
D9_NEXP	15569.15	-0.05	0.10	0.65	0.99	-3.54	0.10	0.68	0.99
D10_NEXP	17221.55	-0.22	0.12	0.84	0.96	0.87	0.09	0.77	0.97

**Table Annex III.6:** the evolution of the coefficients of multilinear regression for the second CP/PARAFAC component for the irradiation experiment I110( river water filtered , seawater filtered , wwtp water non-filtered . (November 10-20th 2015 experiment)

Coefficient C2 à I110	Voltage (Volts)	$A^{SW,EN}_0$	$A^{SW,EN}_1(f_{RW})$	$A^{RW,EN}_2(f_{WW})$	$r_{EN}^2$	$A^{SW,CR}_0$	$A^{SW,CR}_1(f_{RW})$	$A^{SW,CR}_2(f_{WW})$	$r_{CR}^2$
D0	1.7	4.97	0.07	0.76	0.99	17.20	0.02	-0.17	0.58
D2_EXP	3295.15	-1.60	0.02	0.07	0.94	2.61	-0.02	0.43	0.94
D3_EXP	4704.05	2.53	0.02	0.17	0.99	17.54	0.15	1.19	0.98
D6_EXP	10211.45	1.87	0.02	0.12	0.98	13.37	0.04	0.32	0.96
D7_EXP	11961.6	0.99	0.01	0.07	0.92	4.57	0.06	0.47	0.98
D8_EXP	13725.15	0.63	0.03	0.10	0.96	10.48	0.06	0.31	0.98
D9_EXP	15569.15	3.92	-0.00	0.06	0.97	14.07	0.03	0.24	0.95
D10_EXP	17221.55	1.47	0.02	0.10	0.97	17.79	0.02	0.37	0.97

**Table Annex III.7:** the temporal evolution of the coefficients of multilinear regression for the second CP/PARAFAC component for the irradiation experiment I110( river water filtered , seawater filtered , wwtp water non-filtered . (November 10-20th 2015 experiment) . The 2nd CP/PARAFAC Component Regression parameters or the control samples (dark incubations) .

Coefficient C2 à I110	Voltage (Volts)	$A^{SW,EN}_0$	$A^{SW,EN}_1(f_{RW})$	$A^{RW,EN}_2(f_{WW})$	$r_{EN}^2$	$A^{SW,CR}_0$	$A^{SW,CR}_1(f_{RW})$	$A^{SW,CR}_2(f_{WW})$	$r_{CR}^2$
D0	1.7	4.97	0.07	0.76	0.99	17.20	0.02	-0.17	0.58
D2_NEXP	3295.15	-2.62	0.07	0.68	0.98	5.27	-0.07	0.04	0.10
D3_NEXP	4704.05	4.74	0.08	1.02	0.98	95.38	-0.45	-0.77	0.31
D6_NEXP	10211.45	3.52	0.08	0.80	0.99	18.47	-0.04	-0.18	0.40
D7_NEXP	11961.6	2.30	0.05	0.88	0.99	32.82	-0.14	-0.30	0.41
D8_NEXP	13725.15	0.18	0.13	0.75	0.91	16.77	0.01	-0.13	0.20
D9_NEXP	15569.15	0.39	0.10	0.76	0.99	29.99	-0.09	-0.29	0.71
D10_NEXP	17221.55	1.63	0.12	0.87	0.96	21.32	0.06	0.06	0.06



**Table Annex III.8** : the evolution of the coefficients of multilinear regression for the third CP/PARAFAC component for the irradiation experiment I110( river water filtered , seawater filtered , wwtp water non-filtered . (November 10-20th 2015 experiment)

Coefficient C3 à I110	Voltage (Volts)	$A^{SW, EN}_0$	$A^{SW, EN}_1(f_{RW})$	$A^{RW, EN}_2(f_{WW})$	$r_{EN}^2$	$A^{SW, CR}_0$	$A^{SW, CR}_1(f_{RW})$	$A^{SW, CR}_2(f_{WW})$	$r_{CR}^2$
D0	1.7	59.51	-0.02	-0.16	0.35	1.23	0.07	0.72	0.99
D2_EXP	3295.15	-1.36	0.06	0.08	0.13	0.81	0.00	0.20	0.98
D3_EXP	4704.05	71.27	0.03	0.39	0.89	1.01	0.03	0.23	0.99
D6_EXP	10211.45	35.99	0.12	0.22	0.82	0.65	0.01	0.13	0.99
D7_EXP	11961.6	23.52	0.02	-0.00	0.04	0.16	0.02	0.14	0.97
D8_EXP	13725.15	28.82	0.21	0.24	0.65	0.14	0.02	0.11	0.99
D9_EXP	15569.15	58.48	-0.01	-0.01	0.04	1.26	-0.00	0.08	0.97
D10_EXP	17221.55	48.86	0.10	0.22	<b>0.70</b>	0.55	0.10	0.80	0.96

**Table Annex III.9** : the temporal evolution of the coefficients of multilinear regression for the third CP/PARAFAC component for the irradiation experiment I110( river water filtered , seawater filtered , wwtp water non-filtered . (November 10-20th 2015 experiment) The 3rd CP/PARAFAC Component Regression parameters or the control samples (dark incubations) .

Coefficient C3 à I110	Voltage (Volts)	$A^{SW, EN}_0$	$A^{SW, EN}_1(f_{RW})$	$A^{RW, EN}_2(f_{WW})$	$r_{EN}^2$	$A^{SW, CR}_0$	$A^{SW, CR}_1(f_{RW})$	$A^{SW, CR}_2(f_{WW})$	$r_{CR}^2$
D0	1.7	59.51	-0.02	-0.16	0.35	1.23	0.07	0.72	0.99
D2_NEXP	3295.15	2.24	0.00	-0.04	0.74	-1.47	0.08	1.07	0.99
D3_NEXP	4704.05	70.72	0.18	0.11	0.00	-1.33	0.12	1.07	0.99
D6_NEXP	10211.45	44.86	-0.01	-0.13	0.73	1.40	0.08	0.75	0.99
D7_NEXP	11961.6	7.28	0.26	-0.10	0.67	0.60	0.06	0.90	0.99
D8_NEXP	13725.15	43.46	-2.8E-05	-0.18	<b>0.85</b>	-0.38	0.10	0.70	0.93
D9_NEXP	15569.15	54.50	0.03	-0.05	0.35	-3.50	0.11	0.75	0.99
D10_NEXP	17221.55	58.33	0.01	-0.12	0.72	0.55	0.10	0.80	0.96

**Table Annex III.10** : the evolution of the coefficients of multilinear regression for the first CP/PARAFAC component for the irradiation experiment I101 ( river water filtered , seawater non-filtered , wwtp water filtered ” RIV F MER NF STEP F” ) . (Feb 15th -Mars 4th 2016 experiment)

Coefficient C1 à I101	Voltage (Volts)	$A^{SW,EN}_0$	$A^{SW,EN}_1(f_{RW})$	$A^{RW,EN}_2(f_{WW})$	$r_{EN}^2$	$A^{SW,CR}_0$	$A^{SW,CR}_1(f_{RW})$	$A^{SW,CR}_2(f_{WW})$	$r_{CR}^2$
D0	0	1.68	0.06	0.59	0.97	0.99	0.07	0.64	0.95
D1_EXP	486.95	-3.66	0.10	0.43	0.99	2.17	0.06	0.37	0.99
D2_EXP	1034.15	1.29	0.04	0.26	0.84	2.06	0.04	0.31	0.93
D3_EXP	1520.9	-8.64	0.13	0.40	0.93	-4.72	0.11	0.37	0.95
D4_EXP	2089.1	-0.05	0.07	0.15	0.70	0.22	0.06	0.20	0.80
D7_EXP	3600.15	0.26	0.03	0.20	0.98	0.88	0.03	0.20	0.99
D8_EXP	4285.85	2.50	0.01	0.07	0.96	1.36	0.02	0.14	0.98
D10_EXP	5499.2	0.96	0.01	0.06	0.97	1.04	0.02	0.11	0.98
D11_EXP	6111.35	-0.06	0.03	0.12	0.97	1.22	0.02	0.14	0.99
D14_EXP	7246.55	1.25	0.01	0.07	0.97	1.30	0.02	0.11	0.99
D15_EXP	7894.95	-2.17	0.04	0.13	0.88	-2.12	0.05	0.15	0.94
D16_EXP	9618.75	1.25	0.02	0.07	0.97	1.66	0.01	0.10	0.98
D17_EXP	11688	-0.52	0.02	0.08	0.91	0.85	0.02	0.11	0.98
D18_EXP	13283.85	1.38	0.02	0.08	0.92	1.74	0.01	0.10	0.96

**Table Annex III.11:** the evolution of the coefficients of multilinear regression for the first CP/PARAFAC component for the irradiation experiment I101 ( river water filtered , seawater non-filtered ,wwtp water filtered ” RIV F MER NF STEP F” ) . (Feb 15th -Mars 4th 2016 experiment) for the non irradiated control samples. The 1st CP/PARAFAC Component Regression parameters or the control samples (dark incubations) .

Coefficient C1 à I101	Voltage (Volts)	$A^{SW,EN}_0$	$A^{SW,EN}_1(f_R)$	$A^{RW,EN}_2(f_{WW})$	$r_{EN}^2$	$A^{SW,CR}_0$	$A^{SW,CR}_1(f_{RW})$	$A^{SW,CR}_2(f_{WW})$	$r_{CR}^2$
D0	0	1.68	0.06	0.59	0.97	0.99	0.07	0.64	0.95
D1_NEXP	486.95	1.83	0.10	0.72	0.98	4.29	0.08	0.67	0.97
D2_NEXP	1034.15	-10.97	0.23	1.08	0.97	2.24	0.14	0.63	0.90
D3_NEXP	1520.9	-1.87	0.19	0.69	0.79	-15.08	0.28	0.99	0.93
D4_NEXP	2089.1	-25.54	0.38	1.14	0.93	3.68	0.11	0.70	0.97
D7_NEXP	3600.15	1.74	0.15	0.80	0.96	2.10	0.09	0.77	0.96
D8_NEXP	4285.85	1.48	0.06	0.57	0.98	0.73	0.10	0.79	0.96
D10_NEXP	5499.2	-5.98	0.12	0.82	0.97	4.31	0.08	0.69	0.97
D11_NEXP	6111.35	2.10	0.09	0.73	0.99	1.58	0.11	0.86	0.98
D14_NEXP	7246.55	-1.96	0.11	0.91	0.99	2.53	0.10	0.60	0.87
D15_NEXP	7894.95	-1.47	0.15	0.65	0.79	5.70	0.07	0.78	0.98
D16_NEXP	9618.75	1.78	0.087	0.86	0.99	4.79	0.08	0.76	0.98
D17_NEXP	11688	0.97	0.11	0.83	0.99	0.48	0.12	0.97	0.99
D18_NEXP	13283.85	2.55	0.08	0.95	0.99	-3.75	0.18	0.92	0.97

**Table Annex III.12** : the evolution of the coefficients of multilinear regression for the second CP/PARAFAC component for the irradiation experiment I101 ( river water filtered , seawater non-filtered , wwtp water filtered ” RIV F MER NF STEP F” ) . (Feb 15th -Mars 4th 2016 experiment)

Coefficient C2 à I101	Voltage (Volts)	$A^{SW,EN}_0$	$A^{SW,EN}_1(f_R)$	$A^{RW,EN}_2(f_{WW})$	$r_{EN}^2$	$A^{SW,CR}_0$	$A^{SW,CR}_1(f_{RW})$	$A^{SW,CR}_2(f_{WW})$	$r_{CR}^2$
D0	0	2.76	0.07	0.70	0.96	14.59	-0.02	0.06	0.09
D1_EXP	486.95	-3.15	0.09	0.41	0.99	8.62	0.09	0.53	0.97
D2_EXP	1034.15	4.36	0.02	0.18	0.85	21.36	0.04	0.59	0.93
D3_EXP	1520.9	-4.25	0.10	0.33	0.91	2.93	0.24	0.77	0.93
D4_EXP	2089.1	4.31	0.04	0.12	0.68	20.07	0.10	0.40	0.72
D7_EXP	3600.15	4.40	0.04	0.16	0.98	22.85	0.10	0.48	0.98
D8_EXP	4285.85	4.76	0.02	0.07	0.97	22.60	0.06	0.30	0.97
D10_EXP	5499.2	2.73	0.0	0.05	0.87	10.99	0.03	0.19	0.95
D11_EXP	6111.35	2.26	0.02	0.11	0.97	13.79	0.04	0.28	0.96
D14_EXP	7246.55	2.77	0.01	0.07	0.95	12.81	0.02	0.24	0.98
D15_EXP	7894.95	0.22	0.04	0.11	0.91	4.55	0.11	0.33	0.90
D16_EXP	9618.75	4.32	0.00	0.05	0.89	19.18	-0.02	0.20	0.89
D17_EXP	11688	1.36	0.02	0.08	0.91	11.05	0.03	0.27	0.97
D18_EXP	13283.85	4.62	-0.00	0.07	0.95	20.64	-0.05	0.23	0.81

**Table Annex III.13** : the evolution of the coefficients of multilinear regression for the second CP/PARAFAC component for the irradiation experiment I101 ( river water filtered , seawater non-filtered , wwtp water filtered ” RIV F MER NF STEP F” ) . (Feb 15th -Mars 4th 2016 experiment) for the non irradiated control samples. The 2nd CP/PARAFAC Component Regression parameters of the control samples (dark incubations) .

Coefficient C2 à I101	Voltage (Volts)	$A^{SW,EN}_0$	$A^{SW,EN}_1(f_{RW})$	$A^{RW,EN}_2(f_{WW})$	$r_{EN}^2$	$A^{SW,CR}_0$	$A^{SW,CR}_1(f_{RW})$	$A^{SW,CR}_2(f_{WW})$	$r_{CR}^2$
D0	0	2.76	0.07	0.70	0.96	14.59	-0.02	0.06	0.09
D1_NEXP	486.95	2.75	0.11	0.71	0.98	11.51	0.05	0.67	0.98
D2_NEXP	1034.15	-8.43	0.21	0.95	0.97	17.37	0.19	0.96	0.83
D3_NEXP	1520.9	0.86	0.19	0.58	0.79	17.58	0.26	0.66	0.58
D4_NEXP	2089.1	-20.99	0.36	1.05	0.91	27.56	0.20	0.98	0.96
D7_NEXP	3600.15	5.82	0.15	0.73	0.95	43.92	-0.06	0.17	0.24
D8_NEXP	4285.85	0.39	0.10	0.68	0.97	23.16	0.01	0.28	0.42
D10_NEXP	5499.2	-5.49	0.14	0.85	0.96	14.43	0.12	0.89	0.98
D11_NEXP	6111.35	3.59	0.11	0.71	0.98	33.31	-0.05	0.22	0.26
D14_NEXP	7246.55	-3.17	0.14	0.94	0.99	12.18	0.13	0.70	0.80
D15_NEXP	7894.95	1.02	0.14	0.62	0.77	42.32	-0.10	0.20	0.27
D16_NEXP	9618.75	0.41	0.12	0.89	0.99	13.95	0.09	0.98	0.97
D17_NEXP	11688	1.89	0.11	0.80	0.99	46.44	-0.13	0.08	0.16
D18_NEXP	13283.85	2.37	0.10	0.98	0.99	34.75	0.02	0.55	0.48

**Table Annex III.14** : the evolution of the coefficients of multilinear regression for the third CP/PARAFAC component for the irradiation experiment I101 ( river water filtered , seawater non-filtered , wwtp water filtered ” RIV F MER NF STEP F” ) . (Feb 15th -Mars 4th 2016 experiment)

Coefficient C3 à I101	Voltage (Volts)	$A^{SW,EN}_0$	$A^{SW,EN}_1(f_R)$	$A^{RW,EN}_2(f_{ww})$	$r_{EN}^2$	$A^{SW,CR}_0$	$A^{SW,CR}_1(f_{RW})$	$A^{SW,CR}_2(f_{ww})$	$r_{CR}^2$
D0	0	26.96	-0.05	0.05	0.14	0.42	0.07	0.68	0.95
D1_EXP	486.95	22.24	0.05	0.15	0.79	-1.03	0.06	0.35	0.99
D2_EXP	1034.15	55.02	0.05	0.02	0.07	1.90	0.01	0.22	0.95
D3_EXP	1520.9	35.26	0.22	0.32	0.47	-3.96	0.07	0.31	0.95
D4_EXP	2089.1	66.06	0.07	0.02	0.05	0.45	0.04	0.16	0.83
D7_EXP	3600.15	60.24	0.29	0.35	0.58	1.46	0.02	0.16	0.99
D8_EXP	4285.85	37.26	0.08	-0.00	0.66	1.68	0.02	0.12	0.97
D10_EXP	5499.2	31.71	0.00	-0.06	0.22	0.69	0.01	0.10	0.97
D11_EXP	6111.35	34.07	0.04	0.11	0.73	0.89	0.01	0.12	0.99
D14_EXP	7246.55	33.36	0.02	-0.01	0.08	0.95	0.01	0.10	0.98
D15_EXP	7894.95	27.72	0.12	0.14	0.47	-1.22	0.03	0.12	0.96
D16_EXP	9618.75	47.57	-0.02	-0.10	0.37	1.50	0.00	0.09	0.97
D17_EXP	11688	22.05	0.15	0.16	0.43	0.88	0.00	0.10	0.97
D18_EXP	13283.85	49.48	-0.01	-0.01	0.08	1.70	-0.01	0.09	0.95

**Table Annex III.15** : the evolution of the coefficients of multilinear regression for the third CP/PARAFAC component for the irradiation experiment I101 ( river water filtered , seawater non-filtered , wwtp water filtered ” RIV F MER NF STEP F” ) . (Feb 15th -Mars 4th 2016 experiment) for the non irradiated control samples

The 3rd CP/PARAFAC Component Regression parameters of the control samples (dark incubations) .

Coefficient C3 à I101	Voltage (Volts)	$A^{SW,EN}_0$	$A^{SW,EN}_1(f_{RW})$	$A^{RW,EN}_2(f_{ww})$	$r_{EN}^2$	$A^{SW,CR}_0$	$A^{SW,CR}_1(f_{RW})$	$A^{SW,CR}_2(f_{ww})$	$r_{CR}^2$
D0	0	26.96	-0.05	0.05	0.14	0.42	0.07	0.68	0.95
D1_NEXP	486.95	27.51	0.00	0.03	0.18	2.58	0.09	0.64	0.98
D2_NEXP	1034.15	36.77	0.25	0.46	<b>0.75</b>	0.32	0.14	0.56	0.87
D3_NEXP	1520.9	52.11	0.12	0.14	0.25	-17.30	0.27	0.96	0.92
D4_NEXP	2089.1	41.18	0.37	0.50	0.60	2.13	0.12	0.67	0.97
D7_NEXP	3600.15	81.35	0.09	0.15	0.37	-1.96	0.11	0.81	0.96
D8_NEXP	4285.85	30.60	0.09	0.10	0.36	-4.30	0.12	0.83	0.94
D10_NEXP	5499.2	19.34	0.18	0.18	0.39	2.61	0.08	0.66	0.99
D11_NEXP	6111.35	36.26	0.08	0.20	0.66	-3.96	0.13	0.90	0.97
D14_NEXP	7246.55	18.44	0.25	0.28	0.56	0.91	0.10	0.58	0.86
D15_NEXP	7894.95	38.71	0.02	0.02	0.02	-1.06	0.11	0.83	0.99
D16_NEXP	9618.75	29.38	0.21	0.30	0.69	2.13	0.09	0.73	0.99
D17_NEXP	11688	31.25	0.04	0.08	0.35	-3.65	0.13	0.99	0.99
D18_NEXP	13283.85	41.51	0.10	0.29	0.84	-5.59	0.16	0.82	0.98

**Table Annex III.16** : the evolution of the coefficients of multilinear regression for the first CP/PARAFAC component for the irradiation experiment I011 ( river water non-filtered , seawater filtered , wwtp water filtered ” RIV NF MER F STEP F” ) . (December 3rd -17th 2015 experiment)

Coefficient C1 à I011	Voltage (Volts)	$A^{SW,EN}_0$	$A^{SW,EN}_1(f_R)$	$A^{RW,EN}_2(f_{WW})$	$r_{EN}^2$	$A^{SW,CR}_0$	$A^{SW,CR}_1(f_{RW})$	$A^{SW,CR}_2(f_{WW})$	$r_{CR}^2$
D0	0	3.73	0.06	0.46	0.99	1.04	0.06	0.49	0.98
D1_EXP	752.9	-4.73	0.09	0.55	0.98	7.38	0.02	0.41	0.94
D2_EXP	1514.1	-1.99	0.07	0.40	0.97	0.58	0.07	0.45	0.98
D5_EXP	2565.05	-0.42	0.04	0.30	0.99	-1.06	0.08	0.32	0.98
D6_EXP	3317.65	0.24	0.03	0.21	0.99	1.19	0.03	0.24	0.99
D7_EXP	4036.45	-0.50	0.04	0.20	0.99	1.82	0.02	0.20	0.98
D8_EXP	4800	0.99	0.02	0.16	0.98	1.22	0.02	0.22	0.99
D9_EXP	5539	-0.12	0.03	0.18	0.97	3.16	0.04	0.32	0.87
D12_EXP	7029.95	-0.05	0.03	0.24	0.99	1.29	0.03	0.26	0.99
D13_EXP	7678.65	0.16	0.02	0.22	0.99	2.60	0.02	0.20	0.98
D14_EXP	8400.05	-0.17	0.03	0.20	0.99	1.01	0.03	0.21	0.99
D15_EXP	8984.85	-0.46	0.03	0.21	0.99	1.26	0.02	0.20	0.99

**Table Annex III.17** : the evolution of the coefficients of multilinear regression for the first CP/PARAFAC component for the irradiation experiment I011 ( river water non-filtered , seawater filtered , wwtp water filtered ” RIV NF MER F STEP F” ) . (December 3rd -17th 2015 experiment) The 1st CP/PARAFAC Component Regression parameters or the control samples (dark incubations) .

Coefficient C1 à I011	Voltage (Volts)	$A^{SW,EN}_0$	$A^{SW,EN}_1(f_{RW})$	$A^{RW,EN}_2(f_{WW})$	$r_{EN}^2$	$A^{SW,CR}_0$	$A^{SW,CR}_1(f_{RW})$	$A^{SW,CR}_2(f_{WW})$	$r_{CR}^2$
D0	0	3.73	0.06	0.46	0.98	1.04	0.06	0.49	0.98
D1_NEXP	752.9	-0.56	0.06	1.05	0.99	4.58	0.07	0.84	0.98
D2_NEXP	1514.1	0.54	0.08	1.01	0.99	4.77	0.10	0.89	0.99
D5_NEXP	2565.05	1.15	0.07	1.04	0.99	NA	NA	NA	NA
D6_NEXP	3317.65	5.48	-0.02	0.65	0.98	5.11	0.02	0.67	0.99
D7_NEXP	4036.45	0.99	0.08	0.70	0.99	2.96	0.07	0.64	0.99
D8_NEXP	4800	6.83	0.02	0.64	0.98	5.70	0.05	0.67	0.99
D9_NEXP	5539	0.99	0.09	0.86	0.99	5.22	0.10	1.10	0.98
D12_NEXP	7029.95	7.44	0.05	0.99	0.98	3.03	0.12	0.95	0.99
D13_NEXP	7678.65	1.24	0.11	1.02	0.99	4.50	0.08	0.79	0.98
D14_NEXP	8400.05	6.99	0.05	0.85	0.98	1.26	0.12	0.83	0.99
D15_NEXP	8984.85	0.68	0.12	0.99	0.99	4.46	0.06	0.78	0.98

**Table Annex III.18** : the evolution of the coefficients of multilinear regression for the second CP/PARAFAC component for the irradiation experiment I011 ( river water non-filtered , seawater filtered , wwtp water filtered ” RIV NF MER F STEP F” ) . (December 3rd -17th 2015 experiment)

Coefficient C2 à I011	Voltage (Volts)	$A^{SW,EN}_0$	$A^{SW,EN}_1(f_{RW})$	$A^{RW,EN}_2(f_{WW})$	$r_{EN}^2$	$F_{EN}$	$A^{SW,CR}_0$	$A^{SW,CR}_1(f_{RW})$	$A^{SW,CR}_2(f_{WW})$	$r_{CR}^2$	$F_{CR}$
D0	0	7.41	0.07	0.56	0.98		4.15	0.03	0.03	0.22	
D1_EXP	752.9	1.73	0.04	0.42	0.99		4.15	0.07	0.27	0.69	
D2_EXP	1514.1	1.95	0.06	0.33	0.98		4.56	0.05	0.38	0.97	
D5_EXP	2565.05	2.23	0.02	0.26	0.99		2.52	0.04	0.20	0.97	
D6_EXP	3317.65	2.40	0.01	0.18	0.99		2.85	-0.00	0.15	0.99	
D7_EXP	4036.45	0.92	0.03	0.18	0.99		4.33	-0.01	0.09	0.97	
D8_EXP	4800	2.42	0.01	0.15	0.99		3.11	-0.00	0.13	0.97	
D9_EXP	5539	1.50	0.01	0.16	0.97		25.90	-0.07	0.35	0.52	
D12_EXP	7029.95	4.10	0.01	0.17	0.99		7.27	-0.00	0.24	0.98	
D13_EXP	7678.65	4.15	0.02	0.17	0.99		10.32	-0.03	0.14	0.96	
D14_EXP	8400.05	5.10	0.02	0.14	0.98		7.15	0.01	0.18	0.99	
D15_EXP	8984.85	4.47	0.03	0.19	0.97		9.96	-0.01	0.16	0.97	

**Table Annex III.19** : the evolution of the coefficients of multilinear regression for the second CP/PARAFAC component for the irradiation experiment I011 ( river water non-filtered , seawater filtered , wwtp water filtered ” RIV NF MER F STEP F” ) . (December 3rd -17th 2015 experiment) The 2nd CP/PARAFAC Component Regression parameters or the control samples (dark incubations) .

Coefficient C2 à I011	Voltage (Volts)	$A^{SW,EN}_0$	$A^{SW,EN}_1(f_{RW})$	$A^{RW,EN}_2(f_{WW})$	$r_{EN}^2$	$A^{SW,CR}_0$	$A^{SW,CR}_1(f_{RW})$	$A^{SW,CR}_2(f_{WW})$	$r_{CR}^2$
D0	0	7.41	0.07	0.56	0.98	4.15	0.03	0.03	0.22
D1_NEXP	752.9	2.81	0.08	0.85	0.99	7.13	-0.04	0.45	0.98
D2_NEXP	1514.1	3.50	0.12	0.94	0.99	22.68	-0.11	0.09	0.36
D5_NEXP	2565.05	2.56	0.08	0.98	0.99	NA	NA	NA	NA
D6_NEXP	3317.65	5.13	0.01	0.72	0.98	12.47	-0.10	-0.03	0.37
D7_NEXP	4036.45	1.97	0.10	0.75	0.99	3.00	0.00	0.17	0.95
D8_NEXP	4800	5.05	0.07	0.74	0.99	13.24	-0.09	-0.02	0.26
D9_NEXP	5539	1.79	0.12	0.89	0.99	14.96	0.11	1.27	0.89
D12_NEXP	7029.95	3.18	0.13	0.99	0.99	24.26	-0.12	0.03	0.28
D13_NEXP	7678.65	5.69	0.13	0.90	0.99	8.43	0.01	0.34	0.94
D14_NEXP	8400.05	8.03	0.08	0.84	0.99	19.89	-0.09	0.06	0.39
D15_NEXP	8984.85	7.22	0.14	0.88	0.99	10.93	-0.03	0.33	0.93

**Table Annex III.20** : the evolution of the coefficients of multilinear regression for the third CP/PARAFAC component for the irradiation experiment I011 ( river water non-filtered , seawater filtered , wwtp water filtered ” RIV NF MER F STEP F” ) . (December 3rd -17th 2015 experiment)

Coefficient C3 à I011	Voltage (Volts)	$A^{SW, EN}_0$	$A^{SW, EN}_1(f_R)$	$A^{RW, EN}_2(f_{WW})$	$r_{EN}^2$	$A^{SW, CR}_0$	$A^{SW, CR}_1(f_{RW})$	$A^{SW, CR}_2(f_{WW})$	$r_{CR}^2$
D0	0	47.10	-0.06	0.02	0.33	1.01	0.08	0.51	0.97
D1_EXP	752.9	43.74	0.04	0.15	0.38	3.35	0.03	0.33	0.98
D2_EXP	1514.1	40.85	0.01	0.34	0.95	0.97	0.05	0.35	0.98
D5_EXP	2565.05	25.71	0.00	0.14	0.99	-0.36	0.04	0.26	0.99
D6_EXP	3317.65	21.78	-0.06	-0.00	0.21	0.98	0.01	0.21	0.99
D7_EXP	4036.45	13.34	0.06	0.10	0.5	2.45	0.00	0.16	0.98
D8_EXP	4800	18.89	0.00	0.13	0.76	1.06	0.01	0.18	0.98
D9_EXP	5539	15.27	-0.01	0.04	0.18	5.01	-0.01	0.23	0.87
D12_EXP	7029.95	49.24	0.04	0.12	0.50	1.38	0.01	0.21	0.99
D13_EXP	7678.65	43.29	0.12	0.22	0.75	2.76	-0.00	0.16	0.98
D14_EXP	8400.05	58.28	-0.01	0.01	0.01	1.45	0.01	0.17	0.99
D15_EXP	8984.85	60.34	0.09	0.32	0.53	1.42	0.01	0.18	0.99

**Table Annex III.21** : the evolution of the coefficients of multilinear regression for the third CP/PARAFAC component for the irradiation experiment I011 ( river water non-filtered , seawater filtered , wwtp water filtered ” RIV NF MER F STEP F” ) . (December 3rd -17th 2015 experiment) The 3rd CP/PARAFAC Component Regression parameters or the control samples (dark incubations) .

Coefficient C3 à I011	Voltage (Volts)	$A^{SW, EN}_0$	$A^{SW, EN}_1(f_{RW})$	$A^{RW, EN}_2(f_{WW})$	$r_{EN}^2$	$A^{SW, CR}_0$	$A^{SW, CR}_1(f_{RW})$	$A^{SW, CR}_2(f_{WW})$	$r_{CR}^2$
D0	0	47.10	-0.06	0.02	0.33	1.01	0.08	0.51	0.97
D1_NEXP	752.9	45.76	-0.03	0.26	0.89	2.73	0.03	0.73	0.99
D2_NEXP	1514.1	54.15	-0.08	0.18	0.67	-0.89	0.14	0.93	0.99
D5_NEXP	2565.05	24.12	0.01	0.21	0.99	NA	NA	NA	NA
D6_NEXP	3317.65	15.14	0.04	0.07	0.25	1.80	0.04	0.71	0.99
D7_NEXP	4036.45	19.03	-0.01	-0.00	0.01	1.55	0.08	0.66	0.99
D8_NEXP	4800	18.62	0.02	0.07	0.51	1.47	0.08	0.72	0.99
D9_NEXP	5539	16.12	0.01	0.03	0.20	2.30	0.14	1.22	0.99
D12_NEXP	7029.95	42.84	0.10	0.38	0.89	-2.76	0.14	1.00	0.99
D13_NEXP	7678.65	56.10	0.04	0.20	0.71	2.76	0.09	0.80	0.99
D14_NEXP	8400.05	53.56	0.05	0.30	0.87	0.23	0.11	0.82	0.99
D15_NEXP	8984.85	75.09	0.12	0.19	0.65	3.23	0.07	0.78	0.99

**Table Annex III.22** : the evolution of the coefficients of multilinear regression for the first CP/PARAFAC component for the irradiation experiment I000 ( river water non-filtered , seawater filtered ,wwtp water filtered ”RIV NF MER NF STEP NF” ) . (May 11th -27th 2016 experiment)

Coefficient C1 à I000	Voltage (Volts)	$A^{SW,EN}_0$	$A^{SW,EN}_1(f_{RW})$	$A^{RW,EN}_2(f_{WW})$	$r_{EN}^2$	$A^{SW,CR}_0$	$A^{SW,CR}_1(f_{RW})$	$A^{SW,CR}_2(f_{WW})$	$r_{CR}^2$
D0	0	2.54	0.06	0.98	0.99	1.86	0.07	0.99	0.99
D1_EXP	2311.15	1.74	0.02	0.19	0.99	0.99	0.02	0.19	0.99
D2_EXP	4060	0.16	0.02	0.17	0.99	0.84	0.02	0.16	0.99
D6_EXP	13534.8	0.35	0.01	0.08	0.97	0.84	0.01	0.07	0.99
D7_EXP	15961.15	0.06	0.00	0.07	0.99	0.55	0.01	0.07	0.99
D8_EXP	18580.4	1.04	-0.01	0.05	0.98	1.13	0.00	0.05	0.98
D12_EXP	28400.1	0.09	0.00	0.05	0.99	0.61	0.00	0.04	0.99
D13_EXP	31048.8	-0.20	0.01	0.04	0.99	0.60	0.00	0.03	0.99
D14_EXP	33491	0.50	0.00	0.05	0.96	0.63	0.01	0.04	0.99
D15_EXP	36000.35	-0.41	0.01	0.04	0.99	0.68	0.00	0.03	0.97
D16_EXP	38469.2	0.28	0.00	0.04	0.97	0.70	0.01	0.03	0.96

**Table Annex III.23** : the evolution of the coefficients of multilinear regression for the first CP/PARAFAC component for the irradiation experiment I000 ( river water non-filtered , seawater filtered , wwtp water filtered ”RIV NF MER NF STEP NF” ) . (May 11th -27th 2016 experiment) . The 1st CP/PARAFAC Component Regression parameters or the control samples (dark incubations) .

Coefficient C1 à I000	Voltage (Volts)	$A^{SW,EN}_0$	$A^{SW,EN}_1(f_R)$	$A^{RW,EN}_2(f_{WW})$	$r_{EN}^2$	$A^{SW,CR}_0$	$A^{SW,CR}_1(f_{RW})$	$A^{SW,CR}_2(f_{WW})$	$r_{CR}^2$
D0	0	2.54	0.06	0.98	0.99	1.86	0.07	0.99	0.99
D1_NEXP	2311.15	1.29	0.10	0.99	0.99	-0.06	0.11	1.03	0.99
D2_NEXP	4060	4.55	0.02	0.93	0.99	2.54	0.06	0.97	0.99
D6_NEXP	13534.8	1.22	0.09	0.98	0.99	0.70	0.11	1.01	0.99
D7_NEXP	15961.15	5.53	0.01	0.89	0.99	3.25	0.05	0.94	0.99
D8_NEXP	18580.4	0.78	0.09	0.99	0.99	0.41	0.11	1.01	0.99
D12_NEXP	28400.1	-0.09	0.09	0.92	0.99	-0.40	0.10	0.95	0.99
D13_NEXP	31048.8	1.07	0.06	0.99	0.99	1.62	0.06	1.06	0.99
D14_NEXP	33491	6.59	0.01	0.93	0.99	3.44	0.06	0.97	0.99
D15_NEXP	36000.35	1.13	0.06	1.01	0.99	NA	NA	NA	NA
D16_NEXP	38469.2	5.40	0.01	0.92	0.9	6.87	0.00	0.92	0.99



**Table Annex III.24** : the evolution of the coefficients of multilinear regression for the second CP/PARAFAC component for the irradiation experiment I000 ( river water non-filtered , seawater filtered , wwtp water filtered ”RIV NF MER NF STEP NF” ) . (May 11th -27th 2016 experiment)

Coefficient C2 à I000	Voltage (Volts)	$A^{SW,EN}_0$	$A^{SW,EN}_1(f_{RW})$	$A^{RW,EN}_2(f_{WW})$	$r_{EN}^2$	$A^{SW,CR}_0$	$A^{SW,CR}_1(f_{RW})$	$A^{SW,CR}_2(f_{WW})$	$r_{CR}^2$
D0	0	2.42	0.05	0.94	0.99	24.08	0.02	0.61	0.84
D1_EXP	2311.15	1.21	0.01	0.15	0.98	31.62	-0.07	0.58	0.97
D2_EXP	4060	1.15	0.01	0.12	0.99	11.79	0.01	0.53	0.99
D6_EXP	13534.8	0.94	-0.00	0.07	0.99	23.39	-0.16	0.18	0.98
D7_EXP	15961.15	0.85	0.00	0.06	0.99	13.41	-0.08	0.29	0.90
D8_EXP	18580.4	1.32	-0.00	0.05	0.98	30.00	-0.22	0.11	0.91
D12_EXP	28400.1	0.60	0.00	0.04	0.99	8.01	0.01	0.26	0.98
D13_EXP	31048.8	0.98	-0.00	0.03	0.98	12.33	-0.04	0.18	0.99
D14_EXP	33491	0.47	0.00	0.04	0.89	10.07	-0.01	0.33	0.91
D15_EXP	36000.35	0.96	-0.00	0.02	0.93	10.08	-0.01	0.16	0.95
D16_EXP	38469.2	0.70	0.01	0.03	0.88	9.03	0.00	0.30	0.89

**Table Annex III.25** : the evolution of the coefficients of multilinear regression for the second CP/PARAFAC component for the irradiation experiment I000 ( river water non-filtered , seawater filtered , wwtp water filtered ”RIV NF MER NF STEP NF” ) . (May 11th -27th 2016 experiment) . The 2nd CP/PARAFAC Component Regression parameters of the control samples (dark incubations) .

Coefficient C2 à I000	Voltage (Volts)	$A^{SW,EN}_0$	$A^{SW,EN}_1(f_{RW})$	$A^{RW,EN}_2(f_{WW})$	$r_{EN}^2$	$A^{SW,CR}_0$	$A^{SW,CR}_1(f_{RW})$	$A^{SW,CR}_2(f_{WW})$	$r_{CR}^2$
D0	0	2.42	0.05	0.94	0.99	24.08	0.02	0.61	0.84
D1_NEXP	2311.15	1.04	0.09	0.93	0.99	27.99	0.04	1.02	0.97
D2_NEXP	4060	3.08	0.03	0.93	0.99	28.08	-0.04	0.32	0.83
D6_NEXP	13534.8	1.21	0.09	0.96	0.99	11.22	0.09	0.66	0.96
D7_NEXP	15961.15	3.47	0.03	0.90	0.99	27.90	-0.06	0.30	0.77
D8_NEXP	18580.4	1.31	0.09	0.94	0.99	11.28	0.10	0.70	0.97
D12_NEXP	28400.1	1.22	0.06	0.90	0.99	1.98	0.23	0.46	0.89
D13_NEXP	31048.8	1.42	0.06	0.94	0.99	8.53	0.13	0.66	0.99
D14_NEXP	33491	2.92	0.04	0.91	0.99	31.70	-0.05	0.53	0.82
D15_NEXP	36000.35	1.57	0.05	0.98	0.99	NA	NA	NA	NA
D16_NEXP	38469.2	6.88	-0.02	0.91	0.9	27.09	-0.07	0.33	0.67

**Table Annex III.26 :** the evolution of the coefficients of multilinear regression for the third CP/PARAFAC component for the irradiation experiment I000 ( river water non-filtered , seawater filtered , wwtp water filtered ”RIV NF MER NF STEP NF” ) . (May 11th -27th 2016 experiment)

Coefficient C3 à I000	Voltage (Volts)	$A^{SW,EN}_0$	$A^{SW,EN}_1(f_R)$	$A^{RW,EN}_2(f_{WW})$	$r_{EN}^2$	$A^{SW,CR}_0$	$A^{SW,CR}_1(f_{RW})$	$A^{SW,CR}_2(f_{WW})$	$r_{CR}^2$
D0	0	45.28	-0.00	0.38	0.59	4.51	0.07	0.94	0.99
D1_EXP	2311.15	34.04	0.03	0.63	0.95	3.84	0.00	0.22	0.98
D2_EXP	4060	52.50	0.04	0.60	0.96	1.62	0.02	0.20	0.99
D6_EXP	13534.8	77.17	-0.47	0.10	0.77	1.18	-0.00	0.12	0.99
D7_EXP	15961.15	59.02	-0.06	0.30	0.90	1.14	-0.01	0.10	0.99
D8_EXP	18580.4	73.66	-0.21	0.19	0.93	2.27	-0.01	0.09	0.96
D12_EXP	28400.1	39.34	0.02	0.37	0.98	0.67	0.00	0.08	0.99
D13_EXP	31048.8	64.42	-0.29	0.13	0.82	0.89	-0.00	0.06	0.98
D14_EXP	33491	28.29	0.00	0.32	0.96	0.79	0.01	0.07	0.86
D15_EXP	36000.35	75.78	-0.38	-0.04	0.57	0.49	0.01	0.05	0.94
D16_EXP	38469.2	42.34	0.05	0.41	0.85	0.76	0.01	0.06	0.84

**Table Annex III.27:** the evolution of the coefficients of multilinear regression for the third CP/PARAFAC component for the irradiation experiment I000 ( river water non-filtered , seawater filtered , wwtp water filtered ”RIV NF MER NF STEP NF” ) . (May 11th -27th 2016 experiment) . The 3rd CP/PARAFAC Component Regression parameters or the control samples (dark incubations) .

Coefficient C3 à I000	Voltage (Volts)	$A^{SW,EN}_0$	$A^{SW,EN}_1(f_R)$	$A^{RW,EN}_2(f_{WW})$	$r_{EN}^2$	$A^{SW,CR}_0$	$A^{SW,CR}_1(f_{RW})$	$A^{SW,CR}_2(f_{WW})$	$r_{CR}^2$
D0	0	45.28	-0.01	0.38	0.59	4.51	0.07	0.94	0.99
D1_NEXP	2311.15	35.85	0.06	0.59	0.93	2.18	0.11	0.97	0.99
D2_NEXP	4060	76.94	-0.16	0.09	0.52	4.09	0.06	0.93	0.99
D6_NEXP	13534.8	46.26	0.14	0.67	0.76	0.95	0.13	0.99	0.99
D7_NEXP	15961.15	71.50	-0.02	0.18	0.56	3.83	0.06	0.90	0.99
D8_NEXP	18580.4	58.96	0.12	0.52	0.93	0.69	0.13	0.99	0.99
D12_NEXP	28400.1	37.94	0.21	0.26	0.33	0.06	0.11	0.91	0.99
D13_NEXP	31048.8	44.58	0.24	0.47	0.96	1.73	0.08	1.03	0.99
D14_NEXP	33491	41.94	0.16	0.51	0.70	3.54	0.07	0.92	0.99
D15_NEXP	36000.35	47.54	0.22	0.52	0.93	NA	NA	NA	NA
D16_NEXP	38469.2	76.54	-0.27	0.07	0.39	11.30	-0.04	0.90	0.97

## **Annex IV**

EGU Poster (European Geosciences Union Conference)

# Caracterisation of anthropogenic contribution to the coastal fluorescent organic matter

Ibrahim EL NAHHAL, Ayoub NOUHI, Stéphane MOUNIER\*

Laboratoire PROTEE, Université de Toulon, BP 20132, 83957 La Garde Cedex

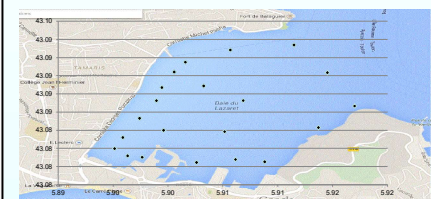
Corresponding author: mounier@univ-tln.fr

## Introduction

The Dissolved organic matter (DOM) has a great importance in the coastal zones (Yamashita et al 2013, Boyer, & Jaffé, 2013). Its importance come in part from the fact that it is the main energy source for heterotrophic bacteria in surface waters (Hoikkala et al., 2015). In addition, It also plays an important role in the transport and availability of trace metals and contaminants in coastal and open-sea waters (Hoikkala et al., 2015). Moreover, the colored (chromophoric) dissolved organic matter fraction (CDOM) which is considered to be the major component of the dissolved natural organic matter (DNOM) in natural waters (Brezonik, Olmanson, Finlay, & Bauer, 2014) has the capability of absorbing and controlling the penetration of UV light into the water column and protecting aquatic organisms (e.g. corals) from photo-inhibition (Baker et al., 2008). And the penetration of light to the deep aquatic environment which affects the primary biological productivity is greatly affected by CDOM (Murphy, Stedmon, Waite, & Ruiz, 2008). In addition, DOM in the coastal zones from terrestrial origins may affect phytoplankton dynamics by providing limiting nutrients in the form of dissolved organic nitrogen (DON) or phosphorus (DOP). The state of art technique for the characterization of CDOM in aquatic environments is Excitation emission matrix (EEM) spectroscopy which is often called "total luminescence" (Hall & Kenny, 2007) is coupled with parallel factor analysis (EEM-PARAFAC) in the evaluation of the dynamics of the fluorescent fraction of DOM (FDOM) in coastal environments (Stedmon and Markager, 2005). The Toulon bay (SE France) is a small bay situated in the southern east of France which is a quasi-closed coastal area (Tessier et al., 2011). In addition, this bay is divided into two parts (the little bay and the big bay). This bay is subjected to various anthropogenic inputs coming from different non-point sources, among these inputs are the effluents of wastewater treatment plants entering the bay directly or indirectly (through riverine inputs containing the effluents of the wastewater treatment plants). Moreover, aquaculture, mytiliculture and conchyliculture can be seen easily in this bay. Therefore, the objective of this work is to characterize the contribution of urban organic matter during winter event to this coastal zone of Toulon bay. And to find if any the differences between the anthropogenic FDOM and the natural FDOM.

## Methodology

**Sample origin and preparation :** Surface samples were collected from the (Toulon Bay, France) from 21 different sites according to the map here-below; during the month of December, 2014 (12th, 17th, 19th); using glass tubes which were acid-rinsed with nitric acid and milli-Q water for each sampling campaign. The temperature of the samples was conserved using ice pieces. No sample filtration was made, in the way to have a rapid measurement without preparation.



**Fluorescence Measurement methodology :** Fluorescence EEM was measured using Hitachi F-4500 Fluorescence Spectrophotometer. The 3D emission scan was made from the wavelengths of 200–400 nm with 5 nm increments at a stepwise increase of 5 nm for the excitation wavelengths from 220 nm to 420 nm. The scanning speed was set at 2400 nm min<sup>-1</sup>, and the excitation and emission slits were adjusted to 5 nm. Likewise, two 2D measurements were done at excitation wavelength 250 nm and 350 nm for emission wavelengths (250–500) and (350–650) respectively; with a scanning speed of 240 nm min<sup>-1</sup> while the stepwise increase and the excitation and emission slits were the same with 3D measurements. To limit second order Rayleigh scattering, a 25 nm cutoff filter was used for the measurements and mirrored cells were used. No inner filter correction were made.

PARAFAC modeling with DOM Fluor toolbox (<http://www.models.life.ku.dk>) was applied using MATLAB R2013a (Mathworks, Natick, MA, USA) to statistically decompose dissimilar fluorescence components from all the EEM data, in which several different fluorophores could be intertwined with each other (Stedmon and Bro, 2008). A total of 66 EEMs (21 x 3 x 3) of the seawater samples were incorporated into the PARAFAC modeling process. The number of components was determined based on the core consistency test (Stedmon and Bro, 2008); which were four components.

Furthermore, the turbidity and the Suspended Organic matter and the E.Coli were measured.

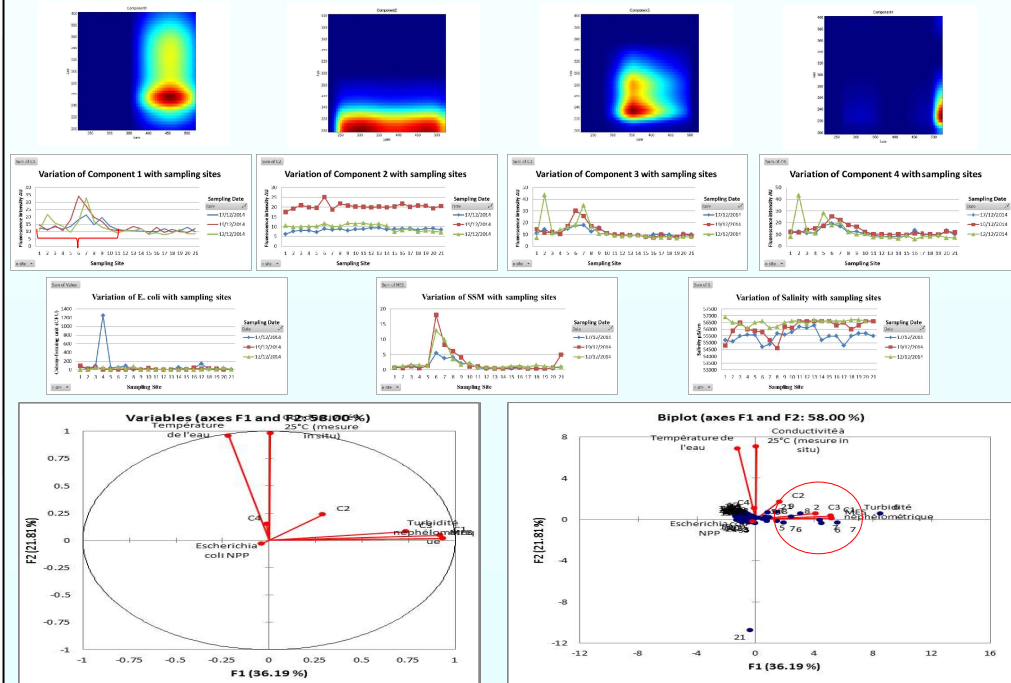
## Conclusions

DOM of anthropogenic origin was detected by fluorescence spectroscopy, however the concentration of E. Coli was not for the only over limit point. The salinity was not correlated with the increase of the fluorescence signal nor the E. Coli concentration.

C1, C2 and C3 are good candidate to monitor the anthropogenic inputs in coastal zones.

More efforts are to be done to directly detect biological pollution by direct fluorescence measurements.

## Results



## Description and Discussion of results:

Four CP/PARAFAC components were extracted from the EEM data set of all samples taken from the Lazaret Bay. The core consistency was 70% for four-component model for this study. Component 1 (C1) exhibited two maxima at the excitation wavelengths of 250 nm and 330 nm, and at the emission wavelength of 450 nm; which is similar to those of typical aquatic DOM with terrestrial sources "humic-like fluorophores" with peak A and C (Coble, 1996; Tedetti et al., 2012). The second component (C2) exhibited also two emission maxima at 300 and 470 nm over excitation at 200 nm, and it seems to be noise, and cannot be associated with any of the known components of CP/PARAFAC in the state of the art. While the 3rd component (C3) exhibited also two excitation maxima at 237 and 280 nm at emission wavelength at 350 nm; which appears to be marine humic-like fluorophores with peak M (Tedetti et al., 2012). Moreover, Component (C4) has two emission peaks at 300 and 550 nm over excitation wavelength at 230 nm.

It can be seen that component 1 varies with the sampling sites and it has greater values associated with the sites (5, 6, 7, 8, 9, 10) for all the sampling campaigns; since these sites were in front of the pipe openings which imports of anthropogenically-impacted riverine input to the Lazaret bay and this enhance the fact that this component is of terrestrial aquatic DOM. The component C2 with sampling sites for the sampling campaigns (12 and 17 Dec.) did not show much variations, meanwhile for the sampling campaign (19 Dec.) showed similar trend with the other ones but with higher values of fluorescence intensities. It may not be explained due to the fact that Component C2 could be considered as noise. For all the sampling campaigns; the values of component C3 showed approximately same variation than C1, except for the sampling sites (2, 6, and 7) which agrees with the fact that these sites correspond to riverine inputs which may be affected by non-intentional leaches from wastewater pipes and this should agree with the variation of E. Coli with the sampling sites since there is a high concentration of it in site 2 and 7. Component C4 showed the same variations as component C3. The Suspended Solids Matter (SSM) varies with the sites 5, 6, 7, 8, and 9 for all the sampling campaign with a maximum value for site 6 of 18 which agrees with the E. coli variations.

E. Coli is found to be over 250 CFU/100 mL only one time at point 4. Even if it is obvious that points 4 to 9 are anthropogenically impacted, no direct correlation was found between E.Coli concentration and CP/PARAFAC components or direct fluorescence intensity. However the components C1, C3 and C4 seems to be related to SSM. No explanation was found for the fluorescence peak in 12/12/2015 at point 2. Salinity in these experiments was not relevant to the anthropogenic inputs, meaning that in this case the pollution is not directly linked to the fresh water inputs.

PCA analysis shows that E.Coli is not correlated to salinity, fluorescence C1, C2, C3 or to the Suspended Solid matter SSM.

## References

1. Yamashita, T., & Prairie, R. (2011). Climate change and coastal zone management: An ecological assessment of long-term impacts. *Current Climate Change Reports*, 1(1), 1-11.
2. Bro, R., & Smilde, A. (2003). Factor analysis of time-course data. *Journal of Chemometrics*, 17(1), 1-17.
3. Coble, P. (1996). Fluorescence spectroscopy of natural organic matter in the environment. *Marine Chemistry*, 51(1-4), 321-349.
4. Hall, J., & Kenny, J. (2007). Estuarine water classification using EEM spectroscopy and PARAFAC-SIMCA. *Applied Chemistry*, 58(1), 11-18.
5. Hall, J., & Kenny, J. (2007). Estuarine water classification using EEM spectroscopy and PARAFAC-SIMCA. *Applied Chemistry*, 58(1), 11-18.
6. Murphy, K. R., Stedmon, C., Waite, T. D., & Ruiz, J. M. (2008). Distinguishing between terrestrial and autochthonous organic matter sources in marine environments using PARAFAC spectroscopy. *Marine Chemistry*, 108(1-2), 1-12.
7. Stedmon, C., & Bro, R. (2008). Characterizing dissolved organic matter fluorescence with parallel factor analysis: a tutorial. *Limnology & Oceanography*, 53(2), 575-591.
8. Yamashita, Y., & Prairie, R. (2011). Climate change and coastal zone management: An ecological assessment of long-term impacts. *Current Climate Change Reports*, 1(1), 1-11.

## ANNEX V

**CP/PARAFAC components from the CP/PARAFAC decomposition of the EEM dataset of the two EEM data acquisition methods (Elnahhal and Croatia). The multilinear regression parameters in Annex I, Annex II and Annex III were calculated based on these CP/PARAFAC components.**

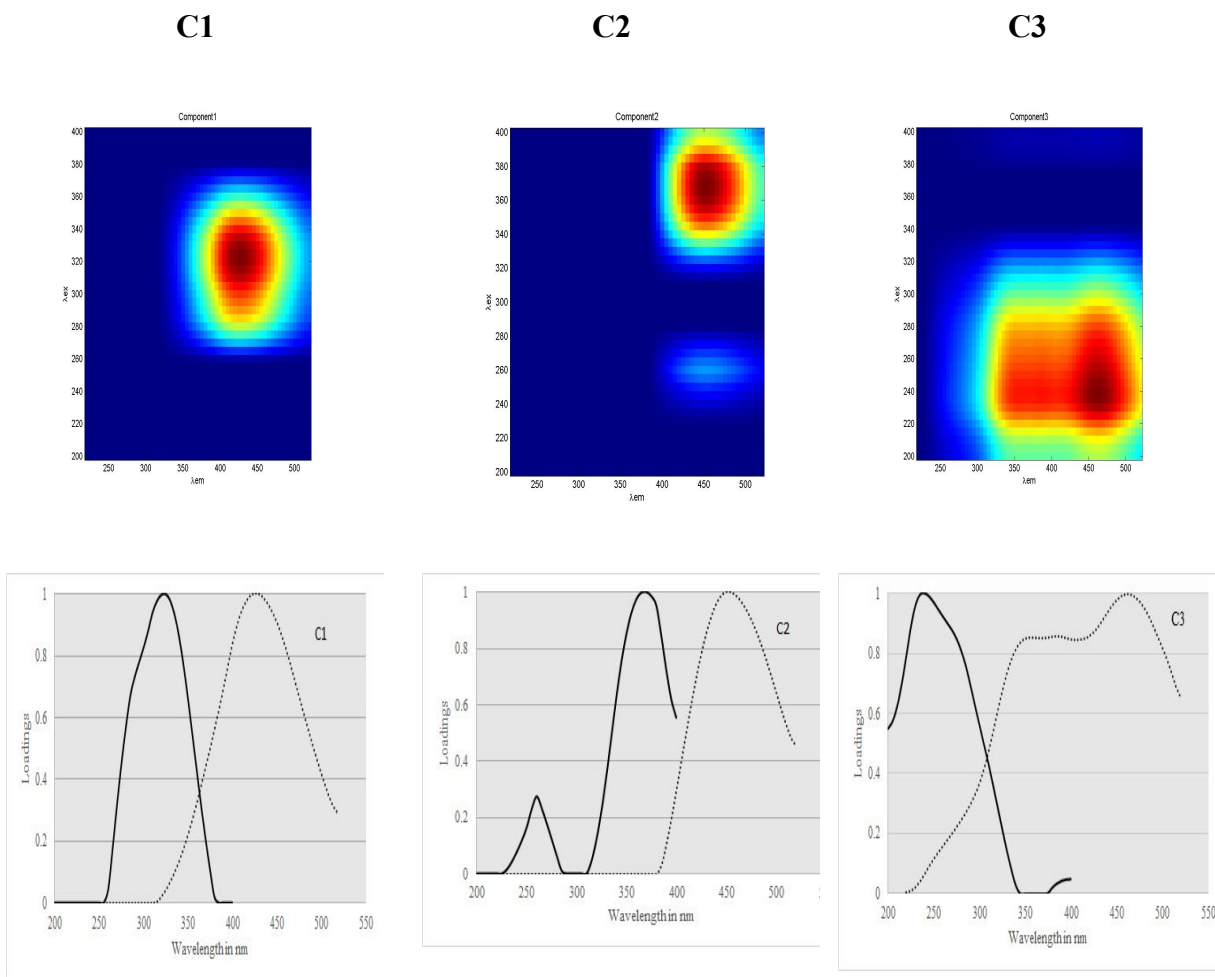


**Fig. Annex V.1** Contour plots of CP/PARAFAC components identified from the decomposition of all EEM datasets from the Elnahhal EEM data acquisition method. Spectral loadings of excitation and emission wavelengths of the three identified CP/PARAFAC in the present study. Excitation loading for CP/PARAC component are solid lines whereas emission loadings are shown in dotted lines.

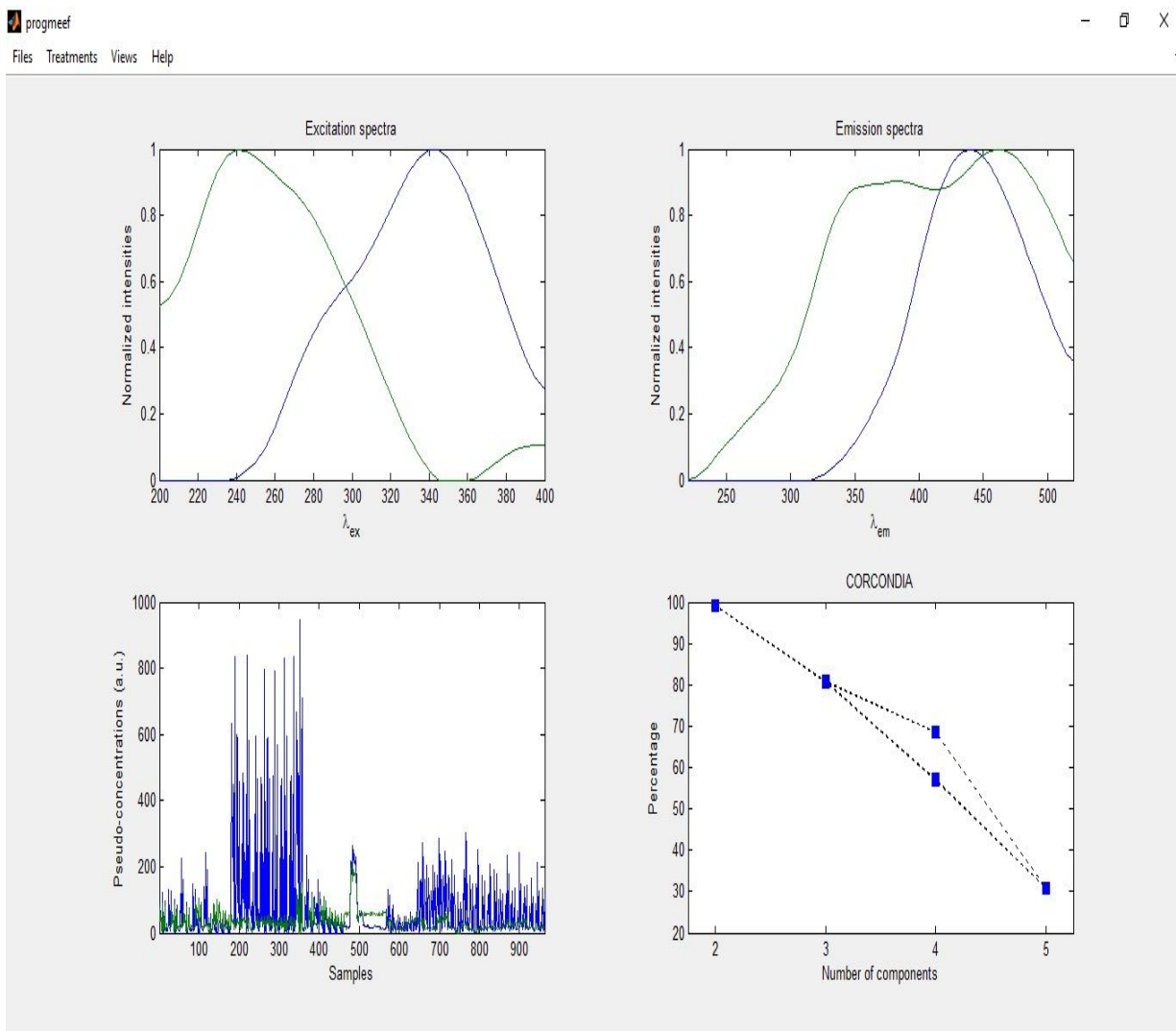


**Fig. Annex V.2 :** results of the Progmeef analysis of the CP/PARAFAC Decomposition of the EEM Dataset acquired by the Elnahhal EEM data acquisition. It shows the results of the concordia scores for each number of CP/PARAFAC components which is on the lower right hand side.

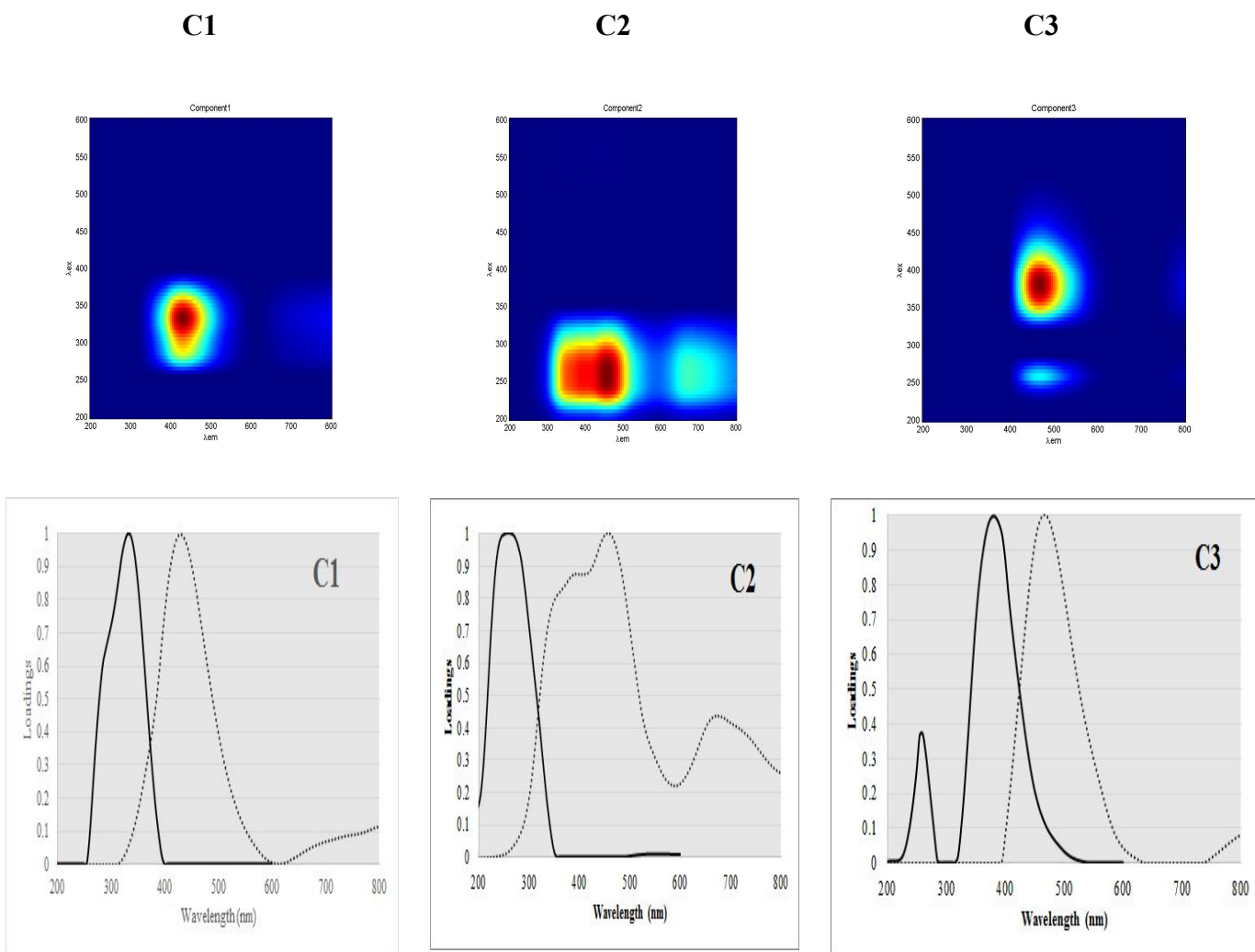


**Fig. Annex V.3.** Contour plots of CP/PARAFAC components identified from the decomposition of all EEM datasets from the Croatie EEM data acquisition method. Spectral loadings of excitation and emission wavelengths of the three identified CP/PARAFAC in the present study. Excitation loading for CP/PARAC component are solid lines whereas emission loadings are shown in dotted lines.

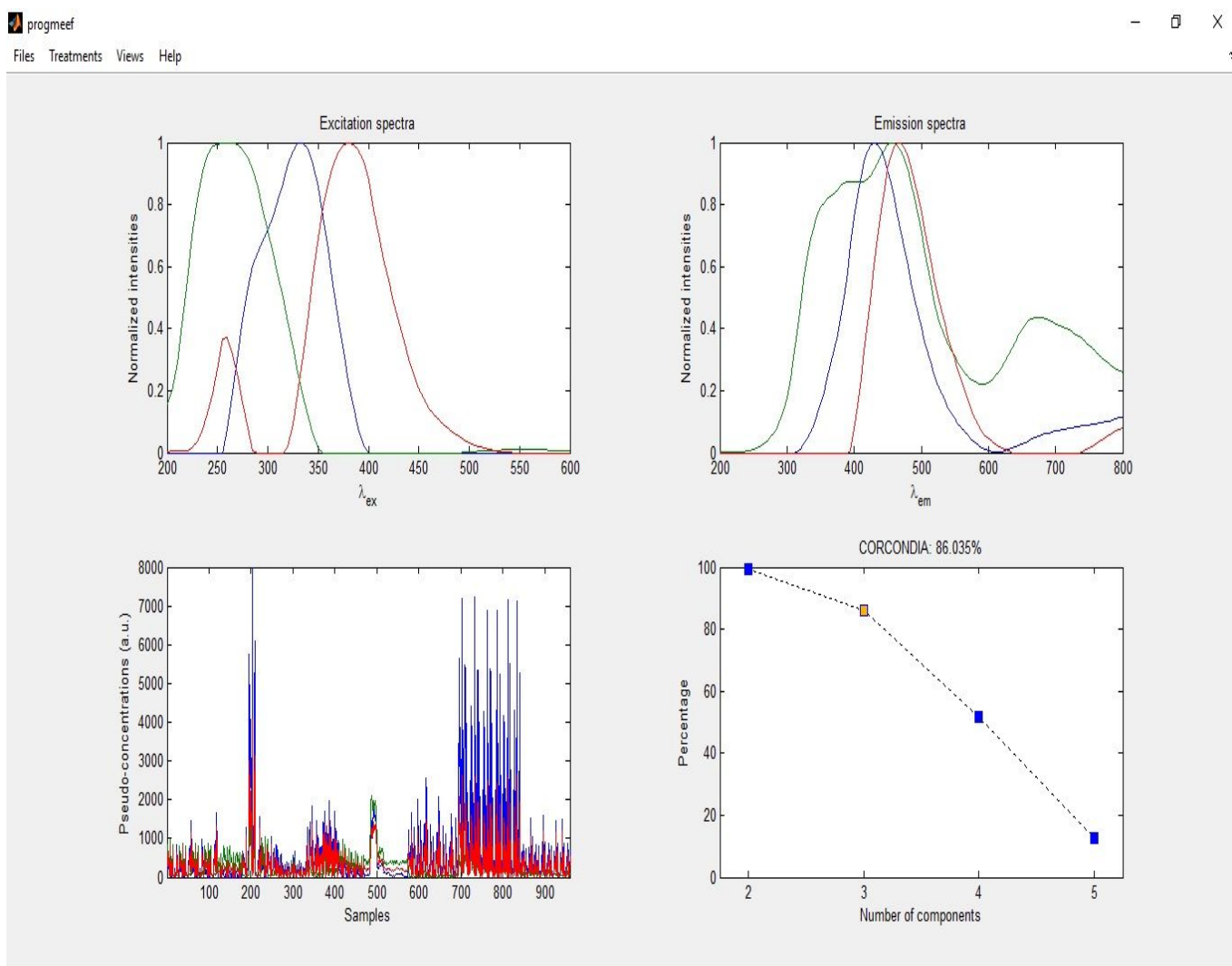


**Fig. Annex V.4:** results of the Progmeef analysis of the CP/PARAFAC Decomposition of the EEM Dataset acquired by the Croatia EEM data acquisition. It shows the results of the concordia scores for each number of CP/PARAFAC components which is on the lower right hand side.



## Annex VI

**Table Annex VI.1** Kinetic order of coefficients of multilinear regression for each CP/PARAFAC from Croatia EEM data acquisition for ( $f_{SW}$  and  $f_{RW}$ ) circular permutation. “NA” means that correlation coefficient for 2<sup>nd</sup> order rate was less than 0.75, and was dismissed.

	C1			C2			C3		
	$A_{1,0}^{WW}$ intercept	$A_{1,1}^{WW}$ ( $f_{SW}$ )	$A_{1,2}^{WW}$ ( $f_{RW}$ )	$A_{2,1}^{WW}$ intercept	$A_{2,1}^{WW}$ ( $f_{SW}$ )	$A_{2,2}^{WW}$ ( $f_{RW}$ )	$A_{3,1}^{WW}$ intercept	$A_{3,2}^{WW}$ ( $f_{SW}$ )	$A_{3,3}^{WW}$ ( $f_{RW}$ )
I111	2	2	2	2	2	2	2	2	2
I110	2	2	2	2	2	2	2	2	2
I011	2	2	2	2	2	NA	2	2	2
I101	2	2	2	2	2	2	2	2	2
I000	2	2	2	2	2	2	2	2	2

**Table Annex VI.2** Kinetic constant for coefficients of multilinear regression for each CP/PARAFAC component from Croatia EEM data acquisition from ( $f_{SW}$  and  $f_{RW}$ ) circular permutation. Values in parenthesis are standard deviation for kinetic constant for second order kinetics

	C1			C2			C3		
$k \cdot 10^6$	$A_{1,0}^{WW}$ intercept	$A_{1,1}^{WW}$ ( $f_{SW}$ )	$A_{1,2}^{WW}$ ( $f_{RW}$ )	$A_{2,0}^{WW}$ intercept	$A_{2,1}^{WW}$ ( $f_{SW}$ )	$A_{2,2}^{WW}$ ( $f_{RW}$ )	$A_{3,1}^{WW}$ intercept	$A_{3,2}^{WW}$ ( $f_{SW}$ )	$A_{3,3}^{WW}$ ( $f_{RW}$ )
I111	15.1(1.4)	1355.5(100.7)	1469.7(107.5)	0.5(0.1)	70.4(3.4)	56.9(9.9)	2.9(0.2)	331.7(15)	330.2(20.2)
I110	5.3(0.8)	471(74.3)	601.3(85)	1.7(0.3)	284.2(52.9)	332.8(47.2)	5.9(0.4)	646.3(61.9)	702.1(55.3)
I011	2.8(0.5)	304.1(51.7)	333.9(60.6)	2.3(0.5)	320.3(101.3)	NA	3.2(0.6)	383.1(65.8)	368.1(63.1)
I101	5.4(0.7)	624(87.4)	732.4(91.9)	1.4(0.2)	237.3(43.9)	311.1(60.4)	8.2(1)	918.8(125)	976.8(148.1)
I000	6.2(0.4)	765.2(47.4)	892.3(42.3)	0.7(0.05)	48.9(11.7)	66.5(13)	3.6(0.4)	401.4(41.4)	470.2(42.5)

**Table Annex VI.3** Kinetic order of coefficients of multilinear regression for each CP/PARAFAC from Elnahhal EEM data acquisition for ( $f_{SW}$  and  $f_{WW}$ ) circular permutation. “NA” means that correlation coefficient for 2<sup>nd</sup> order rate was less than 0.75, and was dismissed.

		C1			C2			C3		
		$A_{1,0}^{RW}$ intercept	$A_{1,1}^{RW}$ ( $f_{SW}$ )	$A_{1,2}^{RW}$ ( $f_{WW}$ )	$A_{2,1}^{RW}$ intercept	$A_{2,1}^{RW}$ ( $f_{SW}$ )	$A_{2,2}^{RW}$ ( $f_{WW}$ )	$A_{3,1}^{RW}$ intercept	$A_{3,2}^{RW}$ ( $f_{SW}$ )	$A_{3,3}^{RW}$ ( $f_{WW}$ )
I111	2	2	2	2	2	2	2	NA	NA	2
I110	2		NA	2	2	NA	2	NA	NA	NA
I011	2	2	2	NA	NA	NA	2	2	NA	2
I101	2	2	2	2	2	2	2	2	2	NA
I000	2	2	2	2	2	2	2	NA	NA	2

**Table Annex VI.4** Kinetic constant for coefficients of multilinear regression for each CP/PARAFAC component from Elnahhal EEM data acquisition from ( $f_{SW}$  and  $f_{WW}$ ) circular permutation. Values in parenthesis are standard deviation for kinetic constant for second order kinetics

		C1			C2			C3		
$k \cdot 10^6$		$A_{1,0}^{RW}$ intercept	$A_{1,1}^{RW}$ ( $f_{SW}$ )	$A_{1,2}^{RW}$ ( $f_{WW}$ )	$A_{2,0}^{RW}$ intercept	$A_{2,1}^{RW}$ ( $f_{SW}$ )	$A_{2,2}^{RW}$ ( $f_{WW}$ )	$A_{3,1}^{RW}$ intercept	$A_{3,2}^{RW}$ ( $f_{SW}$ )	$A_{3,3}^{RW}$ ( $f_{WW}$ )
I111		440.2(75.6)	37578.2(6490.8)	720.9(55)	39.8(5.8)	25422.3(4071.8)	507.4(45)	NA	NA	61.5(3.4)
I110		18.3(3.9)	NA	670.3(124.6)	11.2(2.4)	NA	811.1(208.2)	NA	NA	NA
I011		31(3.8)	3096.5(520.2)	392.7(75.5)	NA	NA	663.6(100.6)	-0.8(0.2)	NA	4919.3(1046.8)
I101		39.9(5.6)	3956.3(453.3)	1054.6(200.3)	15(2.7)	11142.6(2300.4)	1784.2(306.5)	1.2(0.3)	3940.2(696.8)	NA
I000		53.5(9.4)	5803.4(780)	715.3(67.1)	28.8(4.5)	7780.5(1403.3)	907.8(41.2)	NA	NA	36.9(6.9)

**Table Annex VI.5** Kinetic order of coefficients of multilinear regression for each CP/PARAFAC from Croatia EEM data acquisition for ( $f_{SW}$  and  $f_{WW}$ ) circular permutation. “NA” means that correlation coefficient for 2<sup>nd</sup> order rate was less than 0.75, and was dismissed.

	C1			C2			C3		
	$A_{1,0}^{RW}$ intercept	$A_{1,1}^{RW}$ ( $f_{SW}$ )	$A_{1,2}^{RW}$ ( $f_{WW}$ )	$A_{2,1}^{RW}$ intercept	$A_{2,1}^{RW}$ ( $f_{SW}$ )	$A_{2,2}^{RW}$ ( $f_{WW}$ )	$A_{3,1}^{RW}$ intercept	$A_{3,2}^{RW}$ ( $f_{SW}$ )	$A_{3,3}^{RW}$ ( $f_{WW}$ )
I111	2	2	2	2	2	2	2	2	2
I110	2	2	2	NA	2	NA	2	2	2
I011	2	NA	2	2	2	NA	2	2	2
I101	2	2	2	2	2	2	2	2	2
I000	2	2	2	2	2	2	2	2	2

**Table Annex VI.6** Kinetic constant for coefficients of multilinear regression for each CP/PARAFAC component from Croatia EEM data acquisition from ( $f_{SW}$  and  $f_{WW}$ ) circular permutation. Values in parenthesis are standard deviation for kinetic constant for second order kinetics

	C1			C2			C3		
$k \cdot 1e6$	$A_{1,0}^{RW}$ intercept	$A_{1,1}^{RW}$ ( $f_{SW}$ )	$A_{1,2}^{RW}$ ( $f_{WW}$ )	$A_{2,0}^{RW}$ intercept	$A_{2,1}^{RW}$ ( $f_{SW}$ )	$A_{2,2}^{RW}$ ( $f_{WW}$ )	$A_{3,1}^{RW}$ intercept	$A_{3,2}^{RW}$ ( $f_{SW}$ )	$A_{3,3}^{RW}$ ( $f_{WW}$ )
I111	262.5(52.6)	24482.6(4581.2)	1717.8(267.8)	2.8(0.6)	996.6(303.1)	56.9(9.9)	24.6(4.3)	9168.9(959.6)	321.7(19.8)
I110	24.1(5.9)	2061.4(267.6)	672(99.2)	NA	2775.7(741.1)	NA	37.2(4.7)	3352.3(588.1)	515(91.6)
I011	18.1(3.4)	NA	343.5(65.7)	-12.9(2.5)	17225.7(4475)	NA	24.1(3.4)	6252.3(1487.2)	378.9(72.4)
I101	21.2(2.7)	6101.1(778.2)	702.2(108.1)	2.6(0.5)	3131.2(624.1)	311.1(60.4)	55.5(4.8)	32672.9(5278.7)	976.8(148.1)
I000	23.3(3.7)	6325.6(1379.6)	892.3(42.3)	1.8(0.3)	5907.3(1148.1)	90(18.3)	27.5(6.2)	3556.5(332)	470.2(42.5)

**Table Annex VI.7** Kinetic order of coefficients of multilinear regression for each CP/PARAFAC from Elnahhal EEM data acquisition for ( $f_{RW}$  and  $f_{WW}$ ) circular permutation. “NA” means that correlation coefficient for 2<sup>nd</sup> order rate was less than 0.75, and was dismissed.

	C1			C2			C3		
	$A_{intercept}^{SW_{1,0}}$	$A_{(f_{RW})}^{SW_{1,1}}$	$A_{(f_{WW})}^{SW_{1,2}}$	$A_{intercept}^{SW_{2,1}}$	$A_{(f_{RW})}^{SW_{2,1}}$	$A_{(f_{WW})}^{SW_{2,2}}$	$A_{intercept}^{SW_{3,1}}$	$A_{(f_{RW})}^{SW_{3,2}}$	$A_{(f_{WW})}^{SW_{3,3}}$
I111	2	NA	2	2	2	2	NA	NA	2
I110	NA	2	2	2	2	2	NA	NA	2
I011	2	2	2	2	2	2	2	NA	NA
I101	NA	2	2	NA	2	2	2	2	NA
I000	2	2	2	NA	2	2	NA	2	NA

**Table Annex VI.8** Kinetic constant for coefficients of multilinear regression for each CP/PARAFAC component from Elnahhal EEM data acquisition from ( $f_{RW}$  and  $f_{WW}$ ) circular permutation. Values in parenthesis are standard deviation for kinetic constant for second order kinetics

	C1			C2			C3		
k*1e6	$A_{intercept}^{SW_{1,0}}$	$A_{(f_{RW})}^{SW_{1,1}}$	$A_{(f_{WW})}^{SW_{1,2}}$	$A_{intercept}^{SW_{2,0}}$	$A_{(f_{RW})}^{SW_{2,1}}$	$A_{(f_{WW})}^{SW_{2,2}}$	$A_{intercept}^{SW_{3,1}}$	$A_{(f_{RW})}^{SW_{3,2}}$	$A_{(f_{WW})}^{SW_{3,3}}$
I111	170.5(34.5)	NA	721.1(78)	19.4(3.8)	25422.3(4071.8)	498.1(38.3)	NA	NA	74.7(10.4)
I110	NA	1150.4(231.8)	533.1(120.8)	27.3(3)	4260.7(1121)	880.8(192.6)	NA	NA	-119.2(40.3)
I011	231.1(62.3)	3096.5(520.2)	342(62.4)	-44(3.3)	7439(1700)	593.7(93.9)	9.2(1.9)	NA	NA
I101	NA	3725.9(582.9)	884.4(153.5)	NA	20384.6(3351)	920.7(164.7)	-1.7(0.3)	3851.6(745.9)	NA
I000	68.4(17.1)	5803.4(780.7)	603.8(59.4)	NA	7780.5(1403.3)	720.5(42.5)	NA	-954.1(205.4)	NA

**Table Annex VI.9** Kinetic order of coefficients of multilinear regression for each CP/PARAFAC from Croatie EEM data acquisition for ( $f_{RW}$  and  $f_{WW}$ ) circular permutation. “NA” means that correlation coefficient for 2<sup>nd</sup> order rate was less than 0.75, and was dismissed.

	C1				C2		C3		
	$A_{1,0}^{SW}$ intercept	$A_{1,1}^{SW}$ ( $f_{RW}$ )	$A_{1,2}^{SW}$ ( $f_{WW}$ )	$A_{2,1}^{SW}$ intercept	$A_{2,1}^{SW}$ ( $f_{RW}$ )	$A_{2,2}^{SW}$ ( $f_{WW}$ )	$A_{3,1}^{SW}$ intercept	$A_{3,2}^{SW}$ ( $f_{RW}$ )	$A_{3,3}^{SW}$ ( $f_{WW}$ )
I111	NA	2	2	2	NA	2	2	2	2
I110	2	2	2	2	2	2	2	2	2
I011	NA	2	2	2	NA	2	2	2	2
I101	2	2	2	2	2	2	2	2	2
I000	2	2	2	2	2	2	2	2	2

**Table Annex VI.10** Kinetic constant for coefficients of multilinear regression for each CP/PARAFAC component from Croatie EEM data acquisition from ( $f_{RW}$  and  $f_{WW}$ ) circular permutation. Values in parenthesis are standard deviation for kinetic constant for second order kinetics

	C1				C2		C3		
$k \cdot 1e6$	$A_{1,0}^{SW}$ intercept	$A_{1,1}^{SW}$ ( $f_{RW}$ )	$A_{1,2}^{SW}$ ( $f_{WW}$ )	$A_{2,0}^{SW}$ intercept	$A_{2,1}^{SW}$ ( $f_{RW}$ )	$A_{2,2}^{SW}$ ( $f_{WW}$ )	$A_{3,1}^{SW}$ intercept	$A_{3,2}^{SW}$ ( $f_{RW}$ )	$A_{3,3}^{SW}$ ( $f_{WW}$ )
I111	NA	24482.6(4581.2)	1601(263.3)	-0.9(0.3)	NA	64.5(6.7)	15(3.6)	9136.7(403.5)	322.7(16.1)
I110	117.1(27)	2061.4(267.6)	551.9(100.4)	2.7(0.9)	-3351.8(278.7)	274.1(73.4)	536.1(116.6)	3352.3(588.1)	468.4(97.9)
I011	NA	3053.7(505.5)	307(58.2)	-16.1(2.5)	NA	320.3(101.3)	-73.1(85.9)	8106.8(2034.2)	383.9(66)
I101	-37.2(7.9)	6101.1(778.2)	624(87.4)	4.8(1)	3076.9(519.1)	238.2(45.5)	-133.4(24.8)	32672.9(5278.7)	664.8(105.6)
I000	23.9(6.1)	6325.6(1379.6)	765.2(47.4)	1.9(0.4)	5674.6(1070.3)	120.1(14)	34.3(6.5)	3556.5(332)	401.4(41.4)

## Résumé :

Les activités anthropiques ont apporté des changements majeurs à notre système global. Par ailleurs, la matière organique dissoute (MOD) du littoral a une grande influence sur le cycle global du carbone et donc sur le changement climatique. L'apport côtier en MOD représente la matière organique terrestre. Les rivières urbanisées sont fortement impactées par la MOD anthropique provenant des usines de traitement des eaux usées. La MOD chromophorique est un sous-groupe de la MOD qui peut absorber la lumière. La MOD fluorescente est à son tour un sous-groupe de la MOD chromophore. Le signal de fluorescence de la MOD anthropogénique dans la zone côtière n'est pas bien caractérisé et évalué dans la littérature. Les dégradations induites par photochimie et les changements au niveau moléculaire sont peut-être de plus en plus influencés par la MOD. Dans la présente étude, plusieurs expériences d'irradiation solaire ont été menées avec plusieurs modes de filtration de mélange d'eau de rivière, d'eau de mer et d'un effluent de station de traitement des eaux usées dans le but de trouver un signal spécifique de fluorescence comme un traceur de la MOD anthropique en utilisant les matrices d'émission d'excitation de la spectroscopie de fluorescence (EEMs) couplées à la technique statistique chimiométrique de l'analyse factorielle parallèle CP/PARAFAC. Un modèle de régression multilinéaire a été développé entre la contribution des composantes CP/PARAFAC et la composition du mélange. La cinétique des paramètres de régression multilinéaire a également été étudiée. Des suivis géographiques de l'évolution du signal de fluorescence dans la rivière Gapeau jusqu'à la mer ont été menés ainsi qu'une étude temporelle du signal de fluorescence. Le modèle de régression multilinéaire développé a été appliqué pour modéliser les résultats des expériences de champs géographiques et temporelles. Les résultats ont montré que le modèle de régression multilinéaire est excellent. Par contre la recherche d'un signal ou d'une signature de fluorescence spécifique pour l'eau de rivière, les stations d'épuration des eaux usées ou l'eau de mer n'a pas pu être réalisée dans ce travail. Dans la zone côtière affectée par l'homme, les matières organiques fluorescentes résiduelles proviennent principalement sinon uniquement de l'usine de traitement des eaux usées, et aucun signal spécifique provenant de l'eau de mer n'a pu être détecté près de la côte.

Mot Clé : MOD fluorescente, Matrices d'émission d'excitation, fluorescence, CP / PARAFAC, Photodégradation, Usines de traitement des eaux usées, Zone côtière.

## Abstract :

Anthropogenic activities have done major changes to our global system. The coastal dissolved organic matter has great influence on the global carbon cycle and hence climate change. The riverine input of dissolved organic matter represents the terrestrial organic matter. Urbanized rivers are greatly impacted by the anthropogenic dissolved organic matter coming from wastewater treatment plants. Chromophoric dissolved organic matter is a subgroup of the dissolved organic matter which can absorb light. Fluorescent dissolved organic matter in turn is a subgroup of the chromophoric dissolved organic matter. The fluorescence signal of the anthropogenic dissolved organic matter in the coastal zone is not well characterized and evaluated in the literature. Photochemically induced degradations and changes at the molecular level are considered to be a great process which could influence the dissolved organic matter. In the present study, Laboratory mixing experiments, several sunlight irradiation experiments were conducted with several modes of filtration of three endmember mixing components (River water, Sea water, wastewater treatment plant effluent discharge) with the objective of finding a specific signal of fluorescence which could be a tracer of the anthropogenic dissolved organic matter through using the fluorescence spectroscopy excitation emission matrices (EEMs) coupled with the chemometric statistical technique of Parallel Factor analysis CP/PARAFAC. Moreover, multilinear regression model between the contribution of CP/PARAFAC components and two content fraction of River water and Seawater endmember was developed. In addition the kinetics of the multilinear regression parameters were investigated. On top of that, geographical investigations of the evolution of fluorescence signal in the Gapeau river till the sea were conducted. Furthermore, Temporal investigation of the fluorescence signal for four water points in the pathway of Gapeau river were done. The multilinear regression model developed was applied to model the results of the geographical and temporal field experiments. Results have shown that Multilinear regression model for contribution of CP/PARAFAC components is excellent and could be done for the three endmembers. In addition the search for specific fluorescence signal or signature for river water, wastewater treatment plants and sea water couldn't be done in this work. In human impacted coastal zone, residual fluorescent organic matter comes from wastewater treatment plant, and no specific signal from sea water could be detected near the coast.

Keywords : Fluorescent dissolved organic matter, Excitation emission matrices, fluorescence, CP/PARAFAC, Photodegradation, Wastewater Treatment Plants, Coastal zone.